NASA CR - 72981

Final Report

DEVELOPMENT OF OPTIMUM TIG WELDING PROCEDURE FOR PRODUCTION OF WELDMENTS IN 12% NI MARAGING STEEL

By

P. M. Schmidt and R. S. Snow

Prepared for
National Aeronautics and Space Administration

July 1971

Contract NAS 3-11183

Technical Management
NASA Lewis Research Center
Cleveland, Ohio
John A. Misencik

GENERAL DYNAMICS
Electric Boat Division
Groton, Connecticut

FOREWORD

This report summarizes work performed by the Electric Boat division of General Dynamics Corporation from July 1, 1967 to June 30, 1970 under Contract NAS 3-11183. The work was administered under the direction of Mr. John A. Misencik of the NASA Lewis Research Center. Overall responsibility for the contractual performance of General Dynamics was vested in Mr. J. M. Cameron, Manager of Welding and Materials Engineering. Technical responsibility was vested in Mr. J. Lanzafame, Chief of Process Development Engineering through D. R. Smith, Supervisor of Structural Welding Development.

General Dynamics personnel who participated in the work described herein include P. M. Schmidt, project engineer and principle investigator; R. S. Snow, materials engineer; and D. O. Hinchliffe, test engineer. Welding assistance was provided by Process Development Laboratory personnel, A. Sousa, R. J. Root, Jr. and D. Main.

All fracture toughness specimen precracking and testing for this contract was performed by Lehigh University Fritz Laboratory, under the direction of Dr. R. G. Slutter. Del Research Corporation personnel, including Drs. P. C. Paris, R. P. Wei and G. C. Sih, were retained as consultants in the fracture mechanics area.

The information contained in this document is also released as General Dynamics/Electric Boat division Report PDE-154.

ABSTRACT

An optimum gas-tungsten-arc (GTA) welding procedure has been developed for 3/4-inch-thick 12% Ni - 5Cr - 3Mo maraging steel and used to fabricate five 36-inch-diameter test vessels made of this material. Data is reported on the results of extensive studies of base metal, weld metal and weld heat-affected zone mechanical properties and fracture toughness. These studies included heat-treatment response studies of both base plate and weldments. Tensile, conventional Charpy, precracked Charpy, single-edge-notch, surface-flawed and metallographic specimens were tested and the five fabricated vessels were cyclically tested and burst. The results of these tests demonstrated that vacuum-melted 12% Ni - 5Cr - 3Mo maraging steel, welded using the developed gas-tungsten-arc welding procedure, is capable of meeting a leak-before-burst failure design criteria for 260-inch-diameter motor cases at a yield strength of 180,000 psi.

TABLE OF CONTENTS

TABLE OF CONTENTS (Continued)

LIST OF TABLES

LIST OF TABLES (Continued)

LIST OF FIGURES

LIST OF FIGURES (Continued)

LIST OF FIGURES (Continued)

LIST OF FIGURES (Continued)

LSIT OF FIGURES (Continued)

LIST OF FIGURES (Continued)

LIST OF FIGURES (Continued)

LIST OF FIGURES (Continued)

SUMMARY

This program was conducted to investigate the performance and suitability of 12% Ni-5Cr-3Mo maraging steel at a yield strength of 180,000 psi as a 260-inch-diameter rocket motor case material. The principle objective was to demonstrate that full-thickness sub-scale models of such motor cases could be fabricated from this material, using the GTA (gas-tungsten-arc) welding process, which would meet leak-before-burst performance requirements. This involved: (1) the selection of an optimum solution-annealing heat treatment for base plate material; (2) the development of an optimum GTA welding procedure; (3) the selection of an optimum aging heat treatment for weldments, including areas of weld metal, the weld heat-affected zone and base material; (4) extensive mechanical property and fracture toughness testing of heat treated base material and weldments; (5) limited stress-corrosion and flaw-growth rate studies; and (6) the fabrication and hydrotesting to failure of five subscale (full thickness) test vessels.

The results of the programs verified the suitability of this material for large motor case applications. This included a demonstration of leak-before-burst failure capability in 3/4-inch-thick vessel weldments at a yield strength of 180,000 psi.

1.0 INTRODUCTION

Experience gained from the fabrication of large rocket motor cases and other types of pressure vessels has shown that such structures will inherently contain some unavoidable crack-like defects. The presence of these defects can, under certain circumstances, result in premature and catastrophic failure. This was dramatically demonstrated by the failure of a prototype 260-inch 18% Ni maraging steel motor case during proof testing in 1965.[1] This motor case, designated 260-SL-1, failed at only 56% of proof pressure. The failure was concluded to have originated from a submerged crack-like defect approximately 1.4 inches long and extending about 0.10 inch in the thickness direction of the 0.730-inch thick vessel wall. This defect was not detected by either X-ray or ultrasonic nondestructive tests performed on the vessel.

After conducting a special study of the state-of-the-art of nondestructive testing methods as used to inspect this and other motor cases for crack-like defects, the SL-1 failure investigation committee concluded that such large fabricated structures would inherently contain defects similar to the one which caused failure. Consequently, if burst failures are to be realiably avoided, materials, processes and design factors must be selected such that the size of any flaw which could cause fracture must be greater than the vessel wall thickness. This ensures that the vessel will leak rather than burst should failure occur during proof testing or actual operation.

Results of several programs and studies[2,3,4] conducted prior to the initiation of this program indicated the only steels with strengths of 150 ksi or greater which exhibited sufficient weldment toughness to approach leak-before-burst performance in 156-inch diameter or larger motor cases were 12% Ni maraging, and 5Ni-Cr-Mo-V (HY-150).

This program is a further investigation of 12% Ni maraging steel weldments produced using the gas-tungsten-arc (GTA)* welding process.

The work of this contract was divided into five major tasks:

Task I - Review of Existing Data
Task II - Plate Characterization Study
Task III - Optimization of GTA Welding Procedure
Task IV - Fabrication of Test Cylinders
Task V - Hydrotest of Fabricated Cylinders

*As defined by the American Welding Society - also referred to as tungsten-inert-gas (TIG) welding.

All base material used in this program was from a single vacuum-induction-melted and vacuum-arc-remelted heat. Weld filler wires evaluated and used in this program were of 12% and 17% Ni nominal composition.

Mechanical property data obtained as part of this program included results from transverse and all-weld-metal tensile specimens, precracked and conventional Charpy impact specimens, and single-edge-notched bend and surface-flawed fracture toughness specimens.

As a final step in this program, five test vessels were fabricated using a selected optimum welding procedure. Two vessels contained fatigue-precracked flaws in the weld centerline and one was fabricated with an intentionally introduced radial mismatch along one longitudinal seam. These vessels were hydrotested under cyclic and sustained loads to induce leakage or fracture and compared to similar but unflawed vessels statically pressurized to burst.

2.0 BACKGROUND

Investigations of a number of proof-test and in-service failures early in the development of thin-walled solid-propellant motor cases, liquid-propellant tanks, and high pressure-gas bottles showed one predominant feature -- a small defect or flaw was usually observed at the origin of failure, in or near a welded seam. Often, examination of the fracture revealed cyclic-stress-corrosion, or hydrogen-induced flaw growth had occurred prior to failure.

No method was found which completely eliminated the occurrance of such failures, but several materials or design changes were observed to be effective in minimizing them. These changes generally included:(3)

(1) A reduction in heat-treat strength level, which in turn (although only vaguely understood by the designers and materials personnel at the time) resulted in a larger critical flaw size by virtue of both the increased plane-strain fracture toughness and of the lower applied stress level;

(2) Incorporation of more sophisticated fabrication procedures with emphasis on the elimination of longitudinal seam welds;

(3) Improved quality control and inspection procedures, plus a tightening of inspection requirements (again, with little or no actual knowledge as to what flaw needed to be detected);

(4) Introduction of mechanized welding equipment to minimize human error;

(5) Refinement of stress analysis and tool design procedures; and

(6) Use of the gas-tungsten-arc (GTA) welding process.

Although these changes provided an acceptable solution to the problem of fracture of smaller motor cases, they are not adequate to solve the problems encountered in the design and fabrication of considerably larger 156 and 260-inch diameter motor cases. There are several significant differences between large and small motor cases which make the prevention of failures of large cases more important. First, vehicle economics and personnel safety considerations make the prevention of operational failures of the larger cases essential, and second, the cost of a large

motor case makes the prevention of a proof-test failure of major importance. Whereas a proof-test failure of a small motor case is generally a minor setback, representing only one of many cases fabricated, failure of a large motor case may represent a significant portion of the total available motor case budget. Consequently, methods used to prevent the failure of large motor cases must be much more positive and effective than those which can be used for smaller cases.

In addition, the technical problems involved in the manufacture of large motor cases are compounded due to:

(1) The need to fabricate such structures in facilities not usually accustomed to aerospace-quality fabrication procedures and requirements;

(2) The voluminous increase in the amount of welding and the large quantities of plate or base material required; and

(3) The increased wall thicknesses required for such cases.

These requirements tend to increase the probability of flaw occurance, complicate the inspection problem, increase the probability that a critical size flaw will not be detected, and increase the probability of failure rather than leakage during proof-test. The effect of these differences is thus to reduce the reliability of motor cases as they become larger. Consequently, since economic and safety considerations applicable to large motor cases require greater instead of lesser reliability, the use of materials capable of meeting a leak-before-burst requirement becomes necessary.

The work reported herein was consequently conducted to investigate the performance of 12% Ni maraging steel at a yield strength level of 180,000 psi in subscale pressure vessels having wall thicknesses equivalent to a 260-inch motor case.

3.0 MATERIALS AND PROCEDURES

3.1 MATERIALS

3.1.1 BASE MATERIAL -- All base material used in this program was vacuum-induction melted (VIM) and vacuum-arc remelted (VAR) 12% Ni-5% Cr-3% Mo maraging steel, produced by Latrobe Steel Corp. and converted into hot-rolled plate by U. S. Steel Corp. The pressure vessel shells, weld test panels, and all other 3/4-inch thick plate material was from Latrobe ingot number L-50897, which was also the U. S. Steel heat number for this material. All 1-1/8-inch plate, such as used for the vessel heads, was hot-rolled and produced from Latrobe ingots L-50896 and L-50898. The U. S. Steel heat numbers were again the same as the ingot numbers.

Detailed chemical analysis and plate processing data are presented in Tables I and II.

3.1.2 WELD FILLER WIRES-- Two types of weld filler wires were selected for use in this program. The first of these was a 17% Ni-2Co-3Mo composition (Heat No. 01222) and the other was 12% Ni-5Cr-3Mo (Heat No. 04836) nominally matching the composition of the base plate. This wire appeared slightly superior to the 17-2-3 wire and, therefore, it was used to fabricate the final weld test panels and pressure vessels. All wires were 0.062-inch diameter; produced by VASCO, Inc. Chemical analysis data are presented in Table III.

3.2 TASKS PERFORMED AND PROCEDURES

The work of this program was divided into five major tasks, described in the following paragraphs. Test and inspection procedures and the procedures used to conduct several supplementary investigations related to the work of these tasks are separately described in sections 3.3 and 3.4 of this report.

3.2.1 TASK I - LITERATURE REVIEW -- In order to become thoroughly familiar with the state-of-the-art of 12% Ni maraging steel technology, a thorough review of published literature and available information was conducted. This included utilization of the ASM Information Searching Service and personal contact with individuals from International Nickel Company, U. S. Steel Corp., Cameron Iron Works, VASCO Corp. and Air Reduction Company. The results obtained by the Electric Boat division in fabricating a 1/3-scale model of a 12% Ni maraging steel pressure hull[5] were also reviewed.

A summary of this literature review was then written when the task was completed. It is included with this report as Appendix A.

3.2.2 TASK II - MATERIAL CHARACTERIZATION STUDY -- A base material characterization study was conducted to determine the mechanical and metallurgical properties of the 108" x 702" master plate produced for use in this program. Following solution annealing this master plate was cut by the vendor into smaller pieces for shipment. The location and orientation of the items shipped are shown in Figure 1. Figures 2, 3 and 4 illustrate the location and orientation of each piece of material used in this program.

Prior to the production of any weld test panels, a thorough study was made of the mechanical properties and heat-treat-response characteristics of this base plate. This study consisted of two parts, as follow:

Part 1 - Selection of Mill Solution Annealing Treatment

After hot rolling but prior to any mill heat treating, a 21" x 108" sample, Item #1 of Figure 1, was cut from the master plate. This sample was then shipped to the Electric Boat division where it was cut into 6" x 10" test plates as shown in Figure 5. These test plates were designated 1A01 through 1A18. They were subjected to solution annealing and aging treatments as shown in Table IV and tested as follows:

Two	- Standard 0.505-inch round tensile specimens (for determination of T.S., 0.2% Y.S., % Elong. and % R.A.)
Three	- Standard 0.392-inch Charpy V-notch impact bars (to determine toughness, ft.-lbs.)
Three	- Fatigue-precracked Charpy V-notch impact bars (to determine toughness, W/A, ft.-lbs./in.^{2})
One	- Hardness traverse specimen, Rockwell "C" (spacings of 1/16" between readings)

A complete chemical analysis was also conducted.

Specimen locations and orientations are shown in Figure 5, with the hardness transverse test pattern shown in Figure 6.

Based on the results of these tests an optimum solution-annealing heat treatment was selected for the base plate material. Following NASA approval, the selected optimum solution-anneal was applied to the base plate by the mill.

This heat treatment consisted of heating to 1575°F, holding for one hour at temperature, followed by air-cooling.

Part 2 - Evaluation of Heat-Treated Master Plate

Following receipt of the mill solution-annealed base plate, a material characterization study was conducted to confirm the effectiveness of the selected optimum solution-anneal treatment as applied by the mill and obtain additional metallographic, mechanical property and fracture toughness data. The following tests were performed after samples of the mill solution-annealed base plate were aged at 900°F for 8 hours and air cooled:

Two	- Standard 0.505-inch transverse tensile tests (to determine T.S., 0.2% Y.S., % Elong. and % R.A.)
One	- Charpy V-notch impact transition curve, -200°F to +212°F (24 transverse specimens, notch perpendicular to plate surface)
Two	- Fatigue-precracked transverse Charpy V-notch impact bars (tested at 80°F, notch perpendicular to plate surface)
One	- Micro and macro examination of plate mid-thickness
One	- Hardness traverse, Rockwell "C" - surface to surface with approximately 1/16-inch spacings
One	- Edge-notched fracture toughness bend specimen (longitudinal)
One	- Edge-notched fracture toughness bend specimen (transverse)

The plate material used for these tests came from piece II.C of Item #7, with test specimen orientation and locations being as shown in Figure 7. The results of these tests were then compared to the results of subsequent Task III tests of weld-metal specimens aged at various times and temperatures in order to determine a heat-treatment which would optimize both base-metal and weld-metal properties.

3.2.3 TASK III - WELDING PROCEDURE DEVELOPMENT -- The development of an optimum gas-tungsten-arc (GTA) welding procedure for the production of 12% Ni maraging steel weldments was one of the major objectives of this program. This was accomplished in four steps, as follow:

Bead-On-Plate Studies

Numerous bead-on-plate welds were made on 1-1/8" thick 6" x 12" plates to select initial parameters for use in producing the preliminary 12" x 12" weldments in this task. These welds were made using various combinations of weld filler wires, welding currents, arc voltage, travel speeds, wire feed rates, shielding gases, and shielding gas flow rates. Combinations which were obviously unsatisfactory due to unacceptable welding arc characteristics, poor as-deposited weld bead contour and bead wash or which produced defects evident after flush-grinding and liquid penetrant testing were eliminated from further consideration. Twelve combinations were then selected from the remainder for further study and refinement. These combinations were selected such that further refinement would be possible based on consideration of how the following were observed to affect weld properties and quality:

- weld filler wire
- weld bead size
- weld heat input
- type shielding gas
- use of auxiliary shielding
- interpass temperatures
- interpass cleaning techniques
- weld joint design
- weld metal dilution effects

Previous Electric Boat division experience obtained from the fabrication of a 12% Ni maraging steel pressure hull model(5) was also used as a guide in selecting these combinations.

Preliminary 12" x 12" Weldment Studies

Following completion of the bead-on-plate studies, thirteen 12" x 12"x3/4" weldments were fabricated using the parameters and weld joint designs given in Tables V and VI. The location of the specific pieces of base plate used for these weldments is shown in Figure 2. These weldments were aged 900°F for 8 hours and air cooled. They were then liquid penetrant and X-ray inspected for soundness in accordance with the procedures described in Section 3.3.2 of this report. The following mechanical property test specimens were next removed and tested as described in Section 3.3.1:

One - Standard 0.252-inch all-weld-metal-tensile specimen

Four - Standard transverse Charpy V-notch impact specimens, notched in weld

Two - Precracked transverse Charpy V-notch specimens, notched in weld

Transverse 0.505-inch tensiles, reduced section tensiles, 3T-radius weld side bend specimens and macro sections were also taken in some instances.

Test specimen locations and orientations for these weldments are shown in Figures 8 through 15.

The results of these destructive tests and the previously performed nondestructive tests were then analyzed and six welding procedures selected for further study and refinement.

Production of 40" x 40" Test Panels

One 40" x 40" test panel was produced using each of the six welding procedures selected. A seventh panel, 48" long, was also welded to obtain additional information for 60° angle weld joints and higher levels of heat inputs. Figure 2 shows where the pieces used to produce these panels were located in the master plate and their orientation. The welding parameters and weld joint design details are given in Tables V and VII and a typical welding equipment set-up is shown in Figure 16. A drawing of the special auxiliary gas shielding device used in producing these and other weldments is presented in Figure 17.

The welds were liquid penetrant, X-ray and ultrasonically inspected. They were then aged at 900°F for 8 hours and destructively tested as follows:

One - Standard type 0.252-inch all-weld-metal tensile specimen

Two - Standard type 0.505-inch transverse tensile specimens

Five - Transverse standard Charpy V-notch specimens, notched in weld metal

One - 9-1/2" x 40" edge notched (in weld metal) K_Q bend specimen

One - 9-1/2" x 40" edge notched (in HAZ) K_Q bend specimen

One - Metallographic cross section, transverse to weld

Specimen lay-out diagrams are shown in Figures 18 through 23, with specimen details and testing procedures being described in Sections 3.3 and 3.4 of this report. Panel W3C09 contained an extensive amount of lack-of-fusion and therefore no mechanical property tests were conducted. Panel W3C09A was subsequently fabricated using adjusted parameters and liquid penetrant and X-ray inspected for soundness. As shown in Figure 23 only five Charpy V-notch impact and one all-weld-metal tensile specimens were taken from the mid-length area of this panel. No other specimens were tested from this panel.

Production of 40" x 60" Test Panels

Based on an analysis of the results of these tests performed on the 40" x 40" weldments, an optimum welding procedure was selected for use in fabricating four 40" x 60" test panels and the five test vessels of this program.

This procedure is given in Table VIII. Figures 2 and 3 show the location and orientation of the base plate material used to produce these panels. Each panel was liquid penetrant, X-ray and ultrasonically inspected for weld defects after welding was completed but prior to aging.

The first panel welded, #W3D01, was cut into twelve pieces as shown in Figure 24. These pieces were then each subjected to the aging treatments shown in Table IX and tested as follows:

One	- Standard 0.505-inch transverse tensile test specimen
Four	- Charpy V-notch impact specimens, notched in weld metal

Test specimens for each piece were located and oriented as shown in Figure 25.

Panel #W3D02 was fabricated to study the possible effects of repeated weld repairs on weldment mechanical properties. This panel was welded and then selected areas, shown outlined by dashed lines in Figure 26, were ground out and rewelded. The simulated repair welding of these areas was performed three times, with the ground-out areas of the weld being similarly shaped and in the same locations each time. This panel was liquid penetrant and X-ray inspected after the initial welding operation and each repair cycle.

After completion of the last repair cycle, the panel was aged and the following mechanical specimens removed from simulated repair areas and tested:

One	- Standard 0.252-inch all-weld-metal tensile test specimen
Two	- Transverse reduced section tensile specimens
Sixteen	- Charpy V-notch impact specimens notched in weld metal and tested at temperatures from +72°F to -120°F
One	- 9-1/2" x 40" edge notched (in weld metal) K_Q bend specimen
One	- 9-1/2" x 40" edge notched (in HAZ) K_Q bend specimen
Two	- Transverse metallographic weld cross sections, one from an area of no repairs

The location and orientation of these specimens is shown in Figure 27.

The third test panel of this group, #W3D03, was fabricated in order to obtain mechanical property data on a typical weldment produced using the selected optimum welding procedure and aging treatment. Nondestructive and destructive tests on this panel were the same as for weldment W3D02. Specimen locations and orientations are shown in Figure 28.

The fourth panel, #W3D04, was fabricated and inspected in the same manner as #W3D03. Six 10" x 40" surface-flaw test specimens were then cut from this panel as shown in Figure 29. Artificial flaws were then electro-discharge machined (EDM) in base metal, HAZ, and weld metal areas of these specimens and the specimens then fatigue precracked and tested for fracture toughness in both air and salt-water environments. Specific testing procedures and specimen details are described in Section 3.4.2 of this report.

3.2.4 TASK IV - TEST VESSEL DESIGN AND FABRICATION -- Five test vessels were designed and fabricated in Task IV, each one containing two longitudinal seams welded with the optimum procedure selected in Task III and presented in Table VIII. These vessels had a nominal shell wall thickness of 3/4-inch and were approximately 35-inches in diameter. Hemispherical heads, hot spun from 1-1/8" plate, were used as end closures. Figure 30

illustrates the general design configuration of the vessels with weld joint and piping penetration details being shown in Figures 31 and 32. A flow chart of the major steps in vessel fabrication is shown in Figure 33.

Two of these vessels, designated #W4B and #W4E, were fabricated to simulate the highest levels of workmanship and weld quality which can presently be obtained under normal shipyard or boiler shop production welding conditions. The third vessel, #W4C, was fabricated with a radial mismatch of approximately 10%t in one of the longitudinal welds. Figure 34 illustrates the nature of this mismatch. The amount of mismatch was calculated so that the combination of membrane stress and bending stress at the proof pressure would equal the uniaxial yield strength of the steel. In this test, the safety factor and the weld efficiency allowance were "used up" by weld mismatch.

The other two "defective" vessels were essentially defect-free as fabricated. Semi-ellipitical surface flaws with the major axis parallel to the vessel centerline were then cut into the center of one of the longitudinal welds at the mid-length of these vessels. Figure 35 shows typical flaw dimensions and details. The crack-like flaws were made by electro-discharge machining, and were 2-3/8" long, 0.70" deep at the minor axis of the ellipse, and about 1/32" wide. These dimensions were as specified by NASA. The machined flaws were over 80% of the vessel wall thickness, prior to fatigue extension of the EDM flaw. It was assumed they would be representative of the largest "critical flaw size", except for a through-the-wall crack, which could exist for this material thickness at ambient temperature. Thus, in testing, the vessels would either shatter at some pressure less than yield strength if the material were subject to brittle fracture or the slot would simply tear open in a ductile manner and the vessel would leak if the steel possessed sufficient fracture toughness to preclude brittle failure at the temperature and other conditions of the test. Hopefully, a "leak-before-burst" mode of failure would be demonstrated, indicating a sufficient degree of fracture toughness in the weld metal of these vessels to make this material attractive for use in rocket motor cases.

Based on the results of the weldment aging study of Task III, all five vessels were aged at 900°F ± 15° for 8 hours, after welding, followed by an air cool. The artificial flaws were electro-discharge machined after the vessels were aged.

3.2.5 TASK V - VESSEL HYDROTESTS -- While the tensile, notched bend and surface-flawed tensile specimens of Task III of this program provided valuable basic information as to weldment strength, toughness and stress-corrosion resistance, the pressure test of a cylindrical vessel (a "scale model" of a rocket motor case) is the most conclusive test of the weldment properties. Consequently, each of the five test vessels was hydrotested to a leak or burst failure.

The two unflawed vessels and the one containing the mismatched weld seam were proof pressure tested to stress levels equivalent to Class 632A design factors. They were next subjected to five pressure cycles simulating operational stress levels (10% below proof pressure) and then pressurized to burst.

The two vessels containing the artificial flaws were subjected to cyclic pressure loadings prior to proof testing. This was done to initiate a crack from the bottom of the machined notch and extend it in the thickness direction. The vessels were then pressurized to proof pressure or, in the case of vessel #W4A, to the point where a leak occurred. Vessel #W4D, which withstood full proof pressure, was then subjected to five operational pressure cycles, and subsequently pressurized until a leak failure resulted.

Test Parameters and Requirements

Three levels of pressure are significant to the hydrotest of vessels such as these:

(1) Maximum operating pressure - the maximum pressure to which the rocket case will be subjected during normal operations. (Pop)

(2) Proof pressure - a pressure in excess of maximum operating-pressure to which a case is tested prior to use. (Pp)

(3) Burst pressure (or leak pressure) - maximum pressure which the vessel will withstand without rupture. (Pb)

For the design of rockets in this material, the following values apply:

Uniaxial yield strength of optimum weld = 180,000 psi min.

Weld efficiency factor = 0.95

Safety factor = 1.3

$\bar{\sigma}op$ (max. operating stress) = $\frac{Fty\ (min.)\ x\ W.F.}{S.F.} = \frac{180{,}000\ psi\ (.95)}{1.3}$

and:

$\bar{\sigma}p$ (max. proof stress) = 1.1 $\bar{\sigma}op$ = 1.1(131,500 psi) = 144,650 psi

The uniaxial yield strength of the weld metal is about 3,000 psi less than that of the base metal, hence governs the working strength of the vessels.

The hydrostatic pressures required to develop these stresses for a vessel of the following dimensions:

Inside Radius = 16.3 inches

Wall thickness (measured) = 0.8125 inches

are:

$$\text{Pressure operating (Pop)} = \frac{\sigma_{op} \times t}{R} = \frac{131{,}500\text{psi}(0.8125")}{16.3"} = 6{,}550\text{psi}$$

$$\text{Pressure proof (Pp)} = 1.1\ \text{Pop} = 1.1(6550\text{psi}) = 7210\ \text{psi}$$

Burst pressure for the unflawed vessels would be in the neighborhood of:

$$\text{Pressure Burst (Pb)} = \frac{F_{tu} \times t}{R} = \frac{185{,}000\text{psi}(0.8125")}{16.3"} = 9220\ \text{psi}$$

F_{tu} = ultimate strength of the weld metal. This is less than the ultimate strength of the base metal.

Because of biaxial stress conditions in the cylinders, the shell can support a higher stress than indicated by uniaxial tensile strengths, hence the indicated Pb is conservative for a substantially flawless vessel built of tough material.

The test program for the vessels simulated a program of proof test and multiple firings of a rocket motor.

First pressurization was to the proof pressure with a 5 minute hold at pressure, followed by five cycles to operating pressure with a minimum one minute hold at pressure.

Pressurizing System

The pressurizing system for testing the vessels consisted of a high pressure accumulator, pumps, pressure regulators and fluid reservoirs capable of developing at least 20,000 psi hydrostatic pressure. The original intent was to maintain pressure in excess of operating pressure on the accumulator for the cycling part of each vessel test, so that cycling rate would be limited by rate of fluid flow, controlled by valves and piping system resistance.

Unfortunately, due to pump failure, the system did not function in this manner, and pressurizing rate was dependent on pumping rate of one low volume, high pressure pump serving the accumulator. Loss of the low and medium pressure pumps severely restricted operations.

Automatic cycling controls were provided, and auxiliary pressure transducers were installed in the system for data taking, such as pressure vs crack opening displacement, and acoustic output.

The vessels were tested in a concrete vault and placed in a horizontal position for maximum stability.

An attempt was made to use this pressure system for fatigue precracking of the flawed vessels, but the cycling rate was too slow without the low pressure pump. An auxiliary system was, therefore, assembled to operate at 3500-4000 psi maximum, to provide the 3400 psi pressure required for fatigue precracking. The cycling rate with the auxiliary system was about 90 cycles per hour. Much of the primary system piping, including pressure transducers and the cycle counter was used with the auxiliary pumping system.

Since the only openings into the vessels were 7/8" tapped holes at the center of the hemi-heads, the vessels were evacuated to about 28" Hg and filled with water. A small vent tube was then inserted into the vessel to remove any remaining air. This procedure minimized the amount of air in the vessels and thereby minimized the amount of stored energy developed during hydrotest. City water inhibited with soluble oil was used as the pressurizing fluid. Stress corrosion tests were conducted prior to the vessel tests to show that the inhibited water would not introduce a stress corrosion factor into the hydrostatic test.

Instrumentation of the vessels varied with the test. A pressure time record was made for every pressure cycle, except for fatigue precracking of the machined slots in the flawed vessels.

Pressure vs crack-opening displacement and pressure vs time were plotted for the tanks with machined slots.

Crack-opening displacement measurements were made by means of an extensometer mounted across the machined notch, on a 0.75" gage length to indicate by a shift in the trace of the load-displacement chart when precracking initiated.

Subsequently, in the proof, operational and failure pressure tests, behavior of the vessel in the vicinity of the slot was followed by interpretation of the traces from this displacement gage.

Fatigue crack extension of the machined notches in the two flawed vessels was accomplished by cyclicly pressurizing the vessels. In performing this operation, it was assumed that the cyclic rate would be relatively low due to the size of the vessels. Since it was desirable to keep the time to generate the fatigue crack to a reasonable duration, a stress intensity factor for fatigue cracking, K_f, was determined based on the K_{IC} (estimated) of the material. Because the vessel test procedures had to be finalized before all of the data was available from the weldment fracture toughness tests, K_{IC} was conservatively estimated at 133 Ksi $\sqrt{in.}$ based on the available data. The fatigue cracking stress intensity factor K_f was chosen as one-half the estimated K_{IC} value for the weld metal. Thus:

$$K_f = \frac{K_{IC}\ (\text{estimated})}{2} = \frac{133\ \text{Ksi}\sqrt{in.}}{2} = 66.5\ \text{Ksi}\sqrt{in.}$$

3.3 TEST AND INSPECTION PROCEDURES

3.3.1 MECHANICAL PROPERTY TESTS -- All mechanical property tests were performed in accordance with Federal or ASTM Specifications as follow:

a. Tensile Tests: Tensile tests were in accordance with Federal Test Standard 151, method 211.1. Specimens tested included types R1, R3 and F2. These specimens are 0.505-inch diameter, 0.252-inch diameter and 1/2-inch wide, respectively. Gage lengths are 2-inch, 1-inch and 8-inch. A 0.505-inch specimen is shown in Figure 36.

b. Charpy V-Notch Impact Tests: Impact specimens were all tested on a calibrated Riehle impact machine, in accordance with Federal Test Standard 151, method 221.1. Specimens were as shown in Figure 37.

c. Precracked Charpy Impact Tests: Precracked charpy specimen testing procedures were the same as described in paragraph b, above, except that a precrack was introduced into the specimens as shown in Figure 38 prior to testing. Loads were kept low enough during precracking to avoid the creation of large plastic zones at the tip of the precrack. Approximately 50,000 cycles were required to grow precracks from 0.039 to 0.052-inch deep in the specimens. Results of these tests are reported in terms of W/A, inch-lbs. of energy absorbed per square inch of uncracked specimen cross-section.

d. Hardness Tests: All hardness tests performed were in accordance with Federal Test Standard 151, method 243.1, Rockwell Hardness Test.

3.3.2 NONDESTRUCTIVE TESTS

a. Liquid Penetrant and Radiographic Tests: Inspection techniques and standard of acceptance were in accordance with Sections 6 and 7 of NAVSHIPS 0900-006-9010, Fabrication, Welding and Inspection of HY-80 Submarine Hulls.

b. Ultrasonic Tests: Inspection techniques and standards of acceptance for ultrasonic inspection were in accordance with NAVSHIPS 0900-006-3010, Ultrasonic Inspection Procedure and Acceptance Standards for Production and Repair Welds. An automatic weld scanning unit was used to inspect several test panels in Task III.

3.4 SUPPLEMENTARY INVESTIGATIONS AND TESTING

3.4.1 COMPARISON OF WELD FILLER WIRES -- In addition to the two principle heats of weld filler wires studied in this program, two other heats were briefly investigated.

a. Identical Chemistry Wire: The first of these, VASCO #L50898 of Table III, was drawn from coil stock swaged from 1-1/4" x 1-1/4" x 108" strips cut from the rolled plate material purchased for use in this program. One 12" x 12" x 3/4" test weldment was produced using this filler wire and subjected to nondestructive inspection for soundness. Excessive lack-of-fusion precluded any mechanical testing. This weldment is listed as #WV01 in Table VI.

b. Second Heat of 12-5-3 Wire: A second heat of 12-5-3 wire, VASCO #1686A was obtained for use in welding the girth seams of the test vessels if the supply of the original heat of 12% Ni weld wire were exhausted before all vessel welding was completed. This heat of wire was produced to the same requirements as the original heat of wire except the allowable maximum carbon content was increased from 0.01 to 0.02 percent. Two 12" x 12" x 3/4" test weldments were produced using this wire and the parameters shown in Table VI. The first of these, designated WV02 was manually GTA welded with a low interpass temperature and no auxiliary shield. This weldment exhibited excessive porosity; consequently, a second weldment, #WV02A, was produced using automatic welding and auxiliary shielding. This weldment was liquid penetrant and radiographically inspected and tested for tensile and impact properties for comparison with properties of welds made with VASCO Heat #04836.

3.4.2 FRACTURE TOUGHNESS TESTS -- Fracture toughness of the base metal plate and the welds was evaluated on the basis of notched-beam slow-bend specimens and surface flawed, tensile load specimens using fracture mechanics analytical procedures. Toughness was also evaluated on the basis of Charpy V-notch impact test results, as described in Section 3.3.1, but these results were used only in a comparative sense to rate toughness between welds.

a. Notched Bend Specimens - The notched bend specimens used in this program were 9 inches deep, 40 inches in length (36" between supports) and 0.75" in thickness. The notch, machined at the center of the bar, was 2-3/4" deep, extended by fatigue precracking to a minimum of 2-7/8".

Fatigue precracking required to provide the most acute tip to the notch was introduced by a low load (2.7 kips starting and 2.2 kips finishing) high frequency cycling (7500 - 8000 cycles per minute) in an Amsler Vibraphore. Five-six million cycles were required for 1" of crack propagation. The starting stress intensity factor for base metal specimens was about 28 KSI $\sqrt{in.}$ which was reduced at the finish to about 13 KSI $\sqrt{in.}$ The welded specimens had a starting stress intensity factor of 15.7 KSI $\sqrt{in.}$ and a finishing K_f of 13 KSI $\sqrt{in.}$ As shown in Figure 39, the specimens were machined with a chevron notch, which has a V-shape at the base of the notch. This configuration assists materially in reducing precracking incubation time and allows for load concentricity adjustments as the crack runs down the side of the V, so the final precrack extension can be made straight and uniform across the plate thickness. Despite the use of this notch design, precracking results were not completely satisfactory.

The specimens were tested in three-point loading and a plot of load vs crack-opening displacement was made on an X-Y recorder. Sixteen specimens were tested - 2 with the notch in base metal, 7 notched at the weld center, and 7 notched in the weld-heat-affected zone.

b. Surface Flawed Specimens - The surface flawed specimens were 40 inches long, about 0.80 inches thick, pulling ends 10 inches wide, and test section 6 inches wide by 12 inches long. Figure 40 shows the general shape and details of these specimens. The surface flaw was a semi-elliptical notch made by electro-discharge machining, about 2 inches long on the specimen surface, 0.5 inches maximum depth, and perpendicular to both plate thickness and longitudinal axis of the specimen.

It was then precracked or "sharpened" by low-load tension-to-tension cycling in accordance with procedures specified in ASTM E-399-70T. The maximum load varied from 48 - 60 kips average, the minimum load between 3 - 5 kips average. A total of 60,000 to 200,000 cycles at cyclic rates of 160 - 300 cycles per minute were required. K_f at completion of fatigue precracking varied for each specimen, the highest being 30 KSI $\sqrt{in.}$ and the lowest 14 KSI $\sqrt{in.}$ Results were something less than ideal since there is no way to accurately monitor crack growth, or to control its size and shape, especially in welds and heat-affected zones where variations in hardness and residual stress have an influence.

In addition to providing fracture toughness information, the surface-flawed specimens also were used to evaluate the sub-critical and environmental flaw growth characteristics of base material, weld HAZ and weld metal areas (see Sections 3.4.3 and 3.4.4 on flaw growth rate and stress corrosion studies). At the end of each sub-critical flaw growth experiment, the specimen was fractured in tension, since a critical flaw size was not attained in any of the tests. From the fracture load, stress intensity factors were calculated. The critical stress intensity at room temperature (test temperature) was not obtained due to the section thickness being much less than $2.5 \left(\frac{K_{IC}}{\sigma_{ys}}\right)^2$.

Because the environmental and cyclical testing often resulted in the "crack" extending through the specimen thickness, computation of K values for these specimens was based on the equation for center-notched specimens rather than the surface flawed condition.

Two specimens each were tested for base metal, weld metal, and heat-affected zone -- one in air and one in seawater.

3.4.3 CYCLIC FLAW GROWTH STUDY -- Stress intensification at defect boundaries can often lead to low cycle fatigue crack growth, even if the nominal stress is of reasonable magnitude. In high strength, highly stressed metals, low cycle fatigue can

cause a subcritically sized defect to attain a critical size, frequently quite small, and, as the load of the next cycle is applied, cause complete failure of the structure. For this reason, the low cycle fatigue flaw growth characteristics of 12% Ni maraging steel weldments produced with the selected optimum welding procedure were of interest in this program.

To obtain this information, three of the precracked surface-flawed specimens discussed in Section 3.4.2 were subjected to high stress, low cycle loadings prior to breakage. The fracture surfaces of these specimens were then examined and flaw growth rates determined for various load levels and stress intensities.

These three surface-flawed specimens were subjected to cyclic loading in an air environment. The first one, #W3D04-S1, had the flaw located in the base metal; the second, #W3D04-S3, in the heat-affected zone; and the third, #W3D04-S5, in the center of the weld metal. The other three remaining specimens were tested in a saltwater environment as described in Section 3.4.4. The three specimens tested in air were subjected to 100 cycles of loading for a series of increasing levels of load, and the crack growth per cycle, da/dN determined for each load level, or more precisely, for the stress intensity range at each load level. The measurements and calculations were made after the specimens were fractured, when the fatigue crack surfaces were visible.

Because of the high loads required to perform this testing, the services of the Fritz Engineering Laboratory at Lehigh University were engaged. The specimens, machined and with the EDM notch cut, were forwarded to Fritz Laboratory where fatigue precracking of the notches was accomplished in large Amsler Vibraphores. Testing was accomplished in the 5 million pound universal testing machine.

3.4.4 STRESS CORROSION TESTS -- An evaluation of the susceptibility of both base material and weld areas was included as part of the work of this program. This was done using three surface-flawed fracture toughness specimens, produced and precracked as described in Section 3.4.2. Specimens were taken from weld test panel #W3D04. The environment used was synthetic seawater.

The first of these specimens, #W3D04-S2, was notched in the base metal; the second, #W3D04-S4, was notched in weld metal at the weld centerline; and the third, #W3D04-S6, was notched in the weld heat-affected zone. Precracking was done in an air environment.

Fatigue precracking did not proceed as expected. Sub-surface growth could not be accurately followed, nor did the crack develop uniformly along the edge of the EDM notch. As a result, the crack grew through the plate thickness in Specimen No. 2, and closely approached the back side of Specimen No. 4 before cycling was terminated. The fatigue crack extension of the notch in Specimen No. 6 approached the desired geometry.

For the static stress-corrosion test, the notch was sealed with tape and the synthetic seawater corrodent introduced with a hypodermic syringe. A crack opening displacement gage was mounted across the notch on a 3/4" gage length to monitor crack growth. Crack growth vs. load was plotted with an X-Y recorder.

Preliminary experimental work by Del Research Corporation indicated a K_{ISCC} of about 50 ksi $\sqrt{in.}$ for the particular heat of metal being tested in this program, with rapid crack growth expected above this value. Each of the surface-flawed specimens was, therefore, loaded originally to produce a low K-factor, and held at load for two hours. No crack growth was observed on the X-Y recorder. In the absence of significant growth during this period, the load was increased 100 kips and effects observed for two more hours. This procedure was continued until failure due to stress corrosion was induced, or until the tensile strength of the specimen net section was attained.

At the time that preparations were being made to test the vessels of Task IV, the stress corrosion tests just described had not been performed, and the susceptibility of this material was not known. It was known, however, that it would be preferable to use water, inhibited with soluble oil for the vessel tests instead of hydraulic oil as originally proposed. Consequently, a brief stress corrosion test program was conducted to determine whether or not inhibited water could be used for the test of the vessels or if it would add a stress-corrosion variable to these tests. Because of set-up time, fatigue precracking and testing schedules, the vessels might be filled with the pressurizing fluid for a week or more -- adequate time for stress corrosion effects to show up, especially during fatigue precracking.

Notched, fatigue-precracked and side-grooved cantilever beam specimens were tested in a solution of water inhibited with soluble oil and with potassium chromate to determine whether any stress corrosion effects might occur during the vessel tests. The alternative to using inhibited water would be to use hydraulic oil as the pressurizing medium. This would require a more complicated testing circuit, and the prospect of bathing the test pit with oil in the event of a vessel bursting was not desirable.

Five specimens -- three base metal and two weld metal -- were available for this test. One base metal specimen and one weld metal specimen were broken in cantilever beam loading, in air, to determine K_Q toughness at ambient conditions.

The comparative effects of chromate and soluble oil inhibitors were tested on the two remaining base metal specimens, loaded to a nominal outer fiber stress (by simple beam formula) equal to proof pressure stress in the vessels, specifically 149,000 psi; and the second welded specimen was tested at the same stress in the soluble oil-water solution, in a go/no-go type of test.

Length of test was limited to 500 hours, as it was estimated that this would be about five times the length of time that any of the vessels would be filled with fluid and under test. If failure did not occur, the specimens were to be loaded to fracture in air and the extension of the crack, if any, due to corrosion effects would be evaluated.

The results of this test are discussed in Section 4.9.

3.4.5 ACOUSTIC EMISSION MONITORING OF HYDROTESTS -- Acoustic emission data was obtained as two edge-notched fracture toughness bend specimens were being tested and from flawed and unflawed vessels during hydrotest to failure. As stress levels increase in a load-carrying member, characteristic bursts of acoustic energy are released. These emissions can be detected with ultrasonic transducers, amplified and integrated to determine if the member is approaching a point of failure. The data taken in this program consisted of a continuous plot of the total number of emissions detected as a function of the applied load. A sharp increase in the slope of this plot indicates impending failure. A more detailed explanation of the procedures and equipment used to perform this work is presented in Appendix B. Results are discussed in general in Section 4.10 and in detail in Appendix B.

4.0 RESULTS AND DISCUSSION

4.1 TASK I - LITERATURE REVIEW

A summary of the results obtained from the review of literature is presented as Appendix A of this report. Areas discussed include melting and production of base plate material, structure and strengthening mechanisms, aging response, the effects of residual elements, weld filler wire production and processing, and welding characteristics. In addition, machining and grinding information and typical physical and mechanical property data are presented.

4.2 TASK II - MATERIAL CHARACTERIZATION STUDY

4.2.1 INITIAL BASE MATERIAL HEAT TREAT STUDY -- The mechanical property and metallurgical test results of the first part of the base material heat treat study are summarized in Table X and Figures 42 through 51. Data in Figure 42 shows that for a yield strength of 180,000 psi or greater, the maximum longitudinal CVN toughness, 117 ft.-lbs., was obtained from specimens solution-annealed at 1650°F and aged 950°F for 4 hours. This heat treatment was not selected as optimum, however, since the rate at which impact energy diminished as aging times were extended to 16 and 30 hours was also greatest with a 1650°F solution annealing treatment.

Aging material solution annealed at 1650°F for 30 hours at 950°F produced CVN impact test results of only 65 ft.-lbs., the lowest value obtained from any of the specimens tested. Considering that an optimum heat treatment for weldments had not yet been determined, this sharp drop-off was a potentially serious problem and made the selection of a 1650°F solution annealing temperature undesirable. Another reason for not selecting 1650°F as a solution annealing temperature was that even for short aging times, it was superior to 1550°F only when a 950°F aging temperature was used. A 950°F aging treatment is more likely to result in austenite reversion if applied to weldments than a lower temperature aging treatment. Since austenite reversion degrades properties, it was desirable to avoid 950°F as an aging temperature. When material was solution annealed at 1650°F and aged at 900°F, strength/toughness relations were slightly inferior to those obtained from material aged in the same manner but solution annealed at 1550°F.

The use of a 1550°F solution annealing treatment followed by aging at 900°F for 8 hours produced one of the best combinations of strength and toughness properties obtained from any of the test plates, i.e. 190,000 psi yield strength and average Charpy V-notch energy absorptions of 102 ft.-lbs. at 72°F.

Since solution annealing at 1600°F was not observed to result in more than a minor decrease in properties, a temperature of 1575°F was selected for use in mill solution annealing. Variations of as much as ±25°F could then occur in mill heat treating and the actual solution annealing temperature range would still be within limits proven to produce good properties. The material was air cooled following solution annealing.

The optimum aging treatment for the selected 1575°F solution anneal was 900°F for 8 hours followed by air cooling.

Each of these test plates was carefully ultrasonically inspected for laminations prior to heat treating. No such defects were found.

Figure 43 shows good correlation existed between the results of standard Charpy V-notch impact test specimens and those which were precracked prior to testing. For example, precracked Charpy V-notch toughness values of specimens removed from a plate heat treated at 1650/950°F for 30 hours were 46% lower than those aged for only 4 hours, with standard Charpy V-notch specimens showing a 43% decrease.

As shown in Figure 44, all of the combinations of solution annealing and aging temperatures studied resulted in increased strengths for all increased aging times.

The results of surface-to-surface Rc hardness traverses on these samples are presented in Figures 45 through 47. No variations of more than 3 points were observed for any specimen. The total range for all specimens was Rc42 to Rc48, and midthickness values are typically the same as for near-surface areas.

Microstructures of base material subjected to several combinations of solution annealing and aging temperatures are shown in Figures 48 through 51.

4.2.2 EVALUATION OF MILL SOLUTION ANNEALED PLATE -- Following receipt of the mill-solution-annealed master plate, mechanical property tests were performed as described in Section 3.2.2 of this report. The results of these tests are presented in Table XI and a transverse Charpy V-notch impact energy temperature transition curve is presented in Figure 52. The shelf-energy transition temperature for this material, aged at 900°F for 8 hours, can be seen to be approximately 0°F. Fracture toughness test results are discussed in detail in Section 4.7.

The mill-solution-annealed material did not exhibit properties equivalent to those obtained from the initial heat treat study test plates. Whereas the mill-solution-annealed material had an 80°F transverse CVN toughness of approximately 50 ft.-lbs. with a yield strength of 190,000 psi, test plate 1A-13 of the preceeding initial heat treat study exhibited equal strength and significantly better toughness, approximately 64 ft.-lbs. Although this difference in properties cannot be readily explained, it is most likely due to the fact that the specified mill solution anneal included an air cool. The small test plates of the initial heat treat study had also been air cooled but the larger mass of the master plate would cool more slowly.

A water quench would most likely have produced improved properties.

4.3 TASK III - WELDING PROCEDURE DEVELOPMENT

4.3.1 BEAD-ON-PLATE STUDIES -- The bead-on-plate studies indicated a number of combinations of welding current levels, arc voltages, travel speeds, wire feed rates and shielding gases could produce beads of good appearance with no obvious evidence of porosity or cracking. These test beads did show an accute sensitivity to the presence of rust, however, when the test plates were not ground completely clean and smooth. Weld porosity was the most noticeable effect.

Based on the results of these test beads, a number of different combinations of welding parameters appeared suitable for further development through the production of initial test weldments. The selected combinations are as shown in Table VI.

These combinations included the following:

Welding currents from 160 to 280 amperes
Use of helium and argon as shielding gases
High and low travel speeds
Several different weld filler wires
60° and 40° weld joint openings
High and low weld heat input energies
Use and non-use of auxiliary shielding
Various interpass temperatures
Various interpass cleaning techniques

4.3.2 PRODUCTION OF INITIAL 12" x 12" WELDMENTS -- The results of mechanical property tests performed on each of the twelve weldments listed in Table VI are summarized in Table XII and Figure 53. It can be seen in Figure 53 that the weldments exhibiting superior properties were W3B071, W3B051, W3B30, W3B33, W1A15, and, in particular, W3B31 and W3B27. Figures 54 and 55 show cross sections typical of these latter two weldments. The

following is an analysis of the results of the work of this Task based on data shown in Tables VI and XII and Figure 53:

a. Weld Joint Design. All of the single-"U" weld joint designs used to produce these welds appeared to provide adequate access for welding, and consequently, it was assumed that double "U" joints of the same root radius and included angles could be used with satisfactory results for the larger test panels and vessels. The use of single-"U" joints on these 12" x 12" plates made it easier to accurately evaluate all-weld-metal tensile properties, but double-"U" joints were preferable for vessel fabrication in order to minimize welding distortion effects.

b. Bead Size. The wire feed speed-to-travel speed ratio of four-to-one used to produce these weldments gave small, stringer-type weld beads which were not difficult for the welding operator to control and of finer grained than larger beads. Since no problems were encountered as a result of the use of this wire feed/travel speed ratio, and since the number of plates which could be produced and tested to determine the effects of various welding parameters was limited, this ratio was selected for use in the remainder of this program.

c. Filler Wire Composition. Both of the principle wires investigated in this program, nominally 12 and 17% Ni, proved capable of producing welds with 0.2% offset yield strengths greater than 180,000 psi and Charpy V-notch impact energies in excess of 50 ft.-lbs. at room temperature. Neither wire was clearly superior to the other. When deposited and heat treated in a manner similar to the 17% Ni wire, the 12% Ni wire produced welds of greater toughness but lesser strength. This can be seen by comparing weldment W3B31 to W3B27. It appeared from these results, however, that if these two wires were deposited under optimum conditions in separate welds, and the welds aged with optimum heat treatments to the same strength level, the toughness of the two welds would be the same. This observation was confirmed by data obtained from subsequent tests of larger weldments.

d. Weld Soundness. Both wires produced welds which were sound and free of cracks. Some fine porosity was observed in weldments W3B021, W3B29, W3B30, and W3B33, but not more than 8 pores were observed in any 6 inches of weld and none of these were larger than 1/64-inch in diameter.

e. Weld Metal Dilution. Based on a comparison of weldments W1A15 and W3B07-1, the 17% Ni weld wire was not dependent upon base metal dilution for strength, and the use of wide weld joint openings, if necessary, would not be detrimental in this respect. The 12% Ni filler wire was not similarly investigated since it was essentially of a composition matching the base material.

f. Auxiliary Shielding. Weldment W3B07-1 was produced primarily for comparison with W3B27 to determine whether or not the use of an auxiliary trailing shield would improve 17% Ni weld metal properties. Based on test results from these weldments, the use of auxiliary shielding did not appear to be beneficial in improving weld toughness. It did appear, however, to produce cleaner weld surfaces which were less likely to result in lack-of-fusion defects. Studies of the effects of an auxiliary trailing shield on 12% Ni weld metal properties were conducted on subsequent 40-inch wide test panels.

g. Interpass Cleaning. Based on the results of tests of weldment W3B27, burring or wire brushing the surface of beads prior to depositing subsequent beads did not appear to improve weld toughness. Wire brushing and burring or grinding to remove glass-like oxides which occasionally formed on the weld surface did contribute to the elimination of lack-of-fusion defects.

h. Travel Speed - Operator Limitations. The use of a 10-ipm travel speed, as for weldment W3B33, was found unsatisfactory in that it was too fast and the welding operator was not able to make necessary torch position adjustments during welding. Lack-of-fusion defects resulted.

i. Helium vs Argon Shielding Gas. As shown by the results of W3B30 and W3B38, the use of helium as a shielding gas produced properties at least equivalent to those obtained when argon was used. In this particular instance the weldment made with helium exhibited slightly better properties. These weldments were slightly different in other respects, however, and these differences could have contributed to the difference in properties. Since it was economically desirable to use argon if no degradation of properties would result, it was decided to further investigate the possible differences between these two shielding gases on a subsequent 40-inch wide panel.

j. Interpass Temperature. The effect of interpass temperature on the strength and Charpy toughness of welds made with 12% Ni filler wire is indicated by the differences in test results from weldments W3B05-1 and W3B31.

The welding procedures and aging treatments used to produce these weldments were identical except for interpass temperature. The 100°F higher interpass temperature of W3B05-1 produced an increase in yield strength of 4 ksi and a decrease in average 72°F Charpy toughness of 8 ft.-lbs. This decrease in toughness with increased yield strength was slightly more pronounced, but generally consistent with that observed for all weldments exhibiting maximum toughness at various yield strength levels. The general relationship observed between strength and toughness for such weldments is shown as "Line A" of Figure 53. Since the rate at which toughness decreased with increases in yield strength for these two weldments was only slightly greater than the relation shown by Line A, the effect of interpass temperature on overall weld strength/toughness relationships, could not be determined conclusively. A low interpass temperature did appear, however, to result in slightly better properties.

The effect of changes in weld preheat temperature would be the same as described for interpass temperature.

k. Weld Metal Aging Response. The response of 12% Ni weld metal to variations in aging time and temperature was briefly investigated. The purpose of this was to allow an aging treatment to be selected for the next set of test weldments which, although not intended to be optimum, would at least be close to optimum. A comparison of results obtained from weldments W3B02-2 and W3B11 indicated that the application of a 900°F aging temperature for 12 hours instead of 8 hours degraded strength/toughness combinations to a limited extent.

Strength and Charpy toughness changes for these two weldments were not consistent with the general relationship shown by Line A of Figure 53. The 10 ft.-lb. decrease in toughness for an increase in yield strength of 2,300 psi was greater than expected and, therefore, it was assumed the use of a 12 hour aging time was detrimental to properties. A comparison of the results of W3B02-1 with W3B31 similarly indicated the use of a 950°F/8 hour treatment was inferior to 900°F/8 hours.

l. Weld Heat Input Energy. The results from tests of weldments W3B03 and W3B30 were used to estimate the effect of weld heat input energy on weld metal strength and toughness. Before the results of these weldments could be compared, however, adjustments had to be made to compensate for the longer 12-hour aging time of W3B03. These

adjustments were based on a comparison of the results from weldments W3B02-2 and W3B31, previously discussed in the preceeding paragraph k. These results indicated the use of a 900°F aging treatment for 12 instead of 8 hours produced a yield strength increase of 2,300 psi and a 10 ft.-lb. decrease in Charpy impact energy. Consequently, it was assumed that the yield strength and Charpy toughness of W3B03 would have been 2,300 psi lower and 10 ft.-lbs. higher, respectively, if this weldment had been aged for only 8 hours.

Based on this assumption, the use of a low weld heat input energy appeared to provide a yield strength increase of approximately 2,500 psi with only a one ft.-lb. decrease in Charpy impact energy. This decrease is approximately 3 ft.-lbs. per 2,500 psi less than for the relationship shown by Line A in Figure 53, indicating the use of a low heat input energy improves 12% Ni weld metal strength/Charpy toughness relationships as well as increasing yield strength. Further tests on 40-inch-wide panels confirmed this observation.

There are two reasons for weld yield strength to decrease as heat input energies are increased. First, increasing heat input energy causes the weld heat-affected-zone to increase in size, with a greater volume of material being exposed to the 1100-1300°F temperature range where austenite reversion occurs. Second, the volume of material subjected to temperatures in excess of 2000°F in the weld heat-affected-zone is principally a function of heat input energy. Therefore, higher weld heat input energies will result in more extensive grain coarsening and yield strength losses. Tensile strength losses do not result from such grain coarsening. The fact that welds made with high heat input energies exhibited nearly the same ultimate tensile strengths as those made with low heat inputs indicates yield strength losses due to austenite reversion effects are relatively minor compared to decreases in yield strength occurring in grain-coarsened areas.

m. Weld Travel Speed. The effect of weld travel speed appears to be quite significant when test results from weldment W3B38 are compared to W3B31. Except for travel speed, all of the differences between the welding techniques used to produce these weldments were such that an improvement would be expected in the properties of W3B38. Instead, a degradation of properties was observed - mostly as a loss of Charpy toughness. This is felt to have resulted from the faster travel speed used in welding W3B38. Studies[6] have shown that changes in travel speed can significantly affect weld properties by altering weld metal solidification patterns.

The fact that weldment W3B33, welded at 10 ipm, exhibited mechanical properties superior to those of W3B38 indicates that the effect of increases in travel speed may not be as strong as suggested by a comparison of the results of W3B31 with W3B38. The results from W3B38 are not felt, however, to indicate this effect does not exist. The welding current used to produce W3B33 was much higher than that used to produce W3B38, and the effect of such an increase could be opposite to the effect of a travel speed increase.

n. All Weld vs Transverse Yield Strength. As shown by the data in Table XII and Figure 53, transverse 0.505-inch tensile specimens gave higher apparent yield strength values than all-weld specimens from the same weldments. This is not unusual but is sometimes overlooked when weldments are being compared for toughness at a given strength level.

Based on the results from these 12" x 12" weldments, six different welding procedures were selected for further development through the fabrication of 40" x 40" weld test panels.

4.3.3 PRODUCTION OF 40" x 40" TEST PANELS -- The results of mechanical property tests of the six 40" x 40" weldments of Table VII are summarized in Table XIII and Figure 56. Macro cross-sections through each weldment are shown in Figures 57 through 64. Fracture toughness test results are discussed in Section 4.7.

Two weldments, W3C03 and W3C04, can be seen to exhibit the best properties. These weldments were produced using a low heat input energy, low interpass temperature and auxiliary shielding. 12% Ni filler wire was used to produce W3C03 and 17% Ni wire was used to produce W3C04. Both of these weldments had yield strengths in excess of 180,000 psi and 72°F Charpy V-notch impact energies greater than 50 ft.-lbs. The fracture toughness of these weldments was excellent. Figures 65 and 66 show broken bend specimens from each weldment, and cross sections through the fracture path. The fractures were fully of a shear mode, with very distinct 45° angles of failure. No preferential paths of fracture propagation are evident.

The remaining four panels exhibited fairly good mechanical properties but were found to contain areas of lack-of-fusion. These panels were W3C02, W3C06 and, especially, W3C09. Figure 64 shows a cross section through the worst area of W3C09. This panel was of such poor quality that no mechanical property tests were performed.

Instead, an additional panel was fabricated using a wider weld joint included angle, a higher arc voltage and a 6 ipm weld travel speed with a higher heat input energy. This panel was fabricated

to determine how effectively these changes would eliminate lack-of-fusion defects and what effect they would have on weldment mechanical properties. An analysis of the results from this panel and the six previously fabricated panels indicated the following:

a. Weld Joint Design. Based on observations made during panel fabrication, the use of a 60-degree weld joint included angle was preferable to the 40-degree angle used in most of the preceeding studies. This was primarily because of difficulties encountered in depositing the first few weld beads in the back-ground side of the joint. The included angle of the back-ground joint was substantially less than 40-degrees and torch access was considerably restricted. This was quite likely a major cause of lack-of-fusion defects.

b. Filler Wire Composition. As previously indicated by test results from the 12" x 12" initial weldments, test results from weldments W3C03 and W3C04 showed that both the 12% Ni and 17% Ni weld filler wires provided high quality welds with excellent mechanical properties. In addition, these results confirmed that these two wires produced welds of equal toughness when deposited and aged under identical conditions selected to produce weldments of equal yield strengths of approximately 180,000 psi.

c. Weld Soundness. Except for the previously mentioned problem of lack-of-fusion, no difficulties were encountered in obtaining welds of good soundness. No cracks were found in these panels by either x-ray or ultrasonic inspection.

d. Auxiliary Shielding. Test results indicated the mechanical properties of W3C09A were not as good as those of panel W3C03. One possible reason for this difference was that no auxiliary trailing shield was used when W3C09A was produced. There were other possible reasons, however, since W3C09A had been welded with a wider weld joint included angle, a slightly higher weld heat input energy and a somewhat lower interpass temperature than W3C03. Because the use of an auxiliary trailing shield possibly could have been the reason for the difference in the properties of W3C03 and W3C09A, and since it was not shown to result in property degradations but was, however, shown to result in the production of cleaner welds, less likely to contain lack-of-fusion, it was decided to use the auxiliary shield to produce all of the remaining weldments of this program. When the results of W3C09A were compared to results from subsequent 40" x 60" test panels the effect of weld heat

input energy appeared to have been the more likely reason for the property difference between W3C09A and W3C03. This would indicate the use of the auxiliary trailing shield did not improve weld properties significantly.

e. Helium vs Argon Shielding Gas. The only 40-inch wide panel welded with helium used as a weld shielding gas was W3C06. Panel W3C08, which was welded with the same weld joint design and interpass temperature, and a slightly higher heat input energy, exhibited slightly superior weld properties. Consequently, it was concluded that argon was preferable to helium as a shielding gas since it was less costly and produced welds of at least equivalent quality.

f. Arc Voltage. The extensive amount of lack-of-fusion contained in panel W3C09 was due to several factors. One of these was that the arc voltage used to weld this panel was too low. This resulted in insufficient arc heating of the outer edges of the molten weld puddle, and make it more likely that this area would solidify before melting into crevice areas. This effect would be most pronounced if travel speeds were slow and heat inputs high, since the weld puddle would be wider and the outer edges of the molten weld puddle further away from the arc. It was concluded that when argon is used as a shielding gas and welding parameters are approximately the same as used to produce W3C03, the minimum arc voltage should be 10 volts.

g. Weld Heat Input Energy. The results from these 40" x 40" test panels were not adequate to establish the influence of weld heat input energy on weld properties any more conclusively than previously determined on the basis of results from tests of the initial 12" x 12" weldments. The conclusions reached on the basis of results from these 12" x 12" weldments were further substantiated, however, when the results of these 40-inch panels were later compared to test results of subsequent 40" x 60" panels, especially W3D03.

h. Weld Travel Speed. Except for weld travel speed, the welding parameters used to produce panels W3C09 and W3C03 were quite similar. The fact that W3C09 exhibited extensive lack-of-fusion while W3C03 did not indicate the use of a 6 ipm travel speed was beneficial in eliminating lack-of-fusion defects. Although this probably is the case only where arc voltage is too low, as previously discussed in paragraph f, a 6 ipm weld travel speed was concluded to be desirable for use in all subsequent welding of this program since it would contribute to ensuring the attainment of good weld soundness.

Two additional considerations also made the use of a 6 ipm travel speed desirable. First, all of the 40" x 40" panel welds tested for fracture toughness using edge-notched bend specimens had been welded with a travel speed of 6 ipm or faster. The panel welded with a 4 1/2 ipm travel speed contained too many defects and, therefore, could not be tested. As indicated in Section 4.7 of this report, all of the welds tested exhibited excellent fracture toughness, especially W3C03. Consequently, since the use of a 6 ipm travel speed had been proven to produce welds of excellent toughness, it was decided that any attempt to obtain additional toughness through the selection of a 4 1/2 ipm weld travel speed for use in the remainder of this program could not be justified. Secondly, an additional advantage to the use of a 6 ipm travel speed was that wire feed speeds, and consequently weld metal deposition rates, were approximately 33% greater. This is a significant economic benefit.

Based on test results from these 40" x 40" test panels and from the initial 12" x 12" weldments, the optimum welding procedure shown in Table VIII was selected for use in producing the final weld test panels and five test vessels of this program.

4.3.4 PRODUCTION OF 40" x 60" TEST PANELS -- Four 40" x 60" test panels were fabricated using the selected optimum welding procedure shown in Table VIII. The results of mechanical property and nondestructive tests performed on these panels are as follows:

a. Aging Study Panel. The results of mechanical property tests conducted on the twelve samples of panel W3D01 subjected to various aging treatments are shown in Table XIV and Figure 67. Sample W3D01F, aged at 900°F for eight hours was considered to exhibit the best strength/toughness characteristics at minimum weld yield strength levels of approximately 180,000 psi. The advantages of aging the as-deposited 12% Ni weld metal at 900°F are clearly shown in Figure 67. No sharp drop in toughness occurs at increased strength levels, and there is no evidence of susceptibility to overaging. In addition, for any choosen strength level, the toughness produced by a 900°F aging treatment exceeds that resulting from either 850 or 950°F. Also, the difference in strength between weld and base material subjected to the selected optimum aging treatment was no greater than for any of the other aging treatments.

b. Optimum Weld Panel. The second test panel fabricated and tested was W3D03, produced to be representative of an unrepaired weldment containing no defects and made using the selected optimum welding procedure. The results of mechanical property tests and photographs of test specimens are shown in Table XV and Figures 68 through 71. The results of the fracture toughness bend tests are discussed in Section 4.7 of this report.

Weld metal yield strength and Charpy V-notch impact test results from this panel are compared in Figure 68 with results published by the U. S. Naval Research Laboratory of similar tests of 12% Ni maraging steel and also other high-strength steels. This comparison shows the results from panel W3D03 are close to the technological limit proposed by NRL while the work of this program was underway.

By comparing the curves shown in Figure 69 to the one in Figure 52, low temperature impact properties of the weldment can be seen to exceed those of the base metal in the transverse direction. No sharp drop-off occurs and 20 ft.-lbs. impact energy is absorbed at -120°F. Base metal values were approximately 12 ft.-lbs. at this temperature.

The lower strength of the weld metal as compared to weld HAZ areas or base metal is apparent from Figure 70. The 45° shear angle and ductile nature of the fracture can also be seen in this photograph. The fracture surfaces are shown in Figure 71.

Although this weldment did not exhibit a yield strength of 180,000 psi, such strength level could have been attained through the use of a slightly longer aging time. Based on the aging response shown in Figure 67, aging for twelve hours instead of eight would have resulted in weld yield strengths of 180,000 psi and 50 ft.-lbs. CVN impact energy.

c. Weld Repair Study Panel. The results of mechanical property tests of panel W3D02 are summarized in Table XV and Figure 69. Photographs of test specimens from this panel are shown in Figures 70 and 71. This panel was x-ray inspected after it was initially welded and after each repair cycle. The repair welding was not observed to produce porosity, cracks, or any other type of defects.

The strength and toughness of repaired areas of this panel were found to be equivalent to unrepaired areas of panel W3D03, and no decrease in weld soundness or

quality was apparent. The fracture characteristics were also similar, as discussed in Section 4.7 of this report. No measurable differences were detected in the fracture toughnesses of repaired and unrepaired welds.

A comparison of the metallurgical characteristics of repaired and unrepaired weld areas shown in Figure 72 does not indicate any significant differences except for the greater width of the repaired area and the more irregular heat-affected zone pattern. Figure 73 shows etched Charpy test bars prior to testing. The difference in weld HAZ patterns is quite obvious.

d. Surface Flaw Test Panel. The six surface flaw test specimens removed from panel W3D04 were of such a size that the entire panel was required for these specimens. Consequently, no other specimens could be removed and tested. The six specimens tested exhibited exceptionally good strength and toughness, and a lower sensitivity to stress corrosion effects than expected. Stress intensity factors for fracture loads in air for these specimens ranged from 273 to 305 ksi $\sqrt{in.}$ The procedures used in testing these specimens were previously discussed in Section 3.4 of this report. The results of the testing are described and discussed in detail in Sections 4.7, 4.8 and 4.9.

4.4 VESSEL FABRICATION

Each of the five test vessels of this program was fabricated as shown in the flow chart of Figure 33. This was accomplished as follows:

4.4.1 FORMING AND MACHINING VESSEL CYLINDER SECTIONS -- The cylindrical section of each vessel was produced by joining two brake-formed cylinder sections together with two longitudinal seam welds. Each cylinder section was formed from unaged 3/4" thick plate, with the major direction of rolling in the circumferential direction. Roll forming was attempted as a method of manufacture but was unsuccessful due to the high yield strength of the material, approximately 115,000 psi even in the solution annealed and unaged condition. The cylinder sections were plasma trimmed following forming and the longitudinal weld joint preparations were then machined.

4.4.2 WELDING AND GIRTH MACHINING OF CYLINDER SECTIONS -- The weld joint design used for the longitudinal seams of the test vessels is shown in Figure 31 and Table VIII, which summarizes the welding procedure selected for use in vessel fabrication.

The weld filler wire selected for use was 12% Ni. This wire had been found to produce welds of excellent strength and toughness, at least equivalent to an possibly slightly better than the strength and toughness of welds made with the 17% Ni filler, which were also excellent.

Figure 74 shows the equipment set-up used to weld the longitudinal seams of all five cylinder sections. An automatic arc-voltage-controlled welding head was mounted on the end of a boom manipulator, which provided linear motorized travel along the full length of the seam.

All longitudinal seams were liquid penetrant, x-ray and ultrasonically inspected after completion. Some porosity and lack-of-fusion was left in several welds to verify that, because of the good toughness of the welds, such defects would not affect vessel performance. No cracks were detected. Maximum radial out-of-roundness of the finished cylindrical section was ± 1/16 inch, except for the intentionally mismatched vessel.

Following the completion of welding, the ends of each cylinderical section were plasma trimmed and the girth joint weld preparations machined as previously shown in Figure 31.

4.4.3 HEMISPHERE FORMING AND MACHINING -- Concurrent with cylinder section fabrication, forming and machining of the hemispherical end-closure heads was being accomplished. Ten unaged but solution annealed 54" x 54" blanks were plasma cut from 1-1/8" thick flat plate and hot spun into hemispheres by Phoenix Products Company of Milwaukee, Wisconsin. Forming temperatures were between 1500°F and 1800°F.

Following forming, the heads were solution annealed at 1500°F and air cooled. They were then shipped to the Electric Boat division where the weld joint preparations for the penetration insert pieces and girth joint, previously shown in Figures 31 and 32, were machined.

Data on the thickness and out-of-roundness of the as-received hemispheres is presented in Table XVI.

4.4.4 PIPING PENETRATION REINFORCEMENTS -- The piping penetration reinforcements shown in Figures 32 and 75 were produced by plasma cutting ten 4-inch diameter discs from 1-1/8" flat plate stock, applying a 17% Ni GTA weld overlay to increase the disc thickness to 1-3/4" and finish machining to the dimensions shown in Figure 32. The reinforcements were then GTA welded into heads as shown in Figures 75 and 76 using 17% Ni filler wire.

The welds were liquid penetrant and x-ray inspected. In two instances, lack-of-fusion defects were found which exceeded 1/2-inch in length. These defects were ground out and repaired. No other repairs were performed although several other areas of lack-of-fusion were detected. These areas were less than 1/4-inch long. No cracks were detected in these welds.

4.4.5 WELDING OF HEADS TO CYLINDER SECTIONS -- The two heads attached to the cylinder section of each vessel, each required somewhat different procedures. The first head presented no difficulties since the weld joint design and parameters were very much the same as used in the selected optimum procedure and there was easy access to both sides of the joint. These welds were made from the outside, background and a backing pass deposited to fill the background area. The welds were then liquid penetrant and x-ray inspected for soundness. None of the welds were found to contain defects greater than 1/4" in length. No repairs were made since all of these defects were lack-of-fusion and less than critical flaw size.

In attaching the second, or closure head, it was necessary to complete the welding operation entirely from the outside of the vessel. This was necessary since the vessels were designed to avoid the use of a bolted access cover plate. This simplified the procurement of material and eliminated a considerable amount of machining. These advantages were felt to outweigh the problems involved in making one-side access weld.

During actual vessel fabrication these welds did not prove to be any more difficult to make than expected. However, special techniques were used. These techniques, developed and used by the Electric Boat division to weld heavy wall piping systems, included the utilization of an Electric Boat division patented-design consumable weld insert and a patented surge-arc low frequency plused-arc GTA welding power supply.

Figure 77 shows the end of a cylinder section as prepared for joining to a closure head. Note the consumable insert tack welded along the entire length of the girth joint land.

The finished contour shown in the inside view is typical of that used on all longitudinal seam welds. Figure 78 illustrates the typical method by which the first and closure heads were aligned and fitted to the cylinder sections of the vessels. Typical closure weld underbead contours and penetrations are shown in Figure 79.

The only problem encountered in joining the heads and cylinder sections of these vessels was the detection of a network of base metal cracks in Vessel "E". These cracks are not at all connected with welding and were apparently introduced into the base material

during mill conversion into plate. The cracks were in an area of material at the edge and corner areas of the master plate. Figure 80 shows the general size and locations of cracks in the vessel. These cracks were ground out and repair welded. A cross section through a specimen cut out from a cracked area is shown in Figure 81.

4.4.6 AGING OF VESSELS -- The five vessels were each aged at 900°F for 8 hours and air cooled. This work was performed by CPC Engineering Corp., Sturbridge, Massachusetts.

Temperature was maintained ± 15°F and averaged 900°F. Thermocouples were attached to the vessels at the ends and at mid-length of the longitudinal seams. Weld build-up pads were used as attachment points for those thermocouples attached to the longitudinal seams. Except for one pad on Vessel "B", these pads were ground-off prior to hydrotest.

4.4.7 EDM OF ARTIFICIAL FLAWS -- Following aging, artificial flaws were electro-discharge machined into vessels "A" and "D". Figure 82 shows actual flaw shapes and details. These flaws were similar to those in the surface flaw specimens. Tri-D Corporation of Plainville, Connecticut performed this work. Electro-discharge machining these flaws into these two vessels completed all aspects of work related to vessel fabrication.

4.5 VESSEL HYDROTESTS

Pertinent data for each vessel tested is given in Table XVII. A discussion of each vessel test follows:

4.5.1 VESSEL "A" -- This was the first of the intentionally flawed vessels.

A semi-elliptical slot, major axis parallel to the vessel axis, was cut by electro-discharge machining into one of the longitudinal seam welds at its transverse and longitudinal center. The slot was "sharpened" by low cycle, high strain fatigue cracking. It had originally been proposed that following the test at proof pressure, these flawed vessels would be cycled to operating pressure 100 times to see if the crack would propagate through the wall, or enlarge to a critical size at which the tank would rupture. However, the fatigue precrack of this vessel was extended to too great a depth and the vessel developed a leak at the flaw at 5600 psi pressure, 900 psi below operating pressure. Figure 83 shows this vessel at a pressure of approximately 1500 psi after developing this leak.

This test was monitored with a displacement gage mounted across the "crack", and a pressure-displacement chart was constructed as the test proceeded. At 3900 psi, an over-pressure alarm which had been set for the fatigue precracking, and which had not been disconnected, came on.

The test was interrupted at this point to disconnect the alarm, but pressure was maintained on the system. About 0.001-in. of crack-opening displacement (C.O.D.) took place during this 5-10 minute hold, indicating post-yield stresses acting at the tip of the crack, and probably throughout the ligament from crack tip to vessel I.D. The pressure-C.O.D. trace indicated onset of yielding at 3600 psi by deviation of the trace from linearity at this pressure.

The curve indicated two points of rapid crack extension (similar to, if not actually, pop-ins) at 4500 psi and 4800 psi. Through-cracking occurred very abruptly, as the curve became horizontal at 5600 psi, and the C.O.D. component increased, 0.055". The crack appears to have then closed up to within 0.007-in. of its original width, probably due to rotation of the vessel walls adjacent to the crack, as shown below:

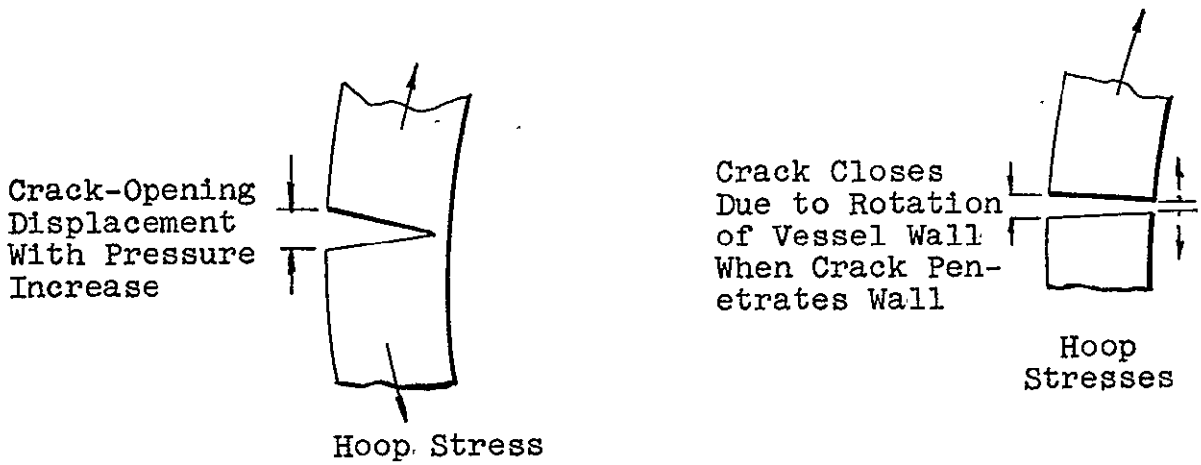

4.5.2 VESSEL "B" -- This was one of two vessels fabricated without defects beyond the extent permitted by specification and sensitivity of the nondestructive test methods employed. Also, it was the first vessel to be tested in this program. The test cycle consisted of:

a. Pressurized to 7320 psi (proof pressure), hold 5 minutes and depressurize to 660 psi.

b. Pressurized to 6650 psi (operating pressure), hold 1 minute and depressurize to 660 psi. Repeat 4 times.

c. Pressurize to burst. (Burst pressure was 10,400 psi.)

Proof and operating pressures used for this test were 110 and 100 psi too high, respectively. These pressures were based on a 33" vessel inside diameter. For all subsequent tests, pressures used were calculated on the basis of a more accurate 32.6-inch value.

Figures 84 through 88 show this vessel after burst failure. The vessel was not under visual observation during pressurization, since it was enclosed with 1/4" steel plate to retain the water when it failed. However, no unusual indications were noted from the instrumentation, either the pressure-time chart or the acoustic emission monitor, which was used on this test.

Fracture in the burst test occurred at the fusion line of the seam weld designated No. 1 at the time of vessel fabrication. There were no indications of a flaw which might have triggered ultimate failure. There was a noticeable bulge at the ruptured seam, about twelve inches from the junction with a hemi-head, and it appears that fracture originated at this location. The fracture path was typical of failure in vessels of similar configuration and of tough material. It traversed the length of the seam weld, then turned 180° after running into the hemispherical heads.

On one end, the crack propagated straight across the girth weld into the head. On the other end, the crack divided -- one branch going into the base metal of the head, and the other branch following the fusion line of the circumferential butt weld about half way around the tank. Another circumferential crack, about 10" long, developed about 12" from the other end of the cylinder from which the fracture apparently initiated. Fracture was full shear type, including the circumferential branches from the longitudinal fracture. No distortion or deformation could be observed in the second seam weld, 180° from the fractured weld.

4.5.3 VESSEL "C" -- This vessel was constructed with a radial mismatch in one seam weld calculated to produce yield stress at proof pressure. Assuming membrane and bending stresses to be additive in the mismatched weld:

$$\sigma_{yield} = \sigma_{membrane} + \sigma_{bending}$$

or:

$$\sigma_{yield} = \frac{PR}{t} + \frac{3\Delta}{t^2} PR$$

where Δ is the mismatch in inches.

When the appropriate values were placed in the above equation, Δ was found to be 0.0665".

Consideration of previous testing of vessels with mismatched welds indicated the maximum mismatch to produce yield stress at proof pressure was close to 10% of the wall thickness -- in the present case, about 0.08". This was the aim in fabrication. The actual average mismatch over the center third of the cylinder part of the tank was 0.067", or equal to the value calculated with the above equation.

This vessel was subjected to a proof pressure test of 7210 psi, followed by five cycles to operating pressure of 6550 psi, and finally to burst pressure.

The vessel burst at 10,250 psi at the fusion line of the mismatched weld. Figure 89 shows the vessel in the test cell after burst. The fracture was completely of a shearing nature, emerging on the vessel surface at the low side of the mismatch for about five-sixths of the length of the cylinder. This part of the fracture was on the shortest shear plane through the weld. For about 10" at that end of the vessel designated "0", the fracture was through the longer shear plane from the high side of the mismatch on the O.D. to the low side on the I.D. The precise origin of failure was not evident on the fracture surface.

The extensive damage done to the test pit as shown in Figure 89 and the fact that the vessel escaped from the restraining fixture and traveled more than 15 feet in the air while more than 1/2 full of water, both demonstrate the danger involved in high pressure hydrotests of pressure vessels such as these. Despite the fact that water was used as the pressurizing fluid, the energy stored in the vessels when pressurizing to 10,000 psi is about one million ft.-lbs.(7)

If oil had been used, the stored energy would have been approximately 50% greater and air would have been more than 200 times greater.

Throughout the hydrotest portion of this program no personnel were permitted in any possible danger areas and a minimum of equipment was located in the test pit with the vessel.

4.5.4 VESSEL "D" -- Vessel "D" was the second vessel to be tested which contained an intentionally-introduced flaw in one longitudinal seam. Fatigue precracking was stopped about 175 cycles after the presence of a crack was detected at a total of 401 cycles of pressure ranging between 340 and 3400 psi. K_f maximum was 100 ksi $\sqrt{in.}$, and nominal hoop stress was 68,000 psi.

The hydrotest sequence for this vessel was:

Proof pressure - 7210 psi, hold 5 minutes and depressurize to 650 psi.

Operating pressure - 6550 psi, hold 1 minute and depressurize to 650 psi. Repeat 4 times.

Maximum pressure - 7150 psi, leak through flaw.

As with Vessel "A", a displacement gage was mounted across the artificial flaw on the vessel surface, using a gage length of 0.75". While monitoring the displacement-pressure cycle during fatigue precracking operation, an indication of precrack initiation was observed at cycle No. 226. At about 300 cycles, the fatigue crack could be seen at the root of the EDM notch by use of a binocular microscope. Cycling was terminated at 401 cycles. At this point, the displacement gage registered about 0.001" increase from the starting displacement. This could not be translated into crack extension since no compliance calibrations were made; therefore, based on the experience with Vessel "A", cycling was terminated at this point.

During subsequent testing, acoustic emission transducers were mounted on the vessel; one less than three inches from the crack, and one near the end of the vessel. Output was recorded on magnetic tape and X-Y chart recorders.

Analysis of the acoustic output during the test is given in Appendix B of this report.

The pressure-displacement diagram for the first test to proof pressure was linear to 4700 psi. The 5% secant offset point, commonly used to determine load for fracture toughness calculations of ductile material, was found at 5500 psi. At proof pressure of 7210 psi, the displacement gage showed the crack to be continuously extending, or the ligament between crack tip and vessel I.D. was continuously plastically deforming during the 5-minute hold. Deformation was still in progress when pressure was reduced.

Final pressurization to failure gave a linear pressure-crack-opening displacement curve to 6300 psi pressure. A step in the curve (about 0.0007" C.O.D.) was noted at 4800 psi, but it is not certain that this was a crack extension -- more probably this was due to a spurious signal to the recorder. Failure occurred as a leak at 7150 psi, somewhat less than the previous proof pressure.

2

The leak was similar in characteristics to that shown in Figure 83 for Vessel "A". The crack extended during the 5 cycles to operating pressure. This conclusion is supported by the change in slope of the C.O.D. curve. Crack opening displacement was 0.0168" on the first operating pressure cycle, and 0.0195" on the fifth cycle.

4.5.5 VESSEL "E" -- This was the second of the unflawed vessels, tested fourth, after the two intentionally flawed vessels. Only a time-pressure record was made of this test. The test program consisted of:

a. Proof pressure test at 7210 psi, hold 5 minutes.

b. Five (5) cycles to operating pressure of 6550 psi, hold one minute at pressure each cycle.

c. Pressurize to burst. For this vessel, the burst pressure was 9880 psi.

The test of this vessel was nearly a duplicate of the first one. Pressure at failure was some 600 psi, or 6% less and there was not as great a degree of bulging evident at the presumed location of fracture initiation. Shown in Figure 90, the fracture appears to have initiated quite near to the center of the cylinder at the fusion line of one of the longitudinal seam welds.

It was a full-shear failure. Two circumferential crack branches developed in the cylinder, one on each side of the longitudinal fracture. The same general crack pattern as in Vessel No. 1 was observed in the heads where the main fracture crossed the butt welds and terminated after turning about 180°. This vessel also escaped from the restraining fixture upon bursting. The resultant damage to the fixture is shown in Figure 91.

4.6 SUPPLEMENTARY INVESTIGATION OF WELD FILLER WIRES

The results of the destructive and nondestructive test performed on weldments WV01, WV02, and WV02A of Table VI are summarized in Table XII. Extensive lack-of-fusion was observed in weldment WV01, and WV02 contained a considerable amount of porosity. As a result, no mechanical property tests were taken from either of these two weldments. The fact that these weldments contained defects should not be interpreted, however, as an indication of poor weld filler wire quality or performance.

In the case of WV01, the parameters and techniques used in welding are considered to have significantly contributed to, or to have been, the cause of the defects. Weldment WV02 was manually welded with no auxiliary shielding and, unlike any of the other weldments produced in this program, interpass temperatures were

maintained during welding by force-cooling with dry-ice. It is possible that any one, or a combination, of these differences could have been the cause of porosity. When weldment WV02A was produced by automatic welding, the techniques and parameters used were the same as selected for the optimum procedure shown in Table VIII. This weldment was of good soundness with no lack-of-fusion or porosity.

Mechanical property test results of WV02A -- the only weldment tested which was produced using weld filler wire from Heat #G-1686A -- were definitely inferior to the properties exhibited by any of the other weldments produced in the course of this program. Although no loss of strength was observed, a sharp loss was apparent in room temperature Charpy V-notch toughness. CVN impact energies at 70°F for this weldment ranged from 30 to 33 ft.-lb. At 0°F, values from 24 to 27 ft.-lb. were obtained.

The reason for this difference in toughness was not investigated but it is likely due to the higher carbon content of Heat #1686A.

Wire from Heat #1686A was used only in completing the last half of two test vessel girth welds. All other girth and longitudinal seam welds were made using weld filler wire from Heat #04836.

4.7 FRACTURE TOUGHNESS TESTS

4.7.1 NOTCHED BEND SPECIMENS -- Fatigue precracking of weld metal and HAZ specimens presented a problem with the bend bars. Instead of developing along a more-or-less straight front, as occurred in the base metal specimens, the precrack tended to form as two nodes, one on each side of the apex of the machined Chevron at the root of the notch. (See Figure 92.) A thin ligament remained at the center of the plate; and the scalloped crack front did not permit uniform extension of the crack over the full specimen thickness. This poorly-developed crack front probably had some effect on crack extension, but it is not readily apparent in the material response curves, probably because most of the applied energy was absorbed in plastic deformation ahead of the notch and little or none in crack extension.

The notched bend specimens exhibited no crack instability in testing. A large plastic zone developed ahead of the crack tip, which was evident from surface indications of lateral contraction; and the specimens failed in a ductile, shearing manner. The material property of a critical stress intensity factor K_{IC} could not be obtained from these 3/4" thick plate test specimens at room temperature.

Therefore, the data is presented in the form of material response curves where in the material's resistance to crack extension is shown as a function of effective crack length; the effective length including the plastic zone ahead of the actual crack.

The curves as presented here, in Figures 93 through 102, originate at the measured crack length (a_o) for each specimen. The difference in a_o is due to variations in the length of fatigue precrack. The inflection of the curve seen in several of the diagrams is believed to derive from excessive deflection at the specimens and friction with the loading tups as the specimen approached final rupture, rather than an actual increase in crack extension resistance.

The material response curves indicate a high degree of base metal and weldment toughness, sufficient to preclude shattering of pressure containing structures such as rocket motor cases, even in the presence of severe flaws.

4.7.2 SURFACE-FLAW SPECIMENS -- Clip-gage-displacement and crack-extension resistance curves from test of the six surface-flaw specimens are presented in Figures 103 through 108. The fatigue precrack extended so far through all specimens except No. W3D04-S6 that, when the environmental or cyclic growth was added, use of the through-plate center crack method of analysis was felt to be desirable. Specimen No. W3D04-S6 was the only specimen considered as a surface-flaw crack. These specimens were precracked and tested in the 5 million lb. test machine shown in Figure 109. Strain gages, as shown in Figure 110, were attached to each specimen during precracking and testing to provide supplementary load and specimen response information.

A stress intensity value was computed for each specimen. In some cases, a limited area under plane strain was observed at the plate center, at the ends of the crack, but failure was predominately plane stress. These "K" values are indicated as K_Q values, applicable only to this thickness of material and essentially ambient temperatures. A critical stress intensity factor (K_{IC}) was not obtained. The computed values of K for these tests are given in Table XVIII. Figure 111 shows the fracture surface of specimen W3D04-S3, a weld-metal specimen tested in an air environment. This specimen is representative of the other two specimens tested in air. The fracture surfaces of the notch area of each of these specimens are shown in Figure 112.

4.8 FATIGUE CRACK GROWTH RATE STUDY

The "beach marks" of the fractured surfaces of the surface flaw specimens of Figure 112 show the extent of crack growth occurring under the several different test loading conditions quite clearly. It is apparent that crack growth along the edge of the EDM slot is not uniform.

The initial low-stress, high cycle fatigue crack "sharpening" of the notch was extended further than desired inasmuch as the low propagation at the ends of the slot on the specimen surface gave no indication of the rate at which the crack was propagating through the plate. As a result, the remaining ligament between the crack front and the "back" surface of the specimen was very narrow. The plastic zone associated with the crack tip, under loads used for low cycle testing, would include the entire ligament. For this reason, in computing the stress intensities associated with fatigue crack propagation, the specimen was considered to be a center-notch type of specimen, the ligament under plastic strain being included as part of the crack. Stress intensity factors were determined with the equation:

$$K_I = 1.77 \left[1 - .1 \left(\frac{2c}{W}\right) + \left(\frac{2c}{W}\right)^2\right] \left(\frac{P\,c}{BW}\right)^{1/2}$$

c = half crack length (average), inches

W = specimen width, inches

B = specimen thickness, inches

P = tensile load, pounds

Computed stress intensity factors and crack growth rates are presented in Table XIX and plotted on a log-log scale in Figure 113. The points do not appear to define a curve, but are in a cluster, being grouped about a central point of 0.001 in./cycle crack growth rate at 150 ksi$\sqrt{\text{in.}}$

Certain of the points on the curve were contributed by Fritz Laboratory personnel, namely those at low stress intensities. Some precrack areas in the specimens had sufficiently well-defined "beach marks" associated with cyclic load changes and sufficiently long runs at constant load range (in the order of 5×10^4 cycles) that reasonably accurate computations of da/dN could be made with respect to ΔK.

Values of ΔK and da/dN were also determined by Fritz Laboratory for the low cycle testing of Specimen 3. Their values fall in the group of points determined by Electric Boat division for the other specimens. The log-log curve shown in the figure for these points coincides with a similar curve plotted by Carmen and Katlin[8] at Frankford Arsenal for several heat treated alloy steels, including maraging grades, in the 240 to 300 ksi yield strength range.

The points are not considered to be highly accurate, because of the general lack of uniformity of the several stages of crack extension. In some instances, only small nodes of crack extension were generated by 100 cycle at relatively high stresses.

For these reasons, whether a precise relationship between K_Q and da/dN can be derived from this data is questionable. It is generally found, however, that the relationship of crack growth to stress intensity will appear graphically as a sigmodal curve in log-log representation, the range between growth rates of 10^{-6} and 10^{-3} inches per cycle being a reasonably straight line. In the present case, most of the datum points are at the extremes of the "straight" portion of the curve, although the three points at the low end (near 10^{-6} in./cycle) appear to define a curve which becomes asymptotic to the growth rate axis at a stress intensity of about 18 ksi$\sqrt{\text{in.}}$, suggesting this value as the lower threshhold of fatigue cracking.

The "straight" portion of the curve has a slope of approximately 4:1, which is in agreement with Paris, Wei, and others [9,10] that for the relationship

$$da/dN = C (\Delta K)^m$$

the exponent "m" should be 4.

Barsom[11] however, found a slope of 2:1 in the log-log relationship of ΔK to da/dN for 12 nickel maraging steel. His data are superimposed in the figure.

Additional flaw growth rate information was obtained by examining the fatigue-extended regions of the artificial flaws in vessels "A" and "D" after the hydrotests of these vessels were completed. The flaw areas were removed by trepanning and broken apart to expose the flaw surfaces.

The fatigue extension of the flaw in Vessel "A" was 0.040", after 401 cycles at 3400 psi maximum pressure. The flaw in Vessel "D" was extended 0.070" after 509 cycles at a maximum 3400 psi. Crack extension which occurred during high-stress, low-cycle testing could clearly be differentiated from that occurring during initial fatigue extension.

It was observed that crack initiation occurred at about 300 cycles; therefore, the crack growth rate was about 0.00035-0.0004 inches per cycle. The cyclic stress intensity factor ΔK had been selected as 100 ksi$\sqrt{\text{in.}}$ The point located by these co-ordinates, on the graph of Figure 113, is very close to the plotted curves. This point is considered to include some error since the number of cycles for crack initiation was not precisely determined.

4.9 STRESS CORROSION TESTS

4.9.1 TESTS OF FLUIDS FOR USE IN VESSEL HYDROTESTS -- None of the three specimens tested in inhibited water showed any tendency toward stress-corrosion extension of the fatigue precrack

in over 500 hours of immersion testing. Dial indicators, mounted at the extremity of each test frame lever arm showed no change in the arm position, indicating no extension of the fatigue-cracked notch in the specimens.

Stress intensity factors (K_Q) were calculated for the two specimens fractured in air. For the base metal specimen, K_Q was 164 ksi$\sqrt{\text{in.}}$, and for the weld metal specimen K_Q was 85.0 ksi$\sqrt{\text{in.}}$ The value for the weld specimen is questionable, as the fatigue crack was only about 1/32" deep across the length of the notch, and extended down the sides of the specimen as two roughly semi-circular cracks of about 1/8" radius, on each side of the notch. In the absence of a straight crack front, the crack tip stress pattern is non-uniform and the stress intensity factor cannot be calculated accurately. Test data are shown in Table XX.

Following the minimum 500 hours in stress corrosion testing, each specimen was fractured to observe any effects of the corroding medium. No corrosive effects and no subcritical crack extension were evident. Unfortunately, the fatigue precrack was seen to extend further down the sides of the specimen than through the center. Therefore, in calculating the stresses and loads to be applied an erroneous crack length measurement was used and actual stresses were significantly lower than desired. Specimen BM-2, for example, showed surface traces of a fatigue crack such that the average crack length dimension "a" was calculated as 0.287". Using the calculated high stress of 149,000 psi developed at a vessel proof pressure of 7210 psi, the bending movement on the specimen was established from:

$$M = S\,\frac{I}{C} = 149{,}000\ \frac{(0.648)(0.460)^2}{6} = 3410 \text{ inch/lb.}$$

When the specimen was fractured, the fatigue crack was found to be incomplete, and the average crack length was actually about 0.175-in. From this (with certain substitution of terms in the above equation), the actual applied stress, σ_{Nf}, was determined.

$$\sigma_{Nf} = 6(3410)/0.648(0.747 - 0.175)^2 = 96{,}500 \text{ psi,}$$
or about 2/3rds the design test stress.

Similarly, the welded specimen WM-7 was found to have an uncracked ligament in the center of the fracture plane, which materially reduced the actual crack-tip stress from the calculated value.

Specimen BM-3, a base metal specimen, was found to have a reasonably uniform crack front, and the actual stress was only about 10% less than the calculated value -- 137,000 psi actual vs 149,000 psi calculated.

Despite the questionable results of the above tests, in view of the fact that no surface corrosion, crevice corrosion, or sub-critical crack extension was apparent, it was concluded that the soluble-oil inhibited water normally used in the Electric Boat division's hydrotest pressurization system would not introduce a stress corrosion factor into the vessel test. Maximum stress to be applied for a significant period of time would be only 68,000 psi during fatigue precracking of the two flawed vessels. This stress is less than the actual stress applied in the corrosion tests.

4.9.2 CORROSION TESTS OF SURFACE FLAW SPECIMENS -- Initial specimen loads were 190 kips, producing K-factors of 62.5 to 71 ksi $\sqrt{\text{in.}}$ in the three specimens (calculated after fracture and when actual notch/crack surface areas could be measured). However, as seen on the load-displacement diagrams of Figures 104, 106 and 108, only minor crack extension was produced in the two-hour hold period. Increasing the load in 100 kip increments and holding for two hours after each increase produced the same results up to loads giving 170 ksi for net section unit stress, or about 94.5% of yield stress. In essence, neither base metal, heat-affected zone or weld metal showed any marked susceptibility to stress corrosion cracking under the conditions of this test, in comparison to preliminary tests by Del Research Corporation.

This apparent anomaly was not investigated, but could have been due to one or more of the following: (1) too short a hold period at low stress intensities, allowing insufficient incubation time; (2) fatigue precrack shape being such that calculated stress intensities based on apparent crack size were actually lower than calculated; (3) corrodent not reaching tip of crack; (4) actual stress intensities being much higher than calculated, causing yielding at the crack tip. It is known that plastic deformation of material inhibits its susceptibility to stress corrosion attack.

Since the original part-through surface flaw was extended by fatigue precracking through specimens 2 and 4, the center-notch analysis was used to compute K-factors for these tests. The surface-flaw equation was used to compute K values for specimen No. 6. These calculated K values are shown, along with flaw dimensions and other details, in Figures 114 through 116. The fracture surface of specimen W3D04-S4, a weld-metal stress-corrosion test specimen, is shown in Figure 117. This specimen had fracture characteristics similar to those of the other surface-flaw stress-corrosion specimens. Close-ups of the flawed areas of these specimens are shown in Figure 118.

Final failure of these specimens, produced by short time tensile loading, occurred at unit stresses approximately equal to the ultimate tensile strength of the base metal or weld metal previously determined in transverse weld and all-weld-metal specimens.

The results of these tests indicate an insensitivity to any stress intensification occurring during static loading.

4.10 ACOUSTIC EMISSION MONITORING OF HYDROTESTS

The results of monitoring Vessels "B" and "D" for acoustic emission during hydrotest are presented and discussed in detail in Appendix B. Considering that 12% Ni maraging steel had never before been monitored for acoustic emission, the results obtained were very good.

Prior to monitoring the vessel hydrotests, one of the edge-notched bend specimens of this program was monitored for emissions during fracture toughness testing. The acoustic emission characteristics of this specimen were then used as a basis to which the acoustic emission signals of the vessels could be compared. The signal characteristics of both vessels, one essentially flawless and the other containing a larger intentionally-introduced flaw, were such that in each case the failure pressure could be predicted substantially before failure occurred.

The results indicate this nondestructive test method has the potential of becoming a very valuable tool in the evaluation of rocket motor cases, propellant tanks and various other structures and pressure vessels.

5.0 CONCLUSIONS

The following conclusions can be stated based on the results of this program:

5.1 The 12% Nickel maraging steel at a yield strength of 180,000 psi can be fabricated to meet the "Leak Before Break" criteria for 260 inch motor cases using the GTA welding process.

5.2 Production-size heats of 12% Ni maraging steel having excellent strength and toughness can be produced successfully.

5.3 Base plate material does not have to be aged prior to welding and a fabrication sequence of solution-anneal, roll, weld, and age can be used in motor case fabrication.

5.4 Both the 17%Ni-2Co-3Mo and 12%Ni-5Cr-3Mo weld filler wires can be used to produce welds of excellent toughness; weld wire residual element content and processing variables appear more important considerations in the selection or specification of weld filler wire than the choice between these two nominal weld wire compositions.

5.5 The optimum GTA welding procedure developed for use in this program is suitable for use in the fabrication of pressure vessels and can consistently produce welds of good soundness and excellent mechanical properties.

5.6 Control of weld heat input energy, preheat, maximum weld interpass temperature and bead size is necessary if optimum weld strength and toughness properties are to be attained.

5.7 Slow bend edge-notched and surface-flawed fracture toughness tests demonstrate that 12% Ni maraging steel weldments which will withstand crack-tip stress intensities in excess of 500 Ksi $\sqrt{\text{in.}}$ at room temperature can be produced from 3/4-inch thick base plate material.

5.8 Welding, fabrication and inspection requirements necessary for the production of 260-inch diameter 12% Ni maraging steel motor cases are within the capability of most modern shipyards and pressure vessel fabrication shops.

REFERENCES

1. J. E. Srawley and J. B. Esgar, "Investigation of Hydrotest Failure of Thiokol Chemical Corporation 260-Inch Diameter SL-1 Motor Case" National Aeronautics and Space Administration Technical Memorandum TM X-1194, January 1966.

2. "Large Motor Case Technology Evaluation", Annual Report of Contract AF 33 (615) - 1623, The Boeing Company, June 1965.

3. C. F. Tiffany, J. N. Masters, D. L. Barclay and R. E. Regan, "A Study of Low-Cost Weldments in Pressure Vessels Made of HY-150 Steel Plates" Final Report of Contract NAS 3-10281, The Boeing Company, October 1968.

4. C. F. Tiffany, J. N. Masters and R. E. Regan, "A Study of Weldments and Pressure Vessels Made of 12Ni Maraging Steel", The Boeing Company.

5. P. M. Schmidt, "General Summary - Welding and Fabrication of the SRV Model" Final Report of Contract NObs-4696, General Dynamics Corporation, June 1969.

6. W. F. Savage, C. D. Lundin and A. H. Aronson - "Weld Metal Solidification Mechanics" Welding Journal Research Supplement April, 1965.

7. L. M. Polentz, "Compressed Water Can Be Dangerous". Chemical Engineering March 23, 1970.

8. C. M. Carman and J. M. Katlin, "Low Cycle Fatigue Crack Propagation of High Strength Steels", ASME Paper No. 66-MET-3, April, 1966.

9. R. P. Wei, P. M. Talda, and Che-Yu Li, "Fatigue Crack Propagation in Some Ultra-High-Strength Steels", U.S. Steel Corp. Applied Research Laboratory, Paper presented at 69th annual meeting of ASTM, Atlantic City, New Jersey, June, 1966.

10. P. C. Paris and F. Erdogan, "A Critical Analysis of Crack Propagation Laws", Journal Basic Engineering (ASME), December, 1963.

11. J. M. Barsom, "Investigation of Sub-Critical Crack Propagation," PHD Dissertation, University of Pittsburg, 1969.

TABLE I - MELTING AND MILL PROCESSING DATA FOR U.S. STEEL HEAT NO.L-50897*

Method of Production:	Vacuum-arc remelted from vacuum-induction melted material.
VAR Ingot Size:	36 in. dia. x 95 in. height.
Conversion Operations:	Ingot heated and upset forged to 75 inch height.
	Reheated and forged to 18 x 65 x 85 inch size.
	Reheated and forged to 13 x 50 x 108 inch slab.
	Reheated and longitudinally rolled to 116 inches.
	Turned 90 degrees.
	Rolled to 3/4 inch thick plate.
Mill Solution - Anneal:	1575°F/1 Hour/Air Cool

*Data as Supplied by U.S. Steel Corporation

TABLE II - RESULTS OF CHEMICAL ANALYSIS OF BASE PLATE MATERIAL-HEAT #L-50897

Source	Analysis, % By Weight									
	C	S	P	Ni	Cr	Mo	Al	Ti	Si	Mn
Vendor Analysis:	0.007	0.003	0.006	11.80	4.85	3.07	0.29	0.31	0.07	0.15
E.B. Div. Analysis:	0.001	0.004	0.002	12.22	5.10	2.95	0.31*	0.32	0.07	0.13

	O_2	N_2	H_2
Vendor Analysis ppm:	14	55	N.D.
E.B. Analysis ppm:	2**	40**	1**

* - Acid Soluble Determination

** - Serfass Gas Analyzer (vacuum fusion)

N.D. - Not Determined

TABLE III - RESULTS OF CHEMICAL ANALYSIS OF WELDS AND WELD FILLER WIRE

Source of Analysis	Analysis, % By Weight											ppm		
VASCO # 01222	C	S	P	Ni	Cr	Co	Mo	Al	Ti	Si	Mn	O_2	N_2	H_2
Vendor Analysis	0.01	0.005	0.003	16.74	N.D.	2.22	3.01	0.01	0.63	0.01	0.05	8	30	1
E.B. Div. Analysis	0.003	0.005	0.001	16.57	0.01	2.35	2.80	.001*	0.62	0.01	0.005	N.D.	N.D.	1(a)
VASCO # 04836														
	0.009	0.005	0.010	11.83	5.04	N.I.	3.18	0.26	0.22	0.05	0.01	16	19	1
	0.006	0.005	0.004	11.91	5.01	N.I.	3.15	0.26*	0.27	0.08	0.01	13**	46**	1(a)
Weld Metal(EB Div)	0.01	0.005	0.010	11.95	5.07	N.I.	3.26	0.23*	0.29	0.09	0.03	8**	23**	1(a)
VASCO # L-50898														
Vendor Analysis	0.01	0.003	0.006	11.87	4.85	N.I.	3.15	0.30	0.30	0.04	0.01	15	60	
VASCO # 1686A														
Vendor Analysis	0.02	0.005	0.008	12.08	5.00	N.I.	3.08	0.31	0.32	0.08	0.04	12	41	1
EB Div. Analysis	0.021	0.005	0.010	11.69	5.04	N.I.	3.16	0.29*	0.32	0.13	0.032	10**	52**	1(a)
Weld Metal(EB Div)	0.02	0.005	0.010	11.97	4.90	N.I.	3.16	0.29*	0.34	0.11	0.03	20**	38**	1(a)

* - Acid Soluble Determination
** - Serfass Gas Analyzer (vacuum fusion)
(a) - Serfass Gas Analyzer (hot extraction)
N.D. - Not Determined
N.I. - Not Intentionally Added Element, Not Measured.

TABLE IV -- SOLUTION ANNEALING AND AGING TREATMENTS USED IN BASE MATERIAL HEAT TREATMENT STUDY.

Specimen Number	Solution Anneal, °F	Aging Treatment Temp., °F	Aging Treatment Time, Hrs.	Specimen Number	Solution Anneal, °F	Aging Treatment Temp., °F	Aging Treatment Time, Hrs.
1A-1, T1	1550	850	4	1A-11, T1	1650	900	8
T2	1550	850	4	T2	1650	900	8
1A-2, T1	1550	850	8	1A-5, T1	1650	950	4
T2	1550	850	8	T2	1650	950	4
1A-7, T1	1550	850	16	1A-6, T1	1650	950	8
T2	1550	850	16	T2	1650	950	8
1A-8, T1	1550	850	30	1A-17, T1	1650	950	16
T2	1550	850	30	T2	1650	950	16
				1A-18, T1	1650	950	30
				T2	1650	950	30
1A-3, T1	1600	900	4	1A-13, T1	1550	900	8
T2	1600	900	4	T2	1550	900	8
1A-4, T1	1600	900	8	1A-14, T1	1550	950	8
T2	1600	900	8	T2	1550	950	8
1A-9, T1	1600	900	16				
T2	1600	900	16				
1A-10, T1	1600	900	30				
T2	1600	900	30				

TABLE V - CONDITIONS AND WELDING PARAMETERS USED TO PRODUCE INITIAL TASK III 12" X 12" WELDMENTS AND 40" X 40" PANELS

Fixed Conditions:

Process:	Gas-Tungsten-Arc (GTA)
Electrode:	2% Thorium - 1/8" Diameter
Shape:	30 Degree Included Tip Angle 1/16" Dia. Flat at End
Current:	D.C.S.P.
Position:	Flat
Base Material:	12% Ni Maraging Steel U.S. Steel Ht. No. L-50897
Weld Filler Wire:	12% Ni - Vasco Ht. 04836, 1/16" dia. 17% Ni - Vasco Ht. 01222, 1/16" dia.
Welding Head:	Voltage Seeking Type
Method of Joint Preparation:	Machined
Pre-Weld Cleaning:	Acetone Wipe
Interpass Cleaning:	Typically Burred and Power Brushed
Type Restraint:	Edges Clamped
Special Shielding:	Backing Gas-Argon Trailing Shield-Argon Linde Gas Lens on Torch
Preheat and Post Heat:	None

Joint Geometry:

Weldments (12" x 12" x 3/4")

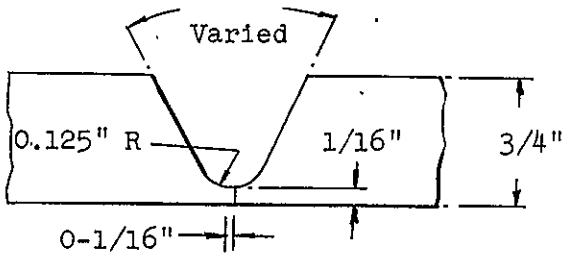

Weldments (40" x 40" x 3/4")

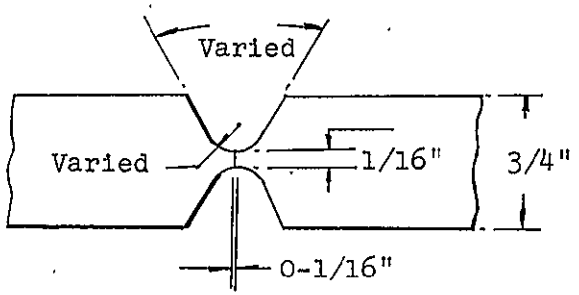

TABLE VI - SPECIFIC SETTINGS AND CONDITIONS, INITIAL 12" X 12" TASK III WELDMENTS

Weldment No.	Filler Wire % Ni	Cup Gas	Flow Rate cfh	Heat Input j/in.	Welding Current Amps	Arc Voltage Volts	Travel Speed ipm	Wire Feed ipm	Maximum Interpass °F	Joint Opening Degrees	Trailing Shield Used?	Comments
W1A15	17	A	20	33,600	210	12	4-1/2	18	300	90	No	Dilution Effects
W3B02-1	12	A	20	29,300	220	10	4-1/2	18	200	40	Yes	Aging Study
W3B02-2	12	A	20	29,300	220	10	4-1/2	18	200	40	Yes	Aging Study
W3B03	12	H	60	26,400	220	12	6	24	200	40	Yes	Helium-High Amps.
W3B05-1	12	A	20	30,000	225	10	4-1/2	18	350	40	Yes	350°F Min. Interpass
W3B07-1	17	A	20	30,000	230	10	4-1/2	18	250	40	No	No Trail Shield
W3B11	12	A	20	17,600	190	9-1/2	6-1/2	24	200	60	Yes	Wide Opening
W3B27	17	A	20	29,300	220	10	4-1/2	18	250	40	Yes	Base Weld - 17%
W3B29-1	17	A	20	35,000	220	12	4-1/2	18	200	40	No	Burred and Brushed
W3B29-2	17	A	20	35,000	220	12	4-1/2	18	200	40	No	Burred Only
W3B29-3	17	A	20	35,000	220	12	4-1/2	18	200	40	No	Minimum Cleaning
W3B30	12	H	60	18,400	160	12	6-1/4	24	200	40	Yes	Helium -Low Amps.
W3B31	12	A	20	30,000	225	10	4-1/2	18	250	40	Yes	Base Weld - 12%
W3B33	12	A	20	17,600	280	10-1/2	10	40	200	40	Yes	High Deposition
W3B38	12	A	20	22,000	220	10	6	24	150	40	Yes	Low Interpass
WV01	12	A	20	21,000	210	10	6	24	150	40	Yes	Ht. L-50898 Wire
WV02	12	A	20	29,000	240	12	6	24	150	60	No	Ht. V-1686A Wire
WV02A	12	A	20	26,000	240	10-1/2	6	24	200	60	Yes	Ht. V-1686A Wire

TABLE VII - SPECIFIC SETTINGS AND CONDITIONS---40" WIDE WELD TEST PANELS

40" X 40" Panels:

Weldment No.	Filler Wire % Ni	Cup Gas	Flow Rate cfh	Heat Input j/inch	Welding Current Amp.	Arc Voltage Volts	Travel Speed ipm	Wire Feed ipm	Maximum Inter-Pass °F	Joint Opening Degrees	Trailing Shield Used?	Comments
W3C02	12	A	30	21,800	255	10	7	30	200	40	Yes	High Current
W3C03	12	A	20	21,500	220	9½/10	6	24	200	40	Yes	Base Weld 12%
W3C04	17	A	20	22,000	220	10	6	24	200	40	Yes	Base Weld 17%
W3C06	12	H	50	18,400	160	12	6-1/4	26	200	40	Yes	Helium-Low Current
W3C07	12	A	30	18,200	200	9-1/2	6-1/4	24	200	60	Yes	60° Joint Opening
W3C09	12	A	20	30,000	225	9-1/2	4-1/4	18	150	40	No	No Trail Shield
W3C09A	12	A	25	24,000	230	10-1/2	6	24	150	60	No	High Voltage Wide Joint

40" X 60" Panels:

W3D01	12	A	20	26,000	240	10½/11	6	24	150	60	Yes	Aging Study Panel
W3D02	12	A	20	26,000	240	10½/11	6	24	200	60	Yes	Repair Study Panel
W3D03	12	A	20	26,000	240	10½/11	6	24	200	60	Yes	Optimum Procedure Panel
W3D04	12	A	20	26,000	240	10½/11	6	24	200	60	Yes	Surface-Flaw Panel

TABLE VIII - SELECTED OPTIMUM WELDING PROCEDURE - CONTRACT NAS 3-11183

Fixed Conditions:

Process----------Automatic Gas-Tungsten-Arc (GTA)

Base Material----------12% Ni Maraging Steel-U.S. Steel Heat #L-50897, Solution Annealed Condition

Weld Filler Wire--------12% Ni-Vasco Heat # 04836, 1/16" Diameter

Position of Welding-----Flat

Welding Electrode-------1/8" Diameter Tungsten, 2% Thorium 30° included Tip Angle 1/16" Diameter Flat at End

Joint Preparation-------Machined

Pre-Weld Cleaning-------Acetone Wipe

Interpass Cleaning------Power Stainless Wire Brush

Welding Parameters:

Current----------230-240 Amp. DCSP

Arc Voltage------10-1/2 - 11 Volts

Travel Speed-----6 i.p.m.

Wire Feed--------24 i.p.m.

Shielding Gas

- Torch---------Argon, 20 cfh
- Aux. Shield---Argon, 70 cfh
- Back-up-------Argon, 15 cfh

Preheat----------80°F

Postheat---------None

Max. Interpass---200°F

Joint Geometry:

See Figure 30

Equipment and Special Devices

D.C. Welding Power Supply

8-Ft. Boom Welding Manipulator

Power-Driven 10,000-lb. Turning Rolls

Automatic Constant-Voltage Welding Head

Auxiliary Trailing Shield

Linde Gas Lens on Torch

TABLE IX- SUMMARY OF WELDMENT AGING STUDY TEMPERATURE/TIME COMBINATIONS

Weldment Number	Aging Temperature	Aging Time	Weldment Number	Aging Temperature	Aging Time
W3D01A	850°F	4 Hrs.	W3D01I	950°F	4 Hrs.
W3D01B	850 "	8 "	W3D01J	950 "	8 "
W3D01C	850 "	16 "	W3D01K	950 "	16 "
W3D01D	850 "	30 "	W3D01L	950 "	30 "
W3D01E	900°F	4 Hrs.			
W3D01F	900 "	8 "			
W3D01G	900 "	16 "			
W3D01H	900 "	30 "			

TABLE X - MECHANICAL PROPERTIES OF 3/4-INCH TEST PLATES SUBJECTED TO VARIOUS SOLUTION ANNEALING AND AGING TREATMENTS (1)

Specimen Number	Heat Treatment °F/°F/Hrs	0.2% Offset Y.S., psi	Ultimate T.S., psi	R.A. %	2" Elong. %	CVN Impact Ft.Lb. (70°F)	Toughness in.lb./in^2 (70°F)	Average Hardness RC
1A-1,T1	1550/ 850/ 4	182,000	191,000	68.0	16.0	89,92,95	6400,6400,6800	44
T2	1550/ 850/ 4	181,200	190,300	68.3	16.0			
1A-2,T1	1550/ 850/ 8	188,500	196,500	67.5	16.0	85,91,95	6000,5600,6000	45
T2	1550/ 850/ 8	188,500	196,500	67.5	16.0			
1A-7,T1	1550/ 850/16	194,100	200,200	67.8	15.5	89,89,91	6400,6400,5800	44
T2	1550/ 850/16	193,000	200,700	66.7	15.5			
1A-8,T1	1550/ 850/30	198,500	204,750	66.5	14.0	81,83,83	5300,5000,5600	47
T2	1550/ 850/30	199,000	205,500	67.7	14.0	47*,43*,44* 42**,41**		
1A-13,T1	1550/ 900/ 8	190,000	196,750	66.5	14.0	101,98,110	7200,7100,6700	45
T2	1550/ 900/ 8	190,000	196,750	70.5	14.0	65*,66*,62* 54**,58**		
1A-14,T1	1550/ 950/ 8	186,000	191,500	66.5	15.0	103,101,109	7200,7600,7200	43
T2	1550/ 950/ 8	185,000	198,750	66.0	16.0			

(1) Longitudinal, Except Where Noted
* Denotes Transverse Property Value @ 74°F
** Denotes Transverse Property Value @ 0°F

TABLE X - MECHANICAL PROPERTIES OF 3/4-INCH TEST PLATES SUBJECTED TO VARIOUS SOLUTION ANNEALING AND AGING TREATMENTS (1) - (Continued)

Specimen Number	Heat Treatment °F/°F/Hrs.	0.2% Offset Y.S., psi	Ultimate T.S., psi	R.A. %	2" Elong. %	CVN Impact Ft.Lb. (70°F)	Toughness in.lb./in^2 (70°F)	Average Hardness RC
1A-3,T1	1600/ 900/ 4	181,000	192,250	68.5	15.0	100,99,104	7400,7800,7700	45
T2	1600/ 900/ 4	181,800	191,600	69.5	15.0			
1A-4,T1	1600/ 900/ 8	187,500	195,600	67.7	14.0	101,100,96	7000,7200,7400	46
T2	1600/ 900/ 8	188,500	196,500	68.0	14.0			
1A-9,T1	1600/ 900/16	190,000	199,250	68.0	14.0	98,94,99	7100,7400,7400	46
T2	1600/ 900/16	186,500	199,500	69.0	14.0			
1A-10,T1	1600/ 900/30	191,900	203,300	66.7	14.0	86,86,90	5600,6000,5800	45
T2	1600/ 900/30	193,000	204,700	67.2	14.0			
1A-11,T1	1650/ 900/ 8	187,500	196,250	70.0	14.0	98,109,104	7100,6700,7600	45
T2	1650/ 900/ 8	188,900	197,500	68.7	14.0			
1A-5,T1	1650/ 950/ 4	184,500	190,500	69.0	16.0	117,115,112	7700,7900,7200	44
T2	1650/ 950/ 4	183,750	190,500	62.5	16.0			
1A-6,T1	1650/ 950/ 8	185,500	193,500	68.0	15.0	102,109,109	7600,7700	43
T2	1650/ 950/ 8	186,000	193,250	58.5	15.0			
1A-17,T1	1650/ 950/16	190,000	198,750	66.0	16.0	90,86,86	6000,6200,6600	45
T2	1650/ 950/16	189,000	200,000	65.5	15.0			
1A-18,T1	1650/ 950/30	195,000	206,000	60.0	16.0	67,66,65	3800,4300,4200	44
T2	1650/ 950/30	192,500	205,000	58.5	16.0			

TABLE XI - MECHANICAL PROPERTY DATA FOR BASE PLATE - MILL SOLUTION ANNEALED AND AGED 900°F FOR 8 HOURS -- TRANSVERSE DIRECTION

Tensile Properties:

Specimen Number	Heat Treatment °F/°F/Hrs.	0.2% Offset Y.S., psi	Ultimate T.S., psi	R.A. %	Elong. % in 2"
2CA T1	1575/900/8	192,000	201,250	13.0	60.5
2CA T2	1575/900/8	190,000	200,750	13.0	58.5

Impact Properties:

Temperature, °F	-200	-120	-40	0°	+32	+80
CVN, ft. lbs.	5,5,5	13,13,11 14,10,16	36,39,38	45,47,50	47,54,53	46,47,50

TABLE XII - MECHANICAL PROPERTIES OF INITIAL WELDMENTS

Weldment Number	Aging Treatment°F	0.2% Offset Y.S.(1) psi	Ultimate T.S.(1) psi	R.A.(1) %	Elong(1) % in 2"	CVN Impact, Ft. Lbs. 80°F	No/Var	0°F	No/Var	Weld Soundness
W1A15	900 /8 Hrs.	186,600 185,000	198,500 189,500	55.7 55.0	13.0 12.1	48	2/3	46	2/4	Good
W3B02-1	950 /8 Hrs.	175,300	184,300	55.6	15.7	63	3/6			Fair
W3B02-2	900 /12Hrs.	178,500	185,500	58.0	14.3	57	3/8			Fair
W3B03	900 /12Hrs.	181,700 186,300*	189,200 190,900*	54.5 57.4*	14.3 11.0*	47	4/12			Good
W3B05-1	900 /8 Hrs.	180,200 182,700*	186,600 187,600*	61.4 58.4*	14.3 12.0*	59	3/3			Good
W3B07-1	900 /8 Hrs.	190,000	199,500	59.0	12.9	50	2/4			Good
W3B11	900 /8 Hrs.	179,000 180,000*	185,000 189,000*2	55.0 54.0	14.3 14.3					Good
W3B27	900 /8 Hrs.	185,000 188,000*	197,000 194,750*	62.0 58.5*	13.6 13.0*	55	2/3			Good
W3B29-1	900 /8 Hrs.	No				42	3/2			
W3B29-2	900 /8 Hrs.	Tensile				46	3/14			Good
W3B29-3	900 /8 Hrs.	Data				45	3/7			
W3B30	900 /8 Hrs.	181,800	187,400 193,300*	57.6	14.3	56	3/9			Good
W3B31	900 /8 Hrs.	176,200	188,100 190,700*	60.4	14.3	67	2/6			Good
W3B33	900 /12Hrs.	183,000 187,400*	189,000 191,200*	54.0 58.6*	14.3 11*	54	4/11			Fair

(Continued)

TABLE XII (Continued)

Weldment Number	Aging Treatment °F	0.2% Offset Y.S.(1) psi	Ultimate T.S.(1) psi	R.A.(1) %	Elong(1) % in 2"	CVN Impact, Ft.Lbs. 80°F	No/Var	0°F	No/Var	Weld Soundness
WEB38	900 /8 Hrs.	177,000	183,500 192,500*	55.0	14.3	59	3/3			Good
WV01	900 /8 Hrs.	No Data Taken Due to Poor Quality								Severe Lack of Fusion
WV02	900 /8 Hrs.	No Data Taken Due to Poor Quality								Excess Porosity
WV02A	900 /8 Hrs.	182,400 182,200*2	186,300 189,000	52.9 53.0	11.0(1") 12.0	32	4/3	25	3/3	Good

(1) All-weld specimen unless otherwise noted

(2) Average of 2 values

(3) Number of specimens and total range of variations in values shown in Table as No./Var.

*Transverse Specimen

TABLE XIII- MECHANICAL PROPERTIES OF INITIAL 40" X 40" WELD TEST PANELS

Weldment Number	Aging Treatment°F	0.2% Offset Y.S.(1) psi	Ultimate T.S.(1) psi	R.A.(1) %	Elong.(1) % in 2"	CVN Impact Ft.-Lbs. 80°F	No/Var***	Weld Soundness
W3C02	900 /8 Hrs.	179,000	185,000 187,500*2	64.0	14.0	57	4/5	Fair
W3C03	900 /8 Hrs.	182,650	188,800 189,000*2 196,400**	57.1	12.0	56	4/10	Excellent
W3C04	900 /8 Hrs.	182,350	192,150 193,000*2 200,300**	60.8	14.0	55	4/10	Good
W3C06	900 /8 Hrs.	177,450	186,250 189,000*2	60.8	15.0	61(3)	3/7	Fair
W3C07	900 /8 Hrs.	181,000	187,000 188,250*2	62.0	14.0	44(4)	4/6	Fair
W3C09	900 /8 Hrs.							Poor - Severe Bridging
W3C09A5	900 /8 Hrs.	181,600	187,800	61.2	14.0	52	5/6	Excellent

(1) All-Weld Specimen Unless Otherwise Noted
(2) Average of 2 Values
(3) One 53 Ft.-Lb. Value Not Included - Defect Visible in Fracture Face
(4) All Specimens Exhibited Visible Defects in Fracture Face
(5) Average Base Metal Hardness was Rc43; Average Weld Hardness = Rc39
* Denotes Value from .505-Inch Transverse Specimen
** Denotes Value from Reduced Section Transverse Specimen
***No/Var Indicates Number of Specimens Tested/Total Range of Variation of Results

TABLE XIV - MECHANICAL PROPERTIES OF AGING STUDY PANEL W3D01

Weldment Number	Aging Treatment °F	0.2% Offset Yld. Str.(1) psi	Ultimate T.S. psi	Elong.(1) % in 2"	CVN Impact, 80°F Ft. Lbs.	No/Var(2)
W3D01A	850 / 4 Hrs.	179,000	183,000	7.0	49	3/5
W3D01B	850 / 8 Hrs.	181,000	187,500	11.0	50	3/4
W3D01C	850 /16 Hrs.	187,500	191,000	6.0	45	3/4
W3D01D	850 /30 Hrs.	186,500	193,000	12.0	43	3/2
W3D01E	900 / 4 Hrs.	175,500	182,000	12.0	63	3/12
W3D01F	900 / 8 Hrs.	179,500	185,000	12.0	59	3/8
W3D01G	900 /16 Hrs.	184,000	189,500	12.0	51	3/3
W3D01H	900 /30 Hrs.	187,500	194,500	12.0	48	3/2
W3D01I	950 / 4 Hrs.	176,250	181,000	12.0	61	3/4
W3D01J	950 / 8 Hrs.	179,500	186,500	12.0	54	3/6
W3D01K	950 /16 Hrs.	180,900	191,000	12.0	47	3/2
W3D01L	950 /30 Hrs.	183,000	194,500	10.0	43	3/3

(1) Based on One 0.505 Inch Transverse Tensile Specimen
(2) No/Var. Indicates Number of Specimens Tested/Total Range of Variation Results

TABLE XV - MECHANICAL PROPERTY DATA FOR TEST PANELS W3D02 AND W3D03, AGED 900°F FOR 8 HOURS

Transverse Weld Tensile Properties:

Specimen Number	Specimen Type	0.2% Offset Y.S., psi	Ultimate T.S., psi	R.A. %	Elong. % in 2"	General Comments
W3D02-TT1	Red. Section	--	192,100	--	--	Broke in Weld
W3D02-TT2	" "	--	192,500	--	--	" " "
W3D02-T1	All-Weld	178,000	186,000	15.0	54.8	Very Fine Porosity
W3D03-TT1	Red. Section	--	194,300	--	--	Broke in Weld
W3D03-TT2	" "	--	193,400	--	--	" " "
W3D03-T1	All-Weld	176,500	181,000	15.0	62.0	No Visible Defects

All-Weld Charpy Impact Properties - Ft. - Lbs.

Weldment Number	-120°F	-40°F	0°F	+32°F	+80°F
W3D03	31,40	42,54	49,56	54,54	53,65,46,48
W3D03	25,30	37,44	44,45	48,50	45,48,61,65

TABLE XVI - HEMISPHERE DIMENSIONAL DATA (1)

Identification		Prior to Solution Annealing				After Solution Annealing			
Set No.	Pc.No.	Avg. I.D.	Out of Roundness	Min.Thk. Equator	Min.Thk. Overall	Avg. I.D.	Out of Roundness	Min.Thk. Equator	Min.Thk. Overall
1	5B	32.685	0.043	0.995	0.915	32.665	0.065	0.984	0.884
	3B	32.696	0.016	1.040	0.940	32.638	0.116	1.040	0.935
2	3A	32.780	0.007	0.988	0.936	32.745	0.043	0.976	0.902
	5A	32.792	0.003	0.915	0.828	32.750	0.050	0.910	0.825
3	4A	32.638	0.025	1.085	0.970	32.635	0.015	1.070	0.920
	1B	32.683	0.017	1.006	0.975	32.630	0.052	1.000	0.934
4	2A	32.766	0.002	0.970	0.890	32.715	0.020	0.970	0.840
	4B	32.745	0.005	0.935	0.860	32.756	0.005	0.930	0.810
5	1A	32.636	0.025	1.038	0.920	32.586	0.132	1.038	0.920
	2B	32.781	0.004	1.000	0.882	32.724	0.098	1.000	0.882

(1) All dimensional values in inches

TABLE XVII - VESSEL DIMENSIONS (ALL VESSELS WERE OF THE SAME DIAMETER, PLUS OR MINUS 1/32", BY ACTUAL MEASUREMENT)

Cylinder Length - 52" Wall Thickness -0.8125"

Inside Diameter - 32.6"

Vessel Description	Proof Pressure Psi	Operating Pressure Psi	Cycles to Operating Pressure Psi	Failure Pressure Psi	Membrane Stress at Failure Psi	Type of Failure
#A	--	--	0	5,600	112,300	Small leak in machined flaw.
#B	7,320	6,650	5	10,400	209,000	Burst in longitudinal seam. Did not shatter.
#C	7,210	6,550	5	10,250	205,500	Burst in mismatched longitudinal seam. Did not shatter.
#D	7,210	6,550	5	7,150	143,500	Small leak in machined flaw.
#E	7,210	6,550	5	9,880	198,300	Burst in longitudinal seam. Did not shatter.

TABLE XVIII- SURFACE FLAWED SPECIMENS, STRESS INTENSITY FACTORS AT FRACTURE LOADS

(Finite Plate Width Correction Added)

Identification	Test Location	Orig. Test* Source	Max. Load(KIPS)	K(KSI $\sqrt{IN}$)
Specimen 1	Base Metal	F	572	305
2	" "	SC	554	256
3	Weld Metal	F	574	273
4	" "	SC	596	244
5	HAZ	F	700	295
6	"	SC	670	303

* F - Low Cycle Fatigue Test Specimen

SC - Stress-Corrosion Test Specimen

TABLE XIX- SUBCRITICAL FLAW GROWTH STUDY
HIGH STRESS CYCLIC LOADING

		Load P (Kips)	K_Q (Ksi $\sqrt{in.}$)	Nominal Stress Ksi	Crack Growth da/dN
Spec. #1	Base Metal	280	135.5	83.8	0.000918
		480	242.0	144	0.00102
Spec. #3	Weld	280	118.5	80.0	0.000625
		380	160.4	112.2	0.00084
		500	227	163	0.00169
Spec. #5	HAZ	300	123.6	83.4	0.0007
		500	215	140.8	0.0007

TABLE XX - STRESS CORROSION TEST OF 12 NICKEL MARAGING STEEL IN INHIBITED WATER

Specimen No.	Maximum Fiber Stress (PSI)	Bending Moment (In-Lbs)	Test Fluid	Deflection-Inches Original	Final	Change	Hours Exposure
BM-1 (Base Metal)	195,000	7443	Air	Fractured — K_Q = 164 KSI $\sqrt{IN}$			-
BM-2	149,000 (Proof Test Stress)	3430	Water & Soluble Oil	0.7867	0.7855	0.0012	674
BM-3	149,000	3658	1 gm Potassium Chromate in 1 litre water	0.6835	0.6776	0.0059	671
WM-1 (Weld Metal)	185,000	10,617	Air	Fractured — K_Q = 85 KSI $\sqrt{IN}$			-
WM-7	149,000	1650	Water & Soluble Oil	0.9921	0.9916	0.0005	503

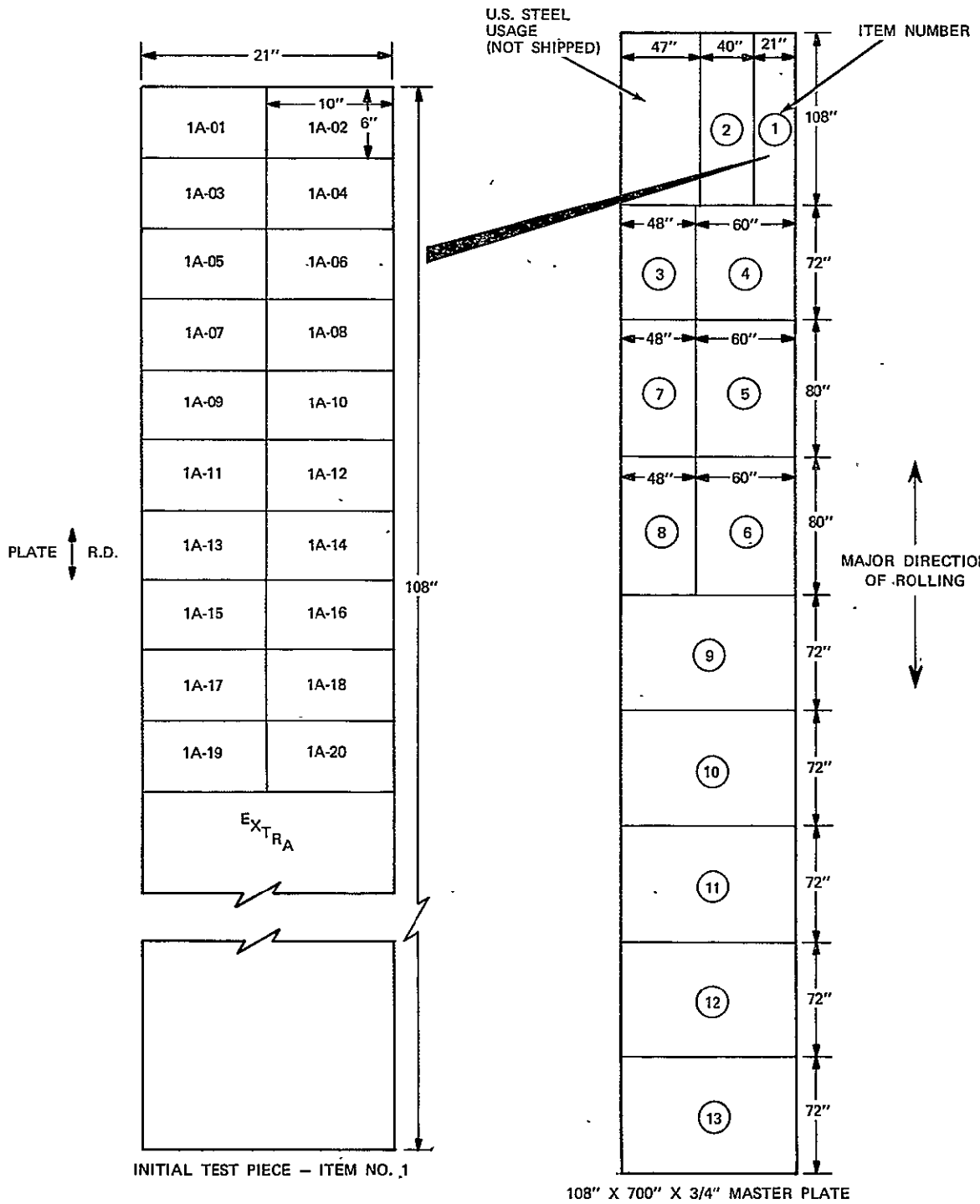

FIGURE 1
MASTER PLATE LAYOUT – ITEMS SHIPPED AND ITEM NO. 1 CUTTING DIAGRAM

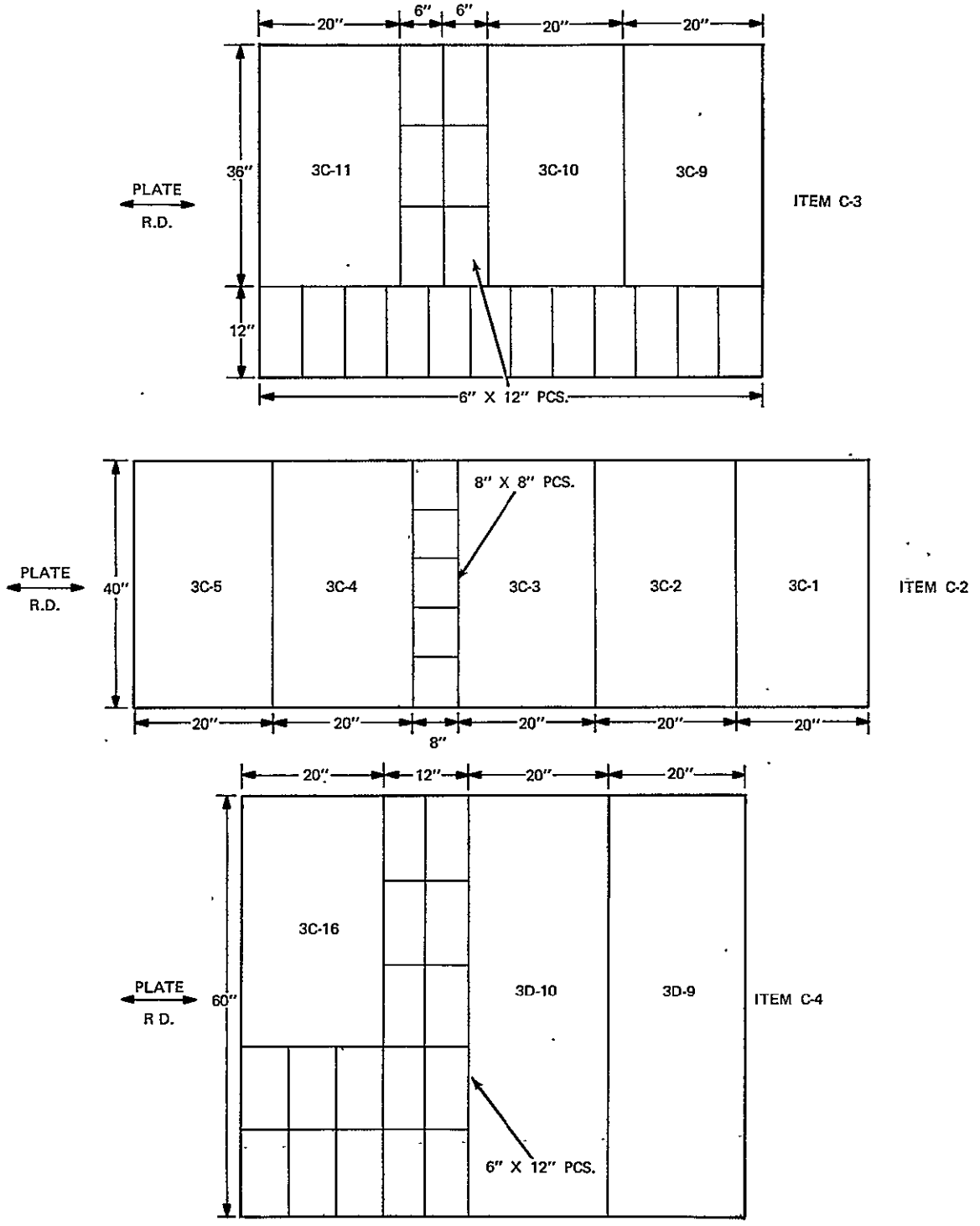

FIGURE 2

ITEMS NO. 2 THROUGH 4 (INCLUDES ALL PCS CUT FROM THESE ITEMS)

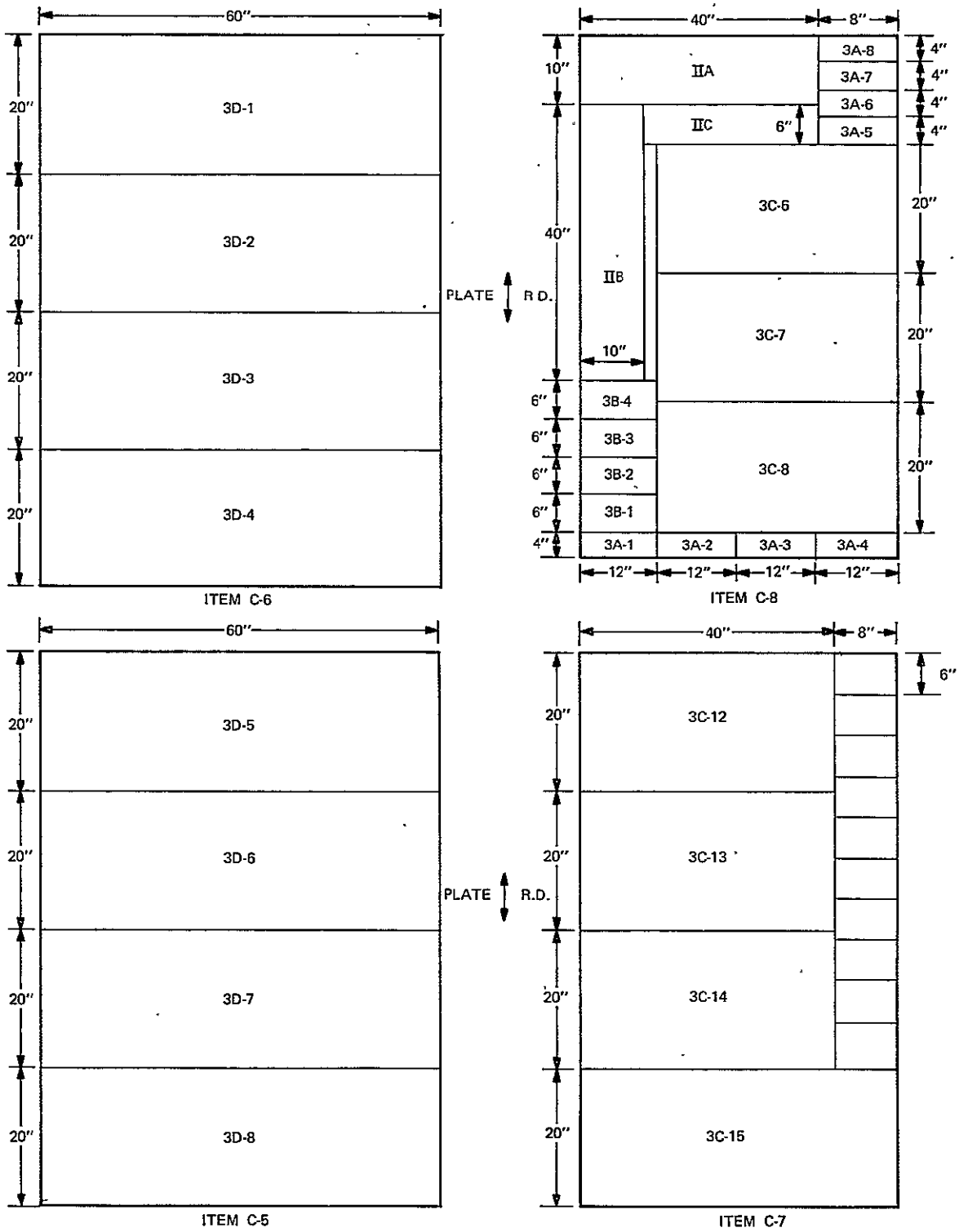

FIGURE 3

ITEMS 5 THROUGH 8 (INCLUDING LAY-OUT OF ALL PIECES CUT FROM THESE ITEMS)

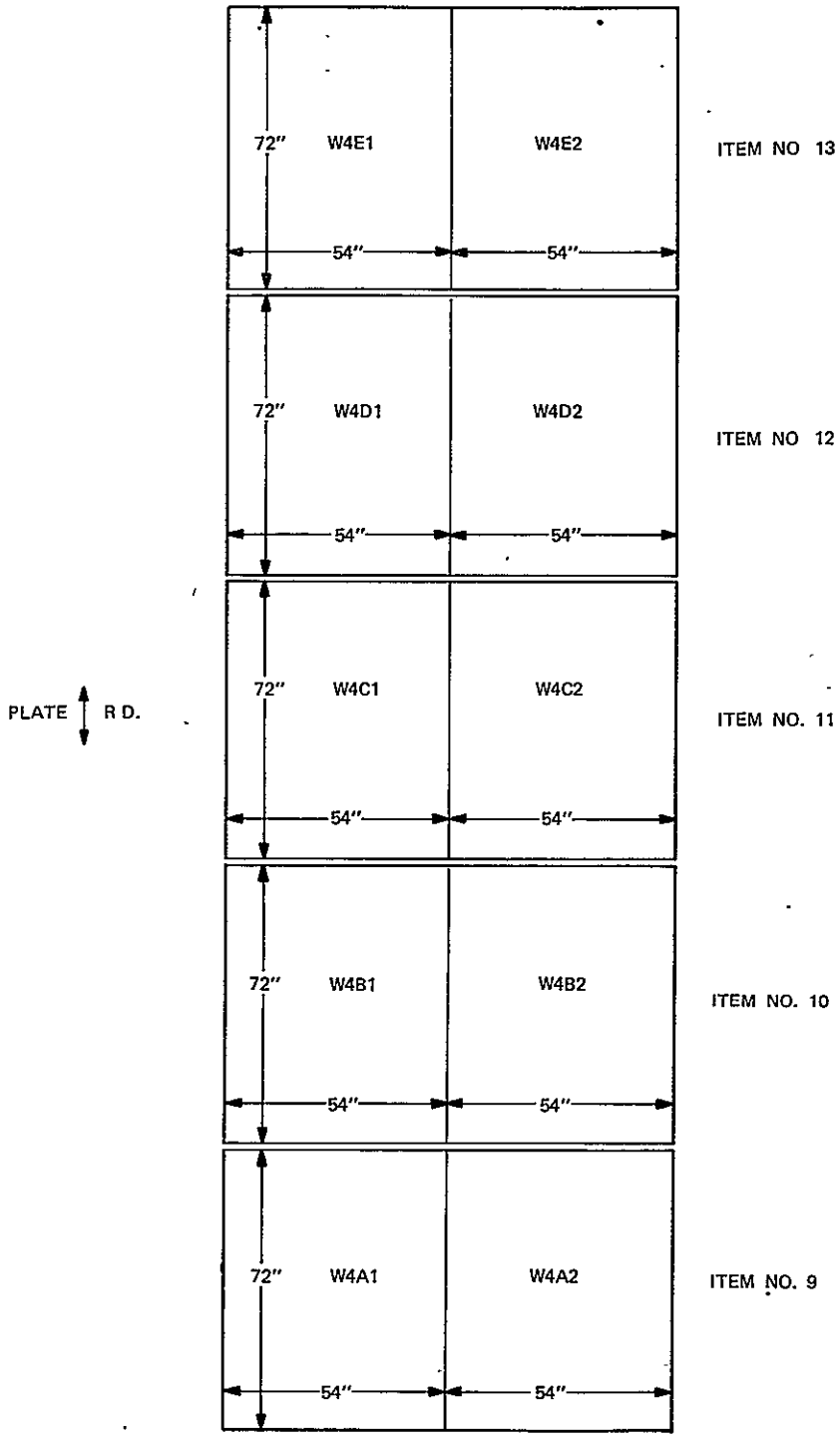

FIGURE 4

ITEMS 9 THROUGH 13 (INCLUDES ALL PIECES CUT FROM THESE ITEMS)

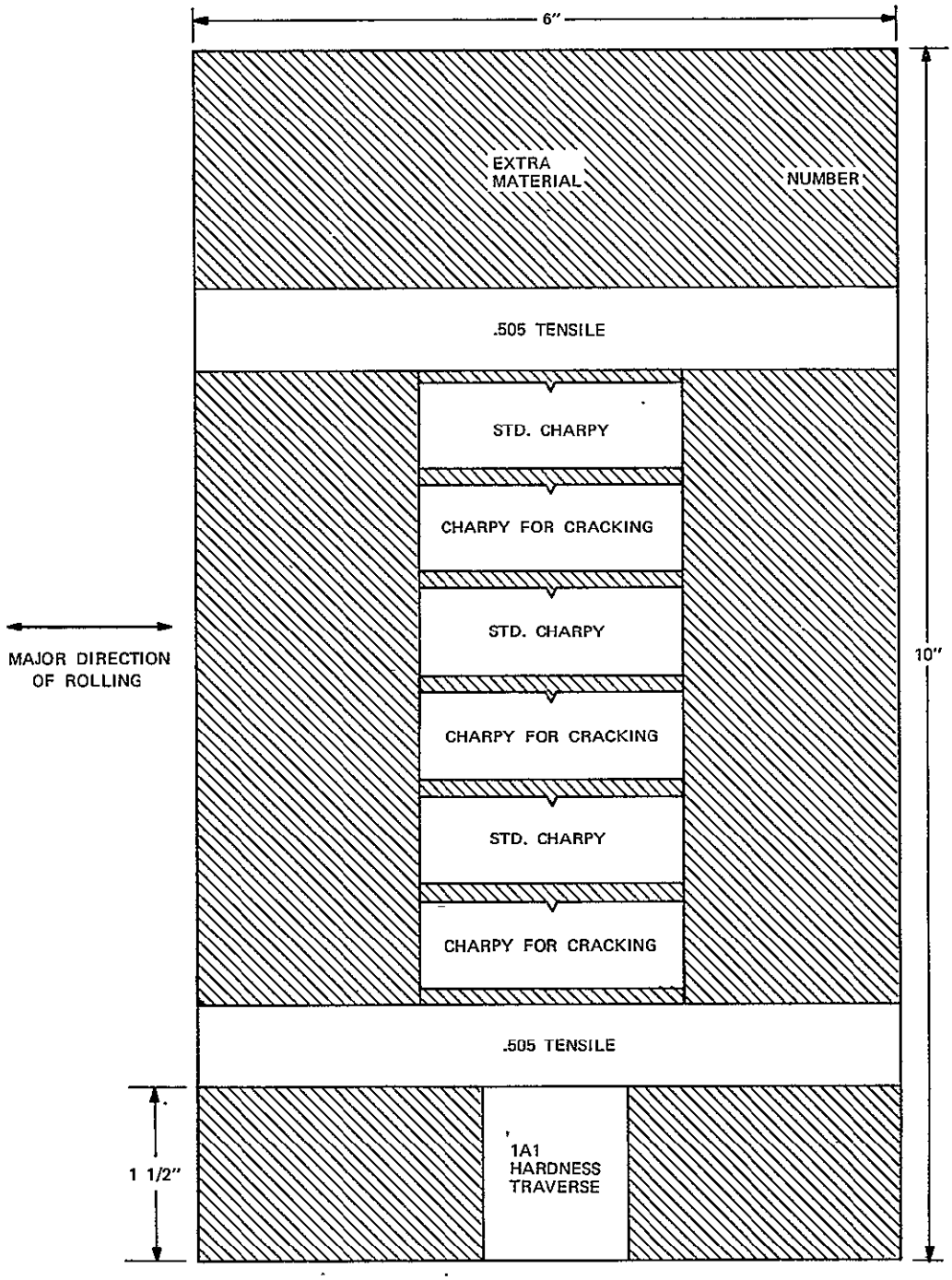

FIGURE 5

BASE MATERIAL HEAT TREAT STUDY – TEST SPECIMEN ORIENTATIONS AND LOCATIONS

NOTE: STATIONS APPROXIMATELY 1/16" APART

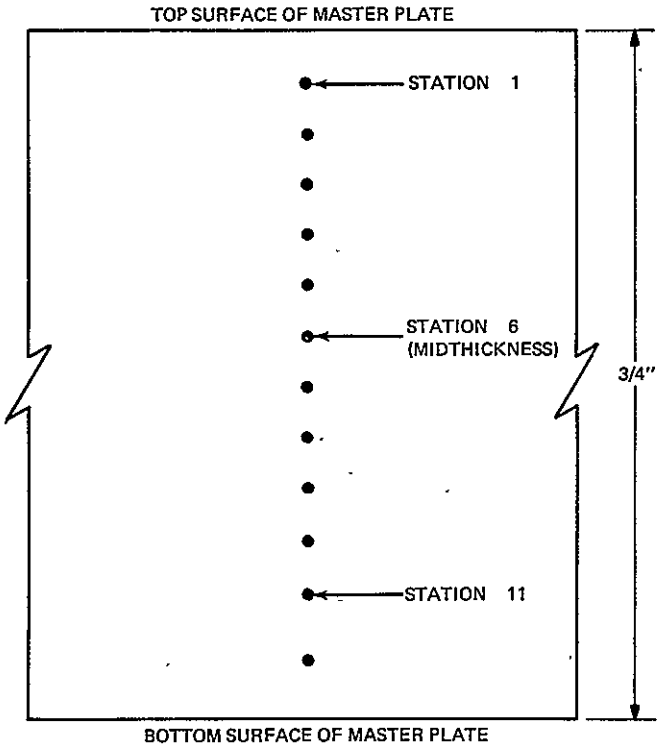

FIGURE 6

R_c HARDNESS TRAVERSE PATTERN FOR BASE MATERIAL HEAT TREAT STUDY

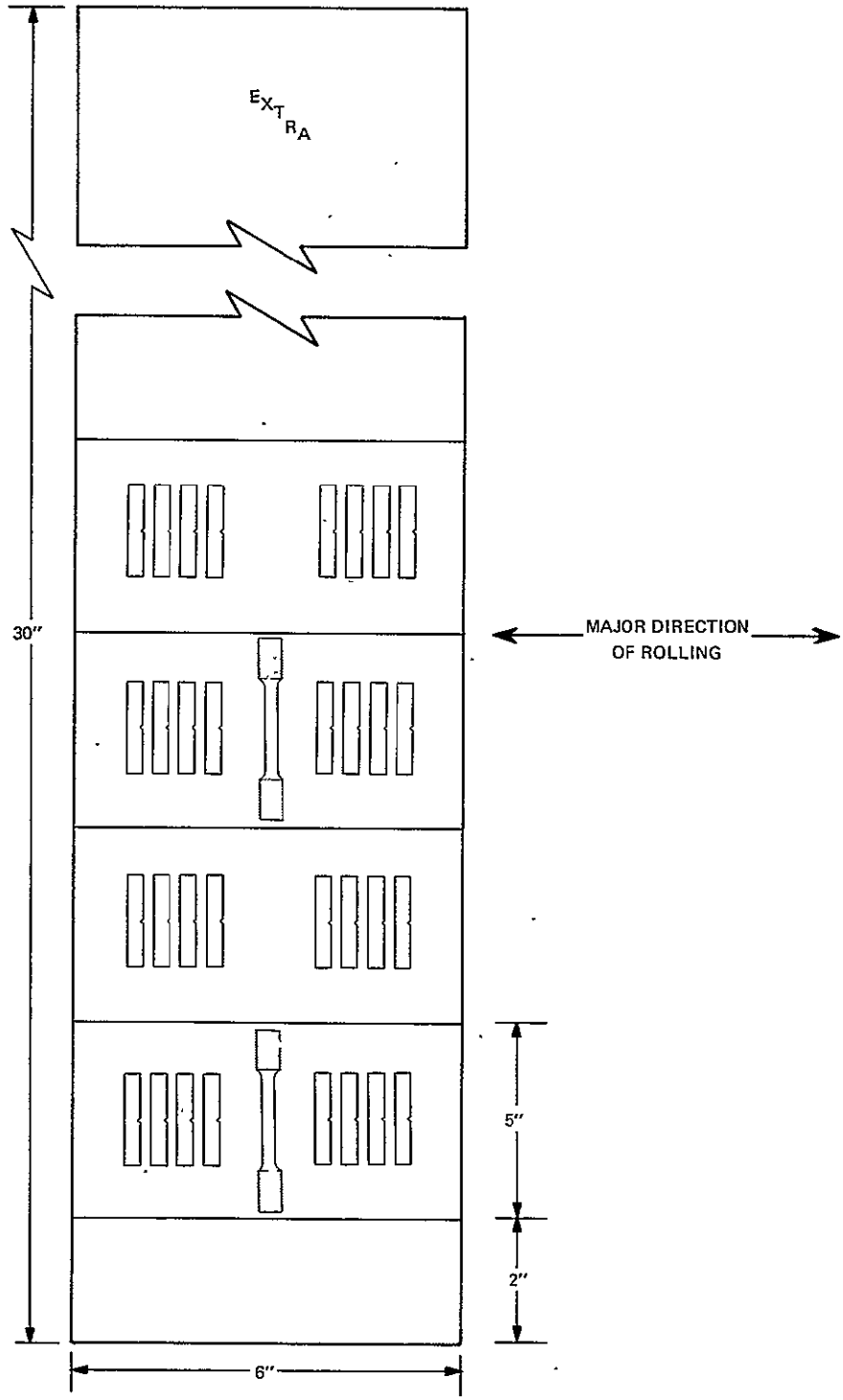

FIGURE 7

MILL SOLUTION ANNEALED BASE MATERIAL-PROPERTY EVALUATION TEST SPECIMENS
FROM PIECE IIC, SPECIMEN ORIENTATION AND LOCATIONS

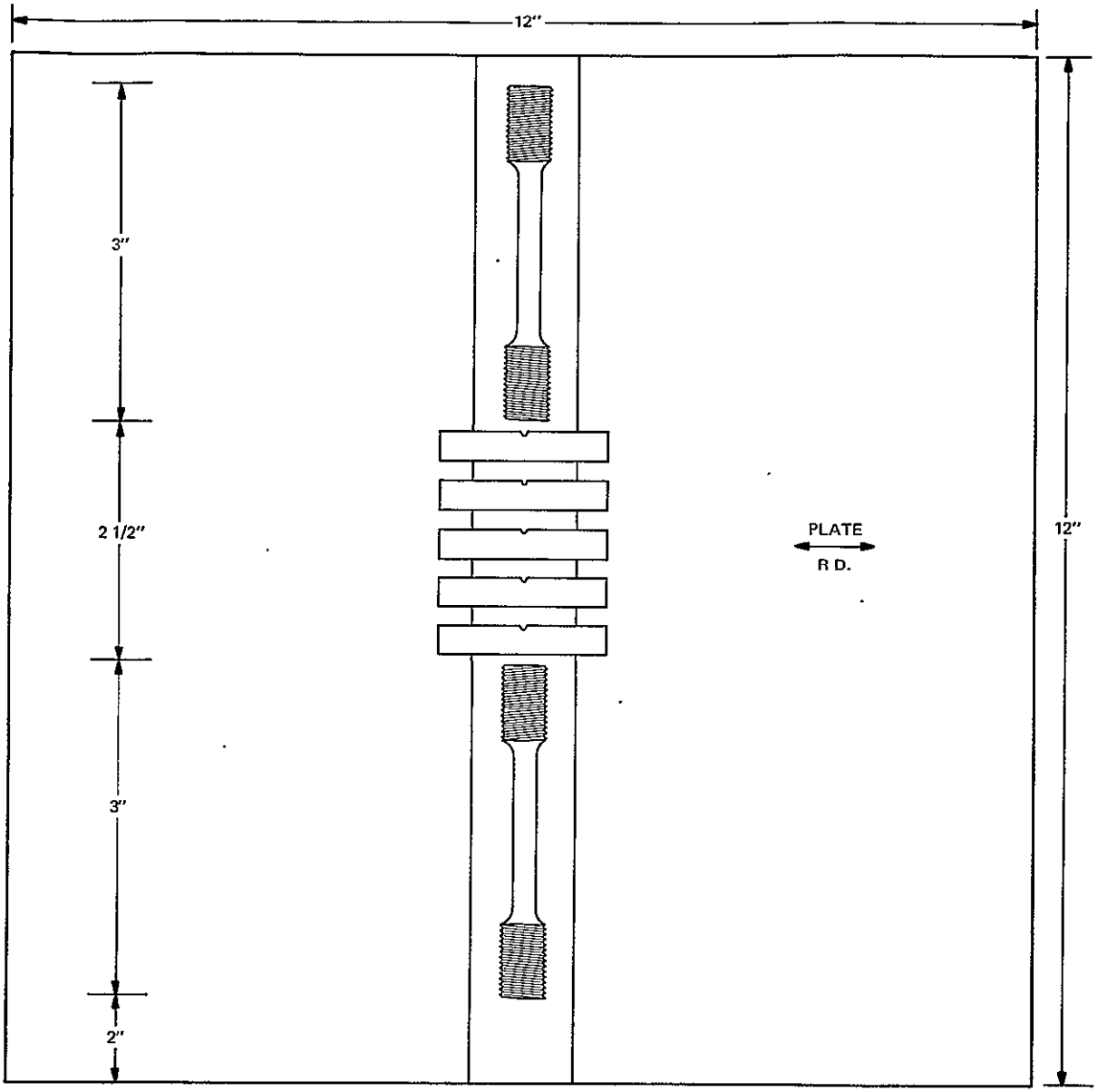

FIGURE 8
TEST SPECIMEN LAY-OUT FOR WELDMENT W1A15

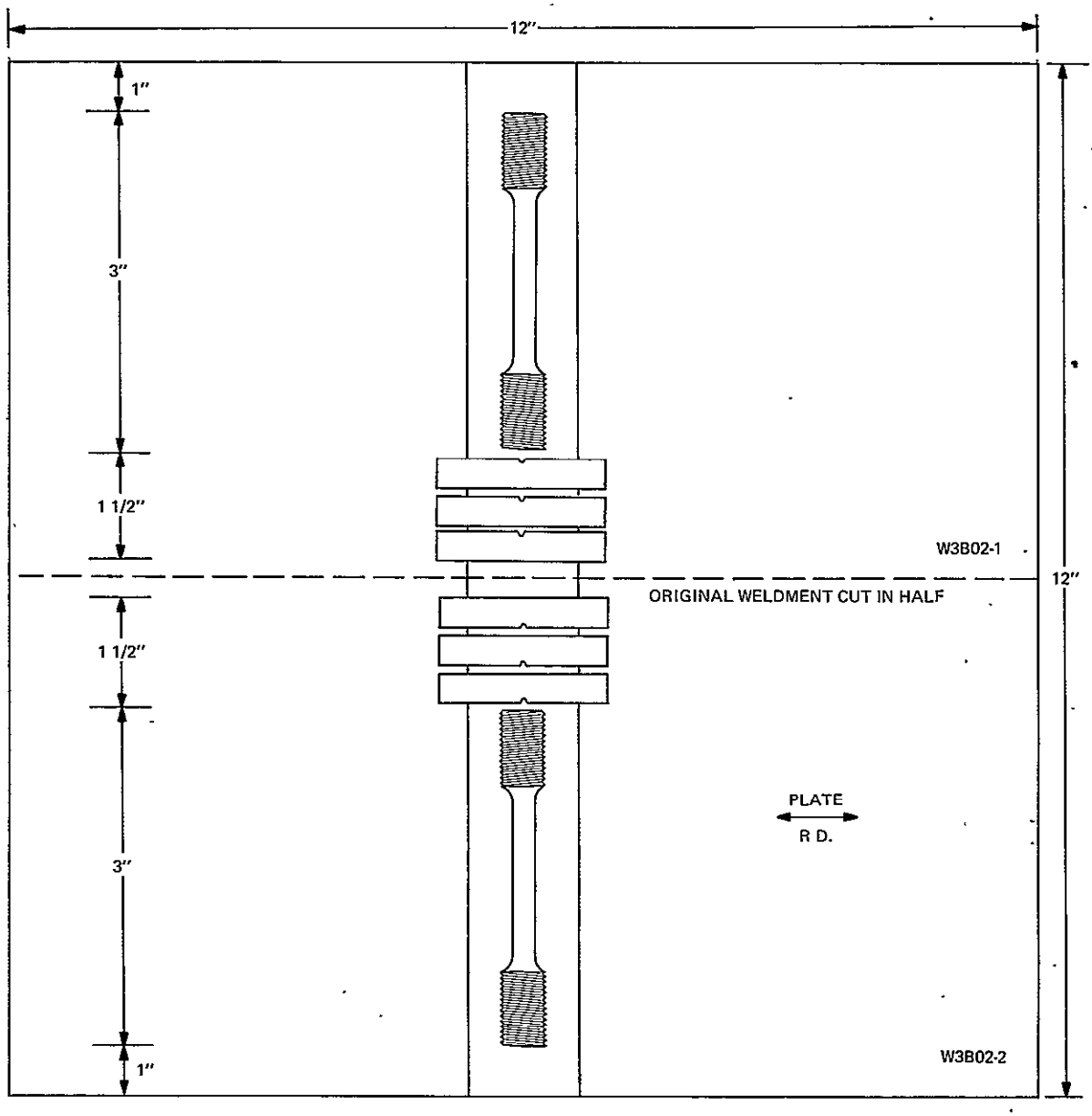

FIGURE 9
TEST SPECIMEN LAY-OUT FOR WELDMENTS W3B02-1 AND W3B02-2

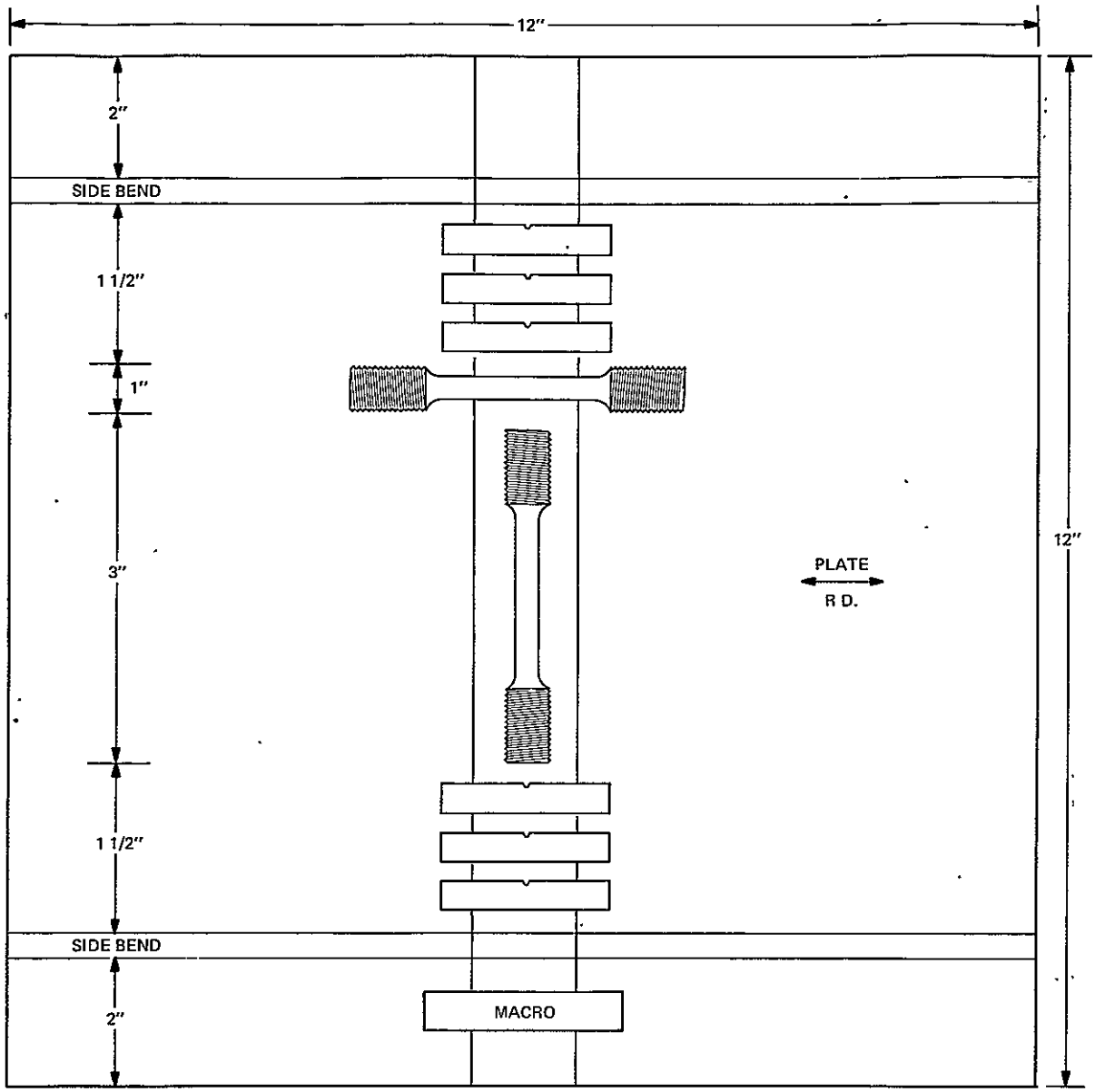

FIGURE 10

TEST SPECIMEN LAY-OUT FOR WELDMENTS W3B03, W3B33 AND W3B38

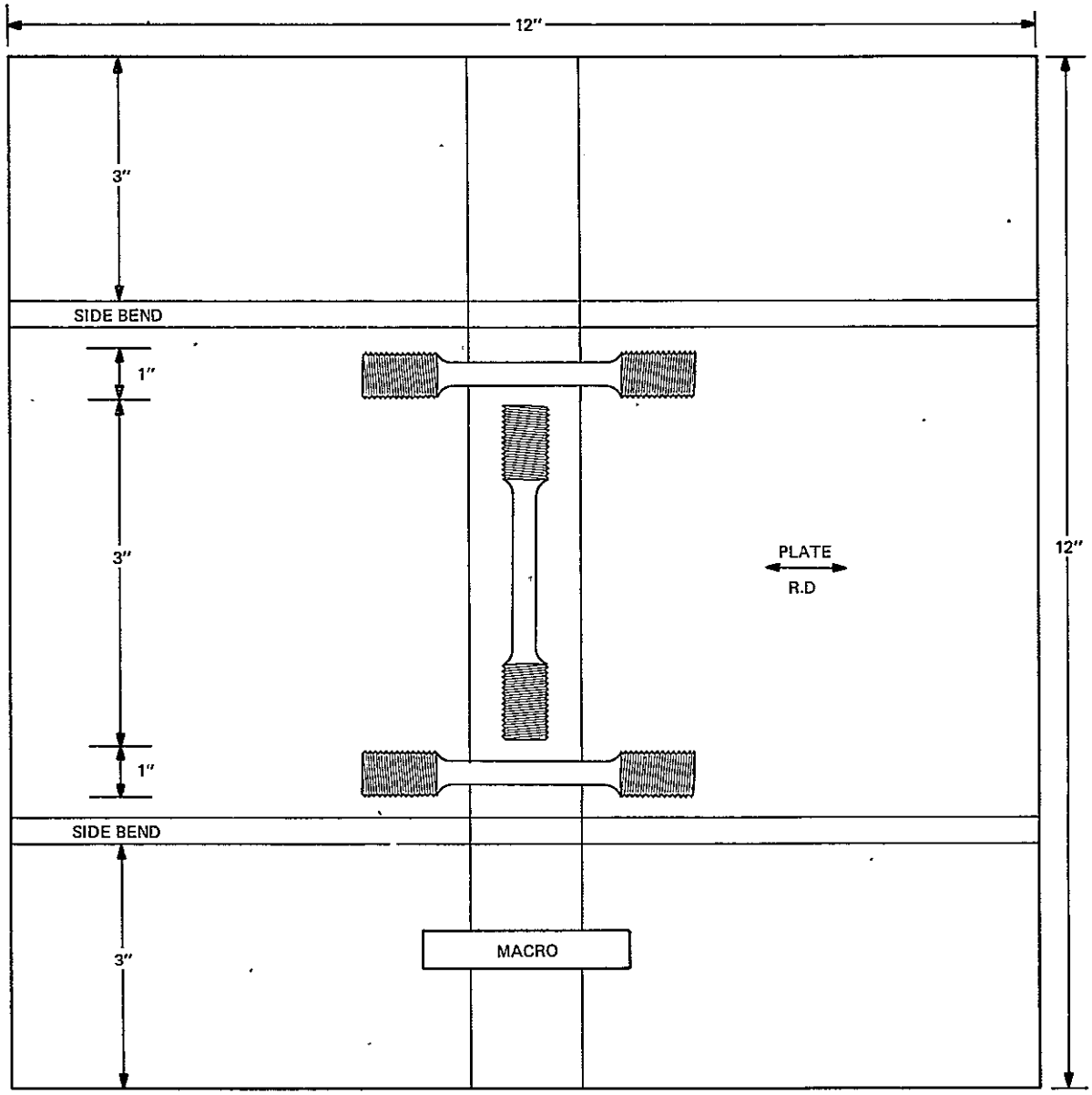

FIGURE 11
TEST SPECIMEN LAY-OUT FOR WELDMENT W3B11

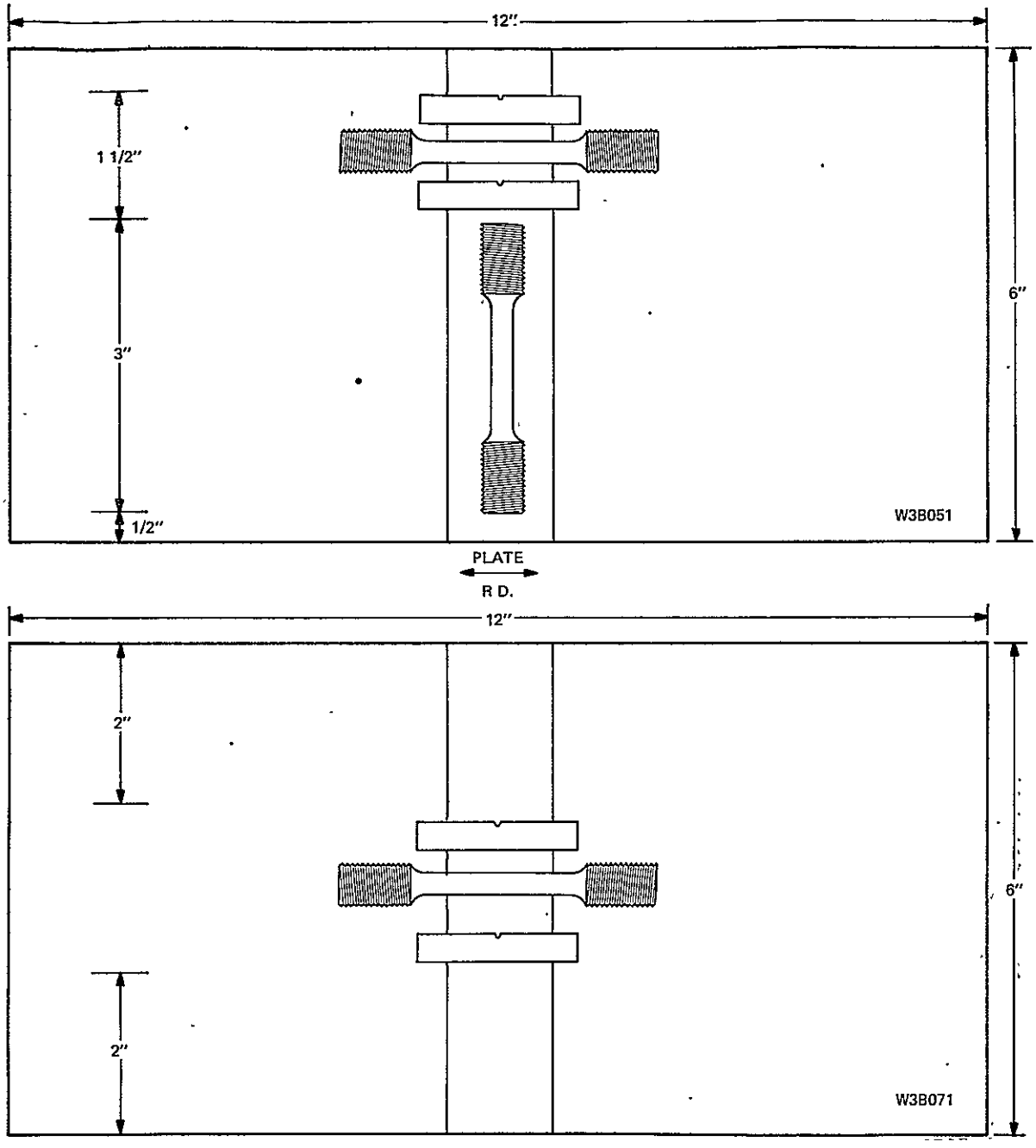

FIGURE 12
FOR SPECIMEN LAY-OUT FOR WELDMENTS W3B051 AND W3B071

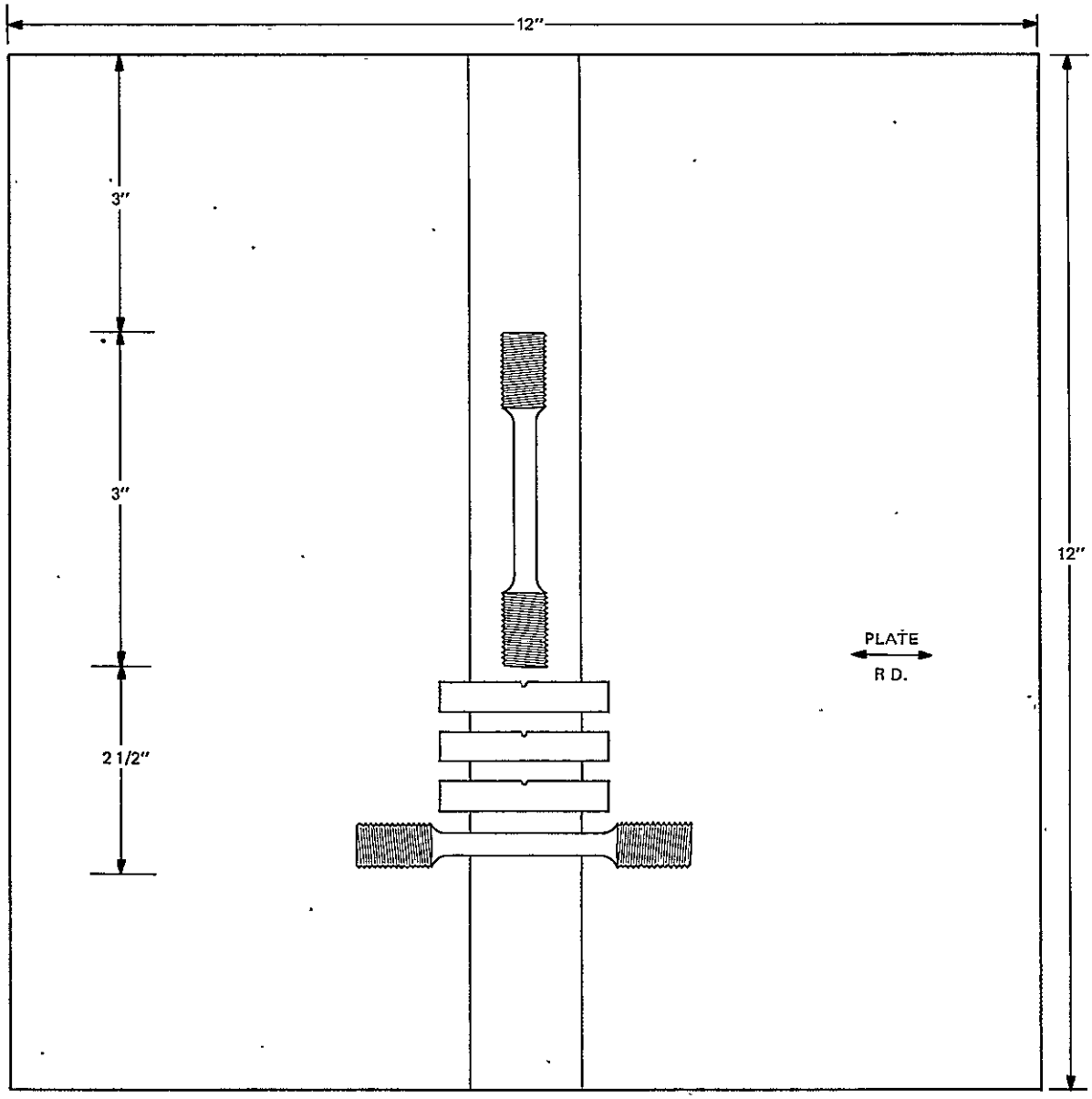

FIGURE 13
TEST SPECIMEN LAY-OUT FOR WELDMENT W3B30

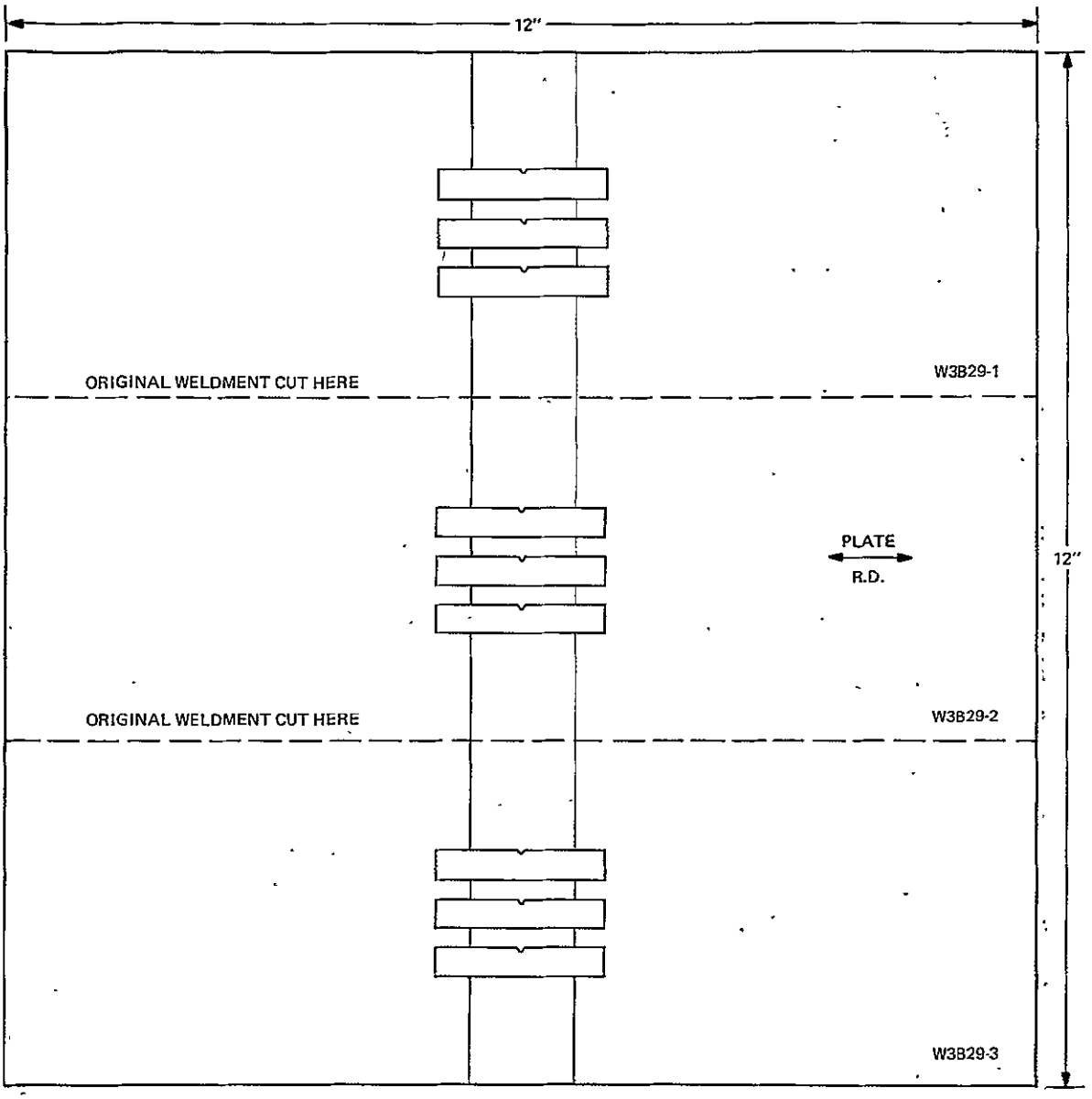

FIGURE-14

TEST SPECIMEN LAY-OUT FOR WELDMENTS W3B29-1, W3B29-2 AND W3B29-3

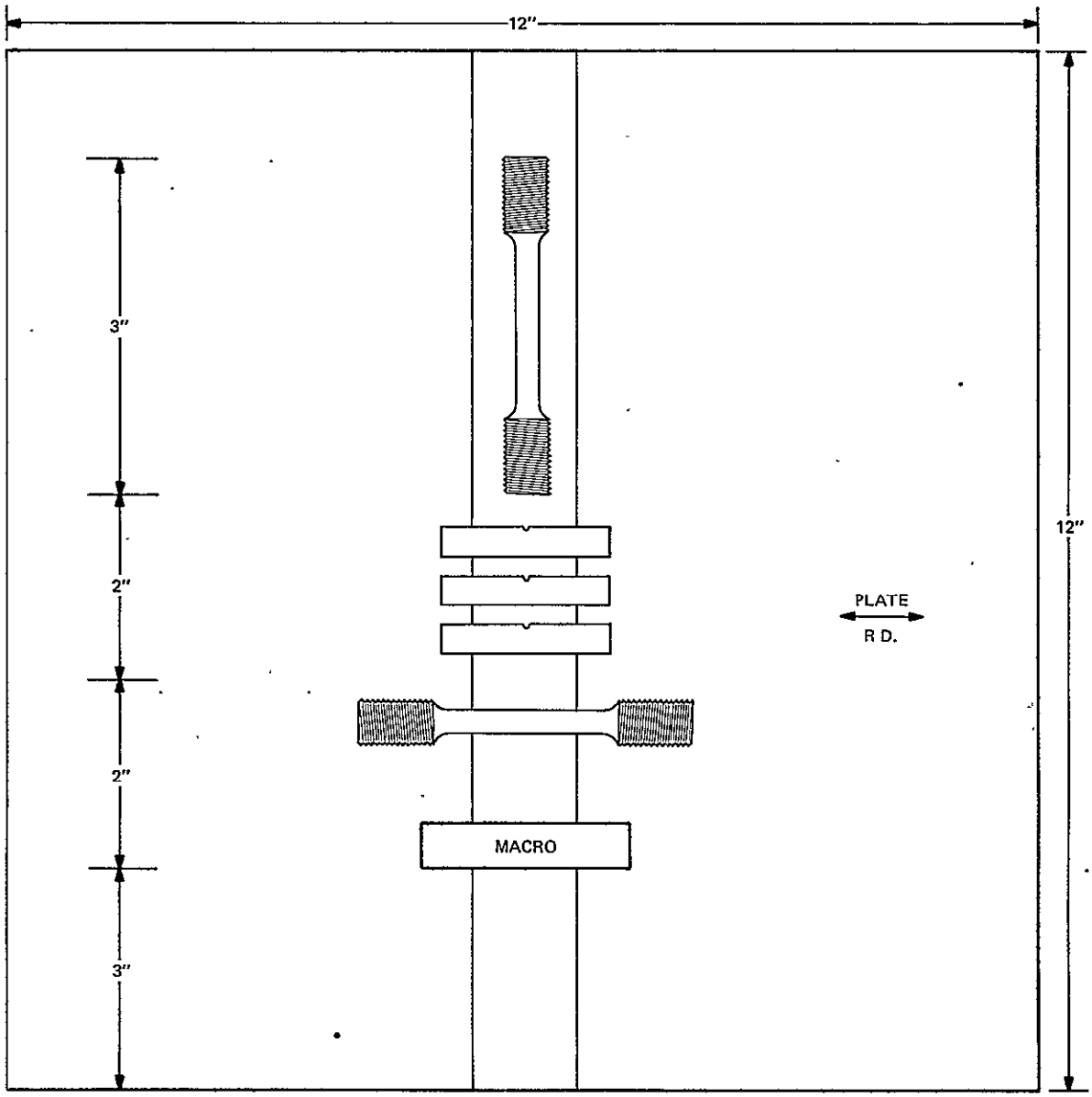

FIGURE 15
TEST SPECIMEN LAY-OUT FOR WELDMENTS W3B27 AND W3B31

FIGURE 16
WELDING EQUIPMENT SET-UP USED TO FABRICATE TASK III WELD TEST PANELS

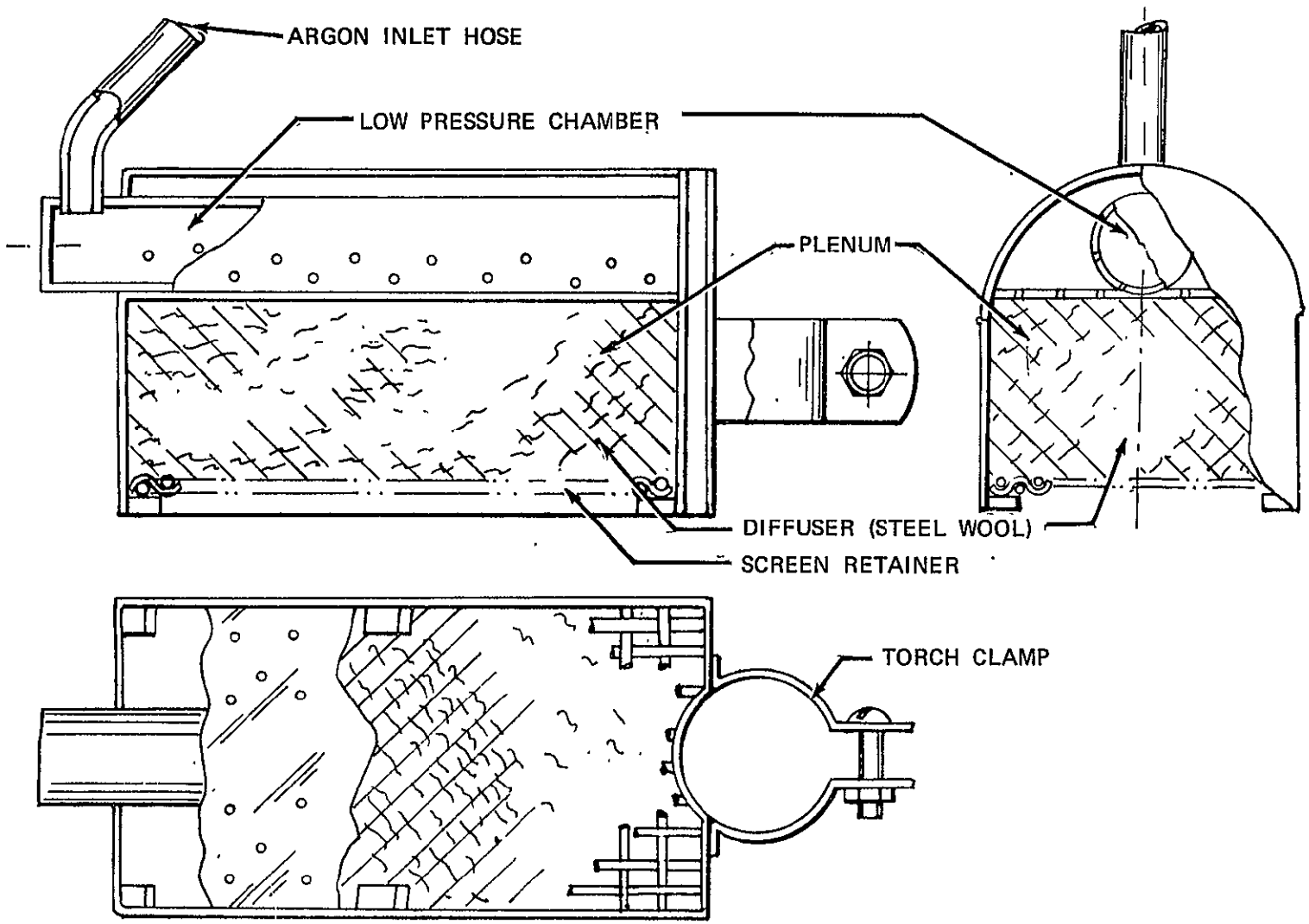

FIGURE 17
AUXILIARY TRAILING SHIELD USED FOR WELDING TEST PANELS AND VESSELS

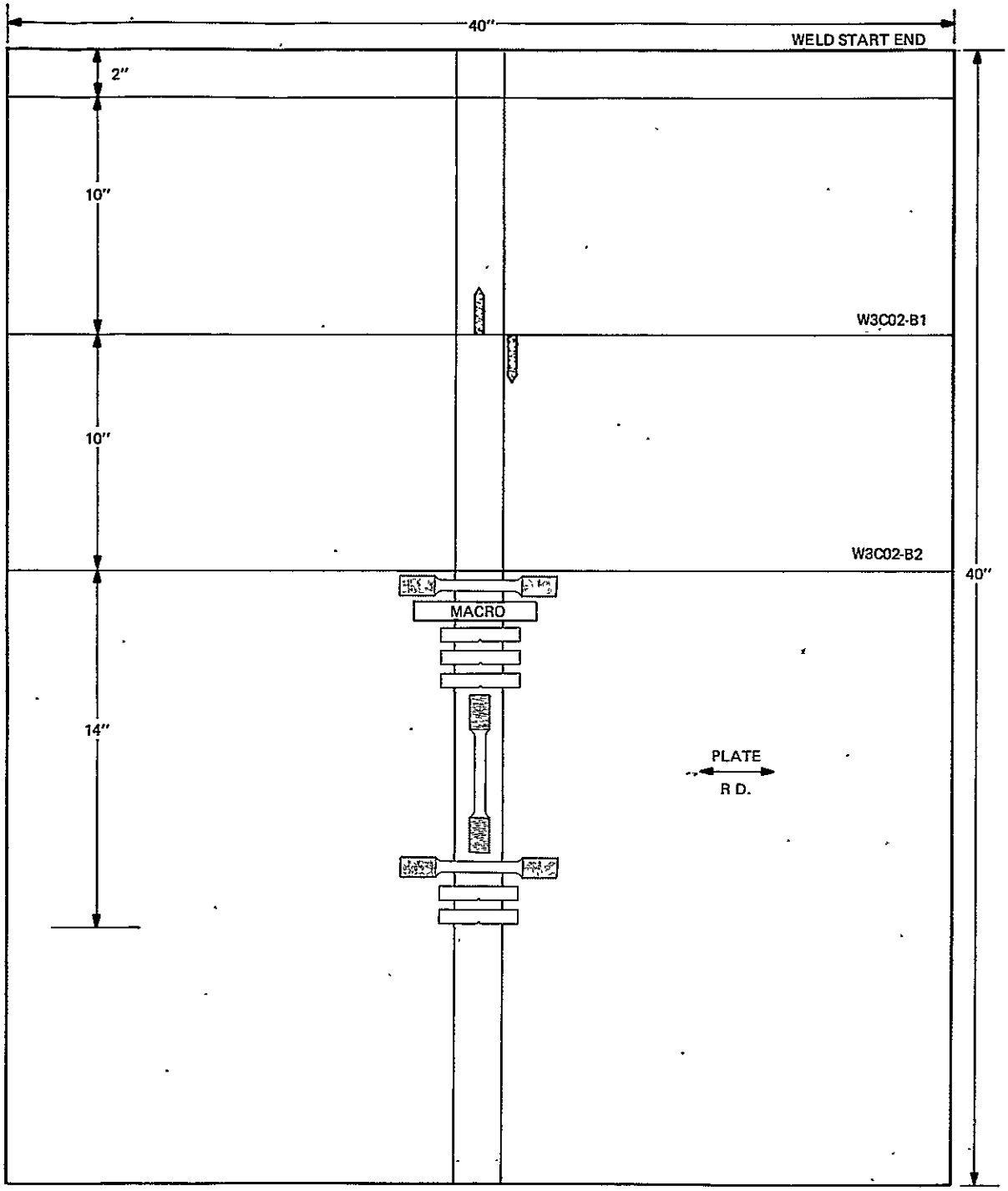

FIGURE 18
TEST SPECIMEN LAY-OUT FOR PANEL W3C02

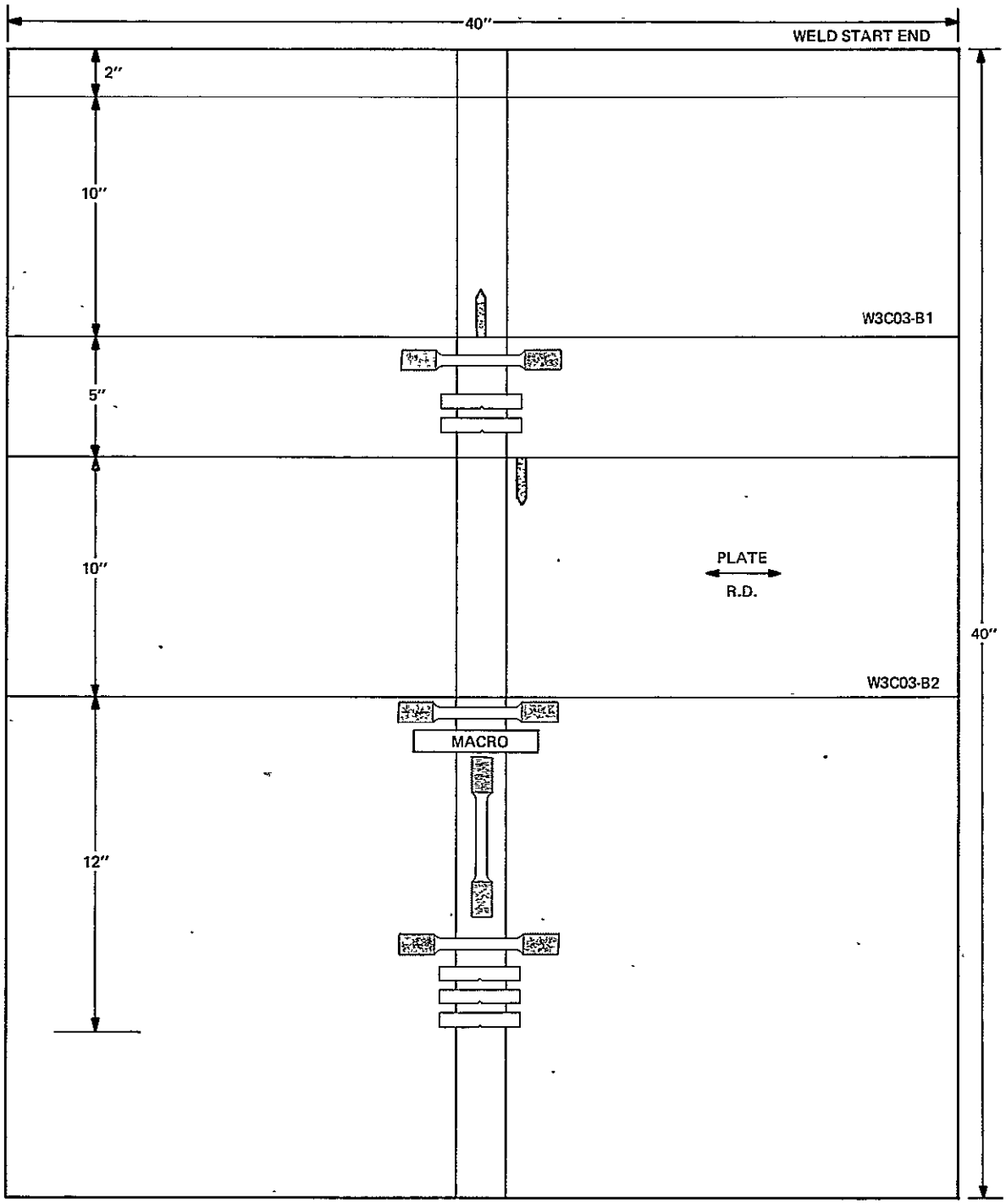

FIGURE 19
TEST SPECIMEN LAY-OUT FOR PANEL W3C03

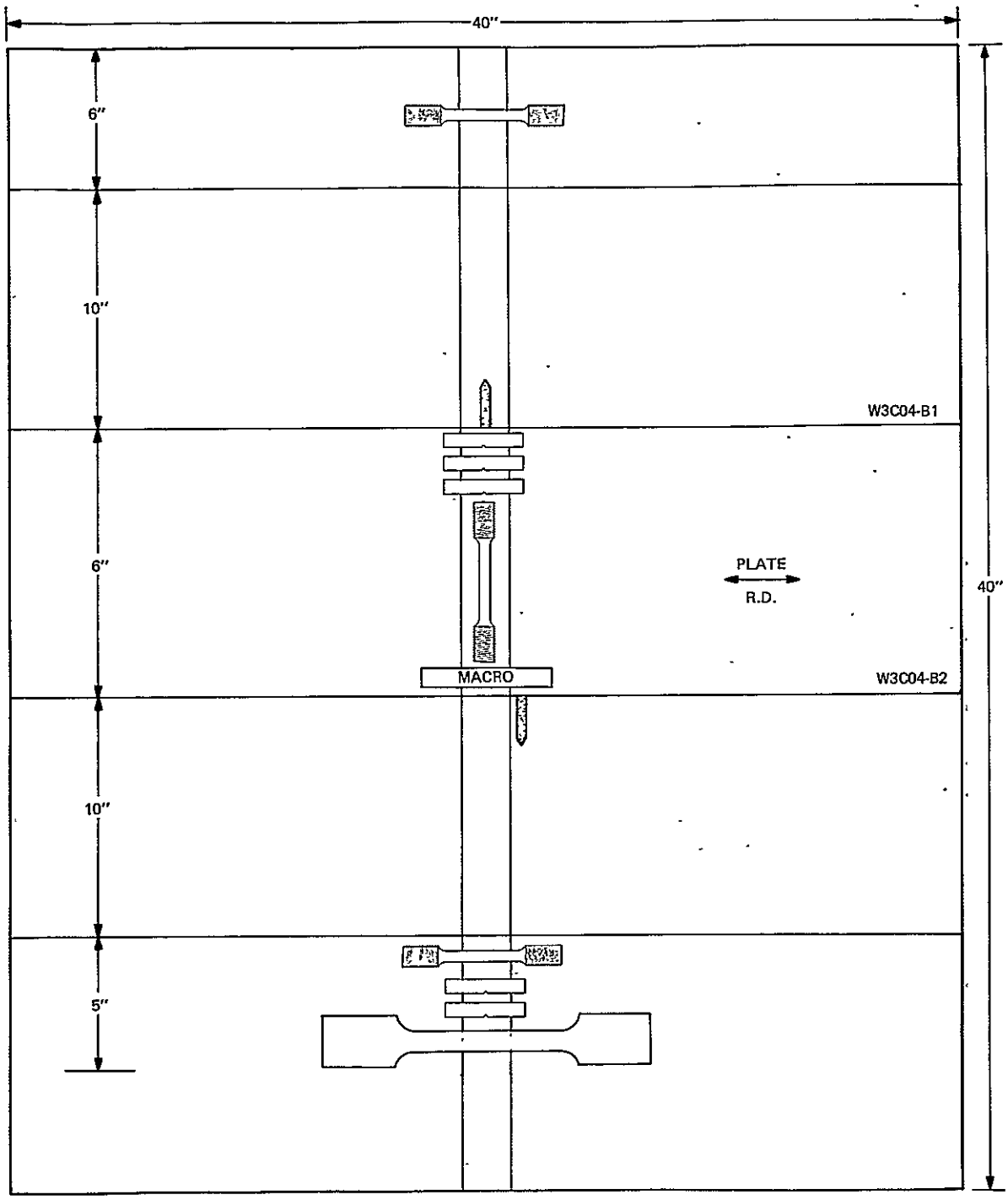

FIGURE 20
TEST SPECIMEN LAY-OUT FOR PANEL W3C04

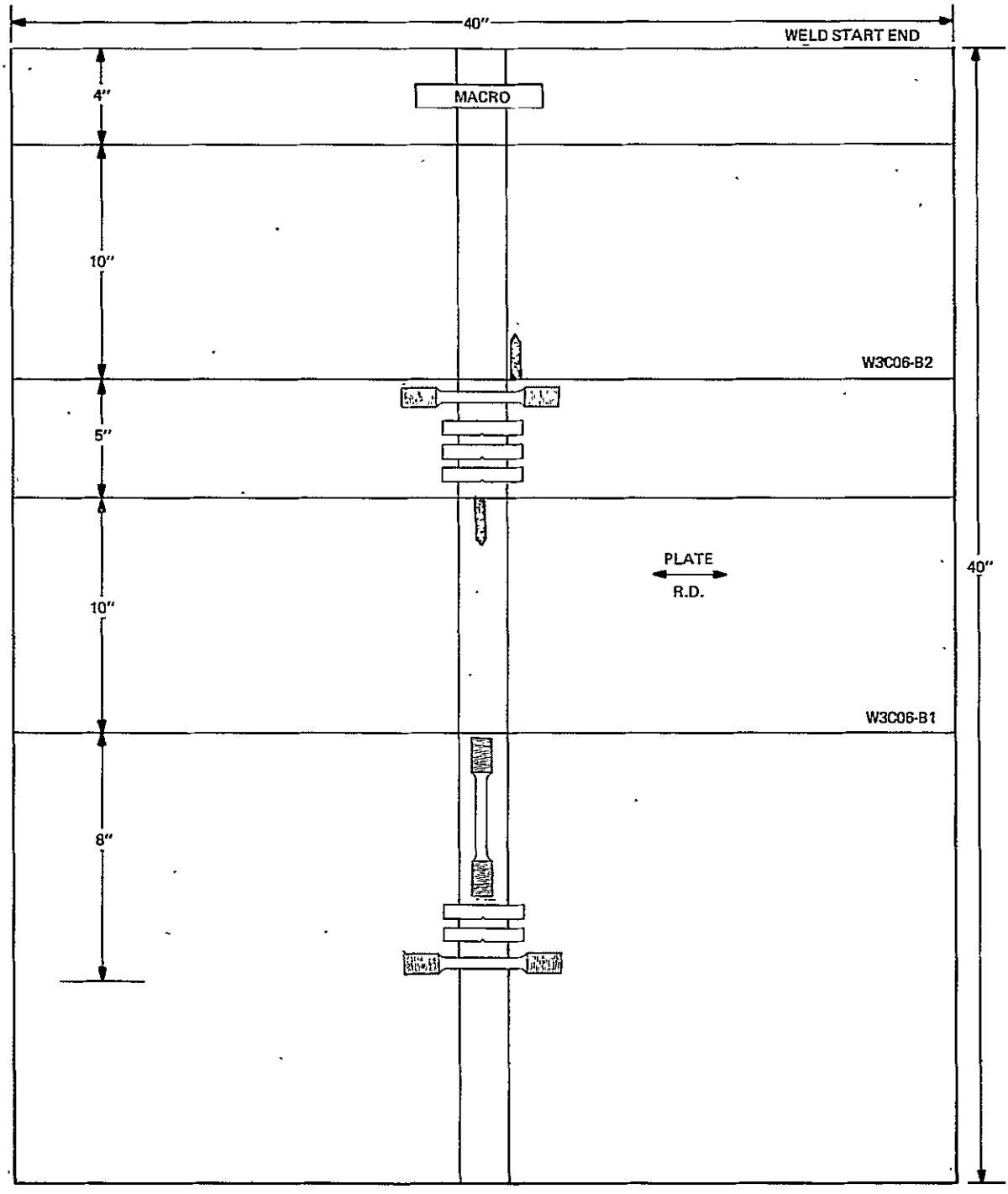

FIGURE 21
TEST SPECIMEN LAY-OUT FOR PANEL W3C06

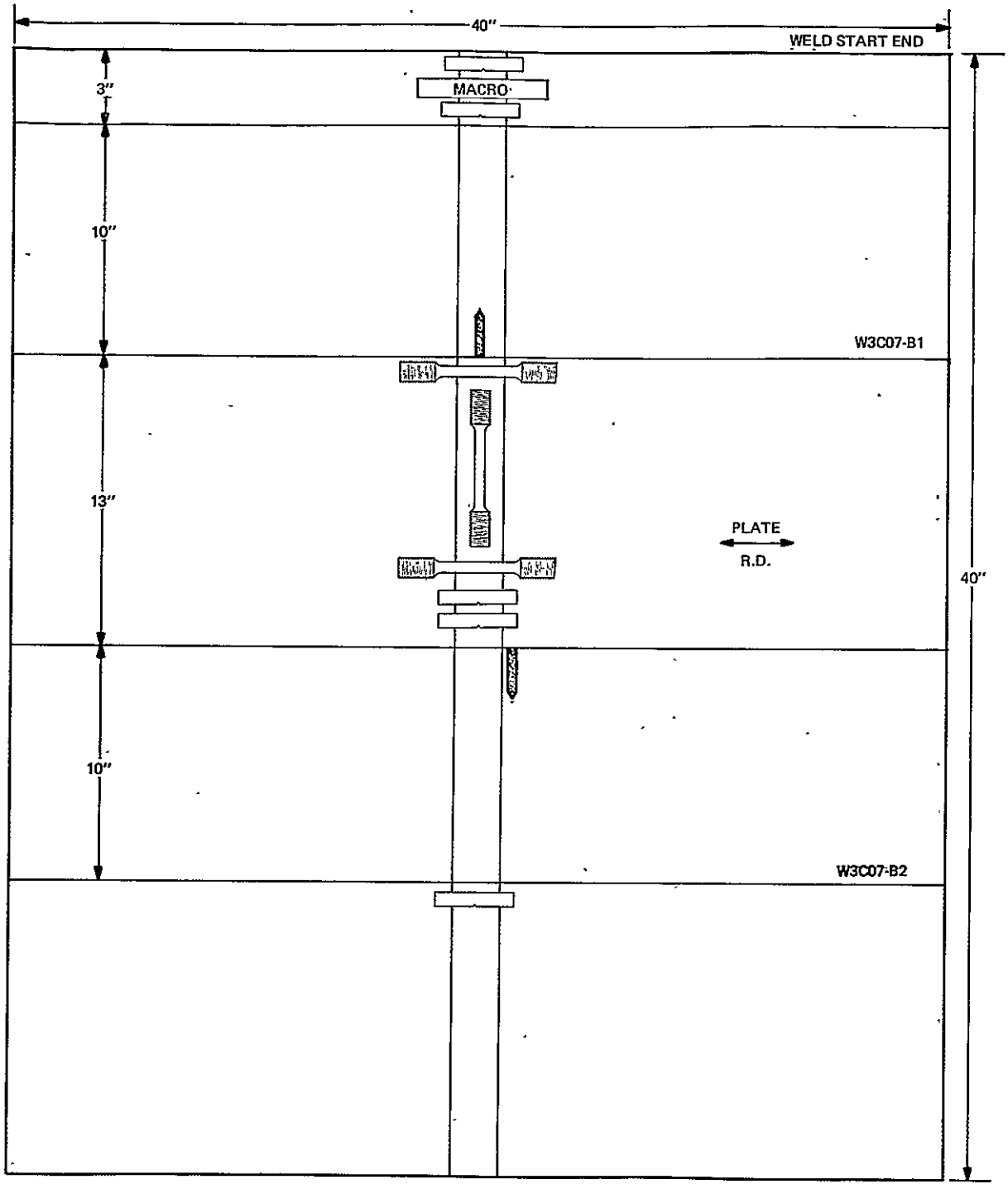

FIGURE 22
TEST SPECIMEN LAY-OUT FOR PANEL W3C07

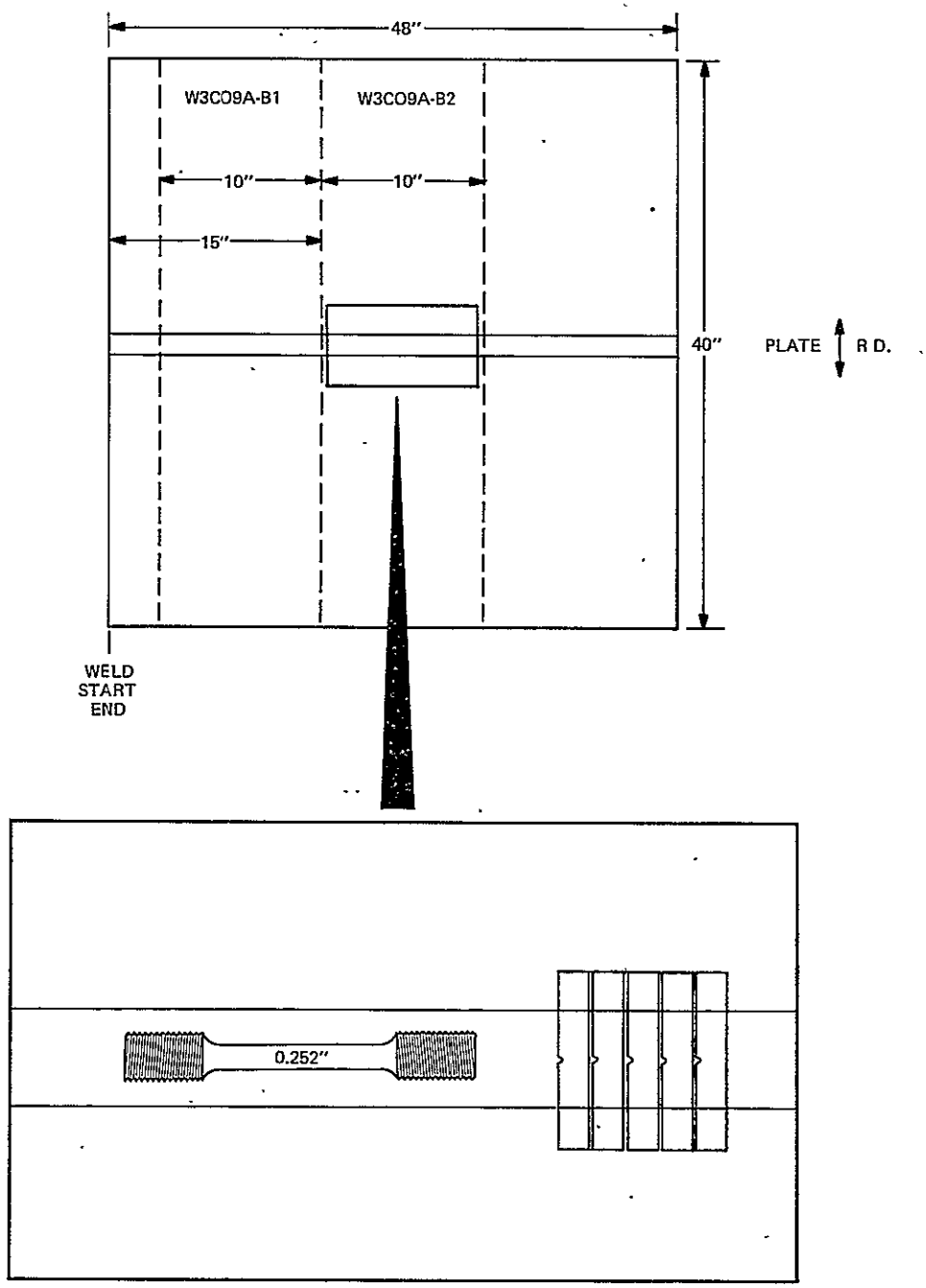

FIGURE 23
TEST SPECIMEN LAYOUT FOR PANEL W3C09A

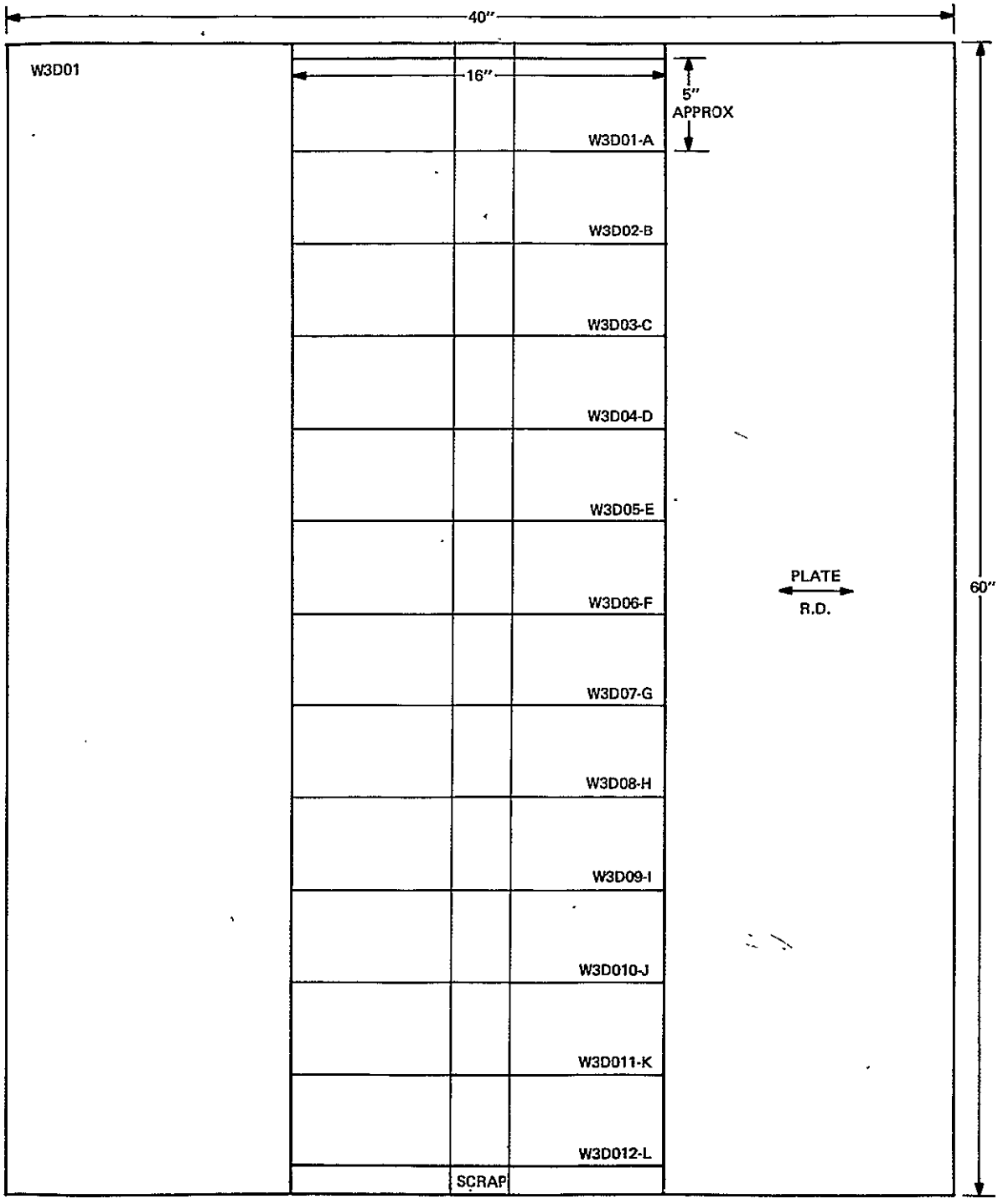

FIGURE 24
LOCATION OF WELDMENT AGING STUDY TEST PIECES, PANEL NO. W3D01

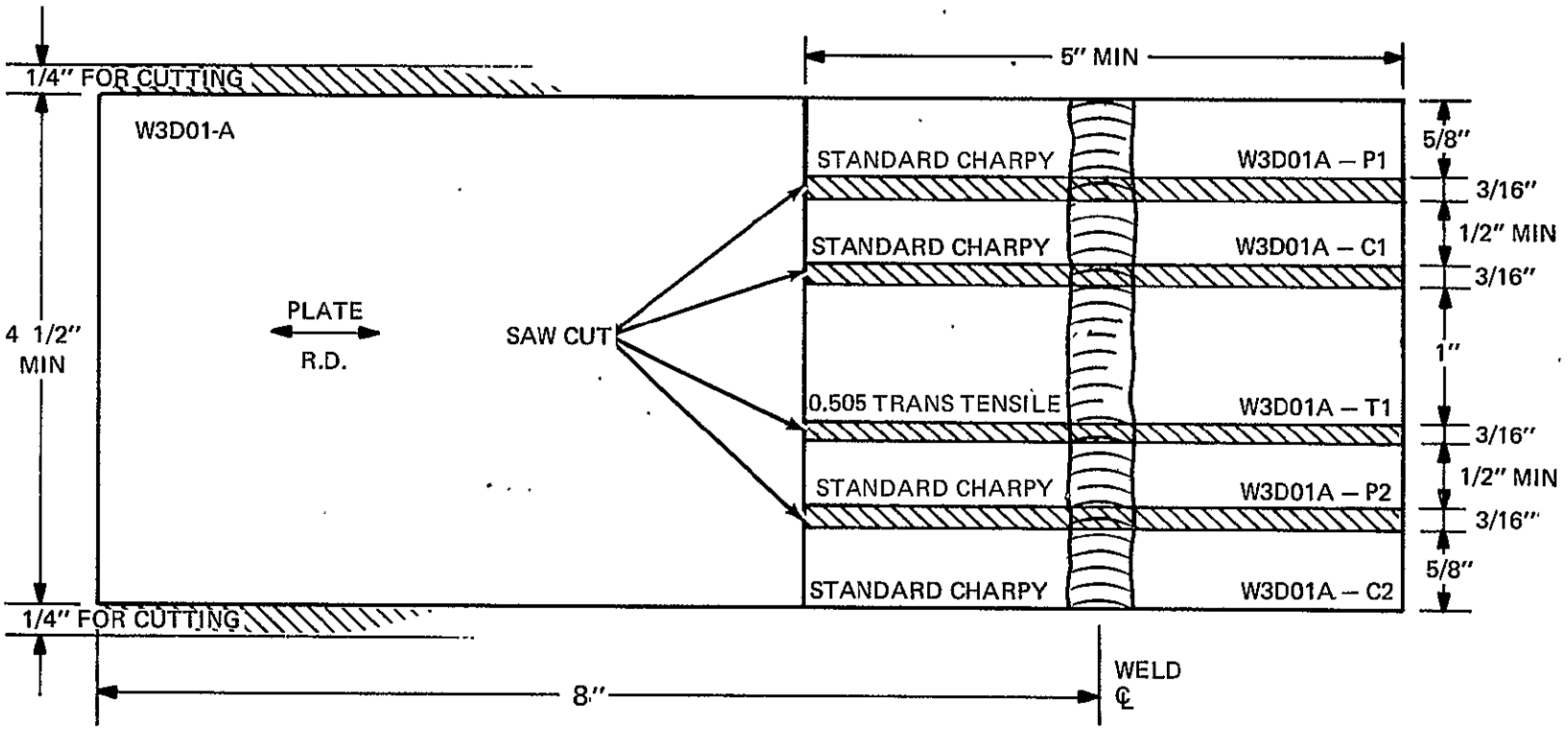

FIGURE 25

TEST SPECIMEN LOCATIONS AND ORIENTATIONS, WELDMENT AGING STUDY TEST PIECES

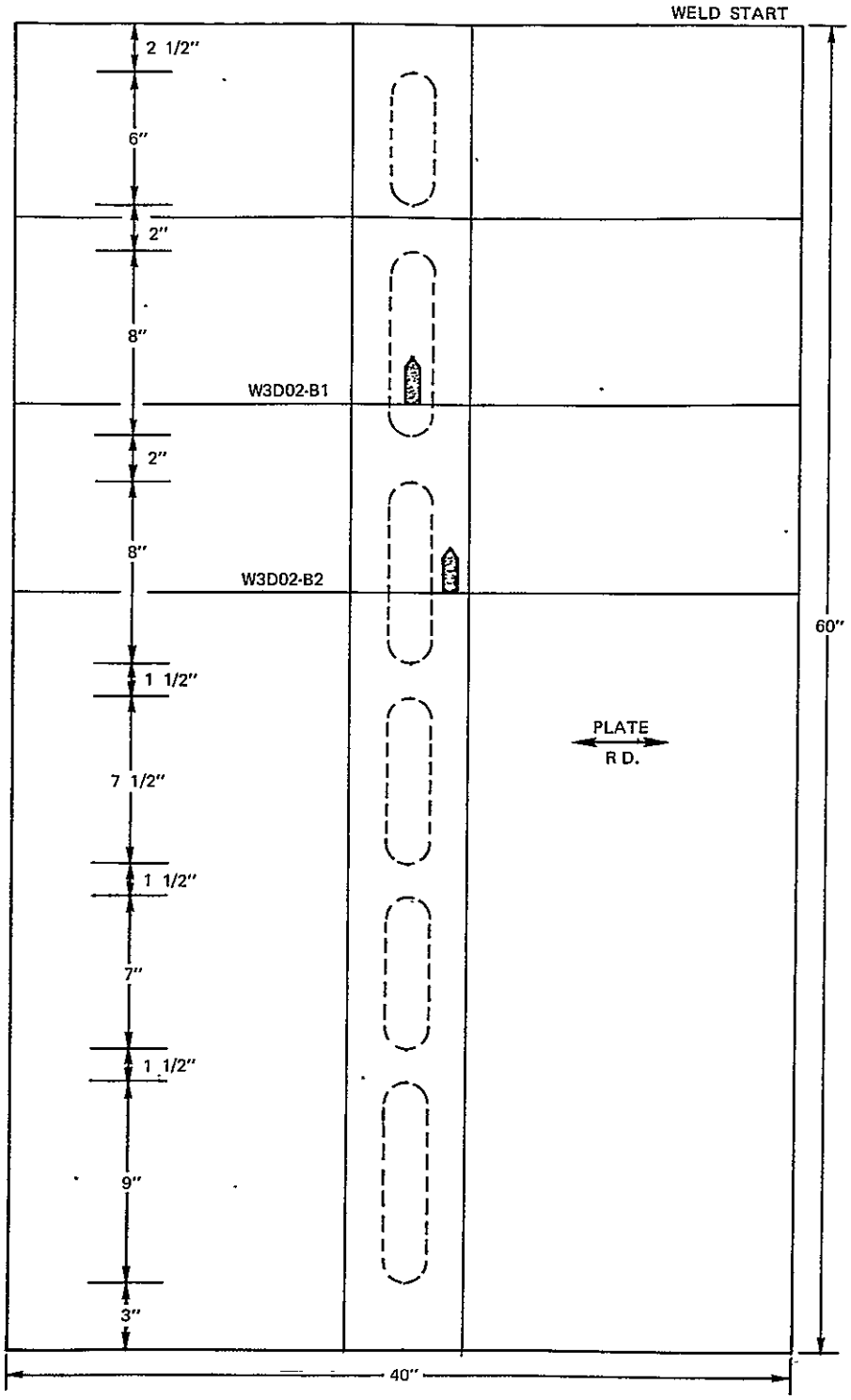

FIGURE 26
AREAS OF SIMULATED REPEATED REPAIRS, PANEL W3D02

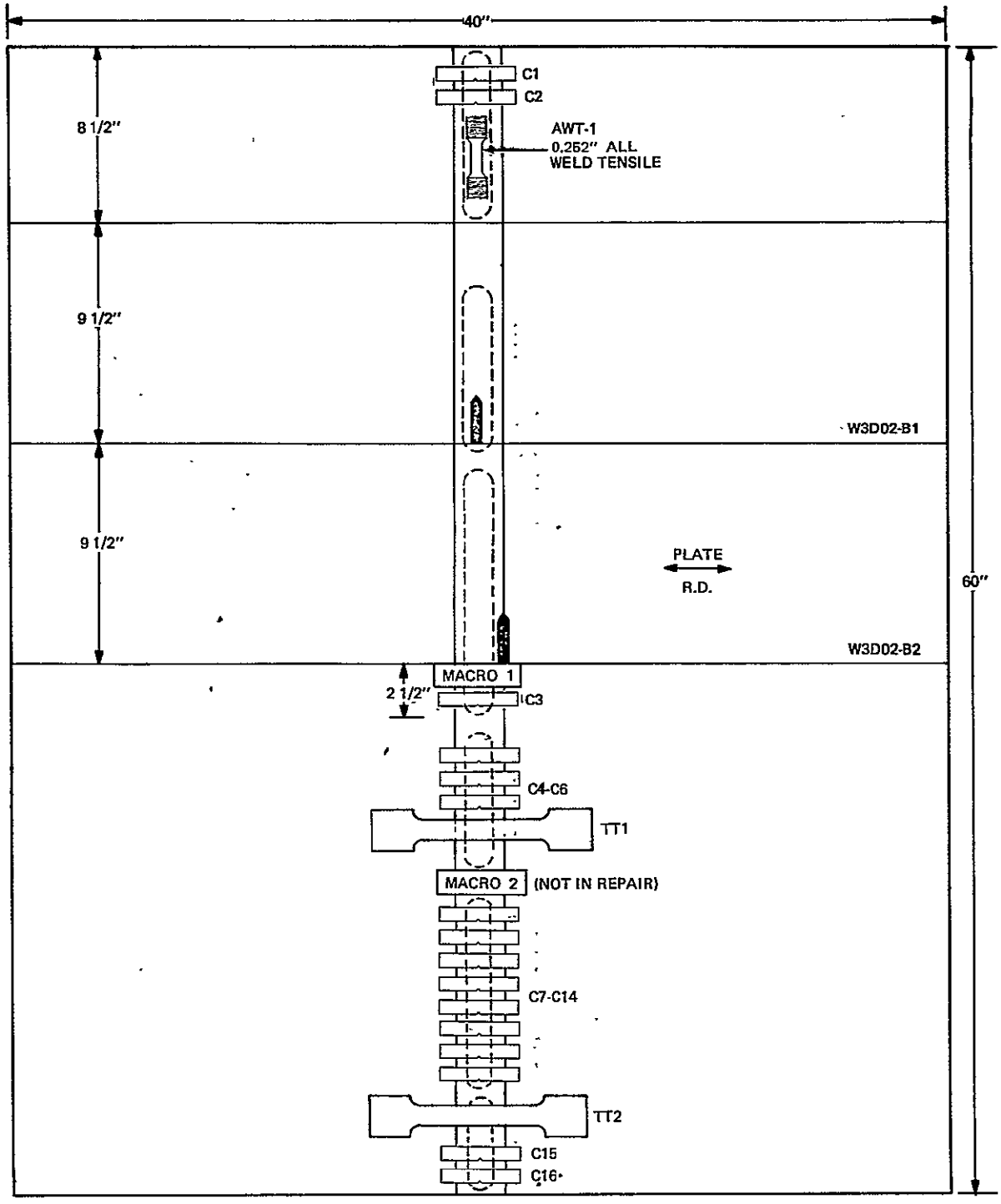

FIGURE 27
TEST SPECIMEN LOCATIONS AND ORIENTATIONS FOR PANEL W3D02

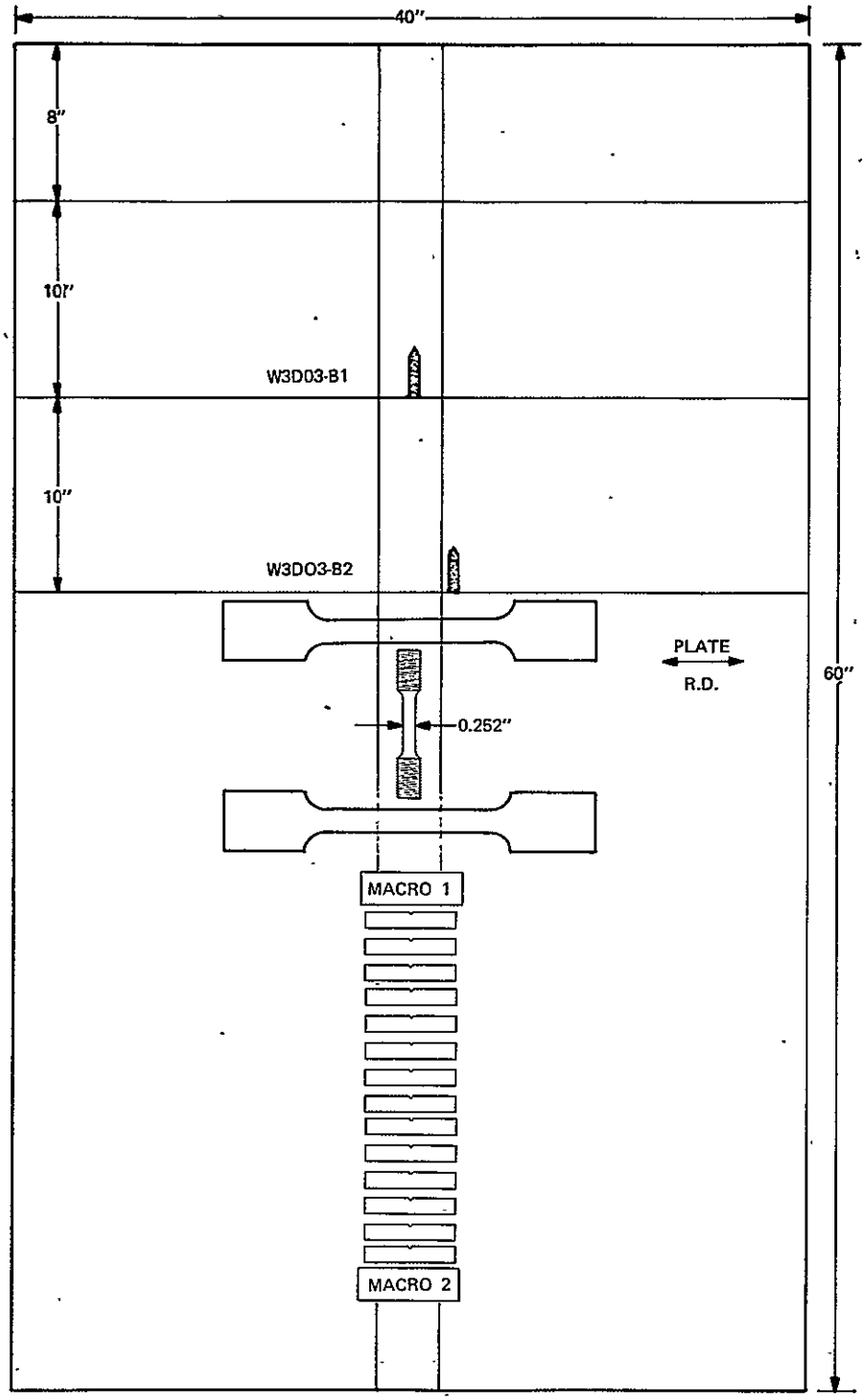

FIGURE 28
TEST SPECIMEN LOCATIONS AND ORIENTATIONS FOR PANEL W3D03

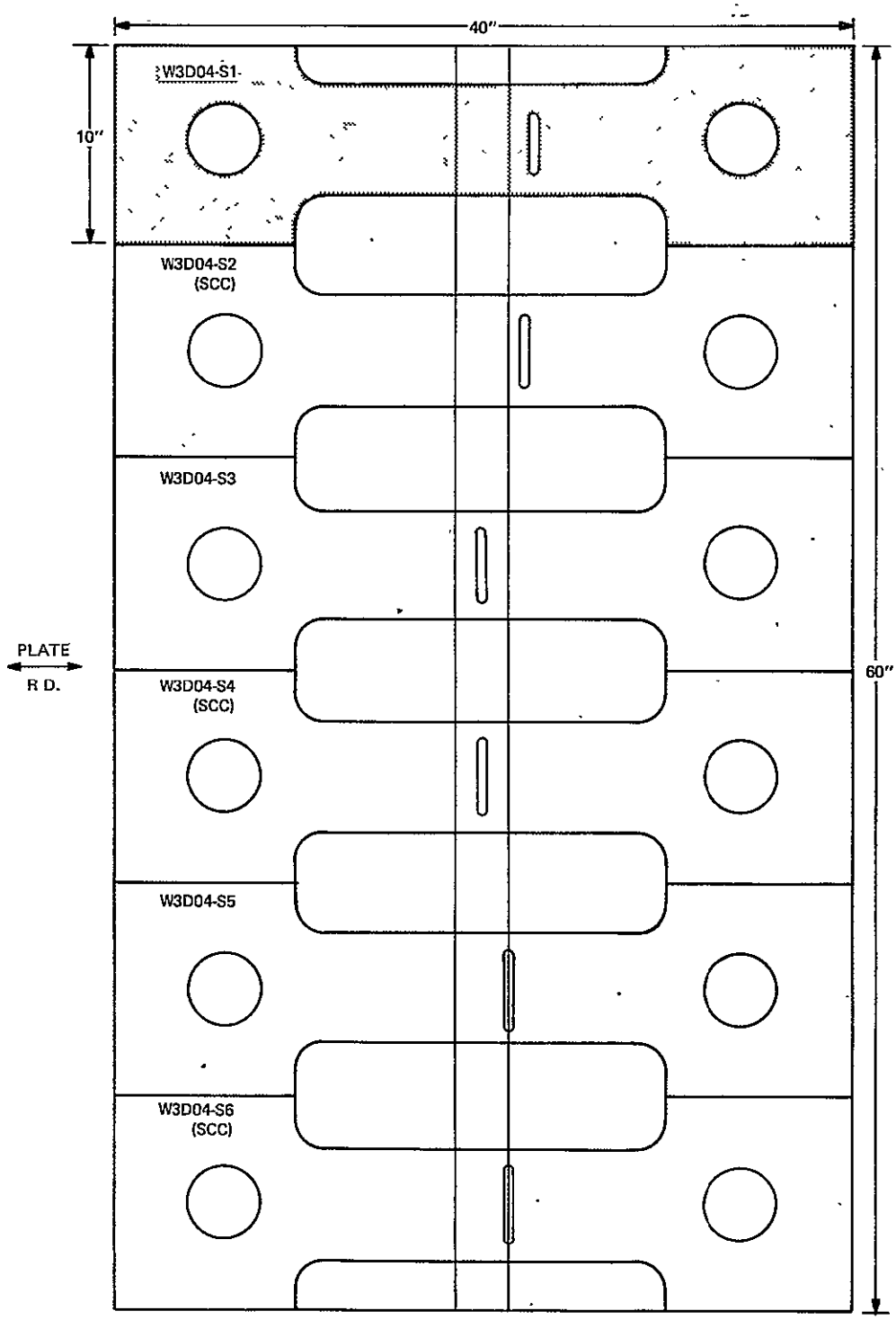

FIGURE 29

TEST SPECIMEN LOCATIONS AND ORIENTATIONS FOR PANEL W3D04

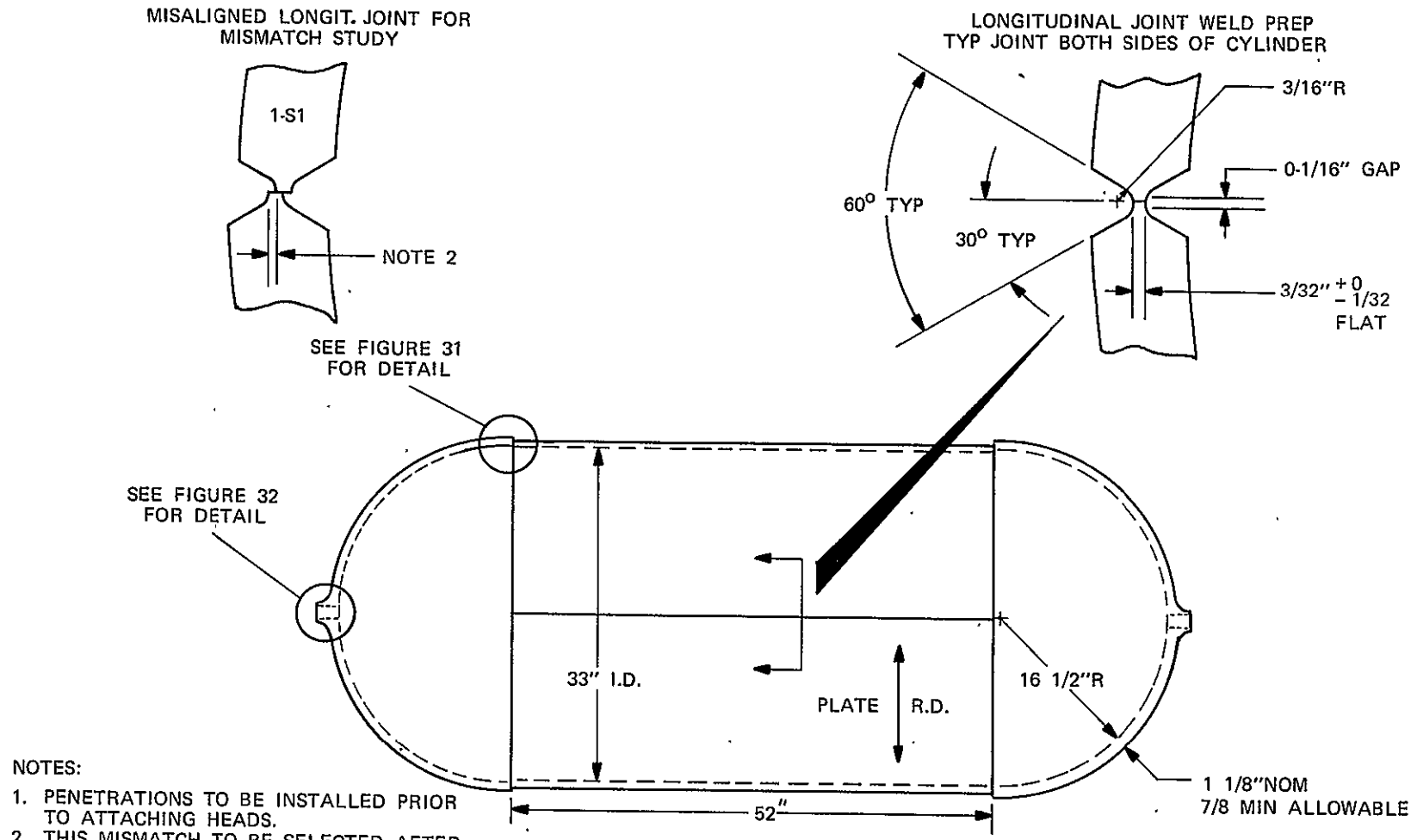

NOTES:

1. PENETRATIONS TO BE INSTALLED PRIOR TO ATTACHING HEADS.
2. THIS MISMATCH TO BE SELECTED AFTER WELD K_Q VALUES HAVE BEEN DETERMINED.
3. MATCH MACHINE EACH HEAD TO MATING CYLINDER. DIMENSIONS TO BE OBTAINED FOLLOWING WELDING OF CYLINDER.

FIGURE 30
GENERAL VESSEL CONFIGURATION AND DESIGN

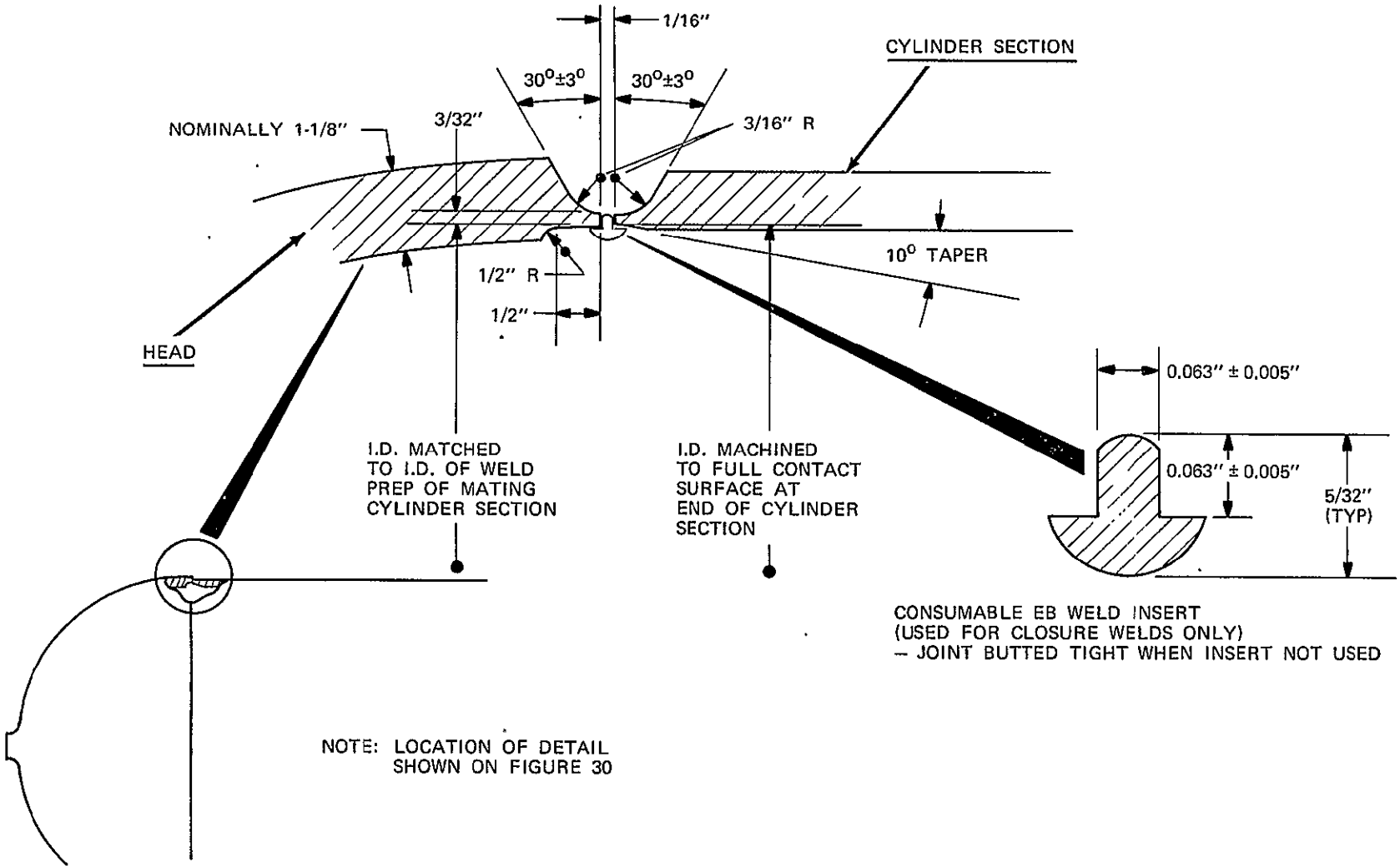

FIGURE 31
GIRTH JOINT WELD PREPARATION DETAILS.

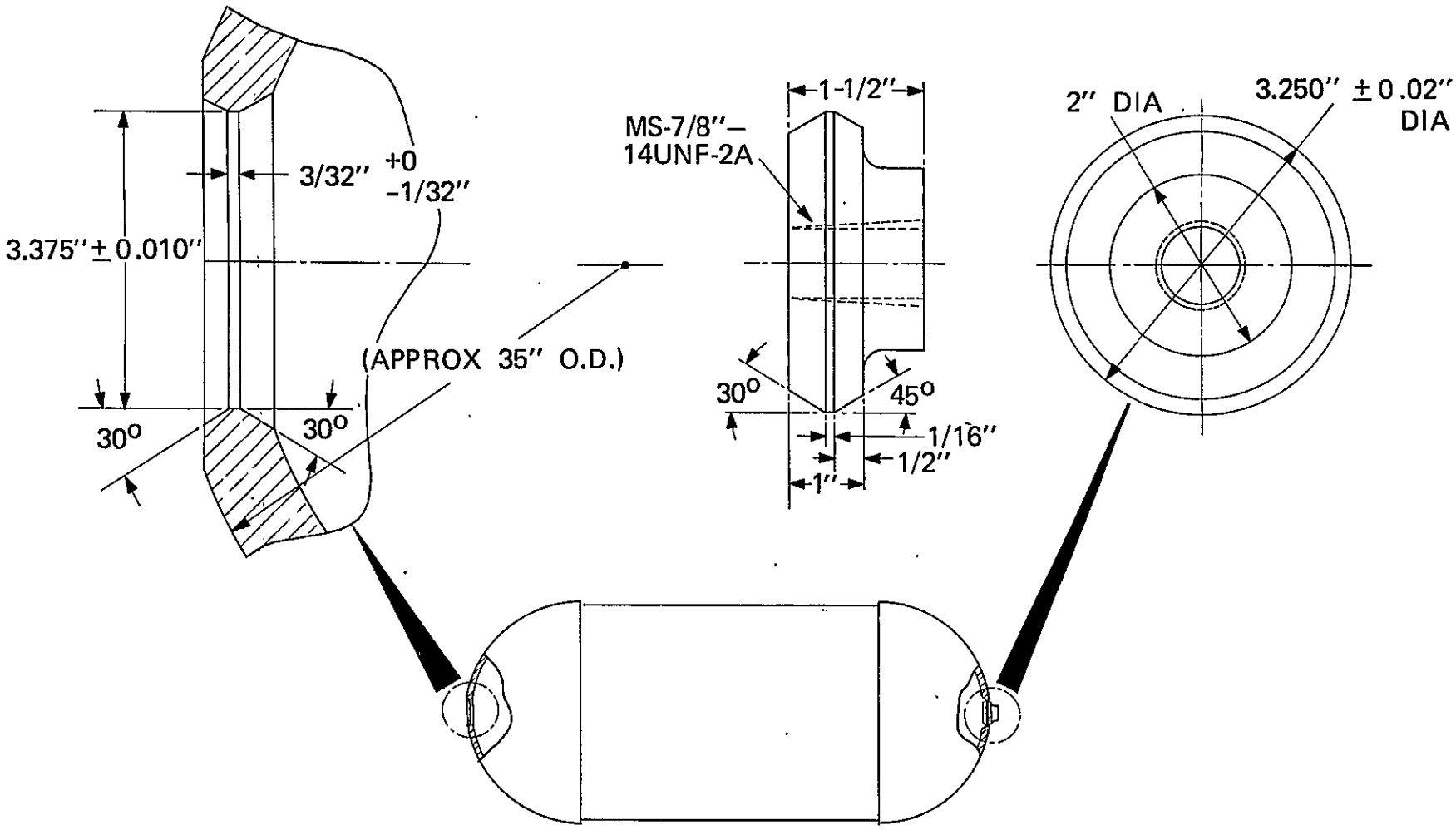

FIGURE 32
HEMISPHERE PIPING PENETRATION JOINT WELD PREPARATION DETAILS

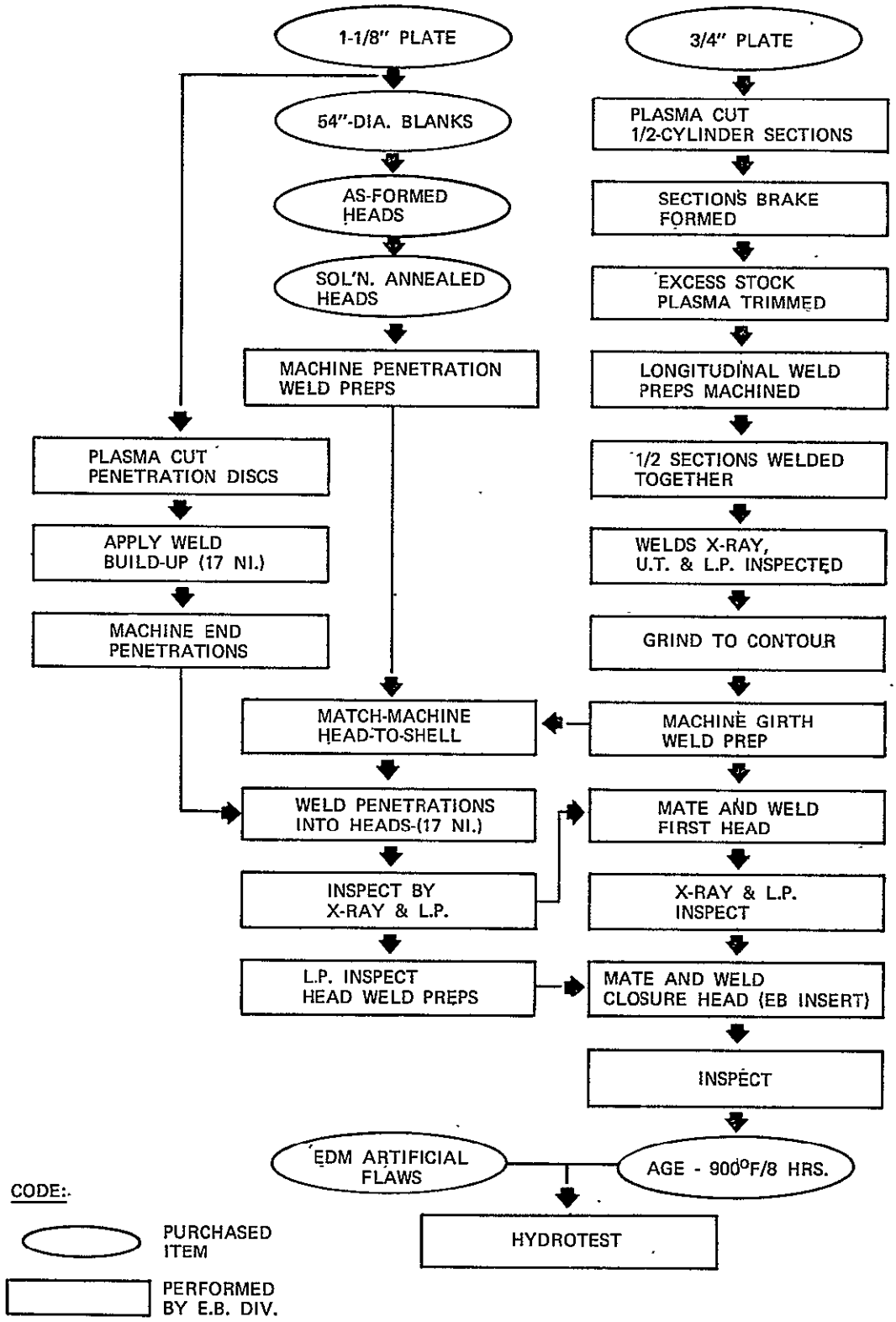

FIGURE 33

FLOW CHART OF MAJOR STEPS IN VESSEL FABRICATION

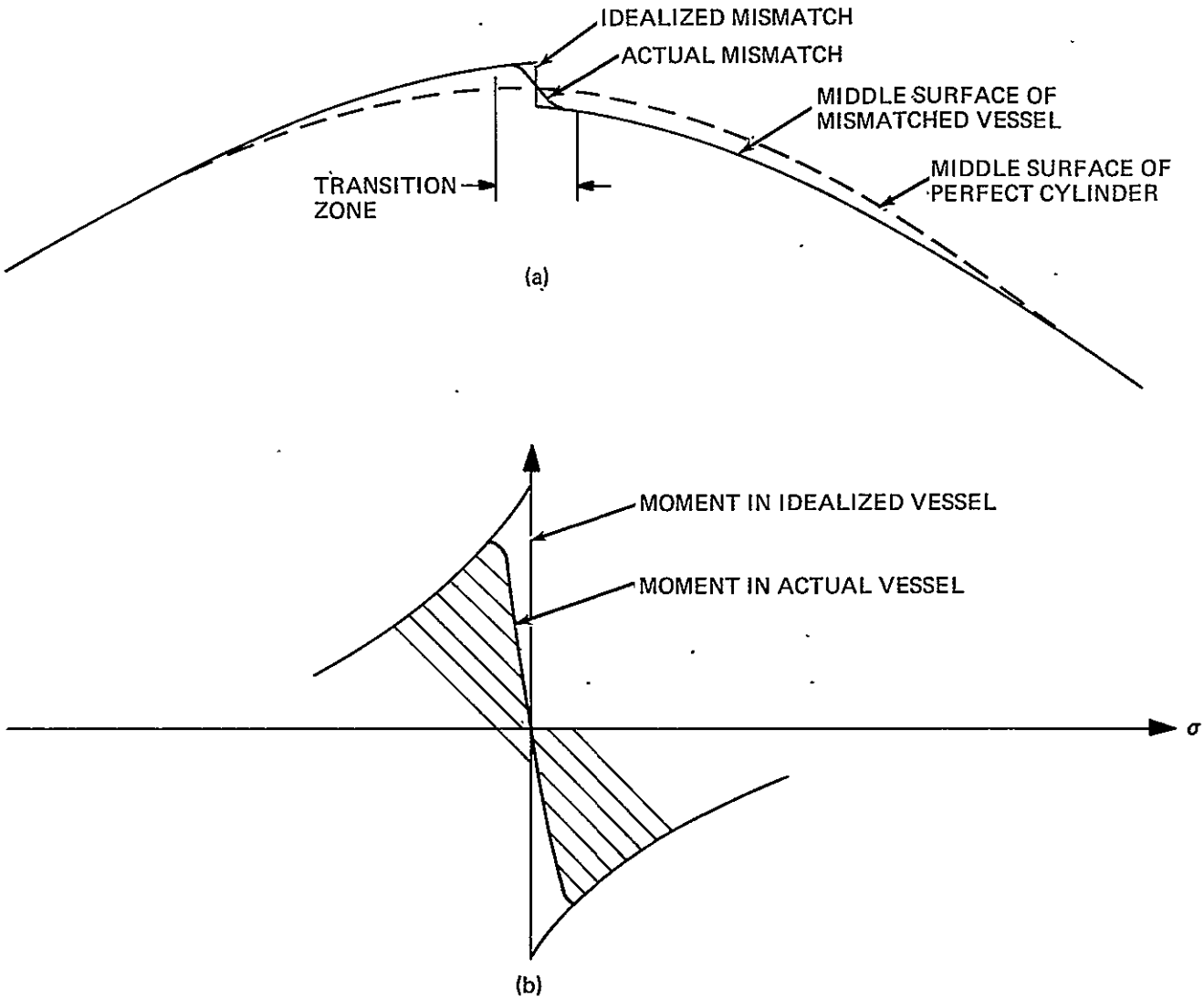

FIGURE 34
COMPARISON OF ACTUAL AND IDEALIZED MISMATCHED VESSELS

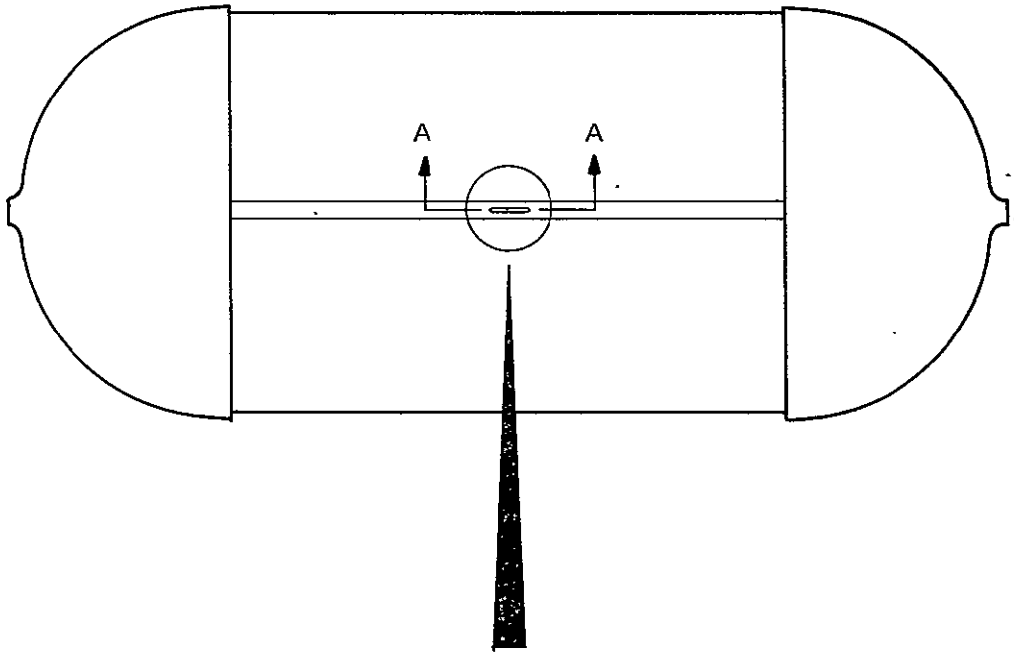

ELECTRO-DISCHARGE MACHINED FLAW IN
ONE OF VESSEL LONGITUDINAL SEAM WELDS

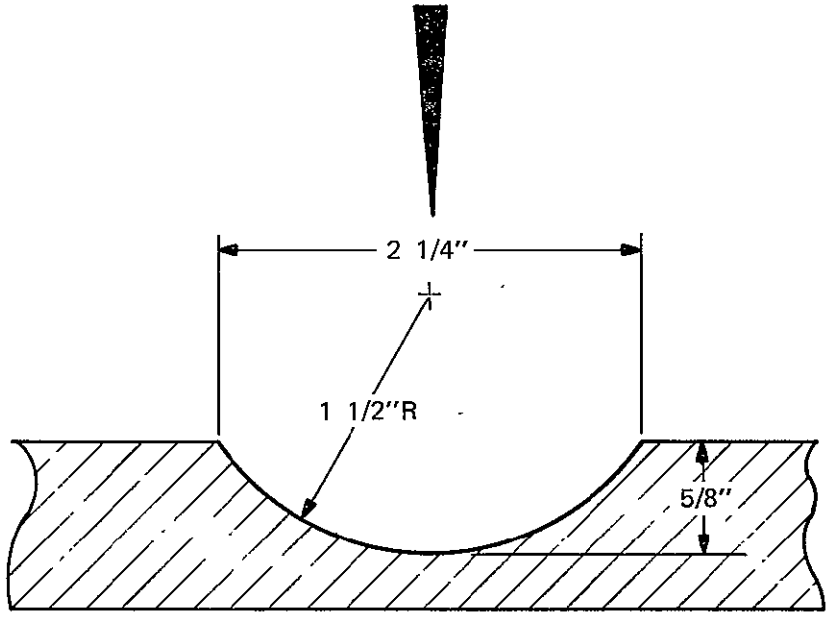

SECTION AA

FIGURE 35
VESSEL EDM FLAW DETAILS

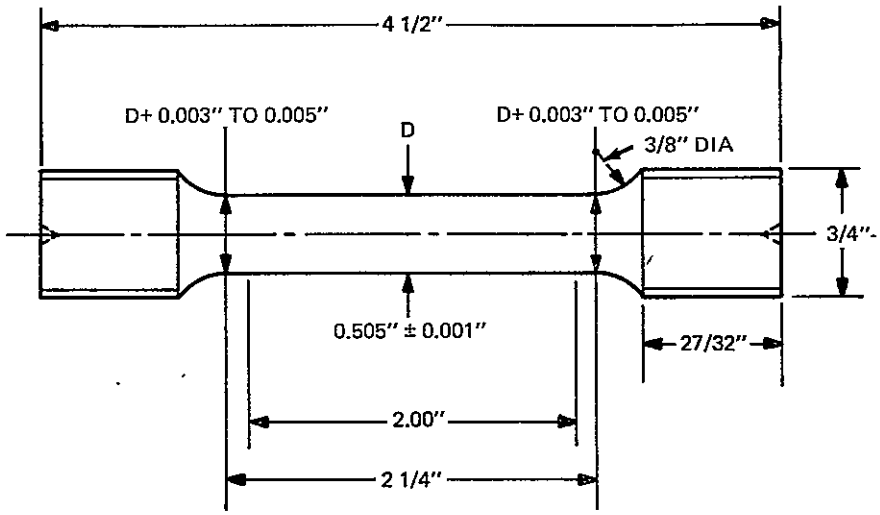

FIGURE 36
0.505 TEST SPECIMEN

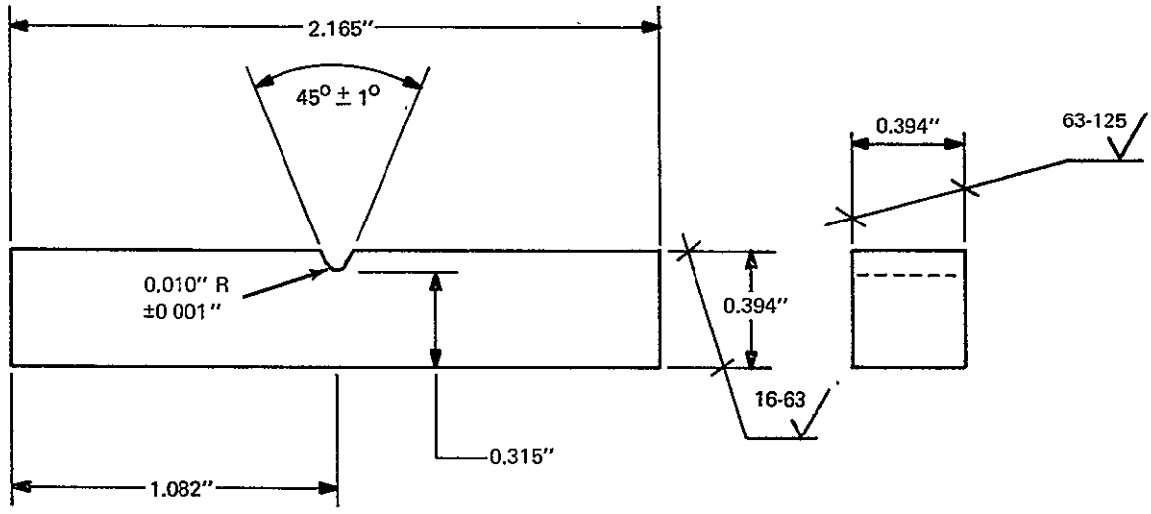

FIGURE 37
CHARPY V-NOTCH IMPACT SPECIMEN

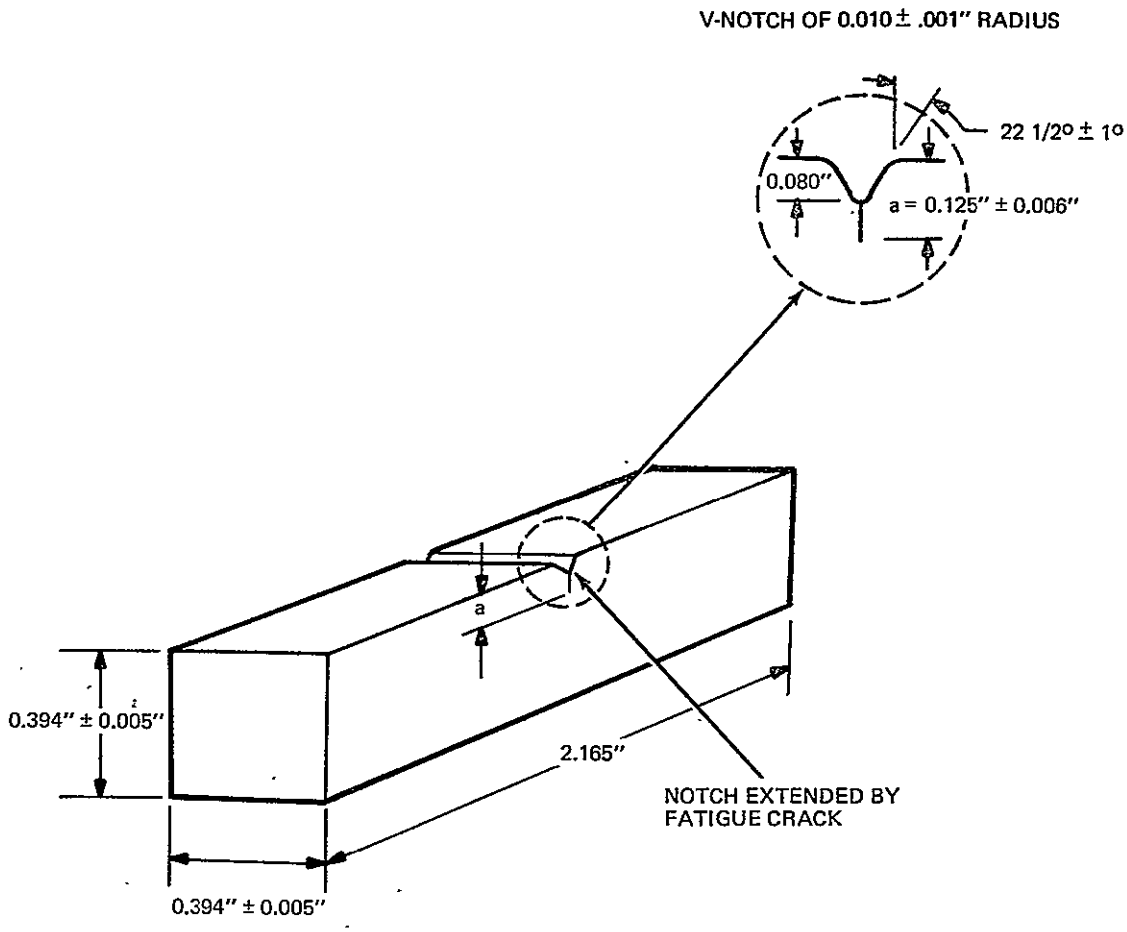

FIGURE 38
FATIGUE PRECRACKED CHARPY IMPACT SPECIMEN

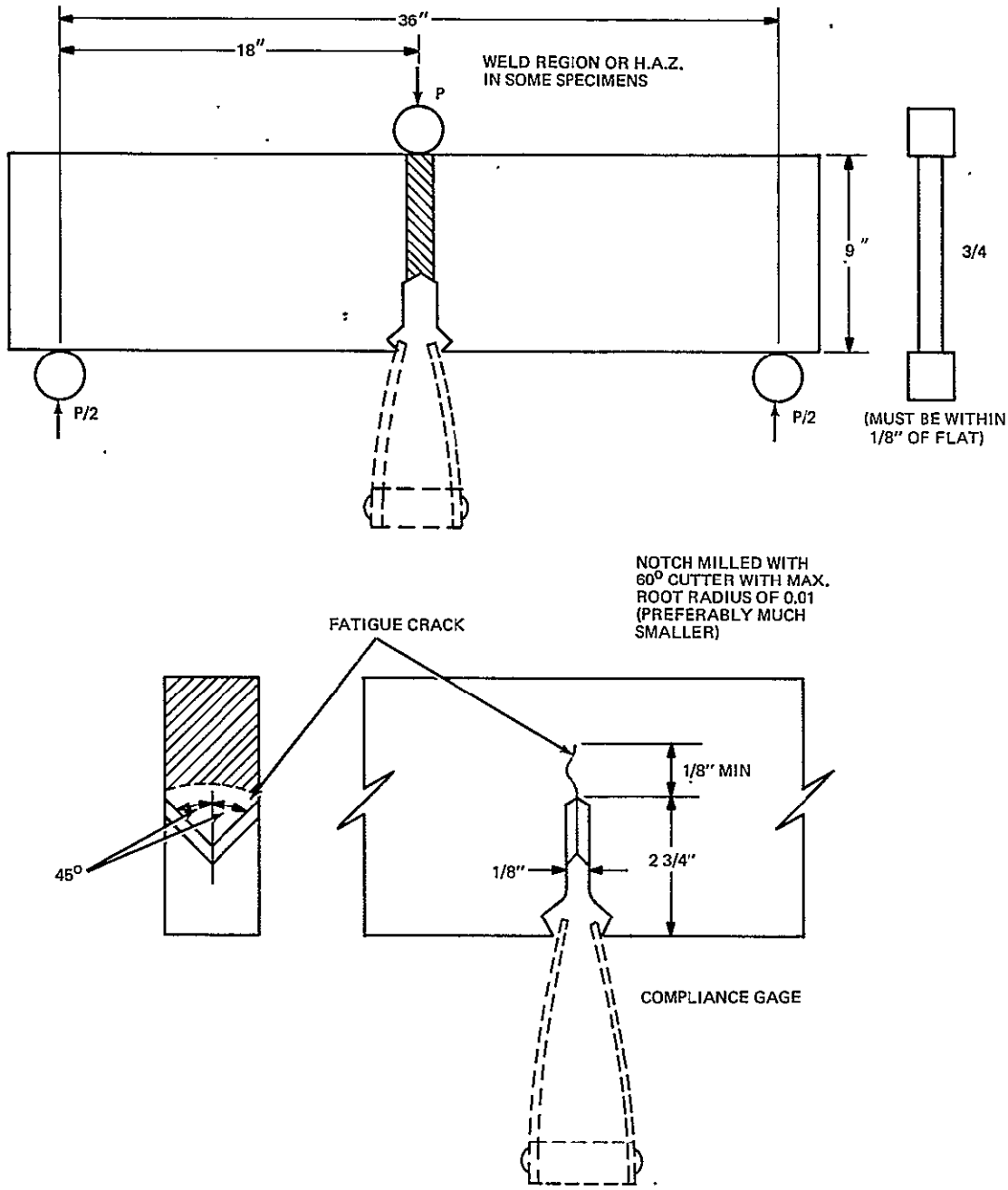

FIGURE 39
BEND TEST SPECIMEN

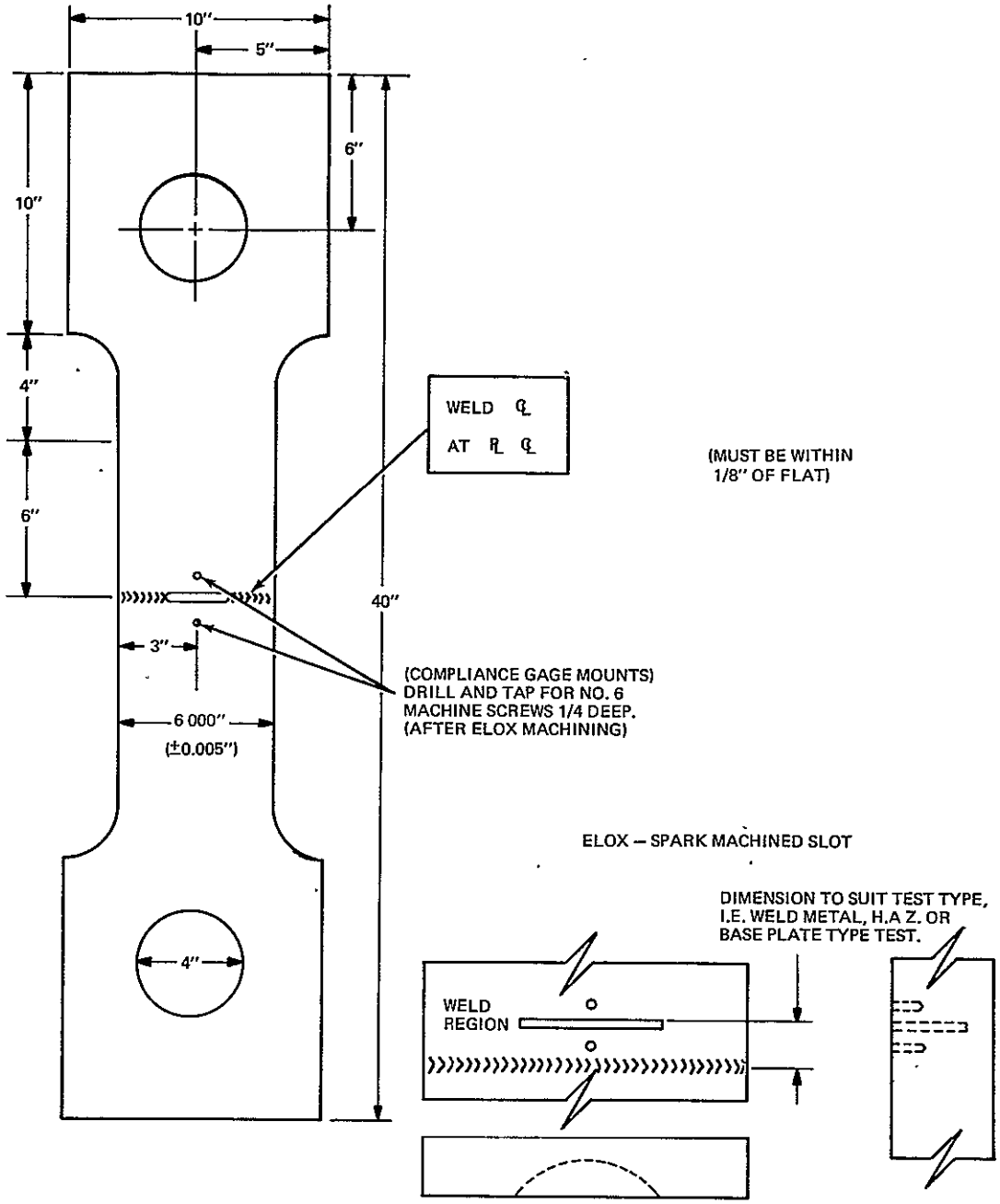

FIGURE 40
SURFACE FLAW TEST SPECIMEN

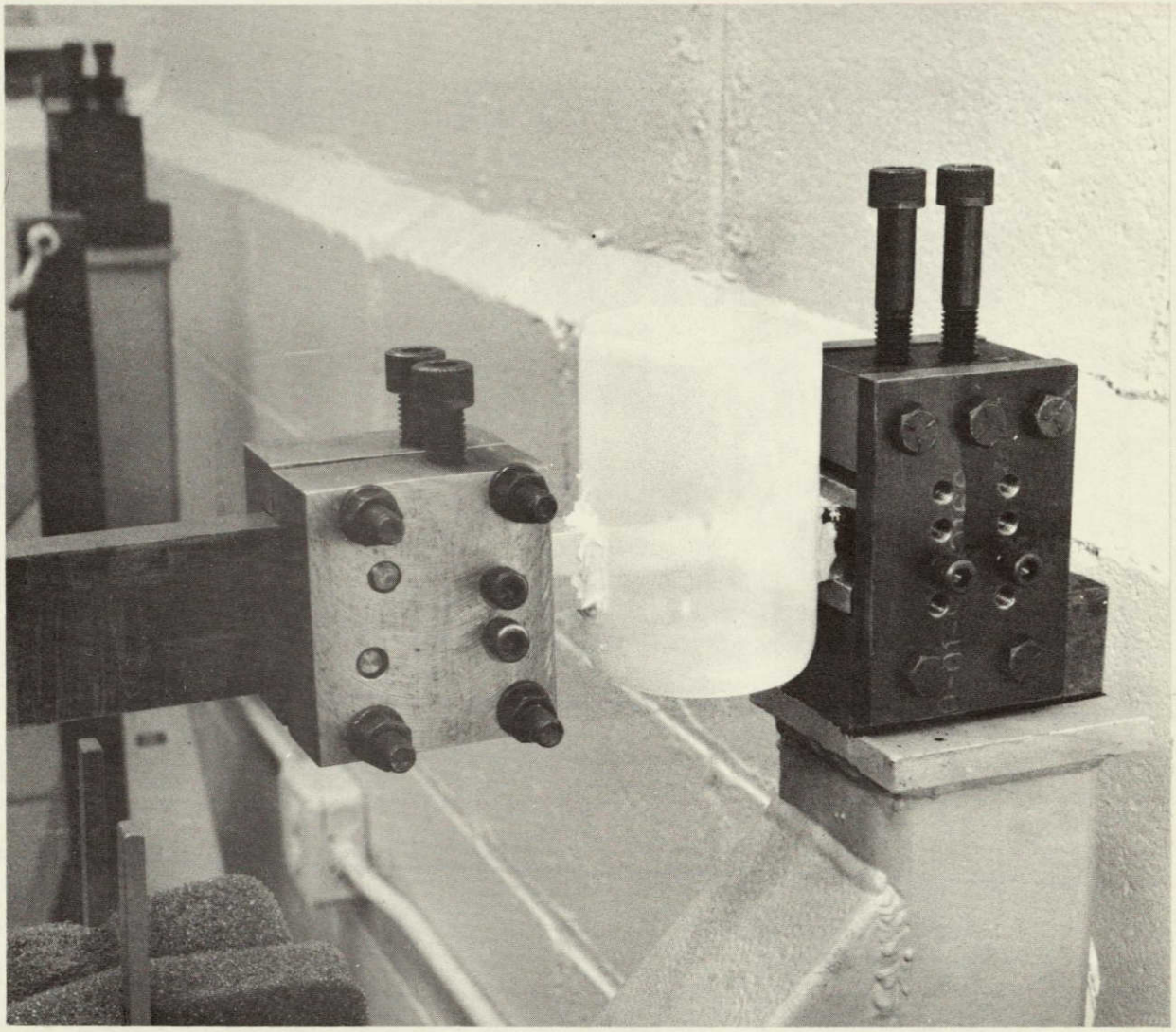

FIGURE 41
STRESS CORROSION TEST OF 12 NICKEL MARAGING STEEL IN INHIBITED WATER

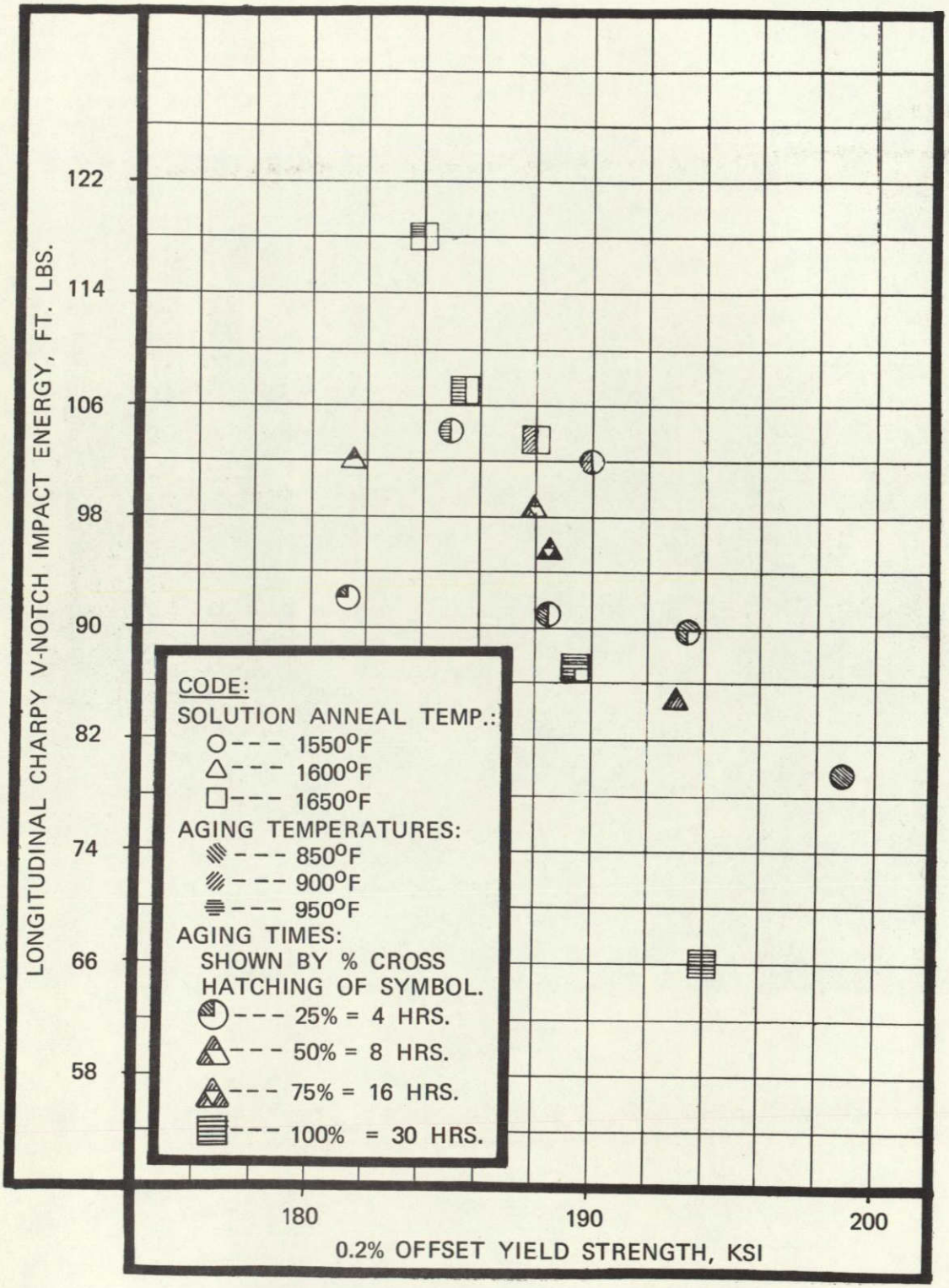

FIGURE 42
CHARPY V-NOTCH IMPACT ENERGY VS. YIELD STRENGTH –
INITIAL BASE PLATE HEAT TREAT STUDY

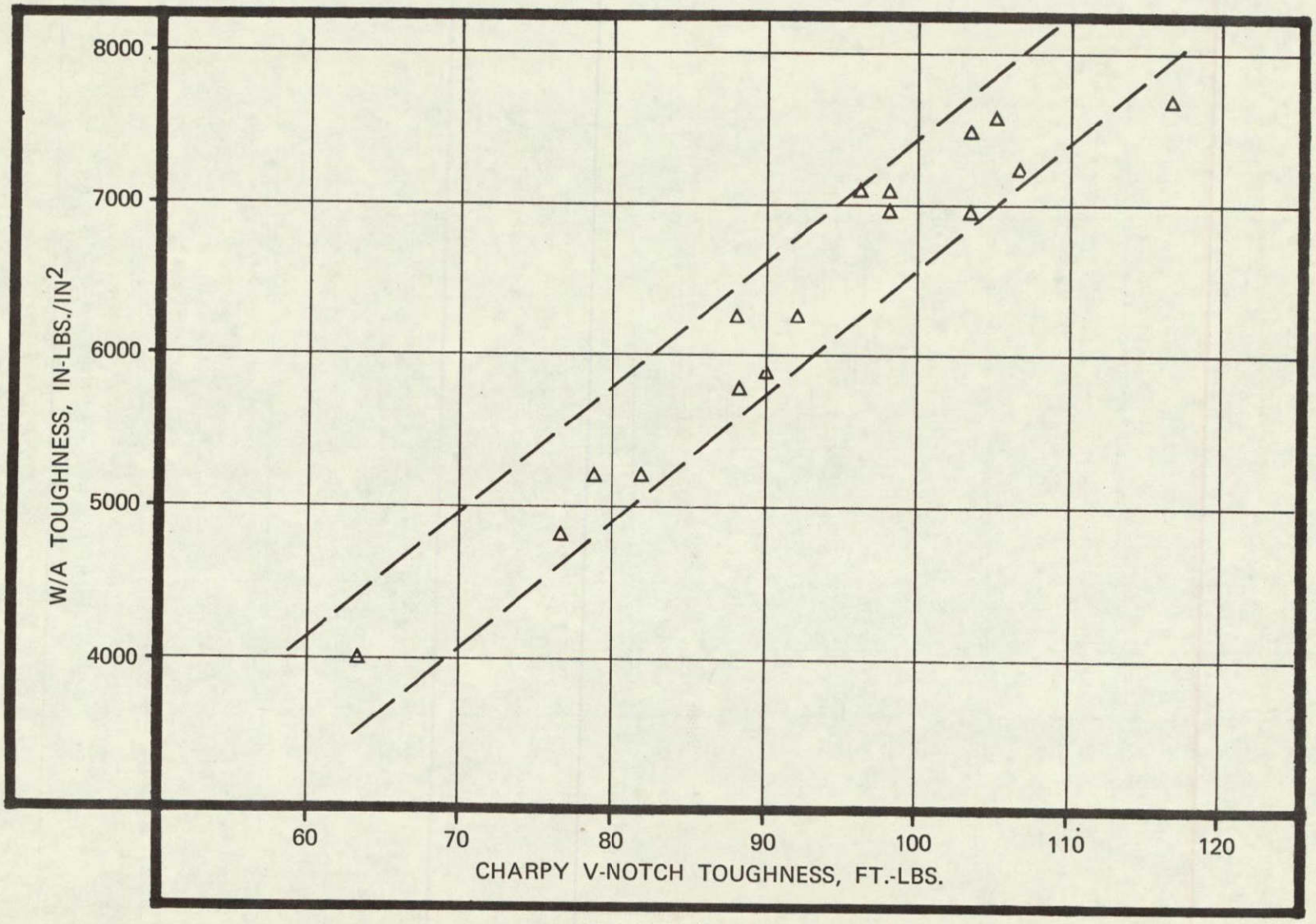

FIGURE 43
W/A TOUGHNESS VS. CHARPY V-NOTCH TOUGHNESS

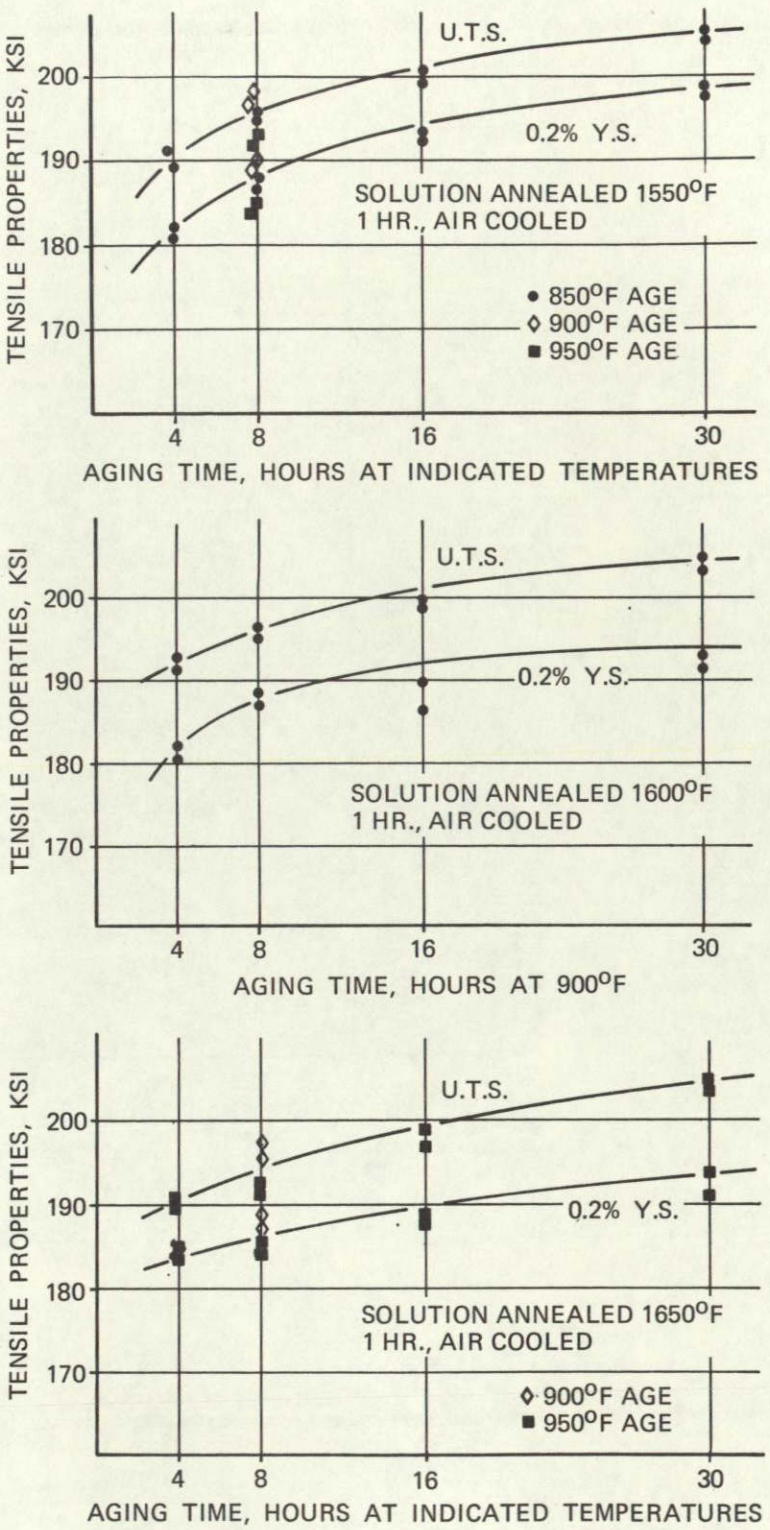

FIGURE 44
AGING RESPONSE DATA FOR BASE PLATE

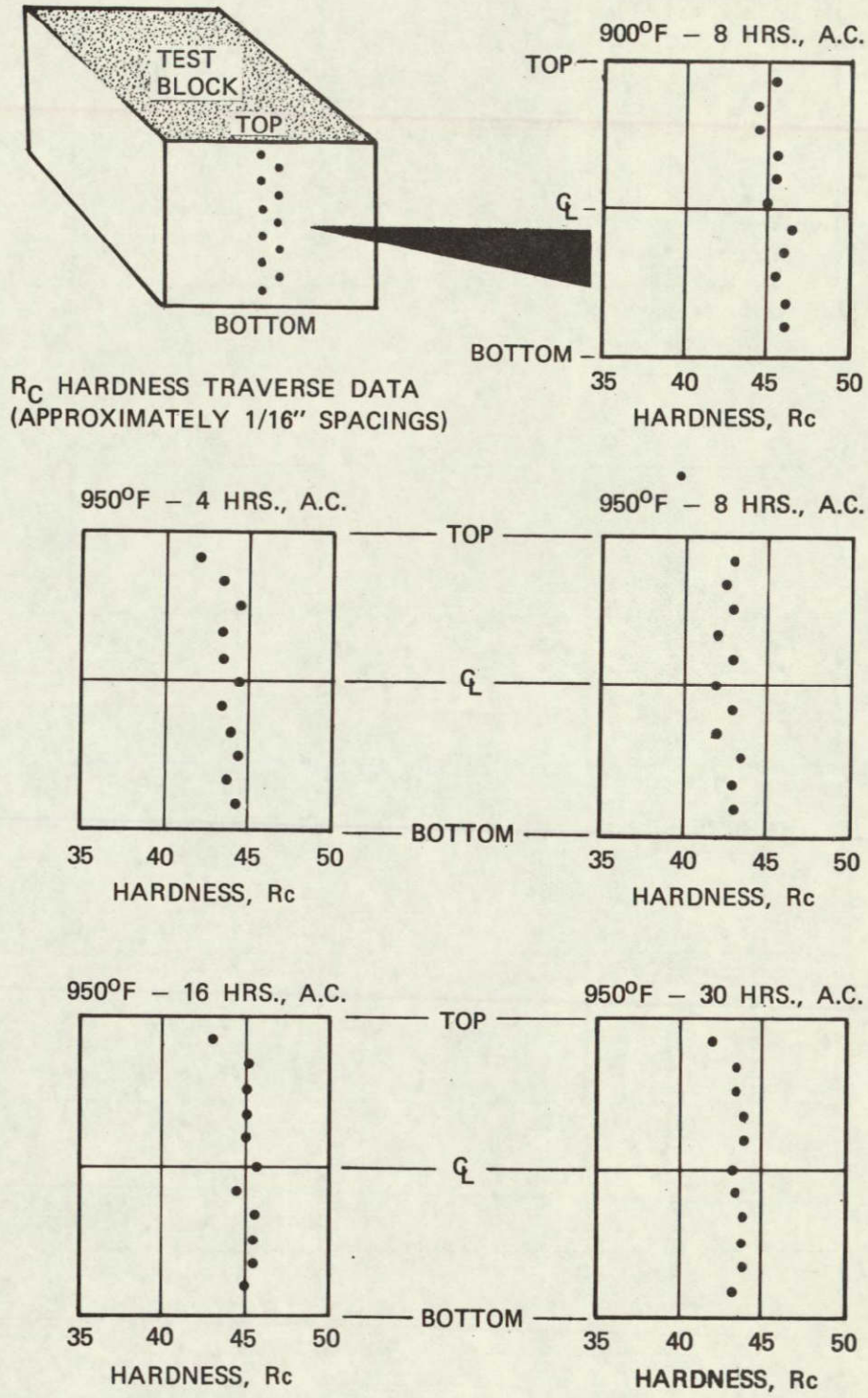

FIGURE 45
HARDNESS TRAVERSE DATA FROM 3/4-INCH 12% Ni MARAGING STEEL PLATE SOLUTION ANNEALED 1650°F AND AGED AS INDICATED

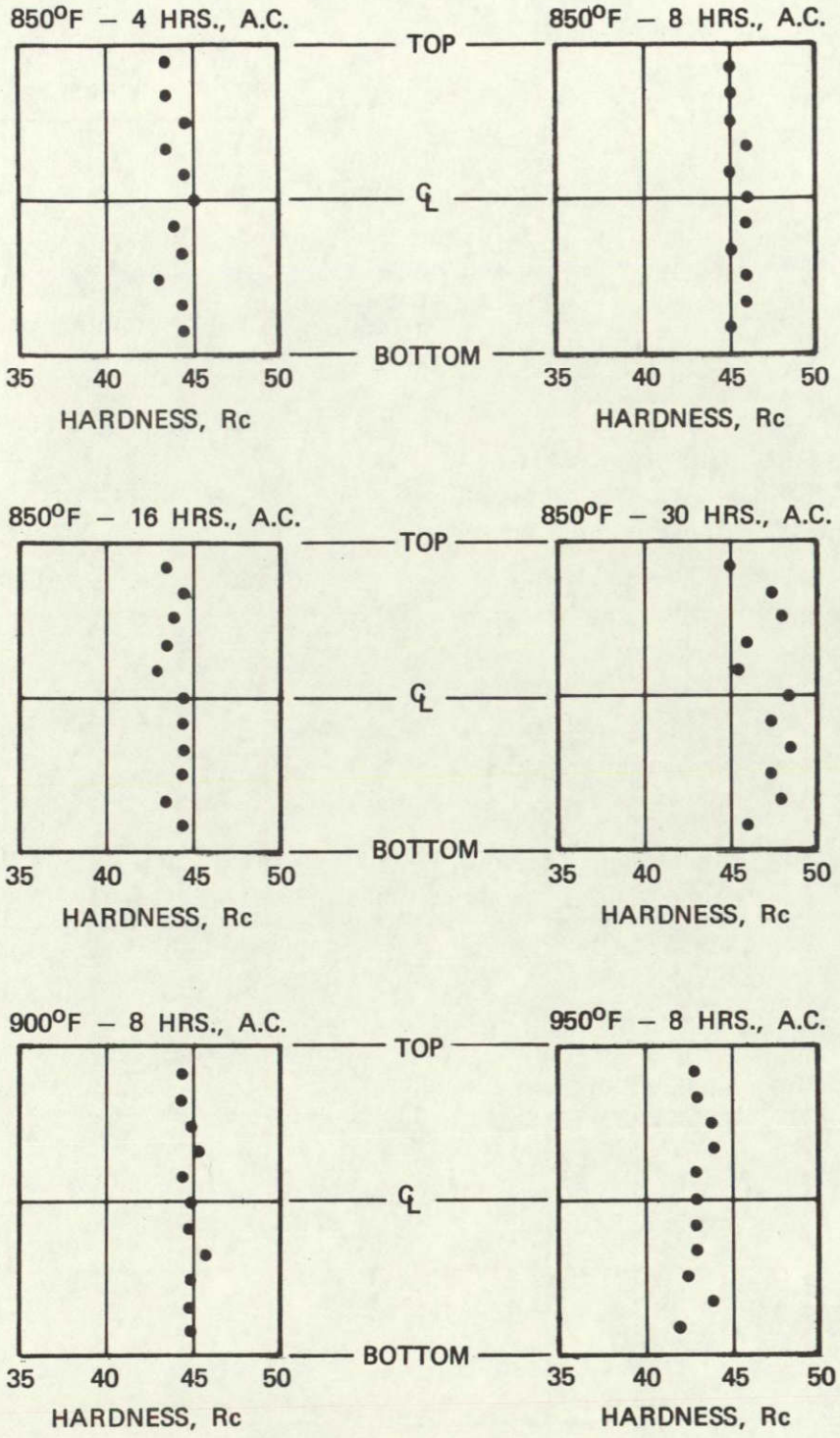

FIGURE 46
HARDNESS TRAVERSE DATA FROM 3/4-INCH 12% Ni MARAGING STEEL PLATE SOLUTION ANNEALED AT 1550°F AND AGED AS INDICATED

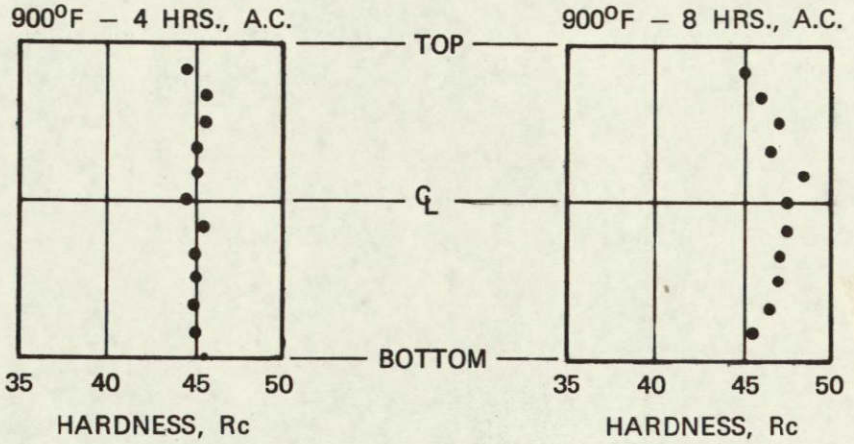

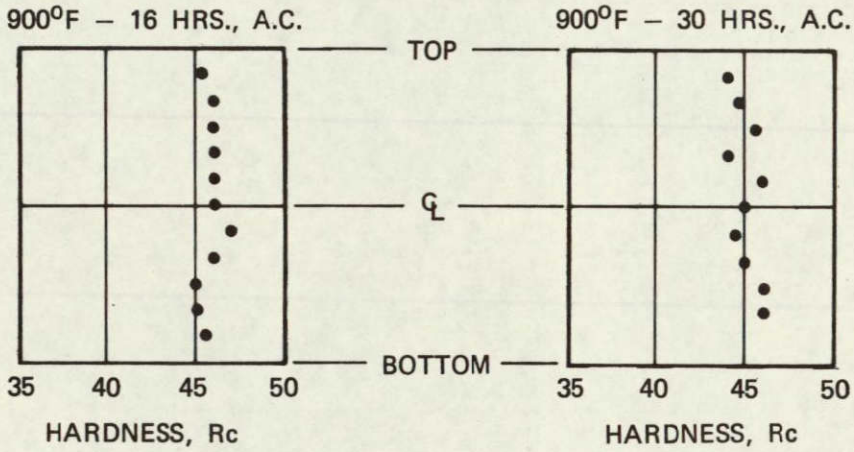

FIGURE 47
HARDNESS TRAVERSE DATA FROM 3/4-INCH 12% Ni MARAGING STEEL PLATE SOLUTION ANNEALED AT 1600°F AND AGED AS INDICATED

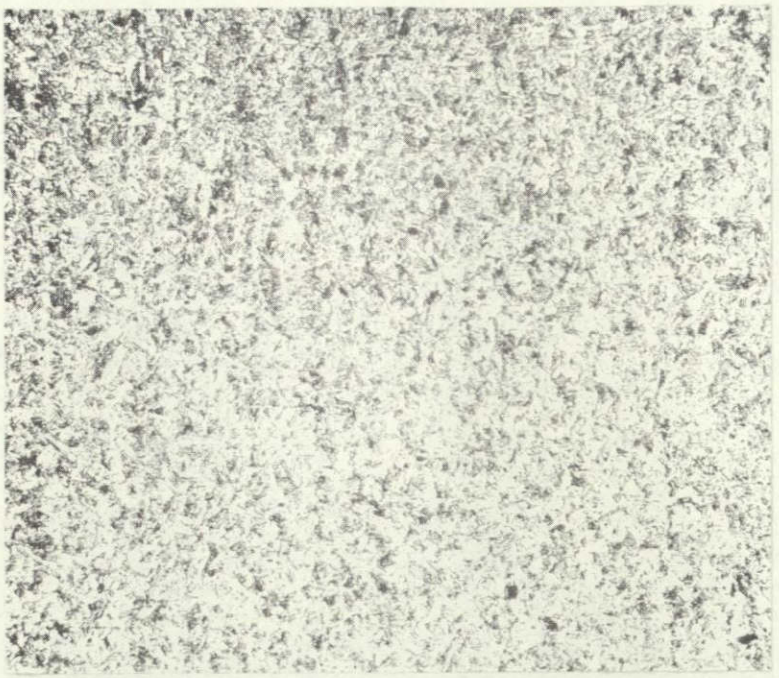

PLATE 1A-13, VILELLA'S REAGENT – 100 X

PLATE 1A-13, VILELLA'S REAGENT – 400 X

FIGURE 48
MICROSTRUCTURE OF BASE PLATE MATERIAL SOLUTION ANNEALED AT 1550°F AND AGED AT 900°F FOR 8 HOURS

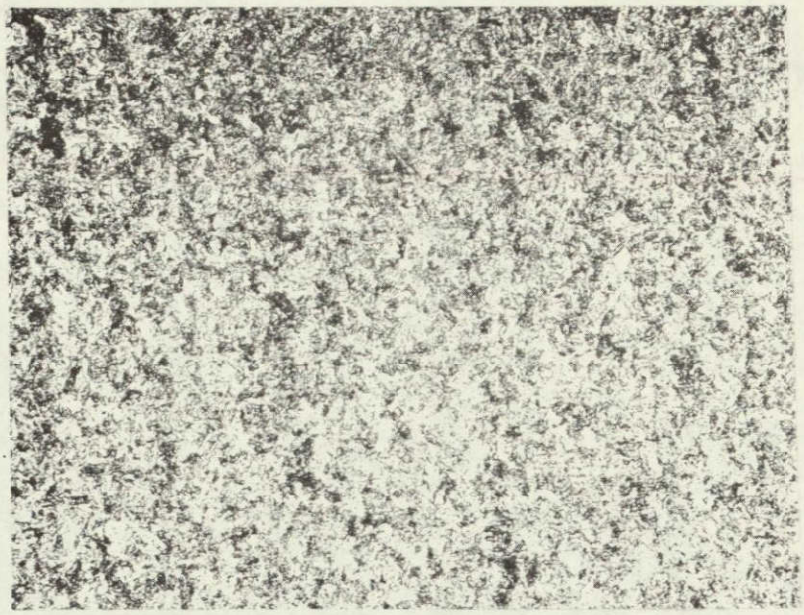

PLATE 1A-14, VILLELA'S REAGENT - 100X

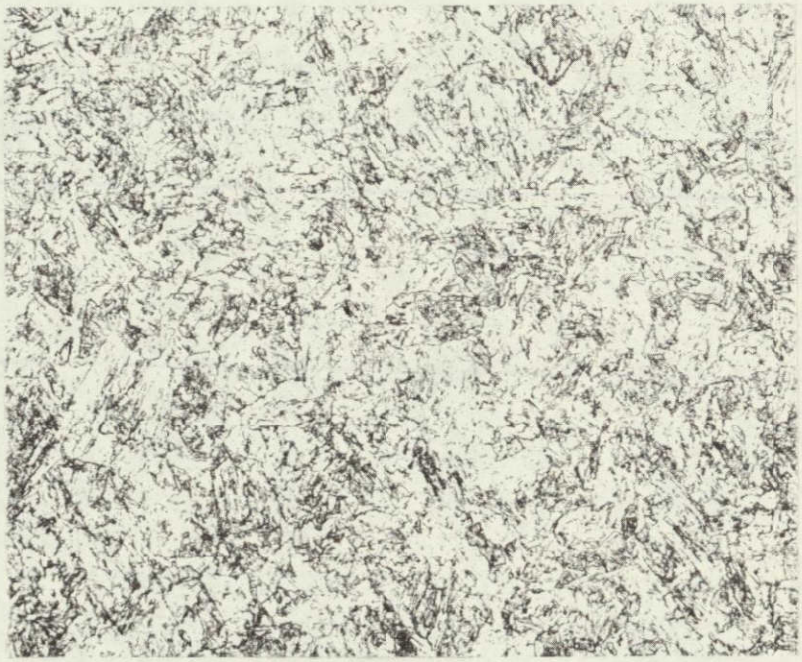

PLATE 1A-14, VILLELA'S REAGENT - 400X

FIGURE 49
MICROSTRUCTURE OF BASE PLATE MATERIAL SOLUTION ANNEALED AT 1550°F AND AGED AT 950°F FOR 8 HOURS

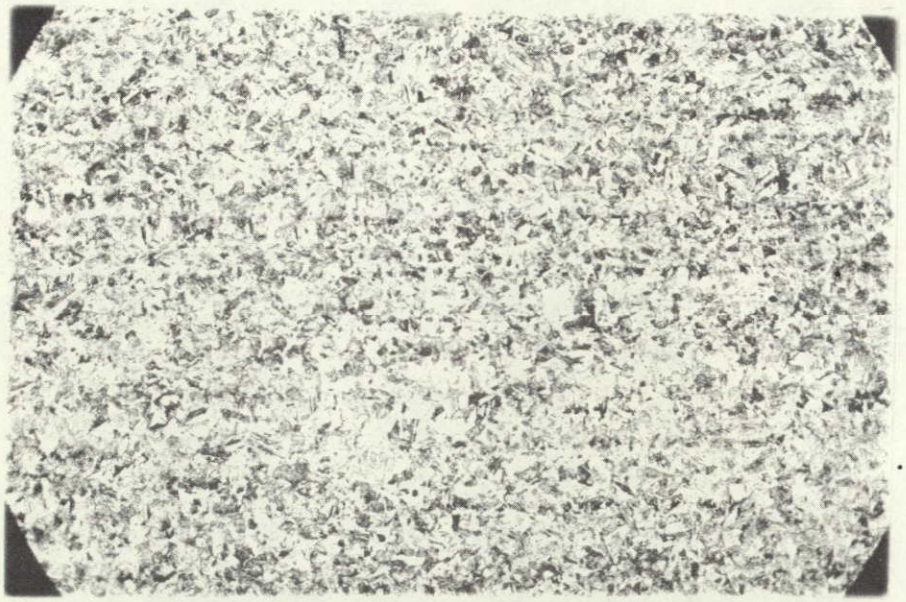

PLATE 1A-3, VILLELA'S REAGENT - 100X

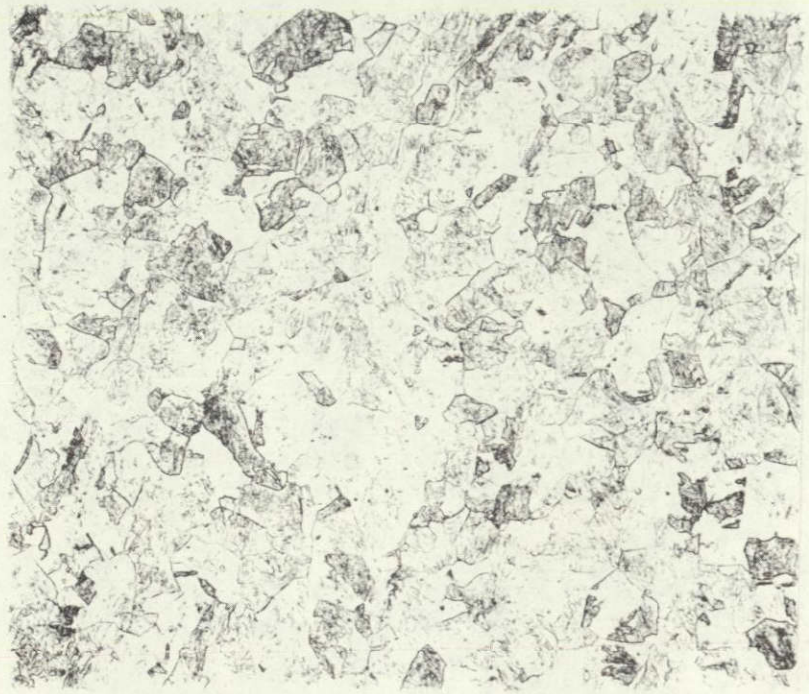

PLATE 1A-3, VILLELA'S REAGENT – 400X

FIGURE 50
MICROSTRUCTURE OF BASE PLATE MATERIAL SOLUTION ANNEALED AT 1600°F AND AGED AT 900°F FOR 4 HOURS

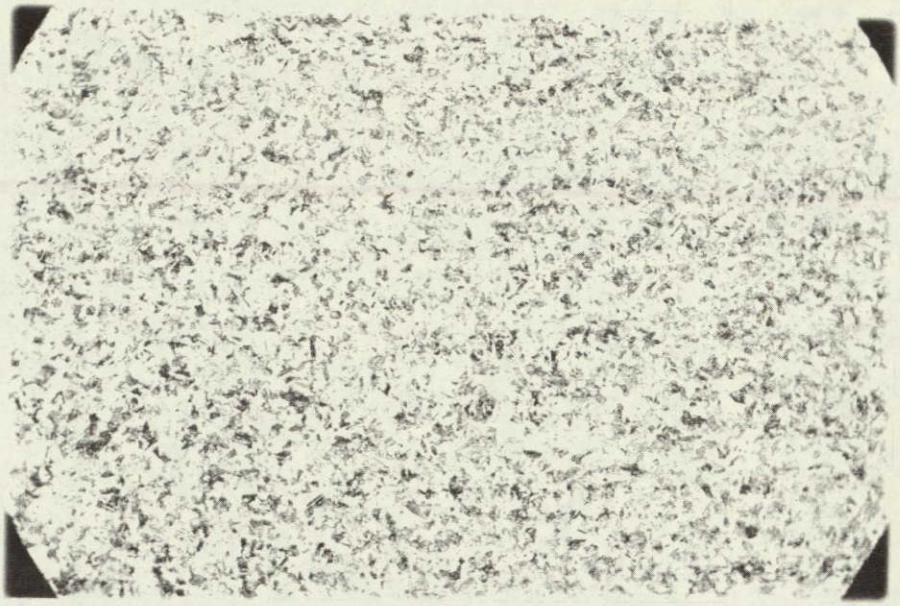

PLATE 1A-6, VILLELA'S REAGENT - 100X

PLATE 1A-6, VILLELA'S REAGENT - 400X

FIGURE 51
MICROSTRUCTURE OF BASE PLATE SOLUTION ANNEALED
AT 1650°F AND AGED AT 950°F FOR 8 HOURS

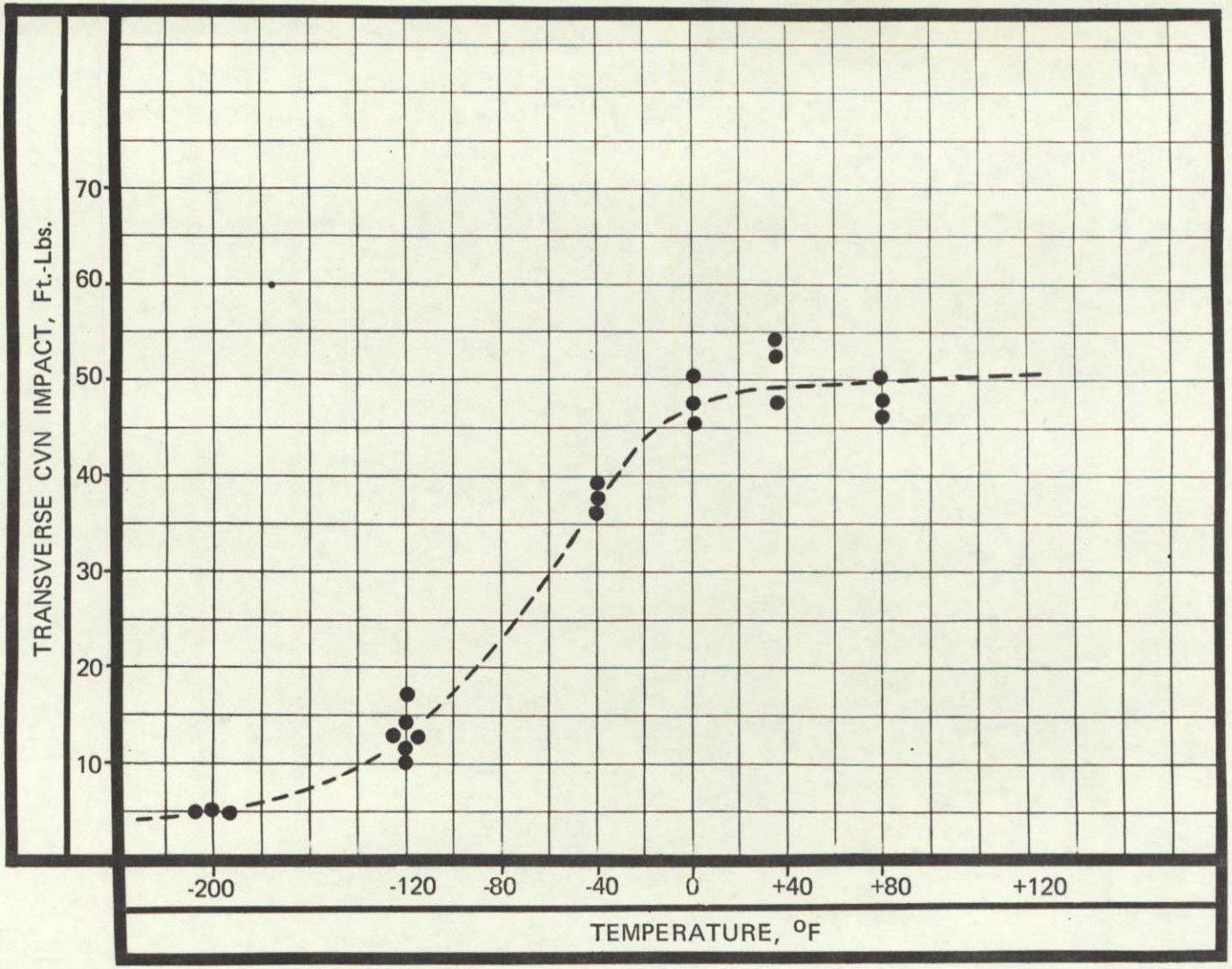

FIGURE 52
CHARPY IMPACT ENERGY VS. TEMPERATURE CURVE FOR BASE MATERIAL SPECIMENS FROM PC. II C. SOLUTION ANNEALED 1575°F, AGED 900°F FOR 8 HOURS

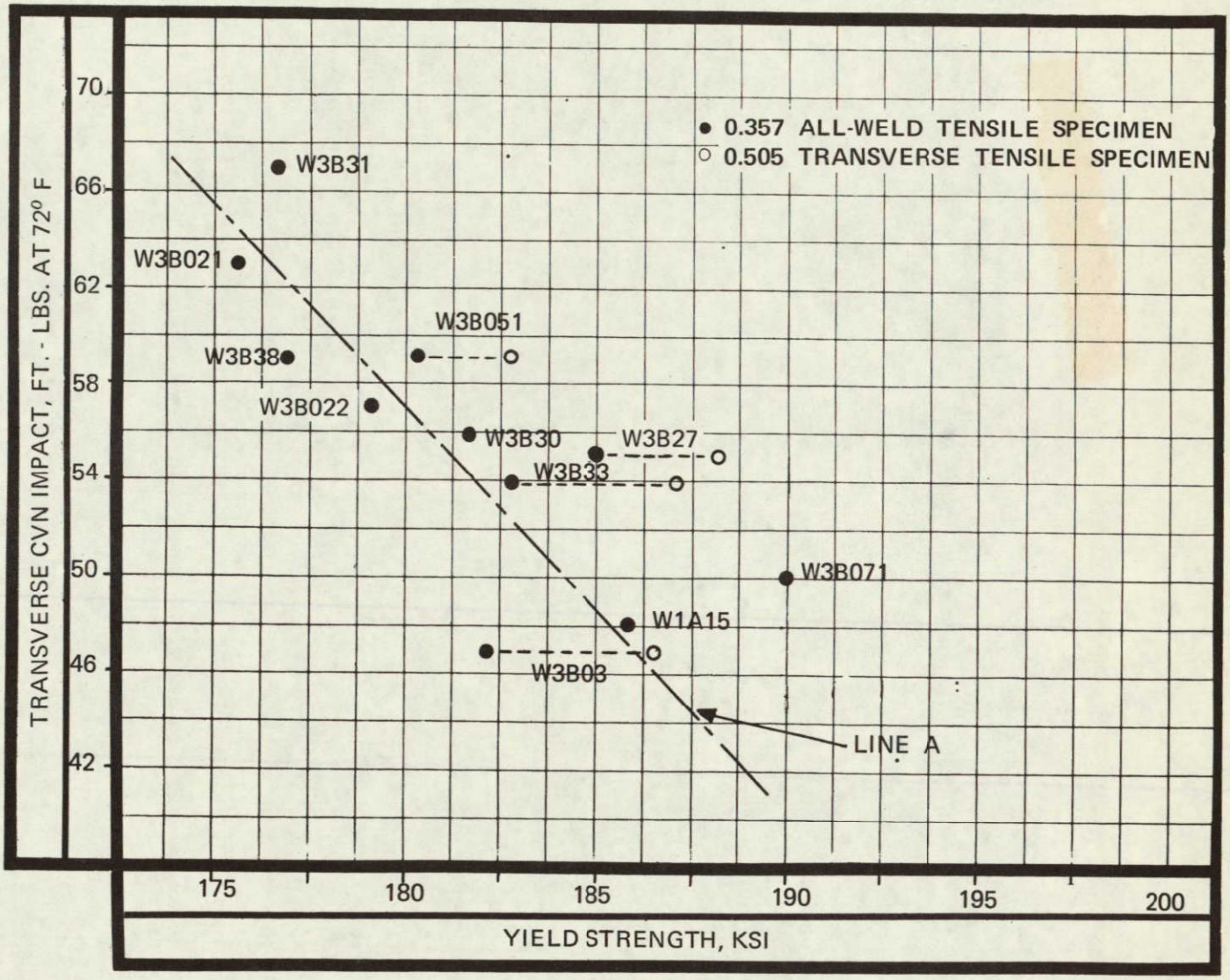

FIGURE 53

COMPARISON OF TRANSVERSE CHARPY IMPACT ENERGY VS. WELD YIELD STRENGTH, 12" X 12" WELDMENTS

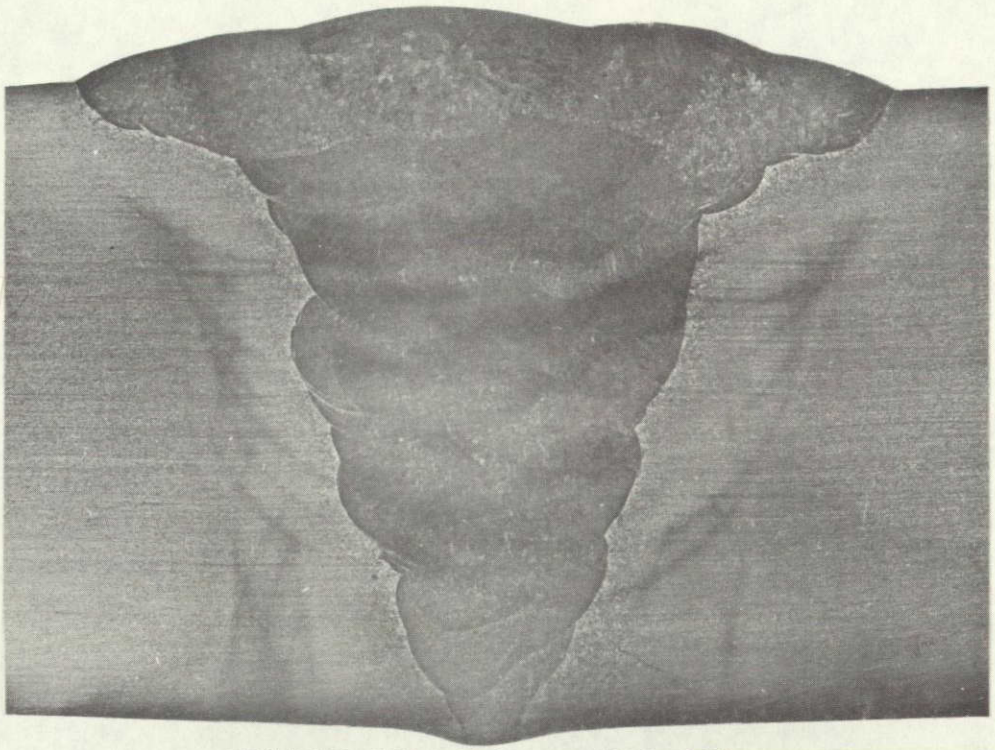

ETCHANT: HCl + H_2O_2 MAG. 4.5X

FIGURE 54
CROSS SECTION OF WELDMENT W3B27 (17% NI WIRE)

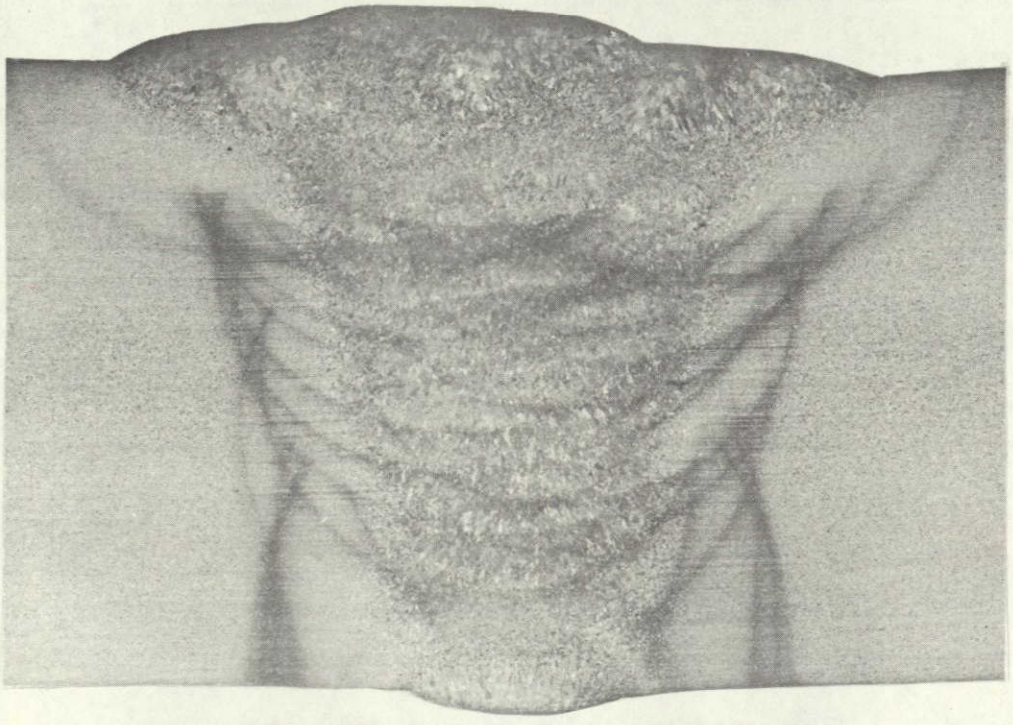

ETCHANT: HCl + H_2O_2 MAG. 4.5X

FIGURE 55
CROSS SECTION OF WELDMENT W3B31 (12% NI WIRE)

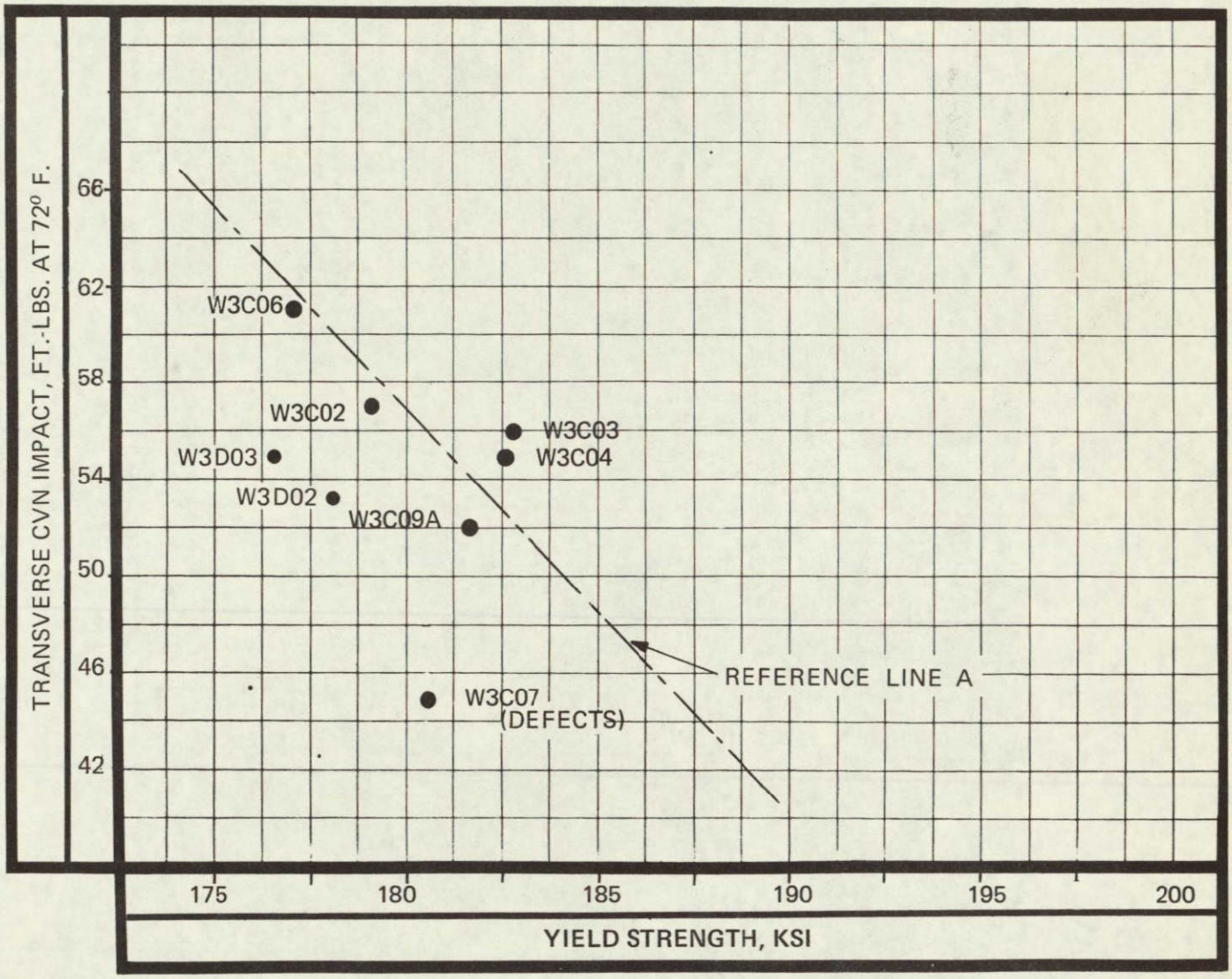

FIGURE 56

COMPARISON OF TRANSVERSE CHARPY IMPACT ENERGY VS. WELD YIELD STRENGTH, 40" X 40" TEST PANELS

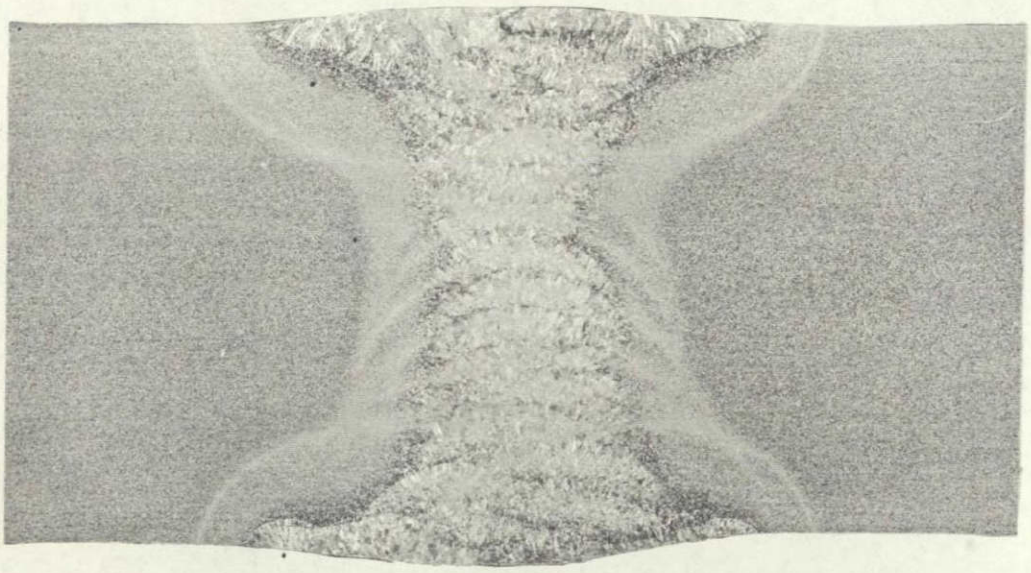

ETCHANT: HCl + H_2O_2 MAG. 3.5X

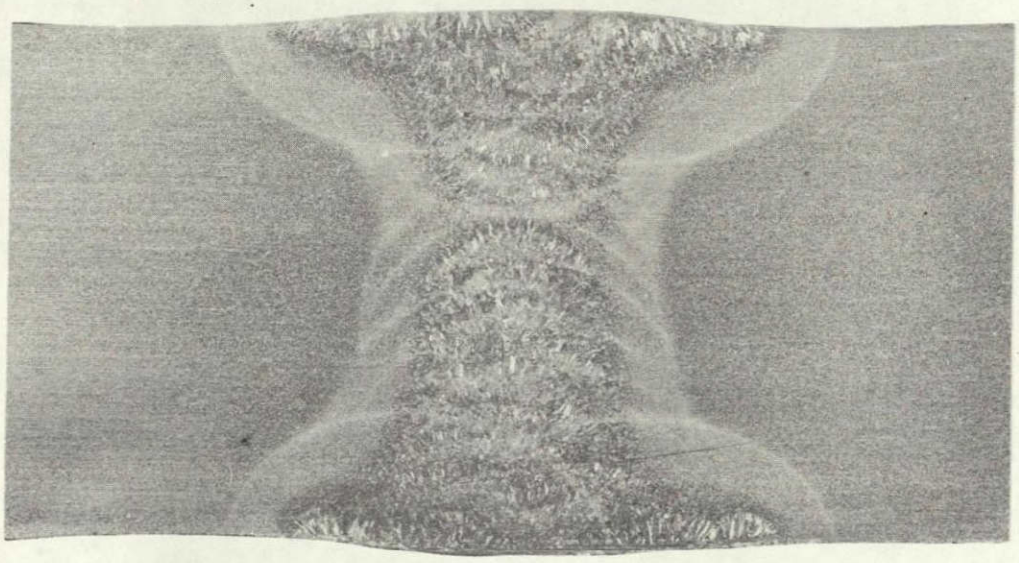

ETCHANT: HCl + H_2O_2 MAG. 3.5X

FIGURE 57
MACRO SECTIONS THROUGH WELDMENT W3CO2

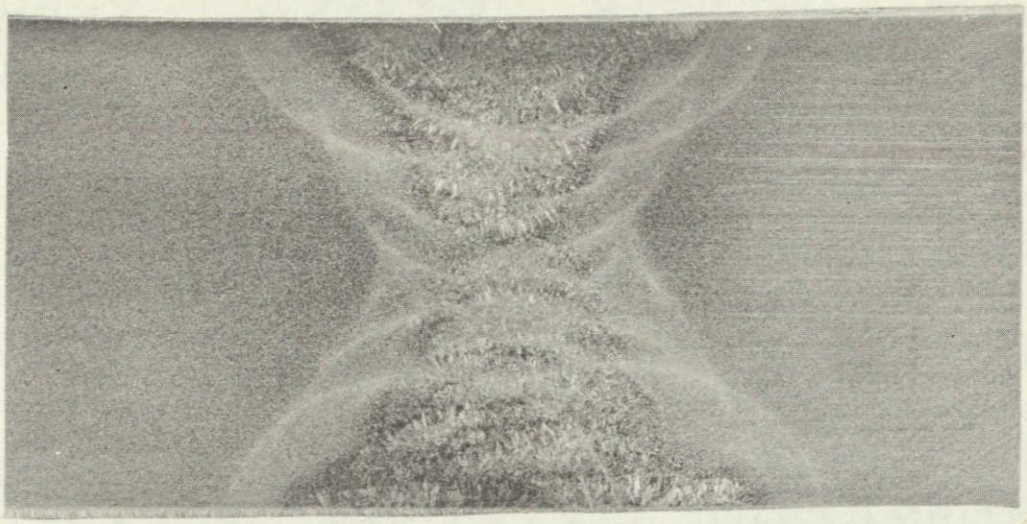

ETCHANT: HCl + H_2O_2 MAG. 3.5X

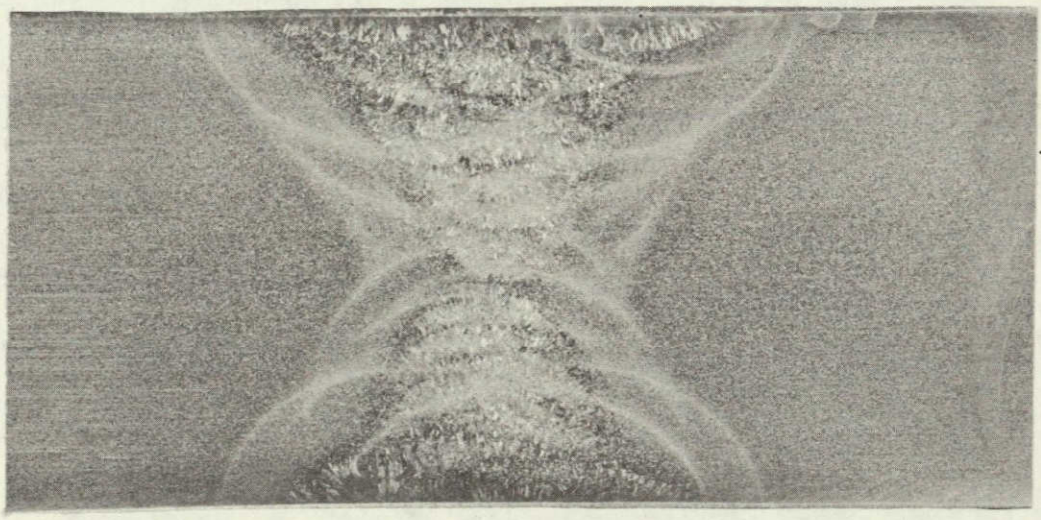

ETCHANT: HCl + H_2O_2 MAG. 3.5X

FIGURE 58
MACRO SECTIONS THROUGH WELDMENT W3C03

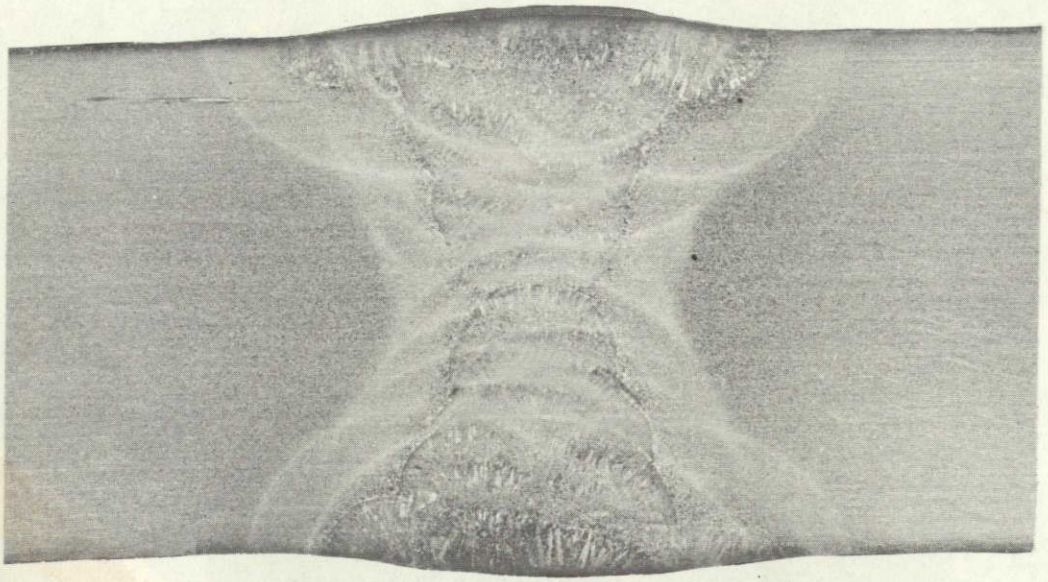

ETCHANT: HCl + H_2O_2 MAG. 3.5X

FIGURE 59
MACRO SECTION THROUGH WELDMENT W3C04

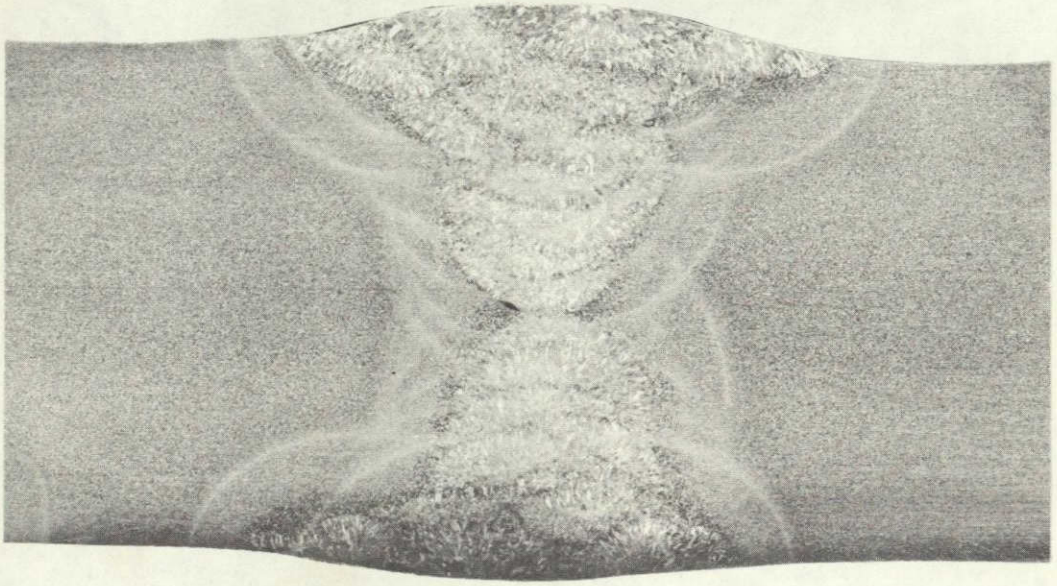

ETCHANT: HCl + H_2O_2 MAG. 3.5X

FIGURE 60
MACRO SECTION THROUGH WELDMENT W3C06

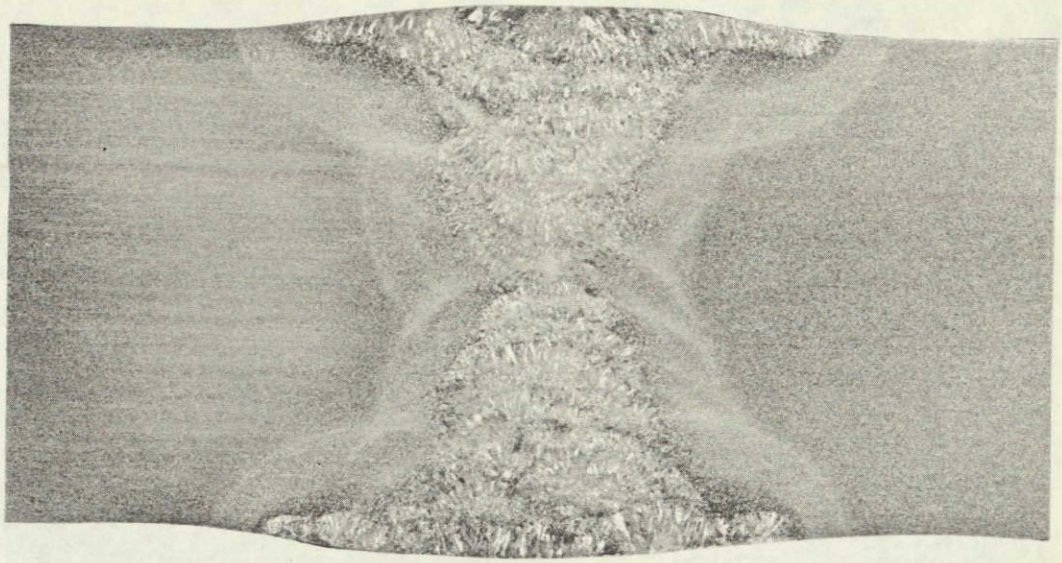

ETCHANT: HCl + H_2O_2 MAG. 3.5X

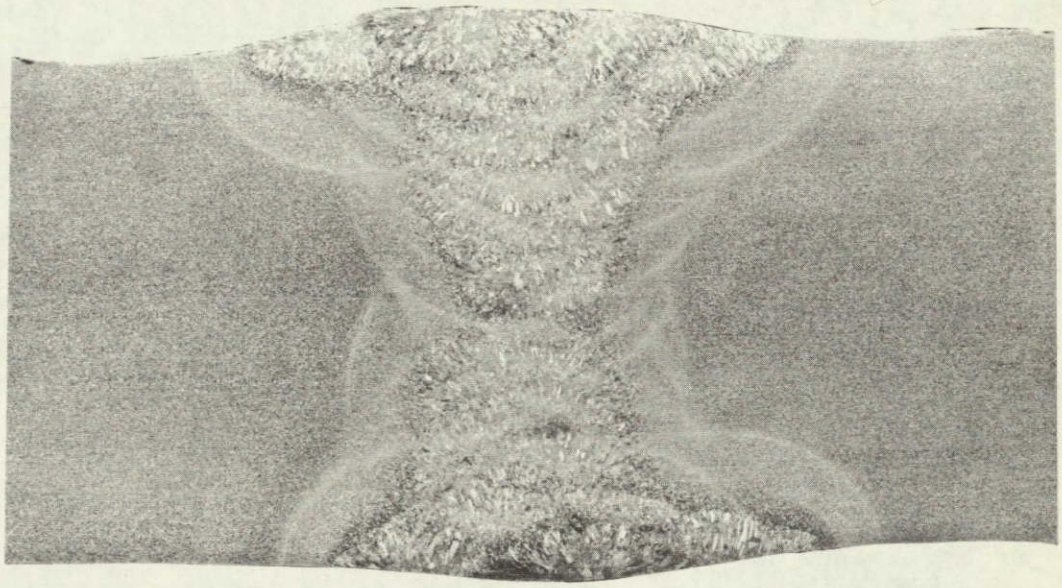

ETCHANT: HCl + H_2O_2 MAG. 3.5X

FIGURE 61
MACRO SECTIONS THROUGH WELDMENT W3C06

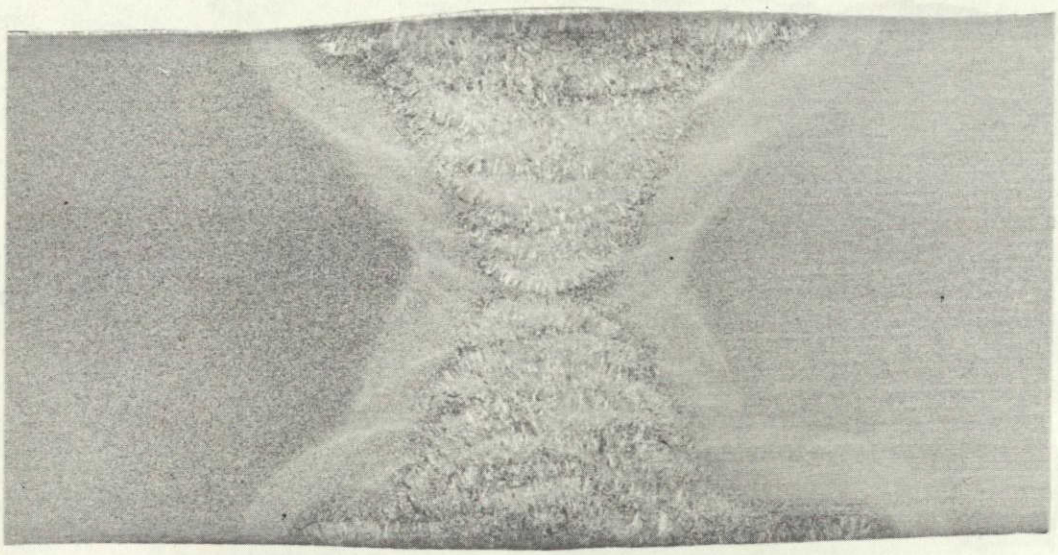

ETCHANT: HCl + H_2O_2 MAG. 3.5X

FIGURE 62
MACRO SECTION THROUGH WELDMENT W3C07

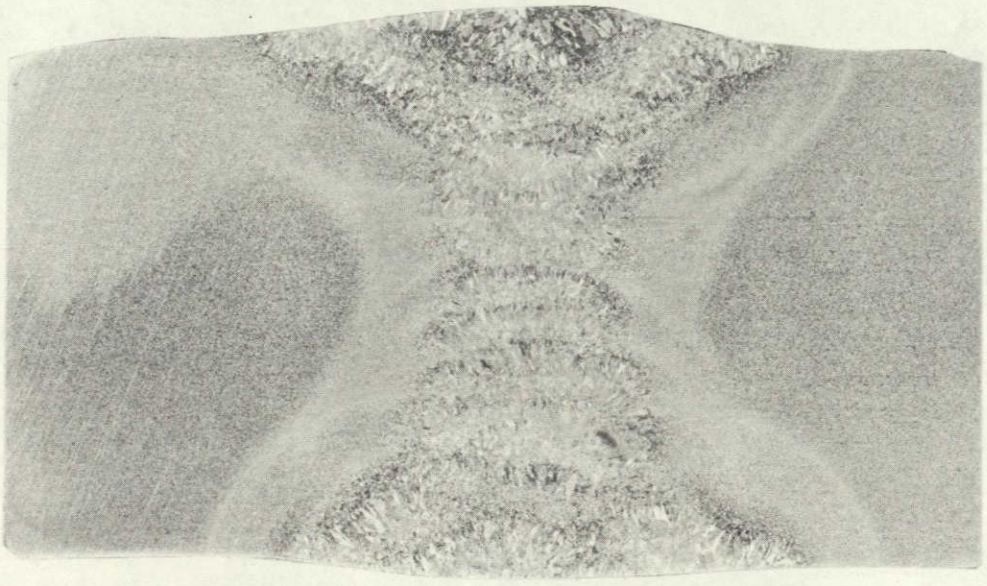

ETCHANT: HCl + H_2O_2 MAG. 3.5X

FIGURE 63
MACRO SECTION THROUGH WELDMENT W3C09

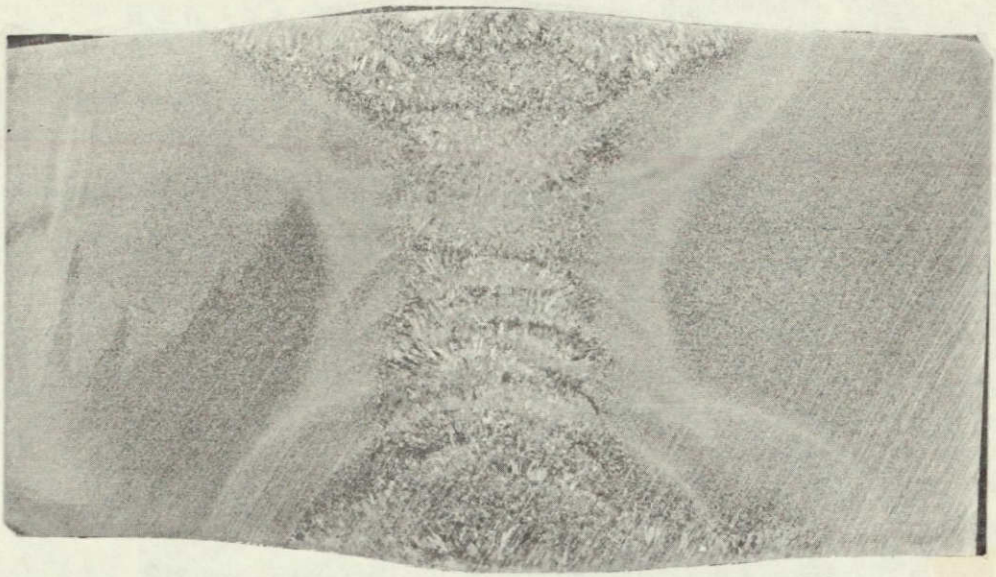

ETCHANT: HCl + H_2O_2 MAG. 3.5X

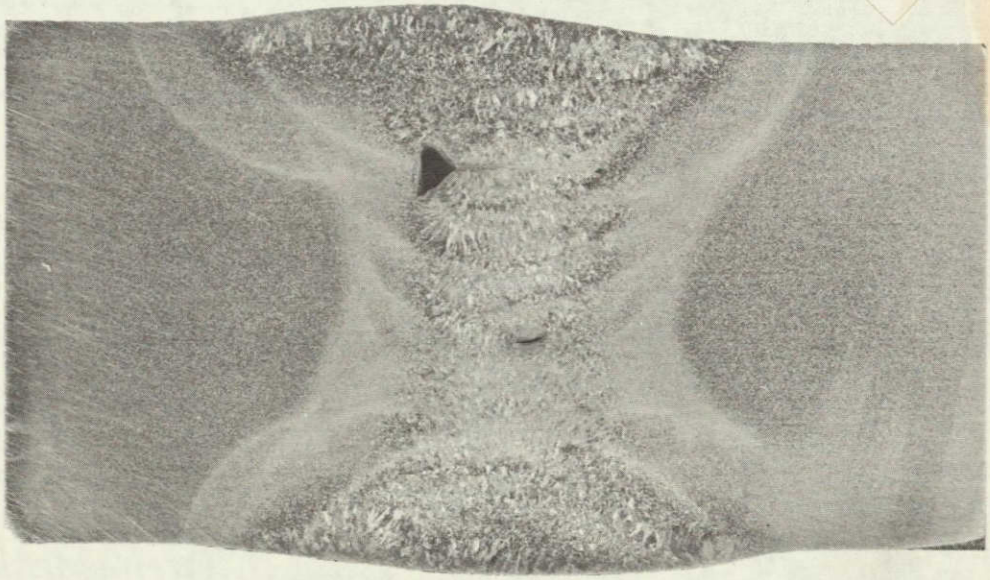

ETCHANT: HCl + H_2O_2 MAG. 3.5X

FIGURE 64
MACRO SECTIONS THROUGH WELDMENT W3C09

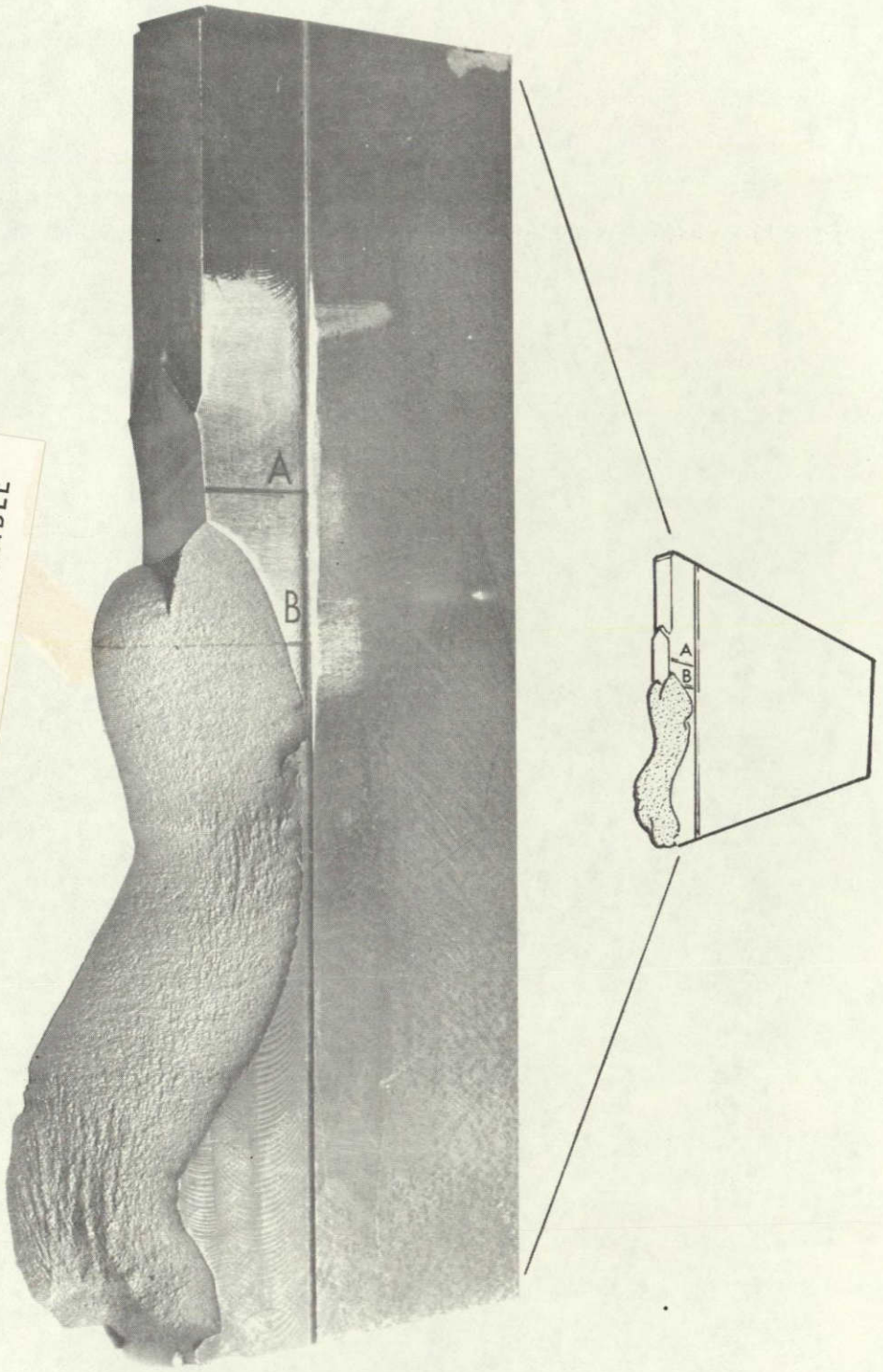

FIGURE 65
FRACTURE SURFACE OF SPECIMEN W3C03-B1

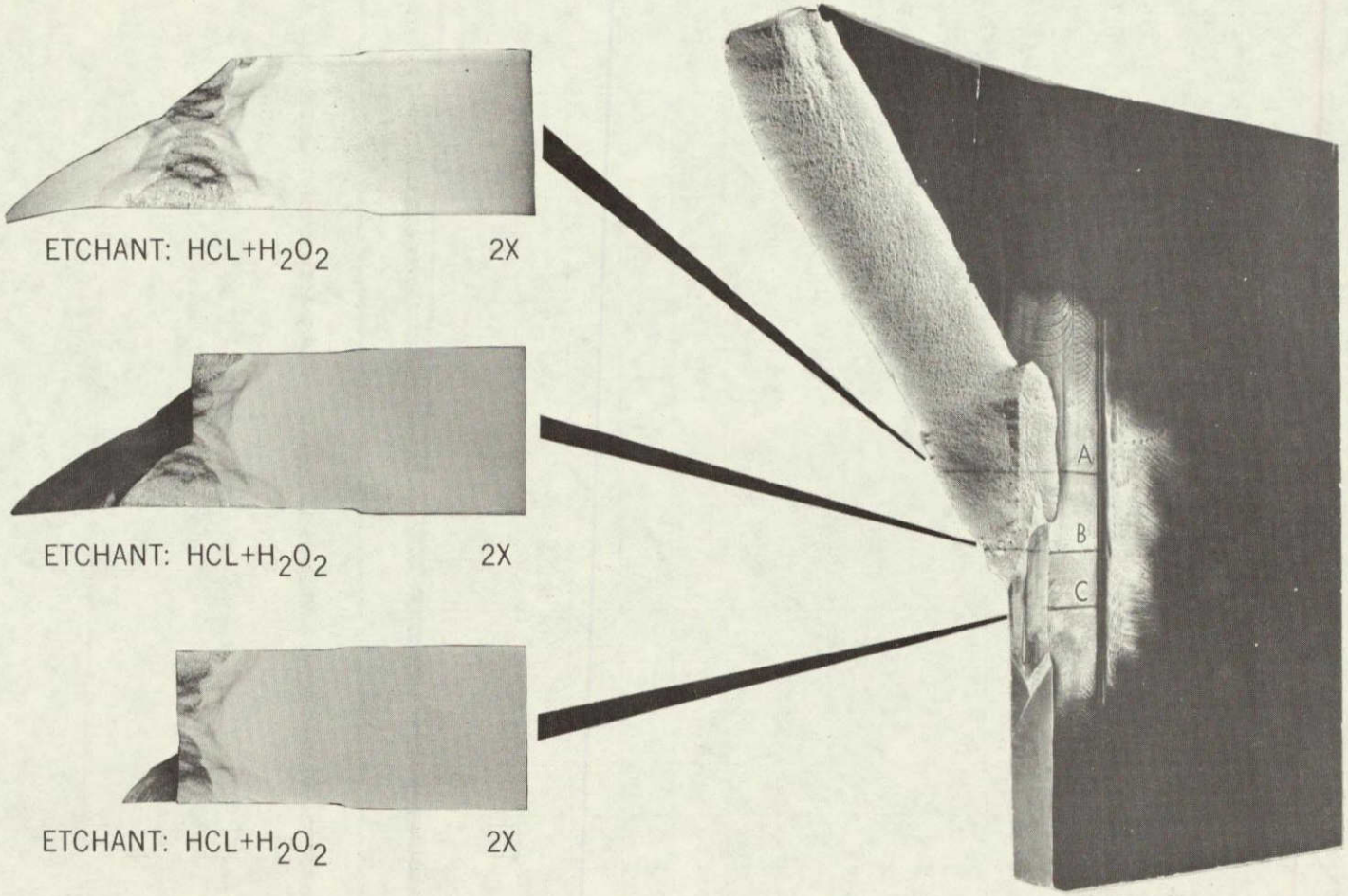

FIGURE 66
GENERAL VIEW AND CROSS SECTIONS THROUGH FRACTURE
OF SPECIMEN W3C04-B1

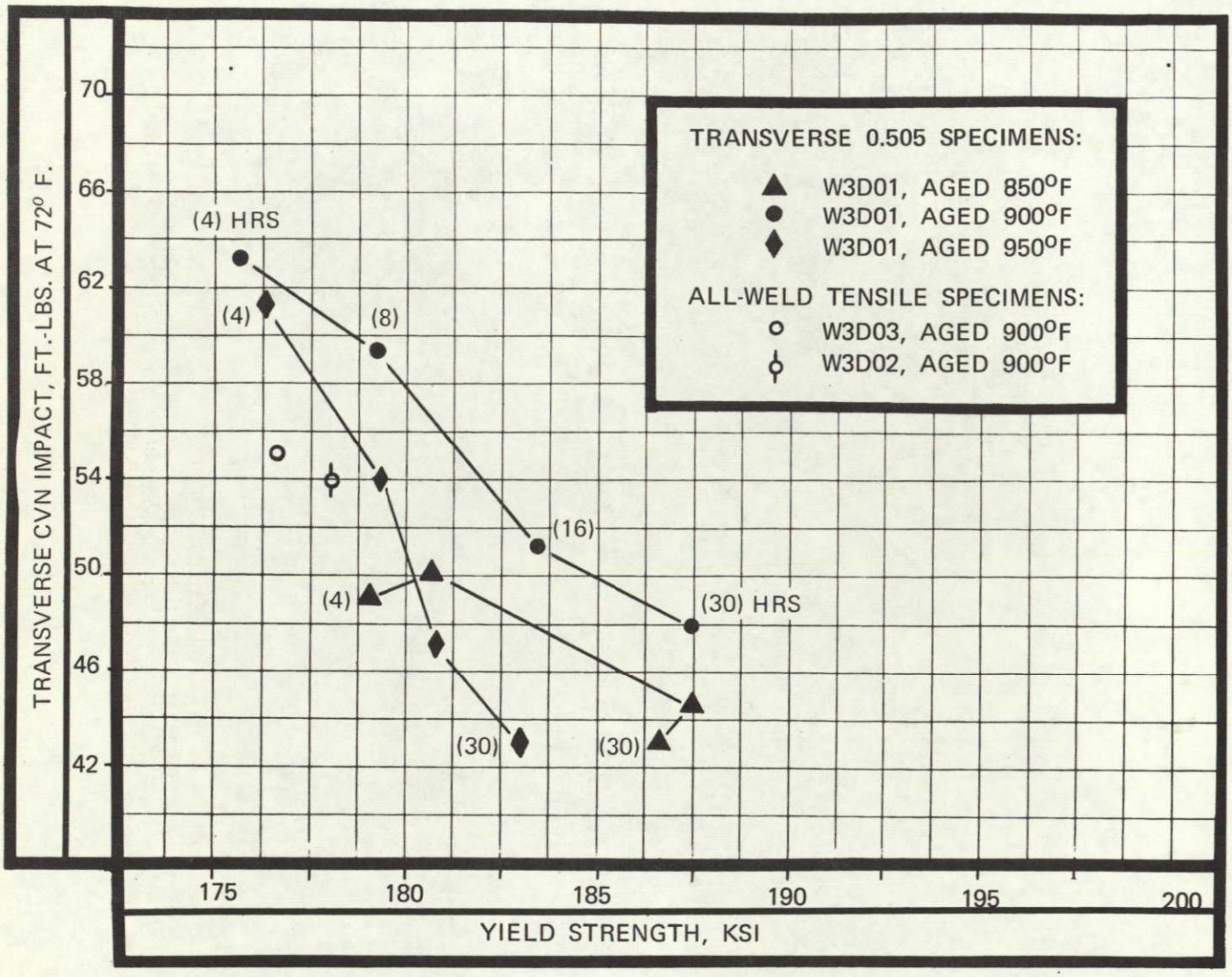

FIGURE 67
COMPARISON OF TRANSVERSE CHARPY IMPACT ENERGY VS. YIELD STRENGTH, AGING STUDY PANEL W3D01

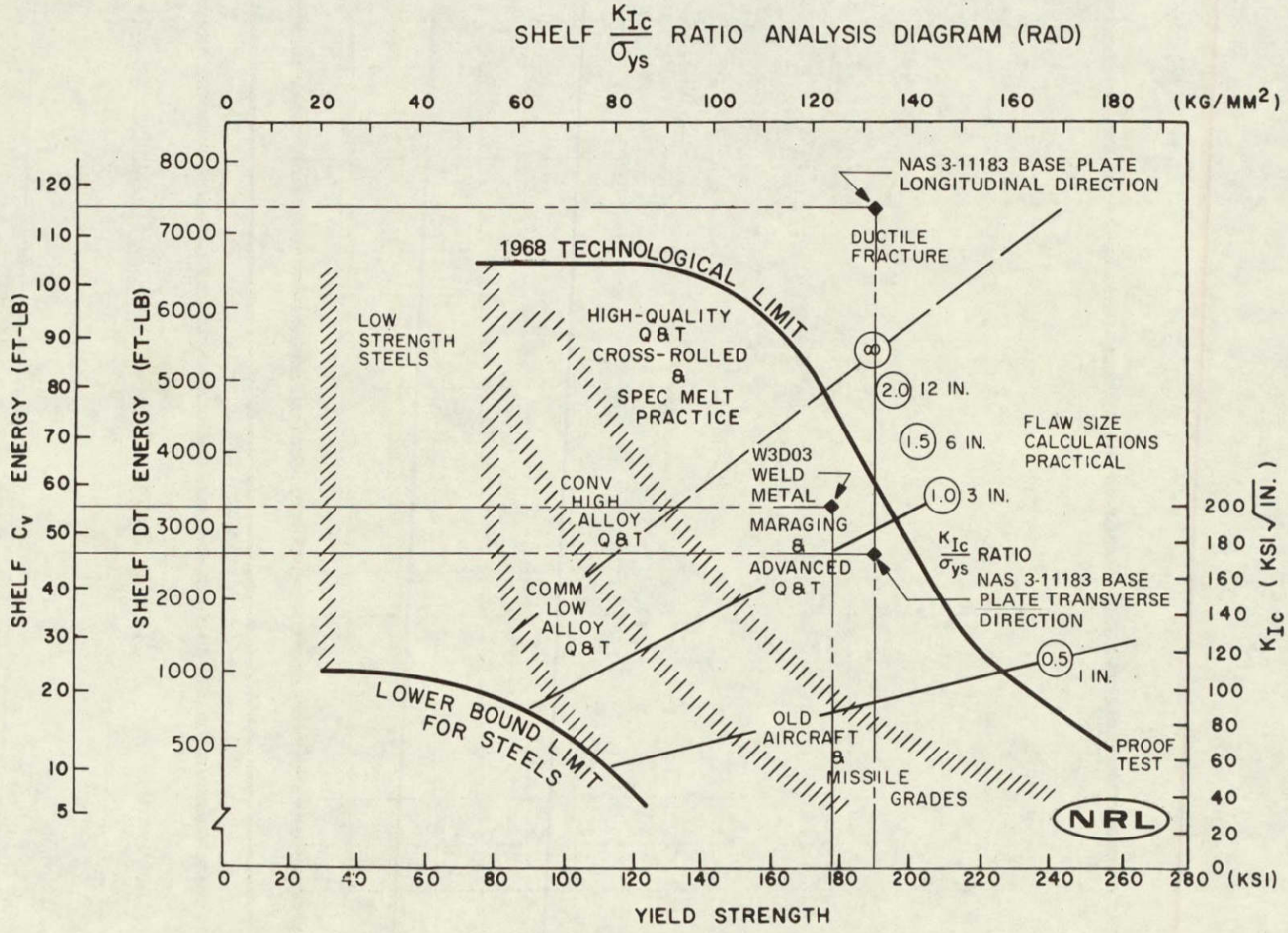

FIGURE 68 COMPARISON OF BASE METAL AND WELD METAL PROPERTIES WITH PROPERTIES REPORTED IN OTHER INVESTIGATIONS BY NAVAL RESEARCH LABORATORY

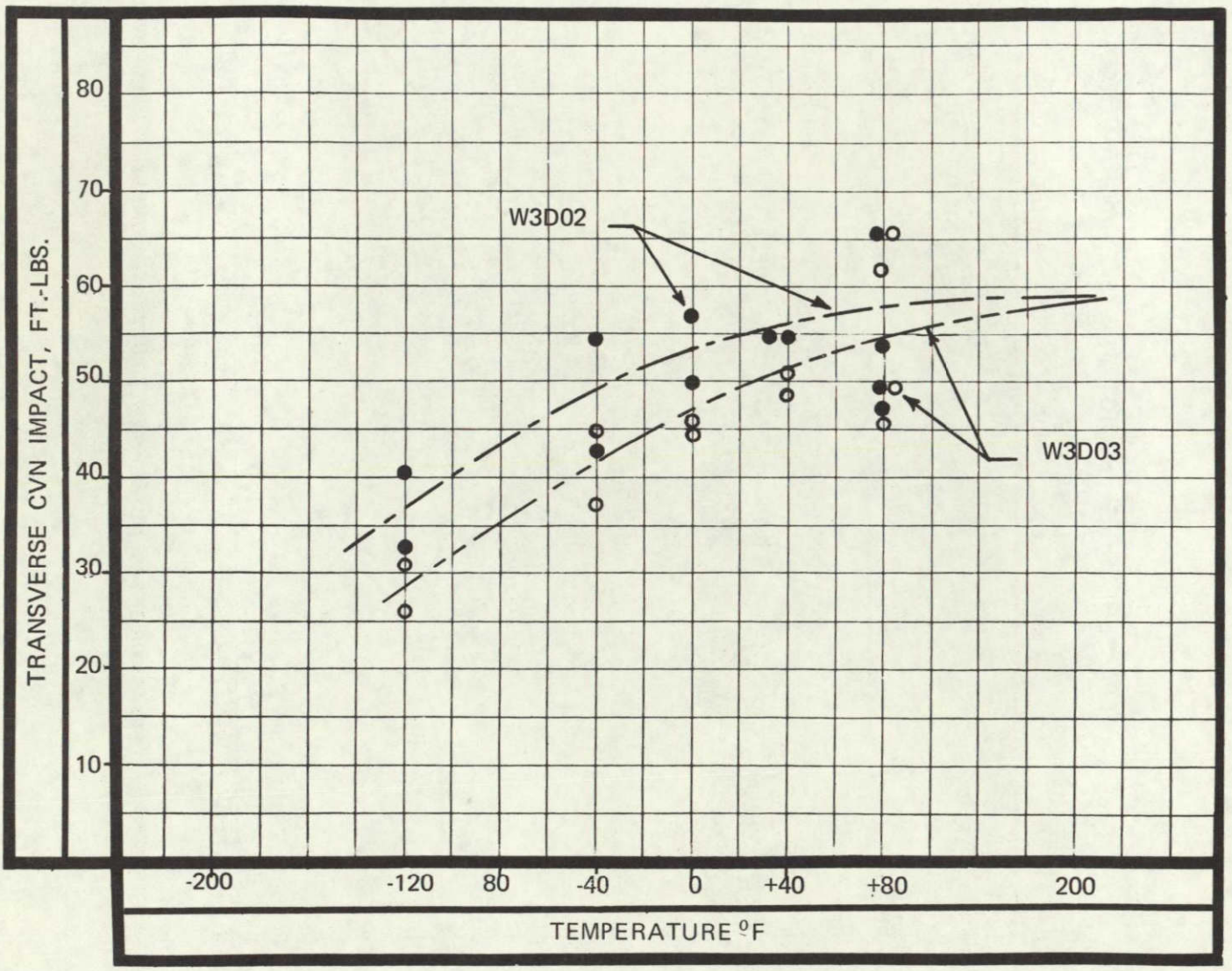

FIGURE 69
CHARPY IMPACT ENERGY VS. TEMPERATURE--ALL-WELD SPECIMENS

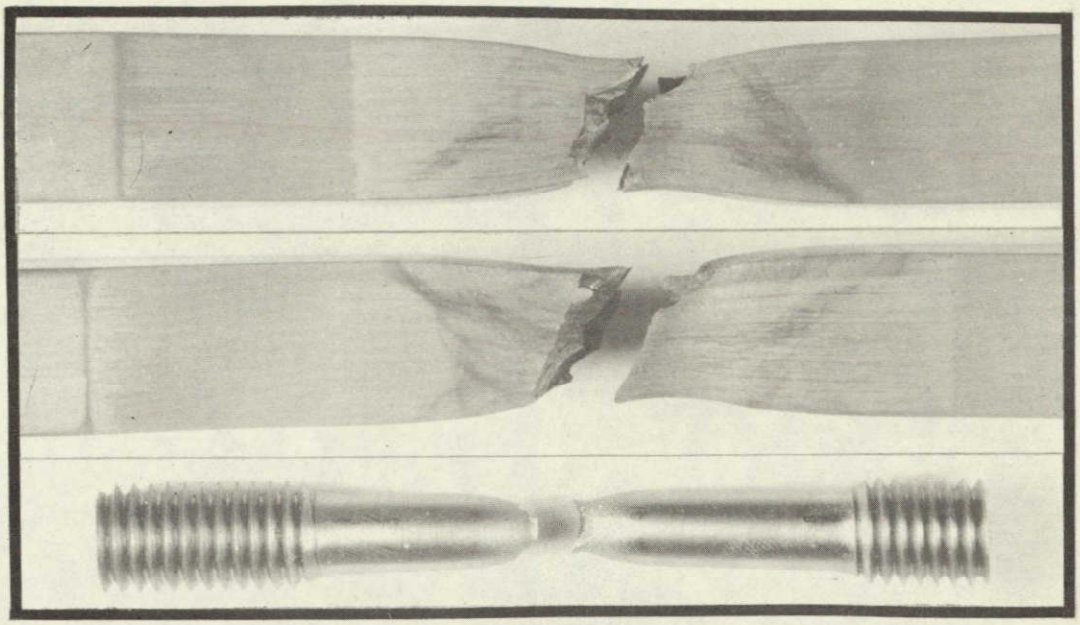

W3D02

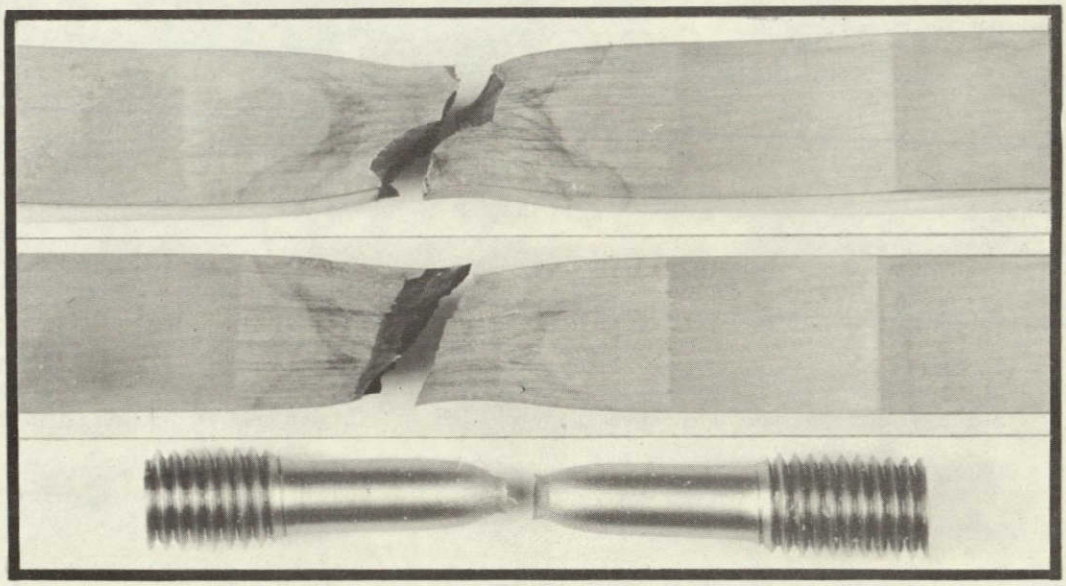

W3D03

FIGURE 70

TENSILE SPECIMENS, WELDMENTS W3D02 AND W3D03

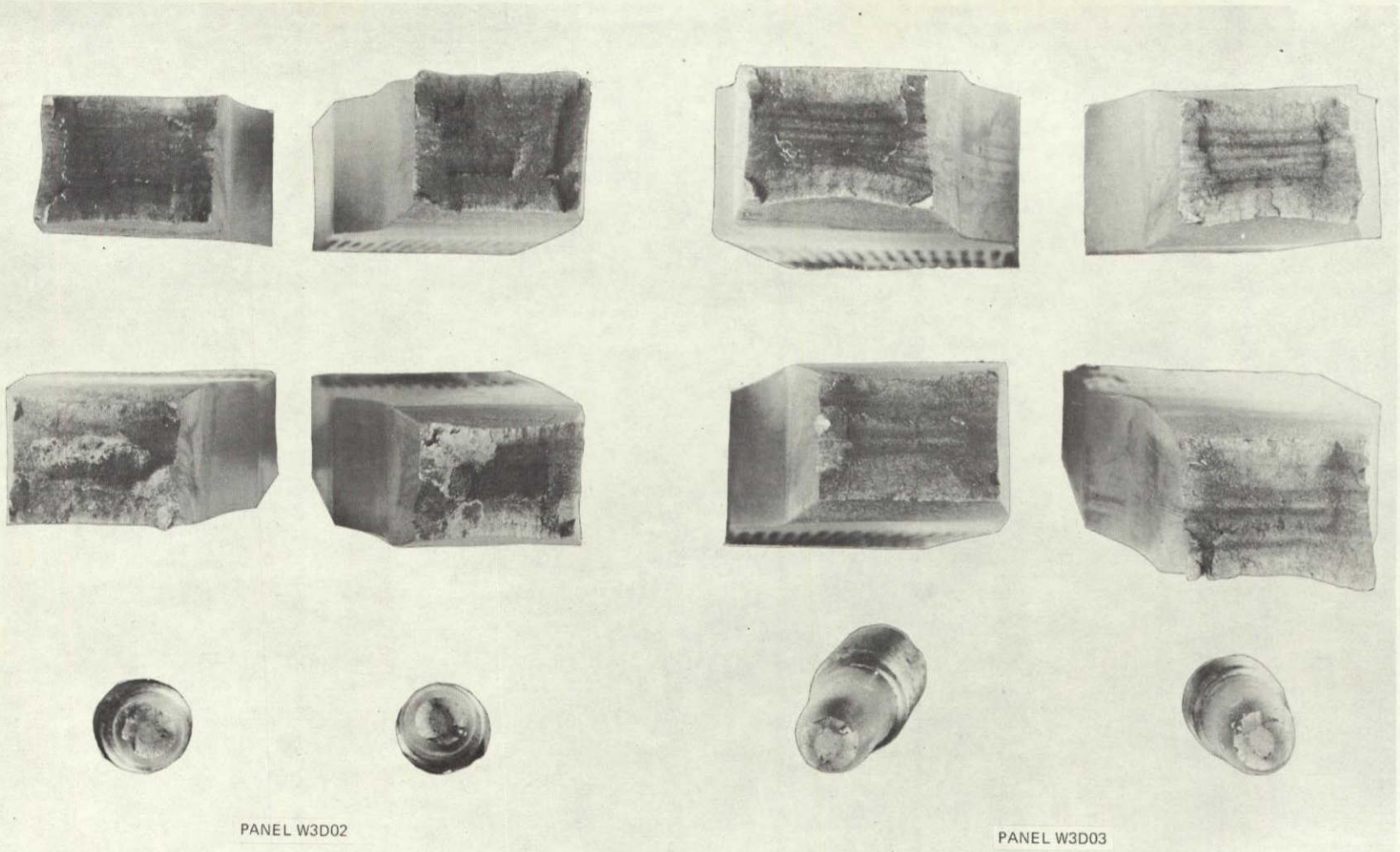

FIGURE 71

FRACTURE SURFACES OF BROKEN TENSILE SPECIMENS
FROM PANELS W3D02 AND W3D03

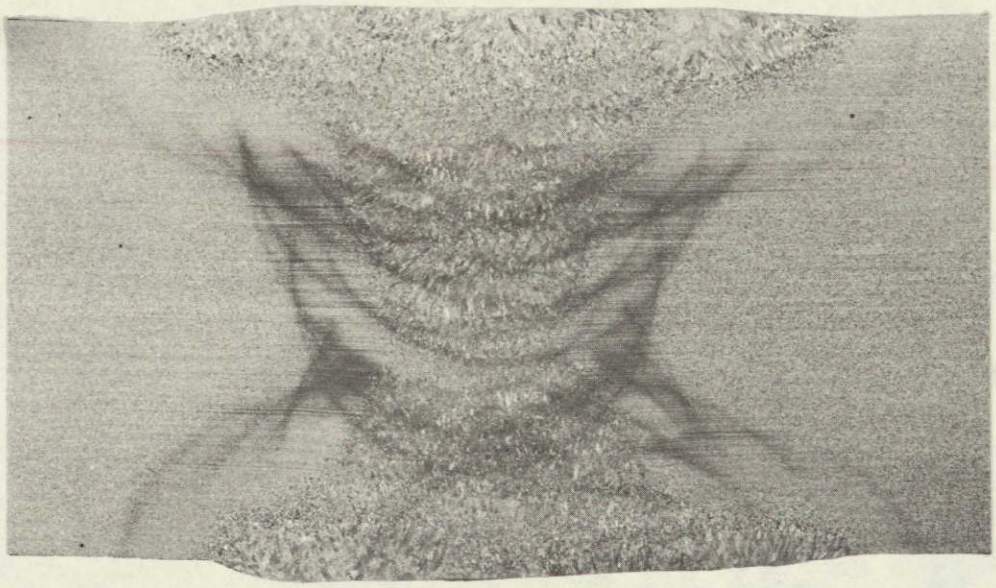

ETCHANT: HCl + H_2O_2 UNREPAIRED AREA MAG. 3.5X

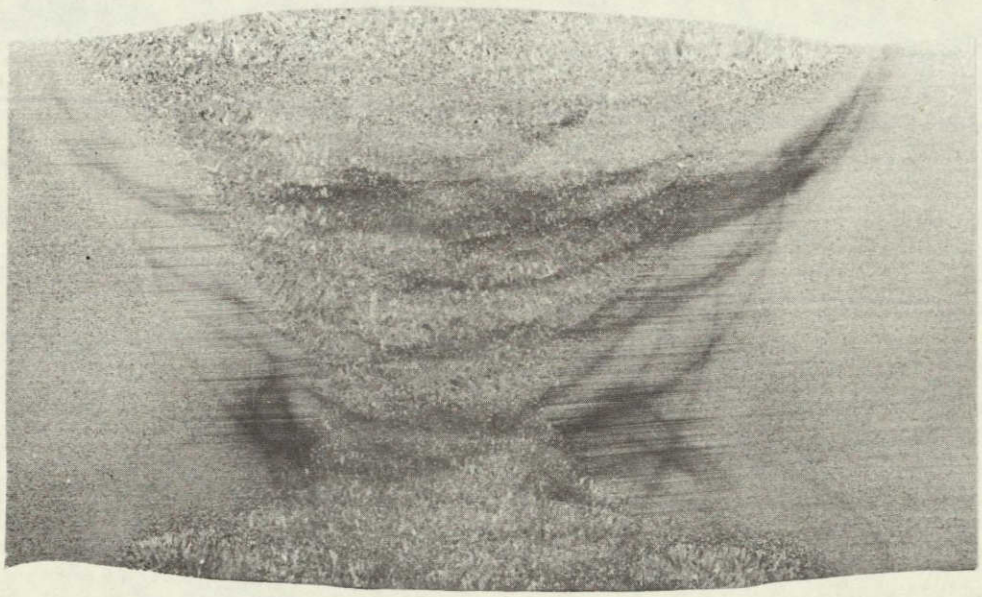

ETCHANT: HCl + H_2O_2 REPAIRED AREA MAG. 3.5X

FIGURE 72
CROSS SECTIONS THROUGH PANEL W3D02

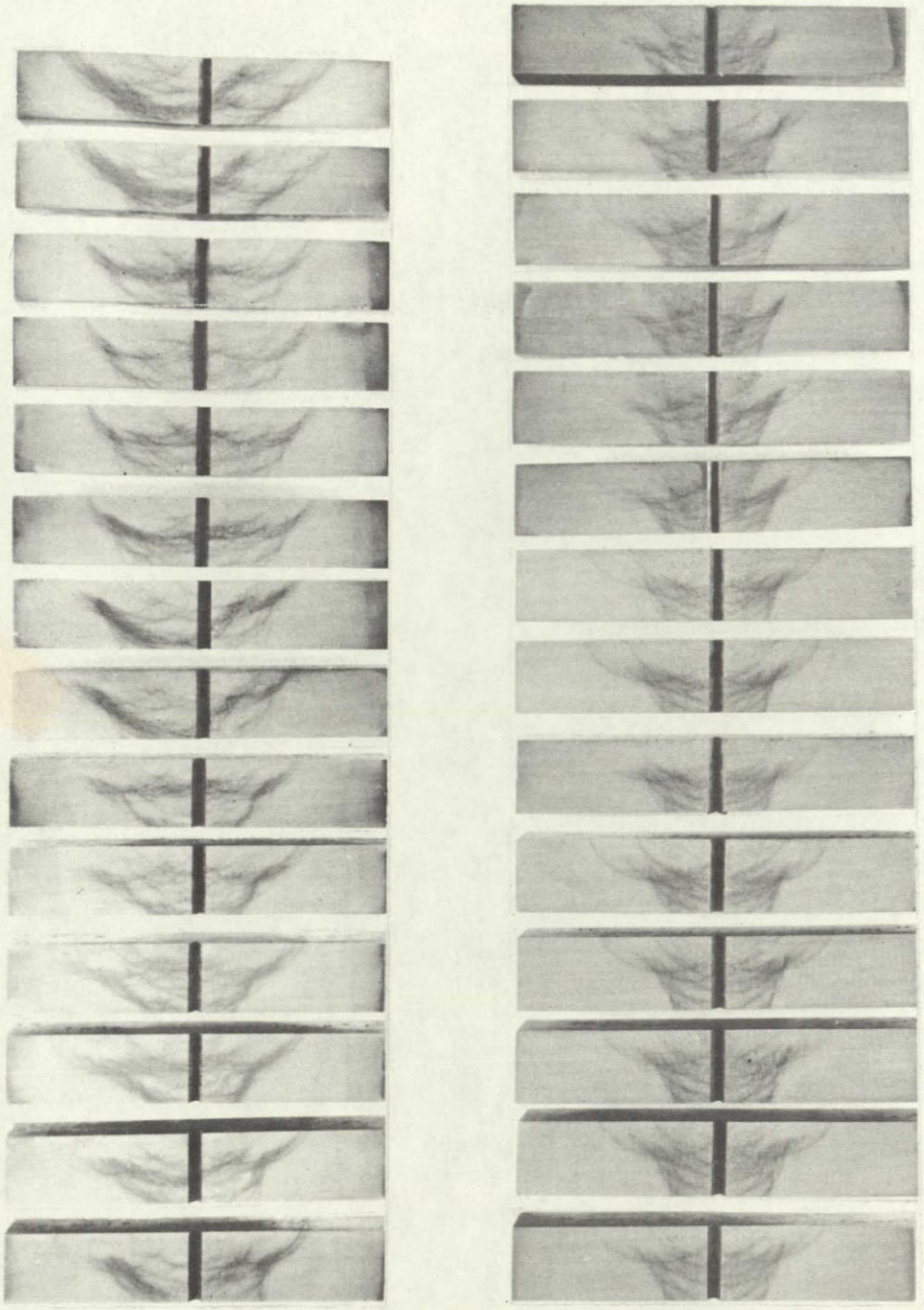

W3D02 W3D03

FIGURE 73

COMPARISON OF WELD HAZ CHARACTERISTICS OF REPAIRED AREAS OF W3D02 WITH UNREPAIRED AREAS OF W3D03

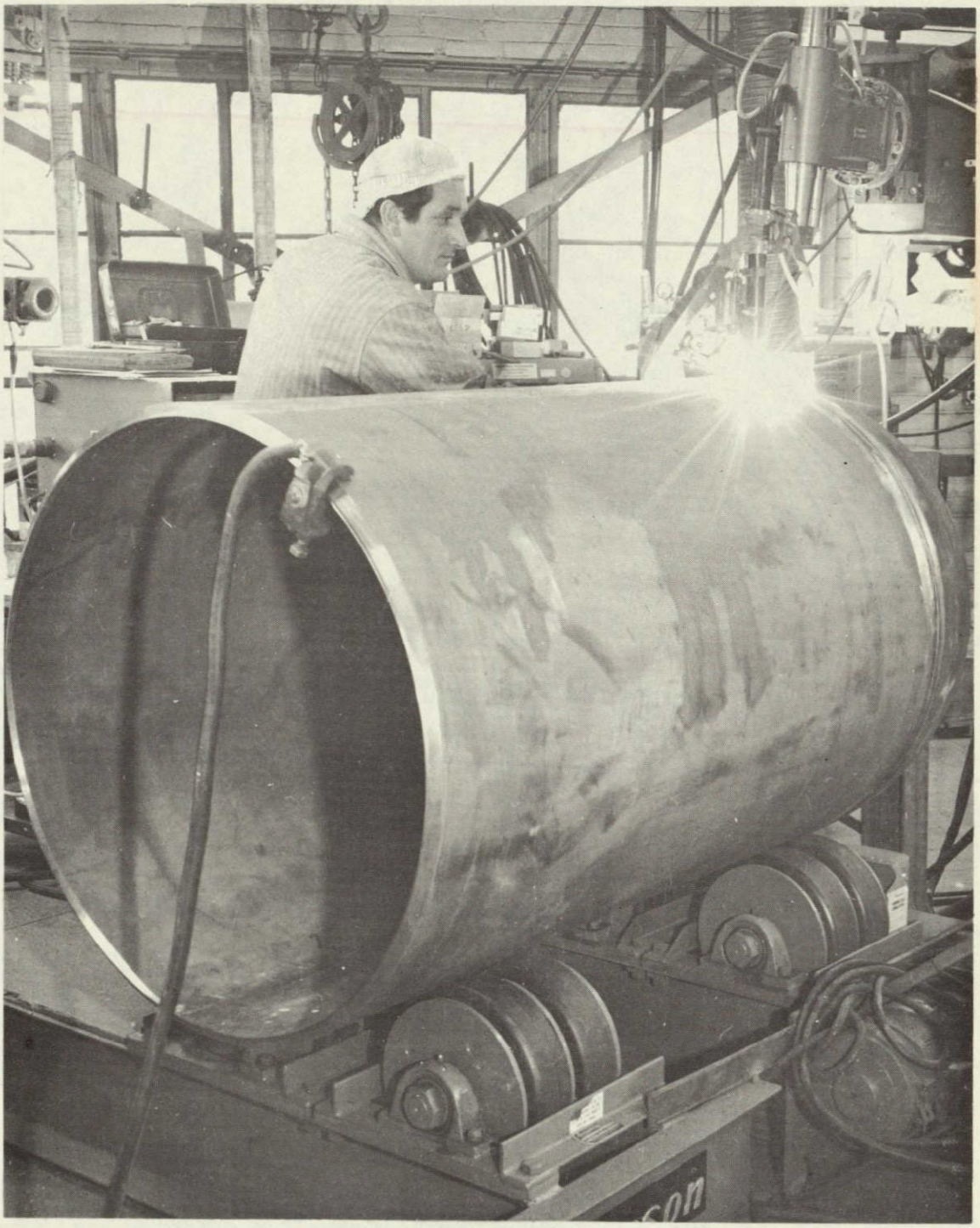

FIGURE 74
EQUIPMENT SET UP USED TO WELD LONGITUDINAL
AND GIRTH SEAMS OF TEST VESSELS

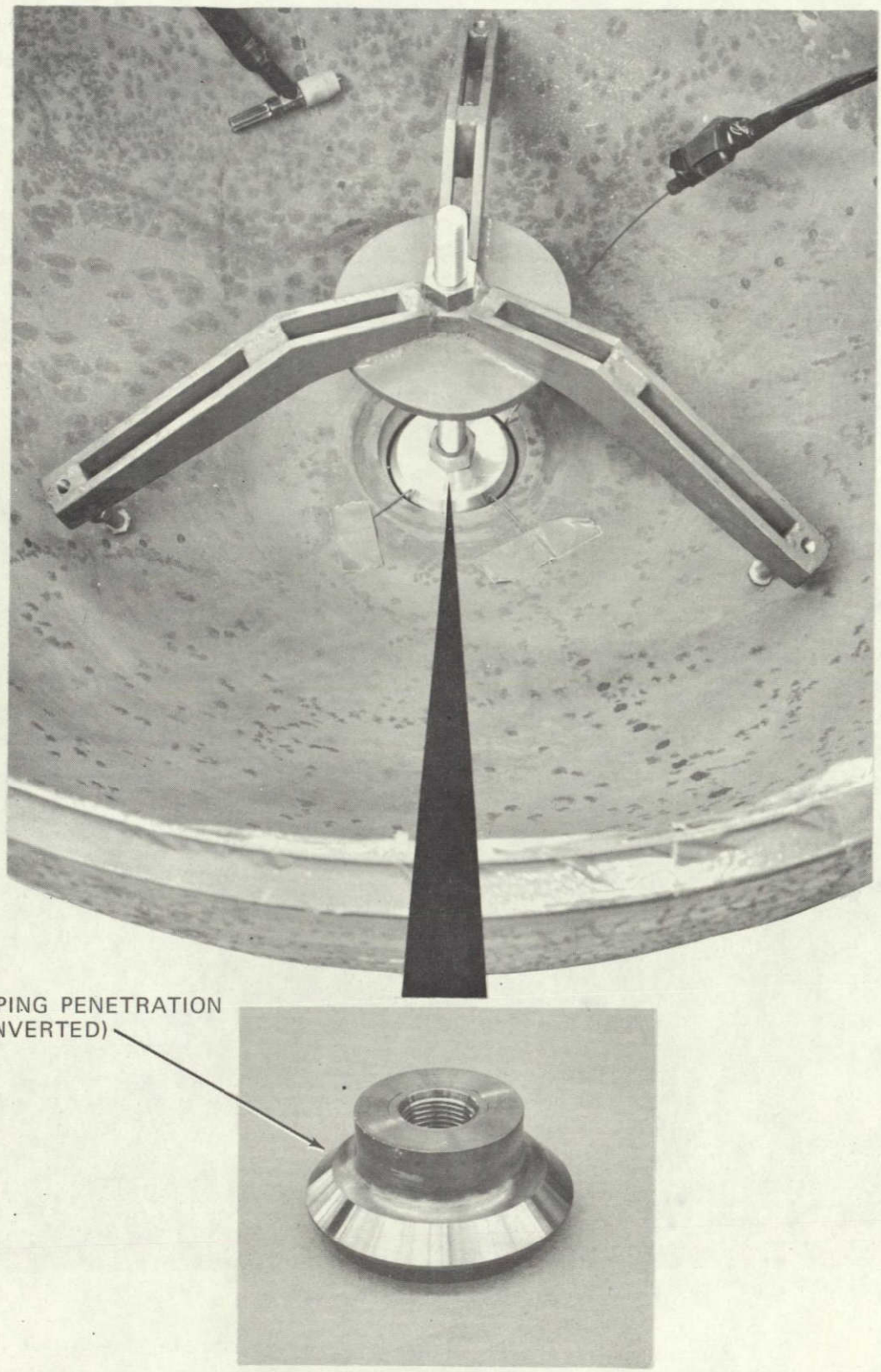

FIGURE 75
TYPICAL PIPING PENETRATION REINFORCEMENT AND DEVICE
USED FOR POSITIONING DURING TACK WELDING

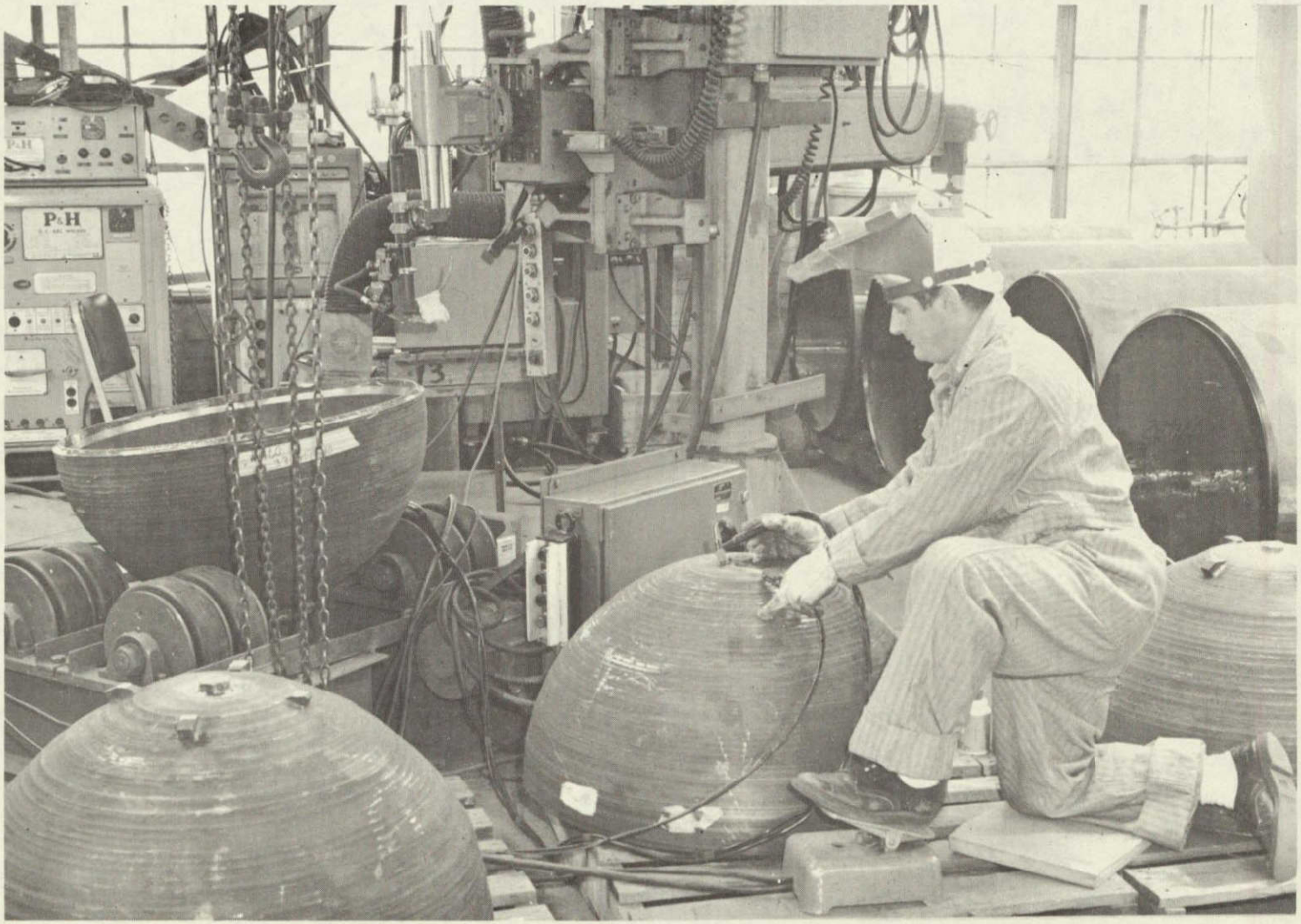

FIGURE 76
GTA WELDING PIPING PENETRATION REINFORCEMENT PIECES INTO VESSEL HEADS

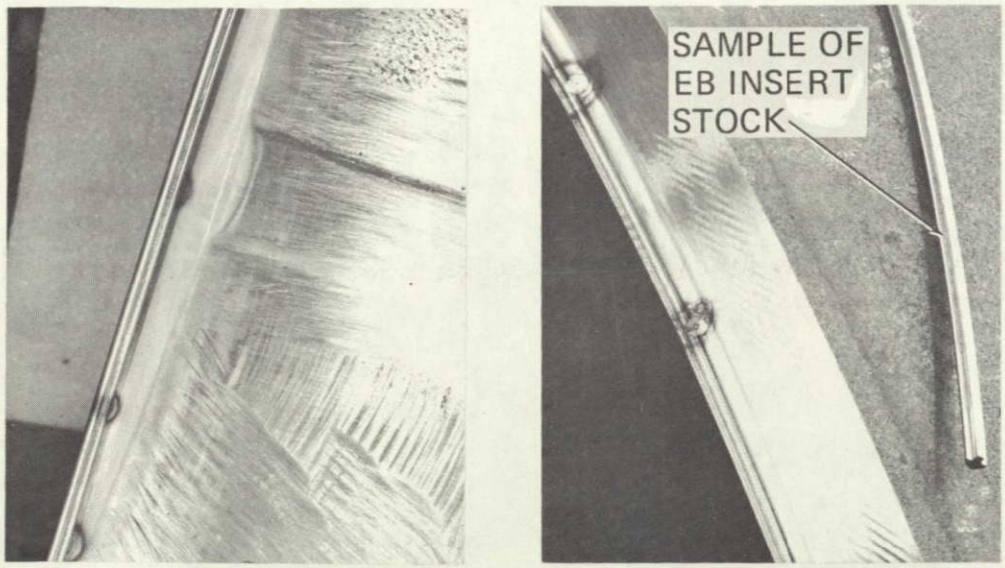

INSIDE VIEW

OUTSIDE VIEW

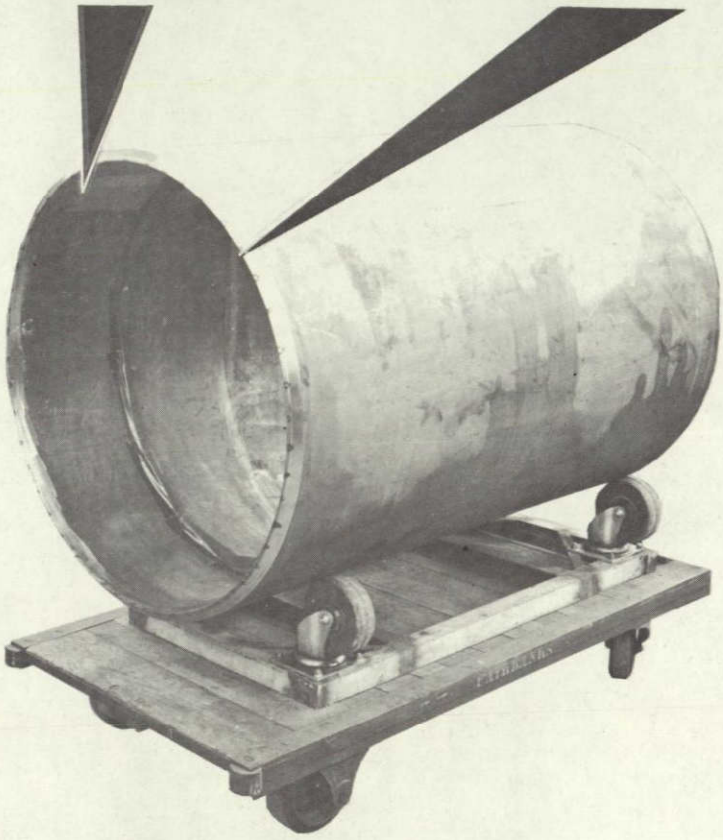

FIGURE 77
CYLINDER SECTION WITH EB WELD INSERT
TACK WELDED INTO PLACE

FIGURE 78
WELDING CLOSURE HEAD OF VESSEL "C"
TO CYLINDRICAL SECTION

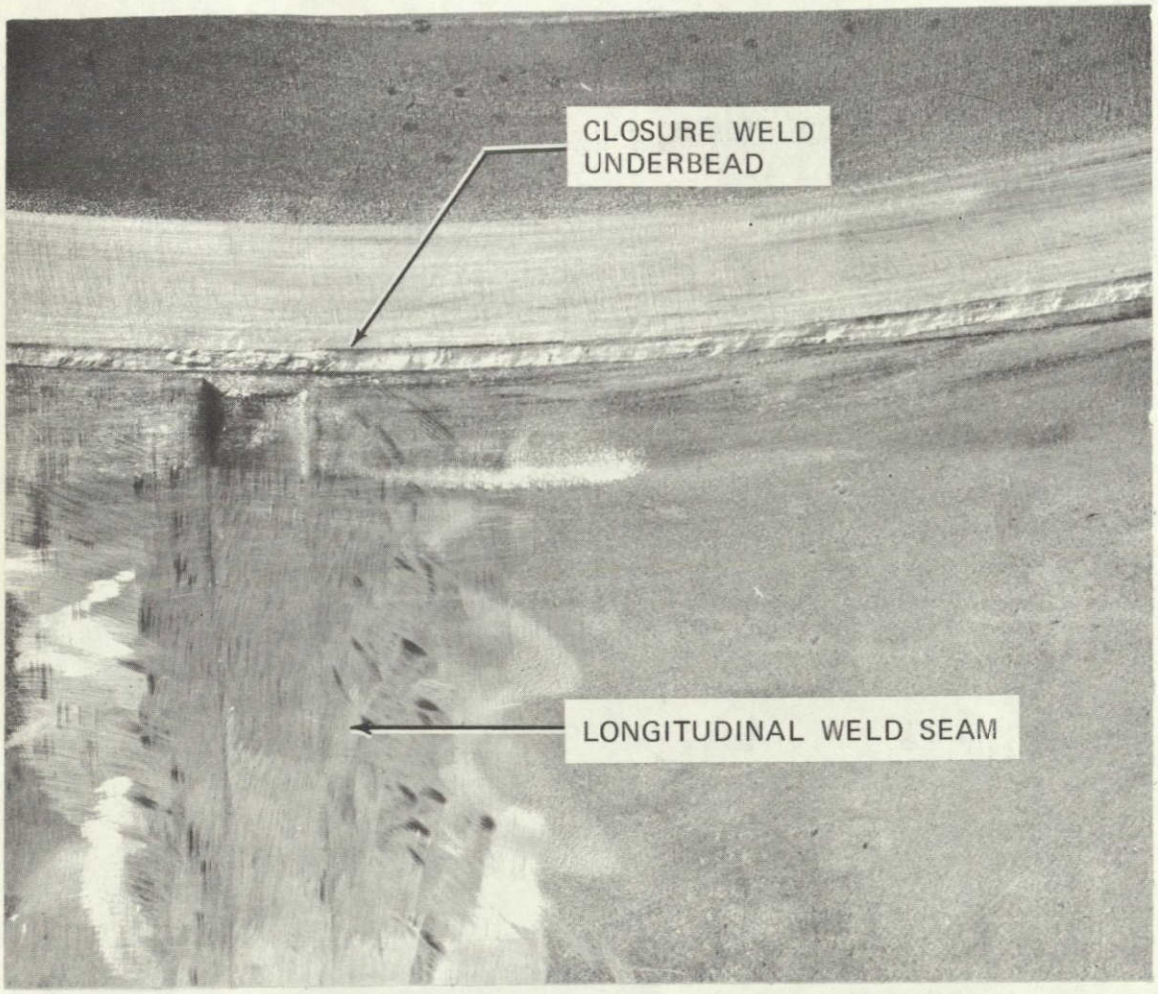

FIGURE 79
INSIDE VIEW OF VESSEL SHOWING TYPICAL CLOSURE WELD
UNDERBEAD AND PENETRATION UNIFORMITY

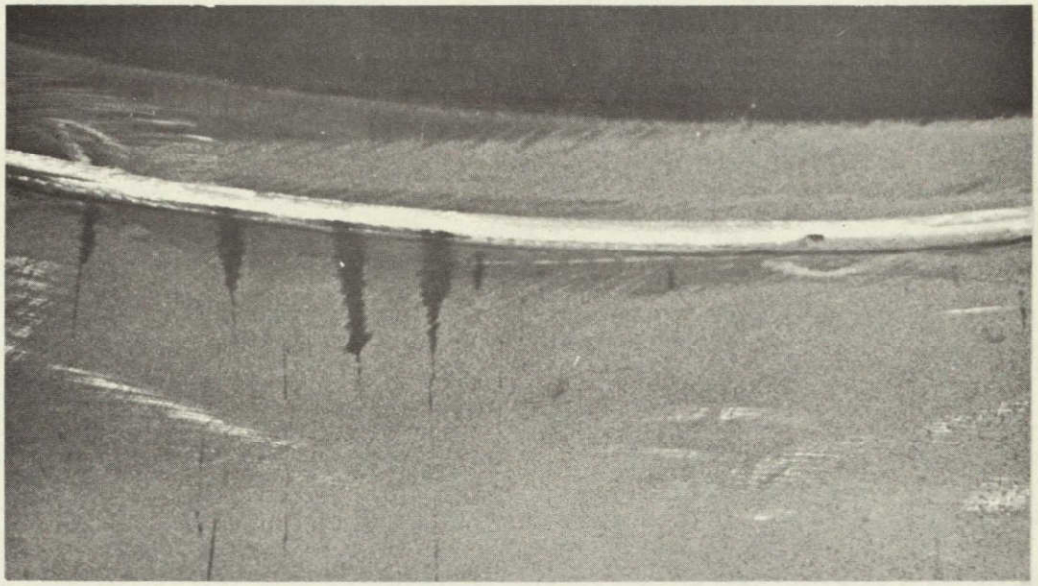

LIQUID PENETRANT DYE ONLY - NO DEVELOPER APPLIED

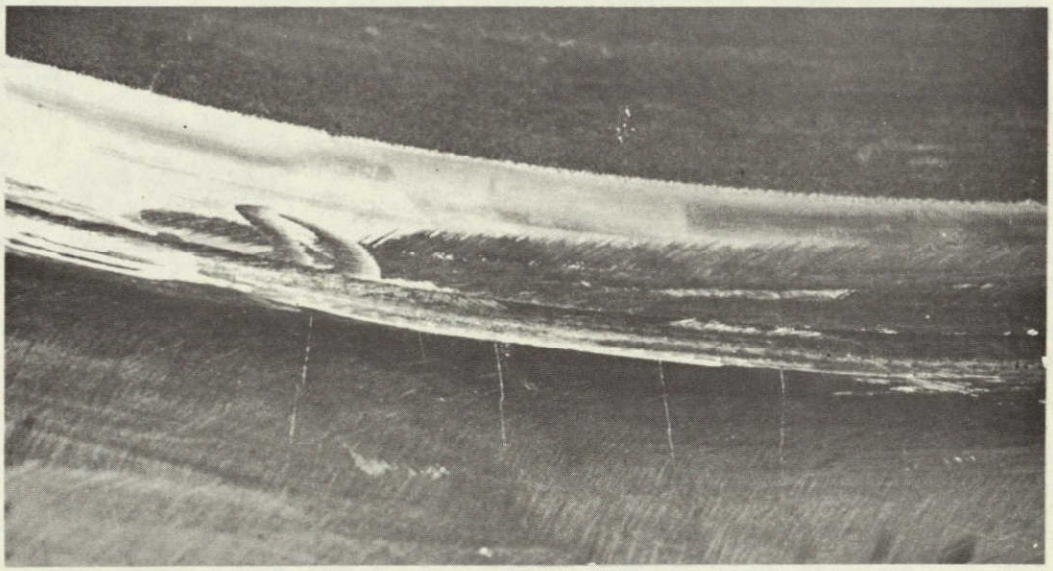

SAME GENERAL AREA - DEVELOPER APPLIED AND WIPED OFF

FIGURE 80
VIEW OF BASE METAL CRACKS FOUND ON INSIDE SURFACE
OF CYLINDER PORTION OF VESSEL "E"

NOT REPRODUCIBLE

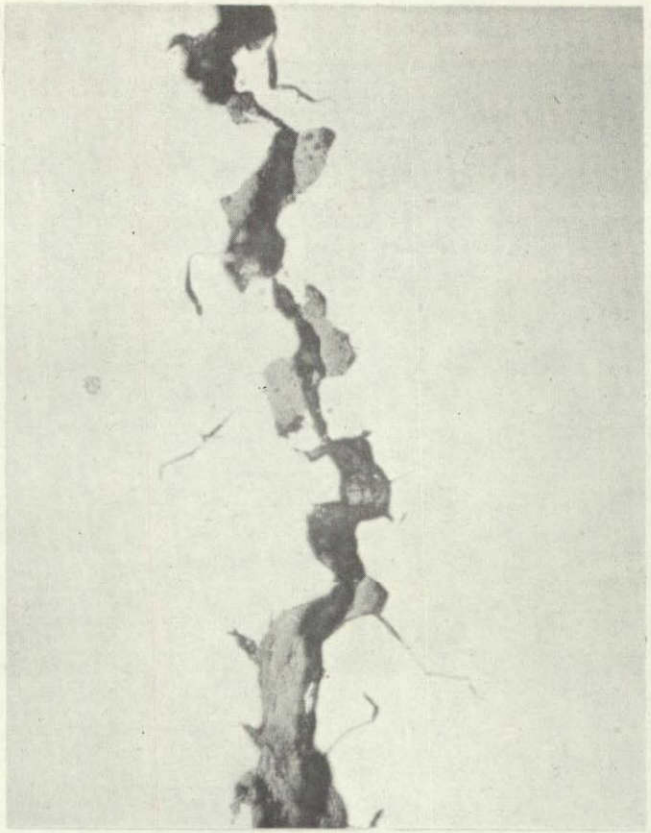

VIEW AT ½ CRACK DEPTH SHOWING OXIDATION ON CRACK SURFACE.

UNETCHED 400X

CRACK TIP AREA ETCHED TO ILLUSTRATE INTERGRANULAR CRACKING

WAZAUS-ETCH 650X

FIGURE 81
SECTIONS THROUGH BASE METAL CRACK FOUND IN VESSEL "E"

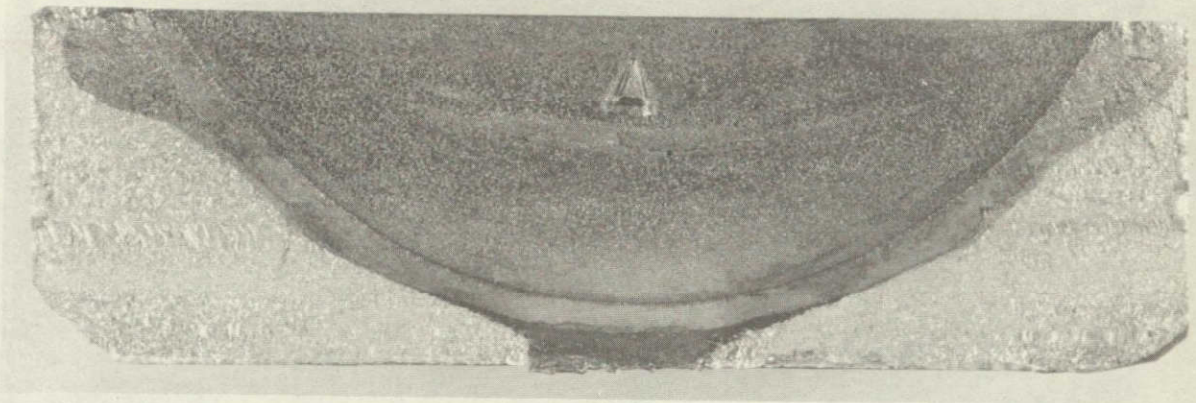

VESSEL "A"

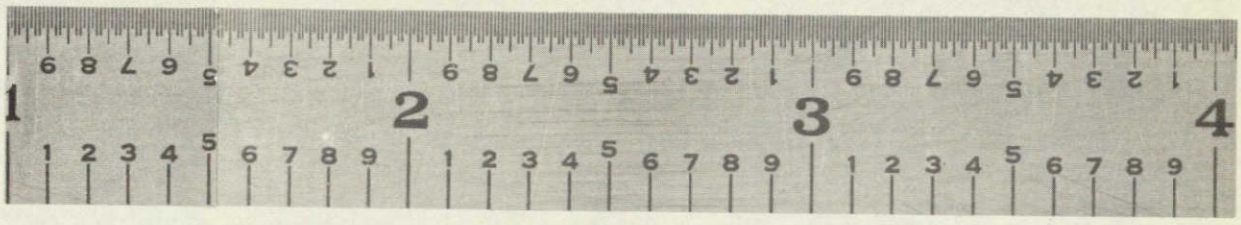

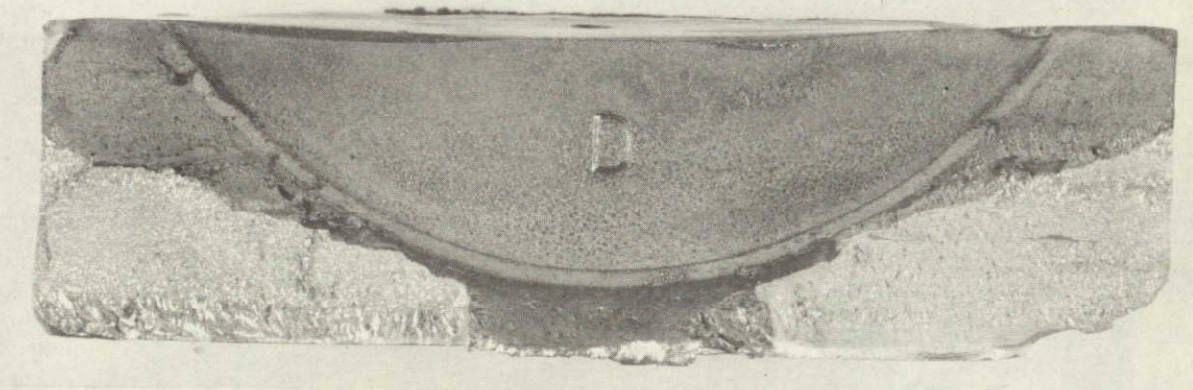

VESSEL "D"

FIGURE 82
EDM ARTIFICIAL FLAWS REMOVED FROM VESSELS A AND D
AFTER HYDROTEST

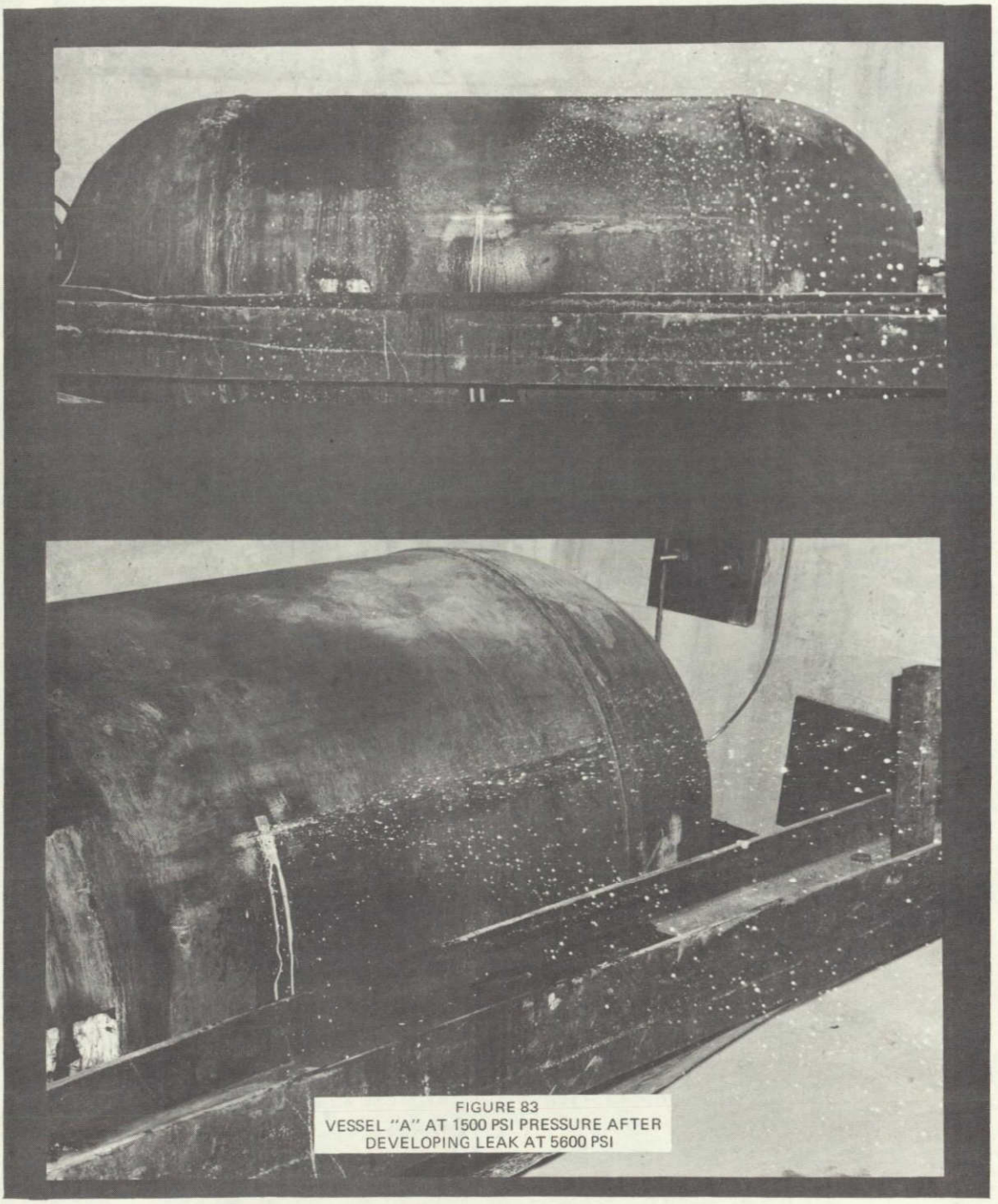

FIGURE 83
VESSEL "A" AT 1500 PSI PRESSURE AFTER
DEVELOPING LEAK AT 5600 PSI

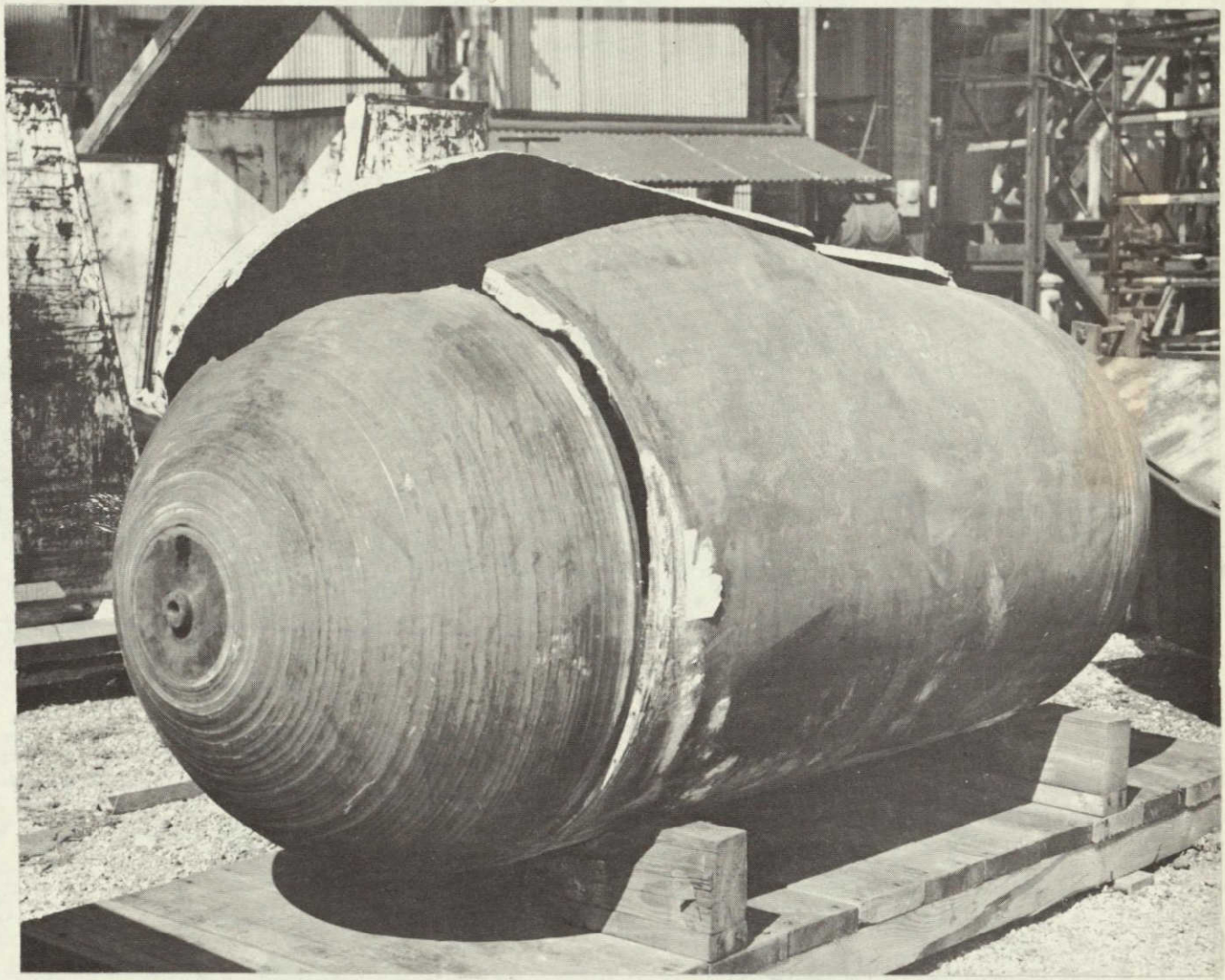

FIGURE 84
GENERAL VIEW OF VESSEL "B" AFTER FAILURE

END VIEW

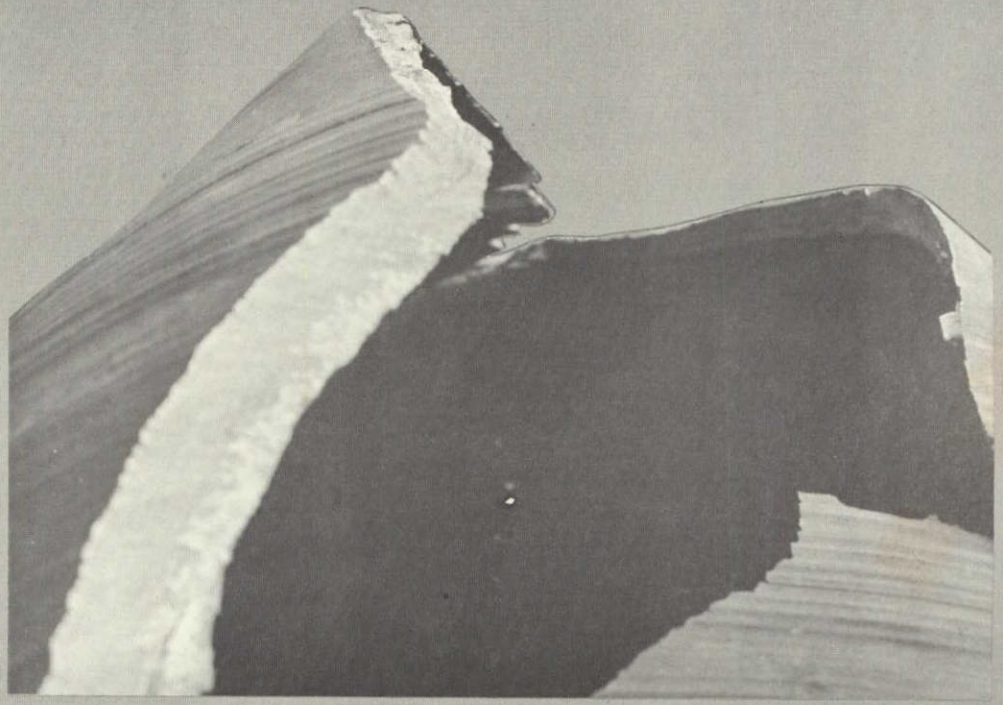

EDGE VIEW OF FRACTURE

FIGURE 85
DETAILS OF FRACTURE PATTERN OF VESSEL 'B'

FIGURE 86
GENERAL VIEW OF TEST PIT AFTER BURST TEST OF VESSEL "B",
STEEL PLATES IN FOREGROUND ORIGINALLY COVERED VESSEL TO RETAIN WATER

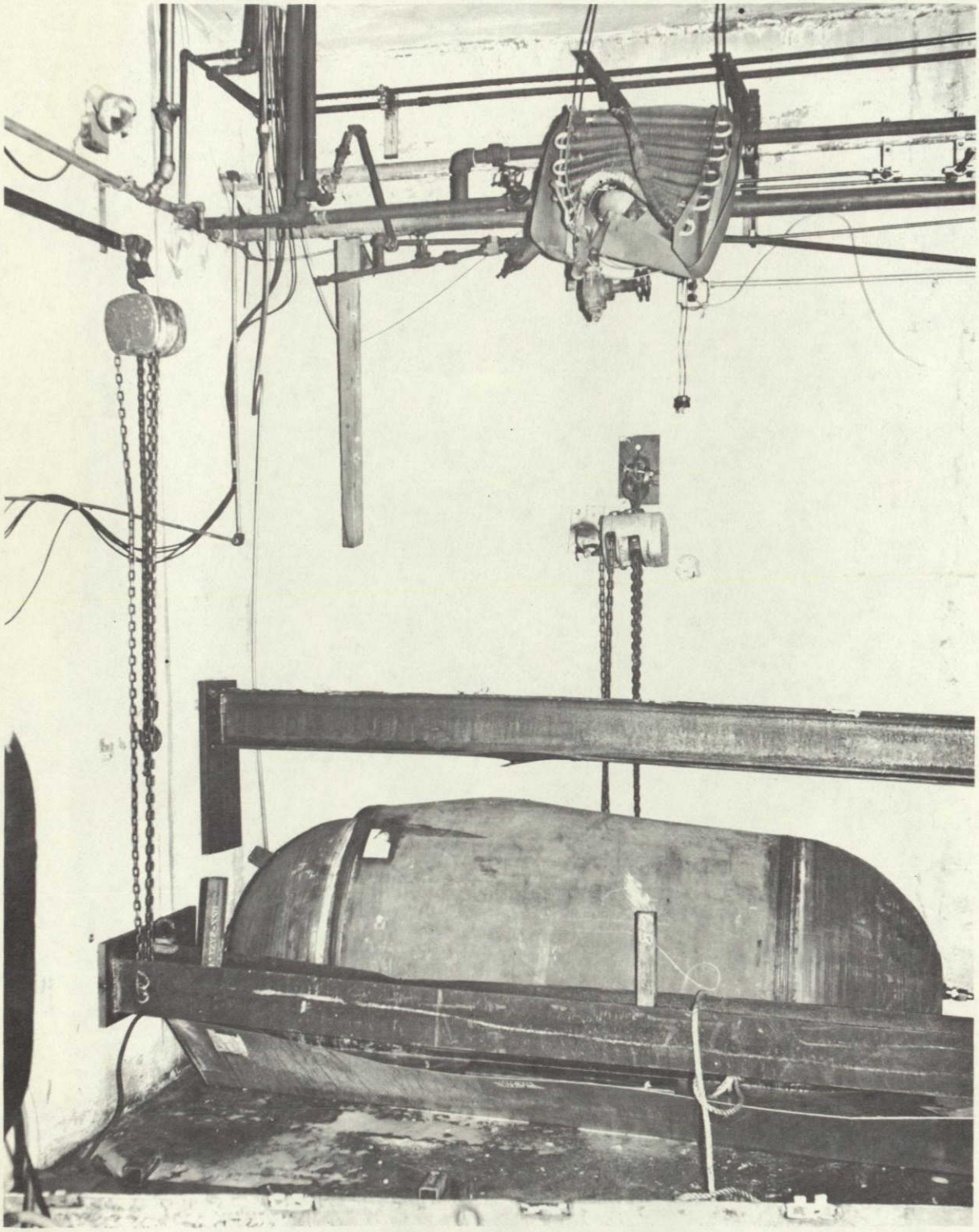

FIGURE 87
VESSEL "B" AFTER BURST TEST. DAMAGE TO HEATER AND
STRUCTURE AROUND VESSEL OCCURRED AT BURST

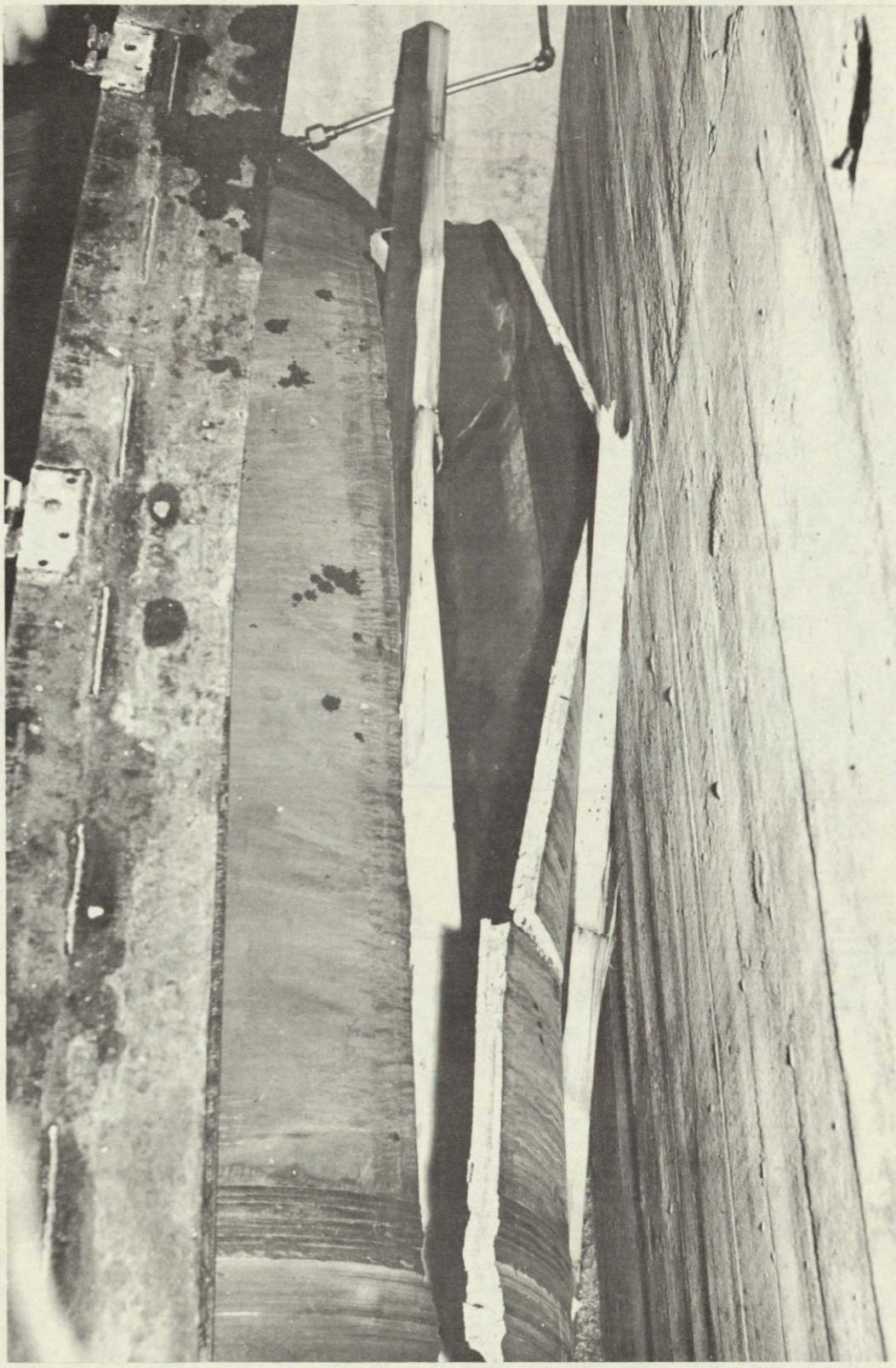

FIGURE 88
VESSEL "B" – CLOSE-UP OF FAILED SEAM SHORTLY AFTER TEST

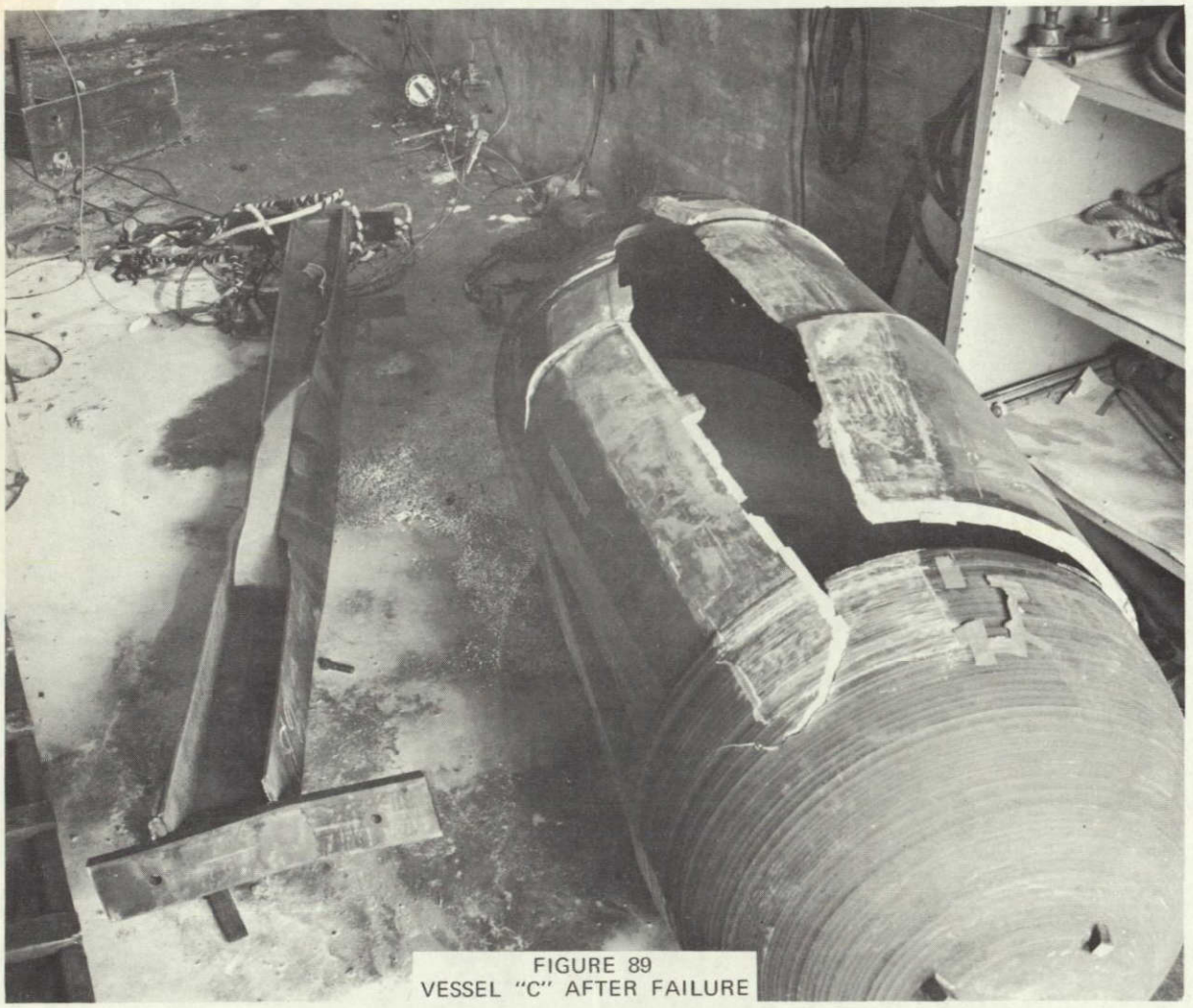

FIGURE 89
VESSEL "C" AFTER FAILURE

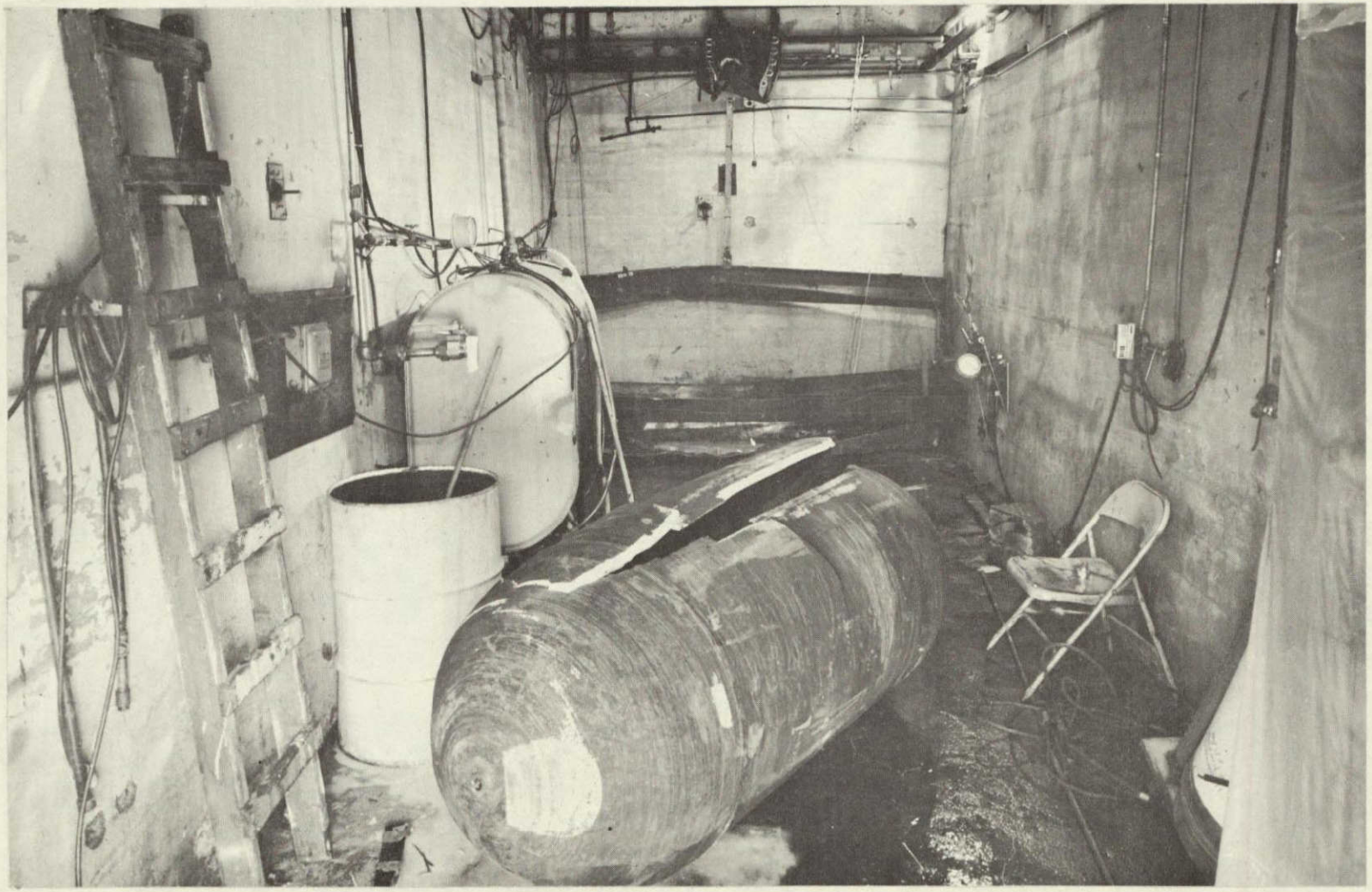

FIGURE 90
VESSEL "E" IN TEST PIT AFTER HYDROTEST

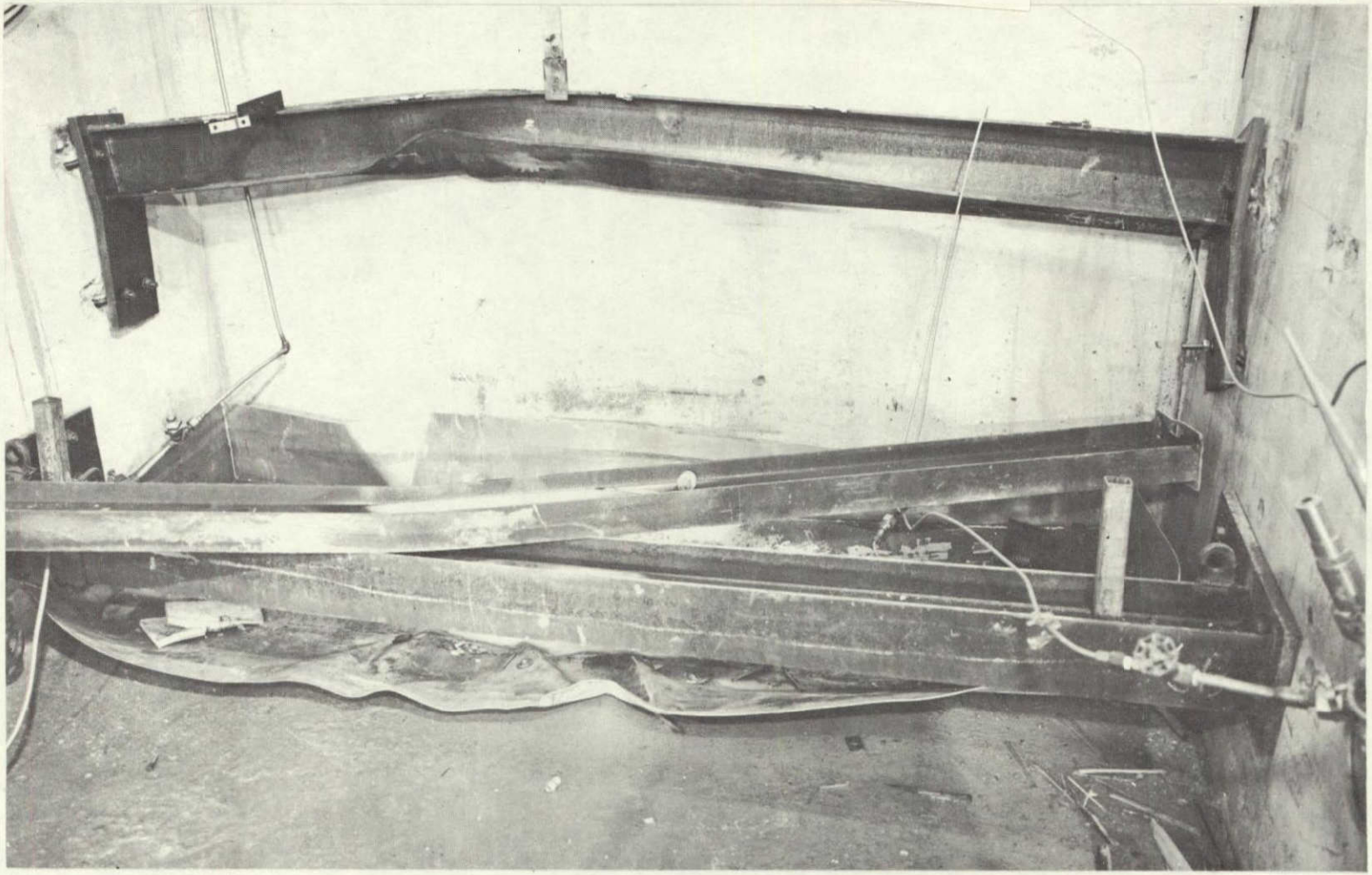

FIGURE 91
RESTRAINING FIXTURE AFTER HYDROTEST OF VESSEL "E"

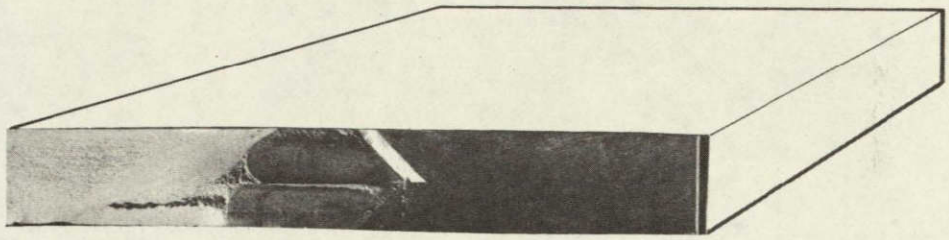

W3D03-B2

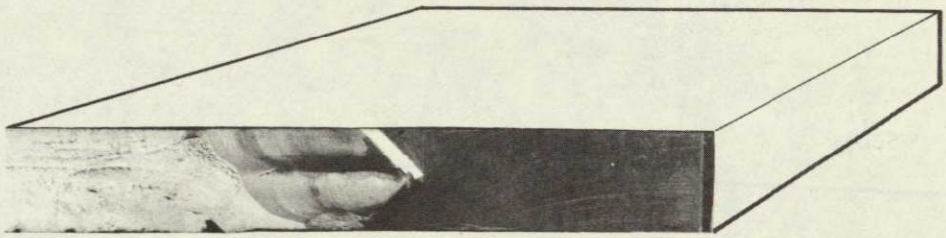

W3D04-B2

FIGURE 92
TYPICAL PRECRACKED AREAS OF WELD HAZ
EDGE-NOTCHED BEND SPECIMENS

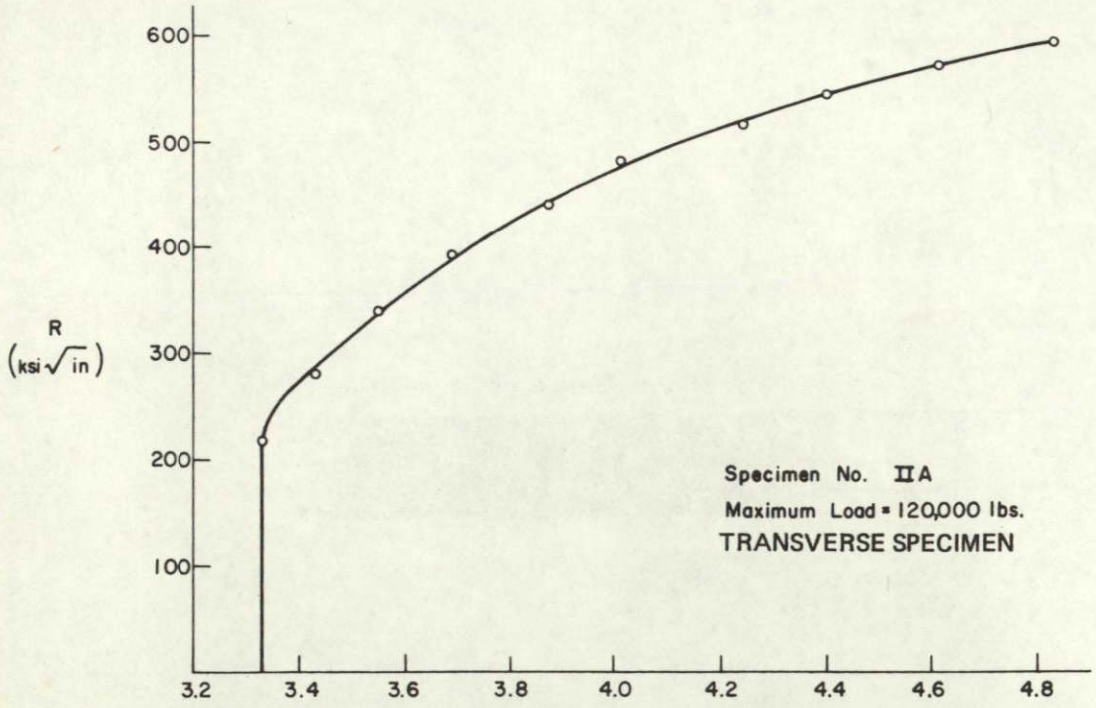

PHOTO CREDIT:
LEHIGH UNIVERSITY

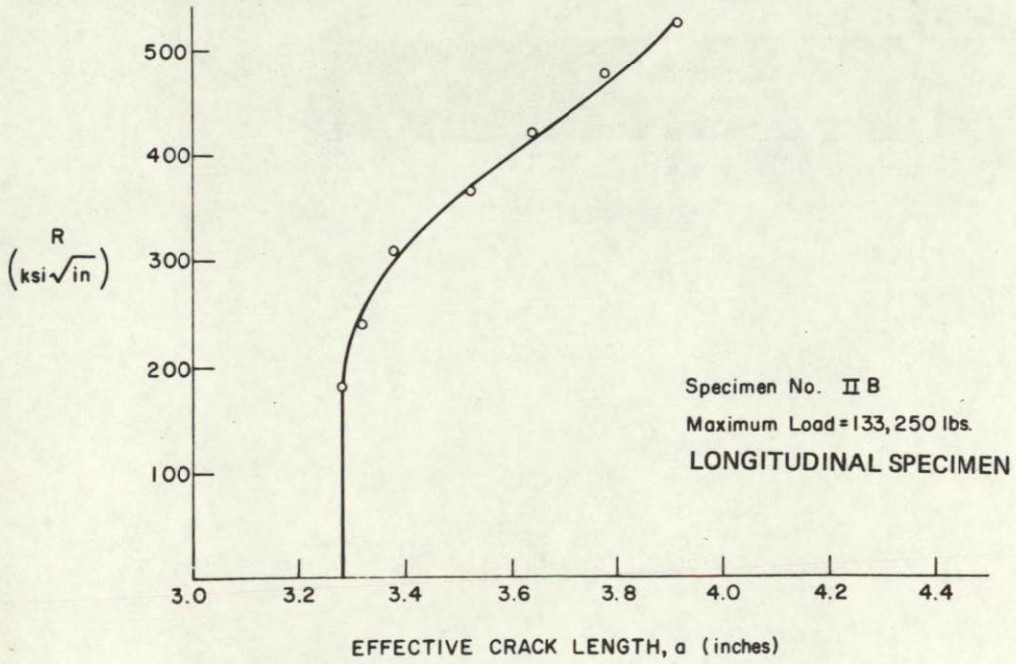

FIGURE 93
BASE METAL FRACTURE TOUGHNESS BEND TEST RESPONSE CURVES, TRANSVERSE AND LONGITUDINAL SPECIMENS

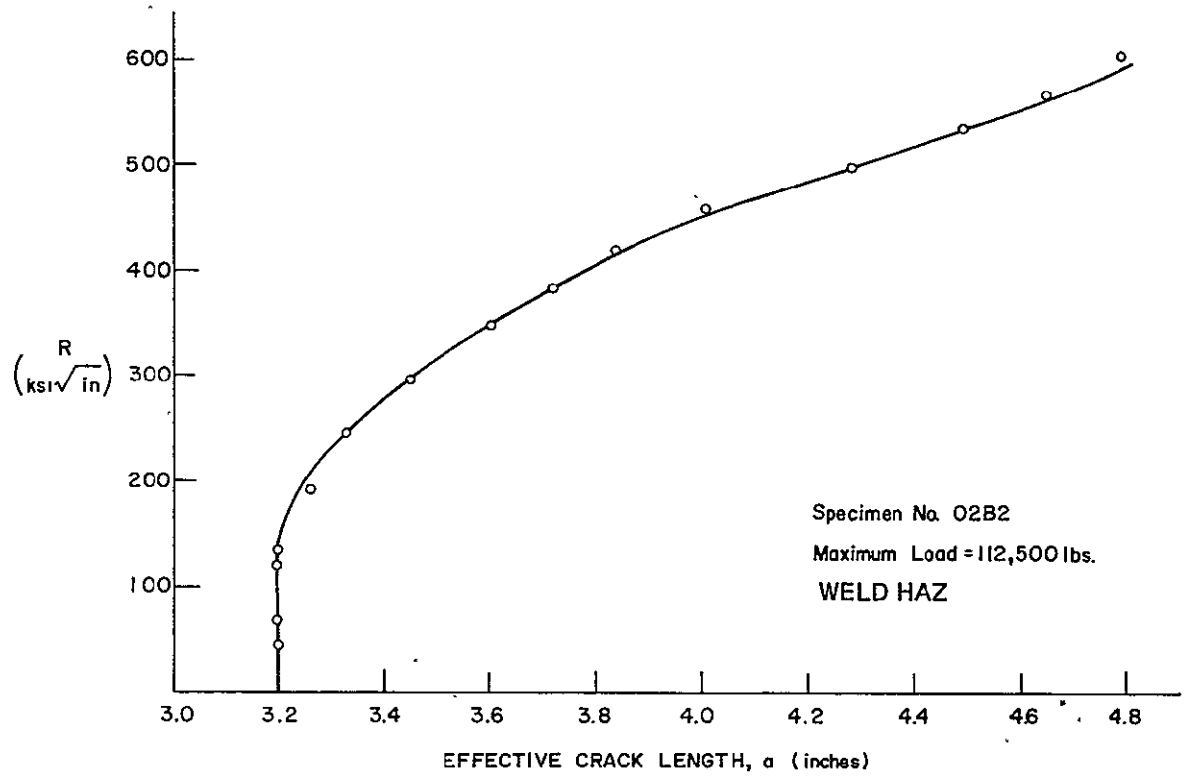

PHOTO CREDIT:
LEHIGH UNIVERSITY

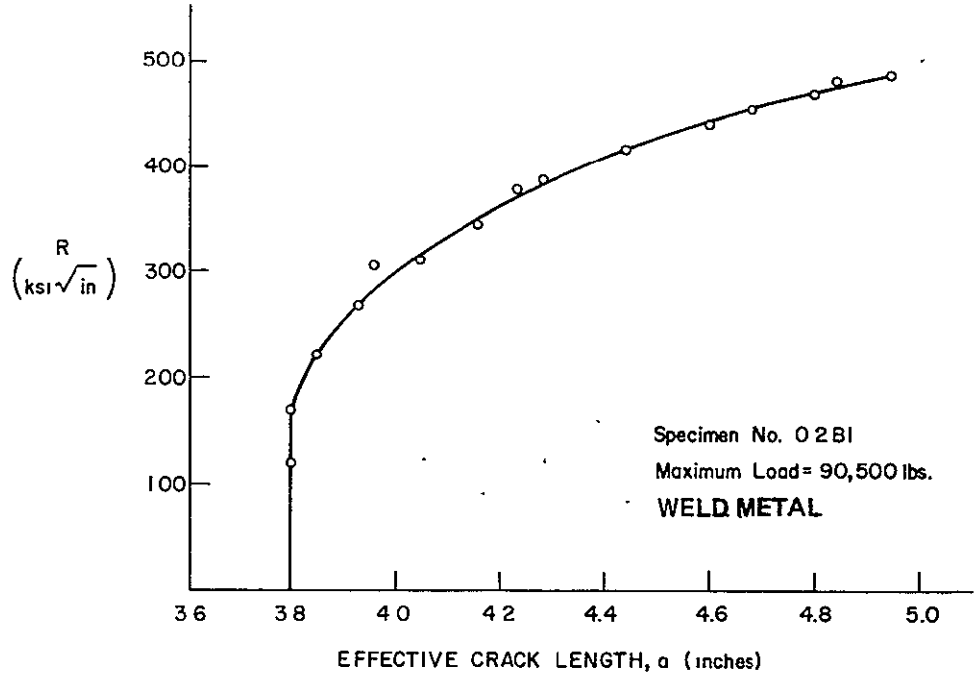

FIGURE 94
WELD METAL AND WELD HAZ FRACTURE TOUGHNESS BEND TEST RESPONSE CURVES, SPECIMENS B1 AND B2 FROM PANEL W3C02.

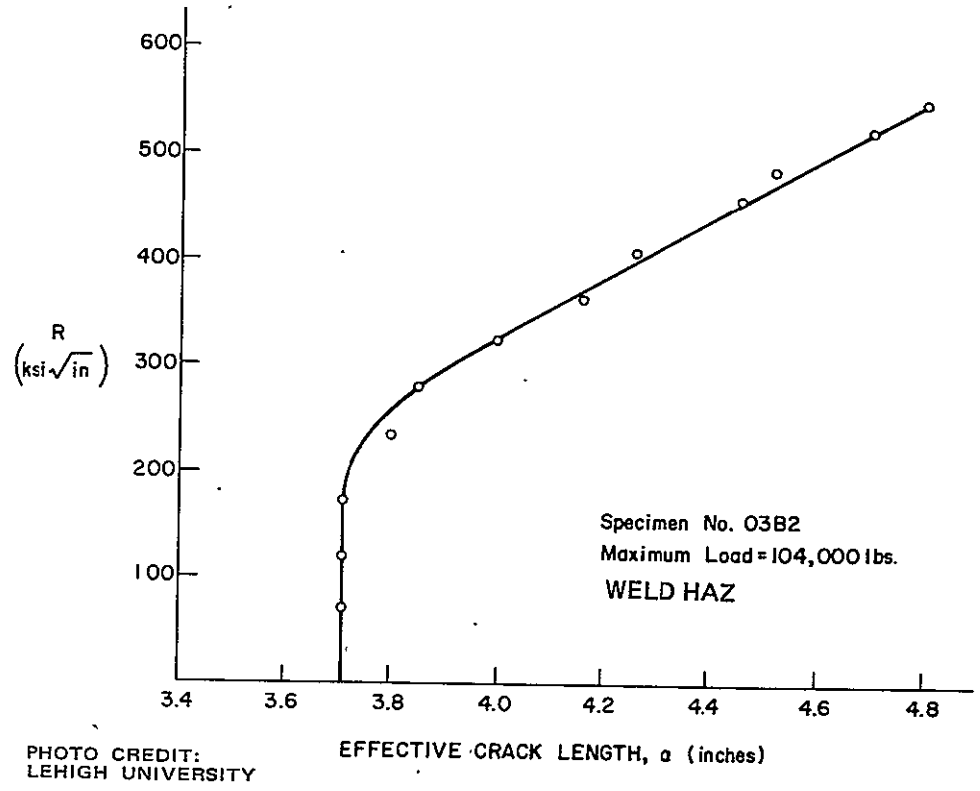

PHOTO CREDIT:
LEHIGH UNIVERSITY

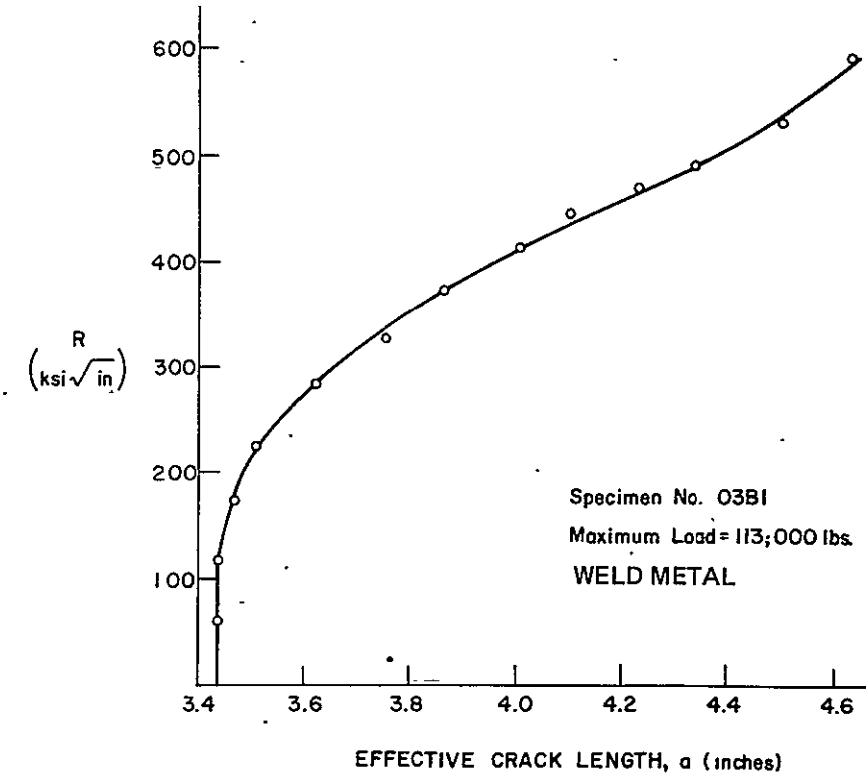

FIGURE 95
WELD METAL AND WELD HAZ FRACTURE TOUGHNESS BEND TEST
RESPONSE CURVES, SPECIMENS B1 AND B2 FROM PANEL W3C03

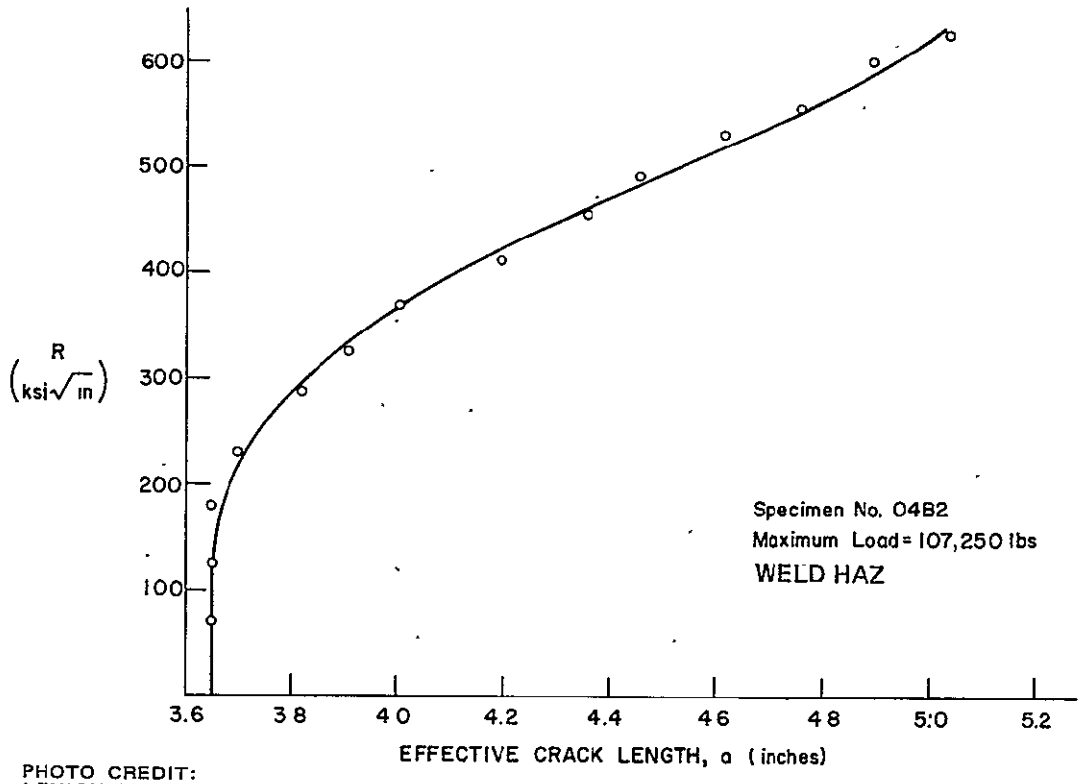

PHOTO CREDIT:
LEHIGH UNIVERSITY

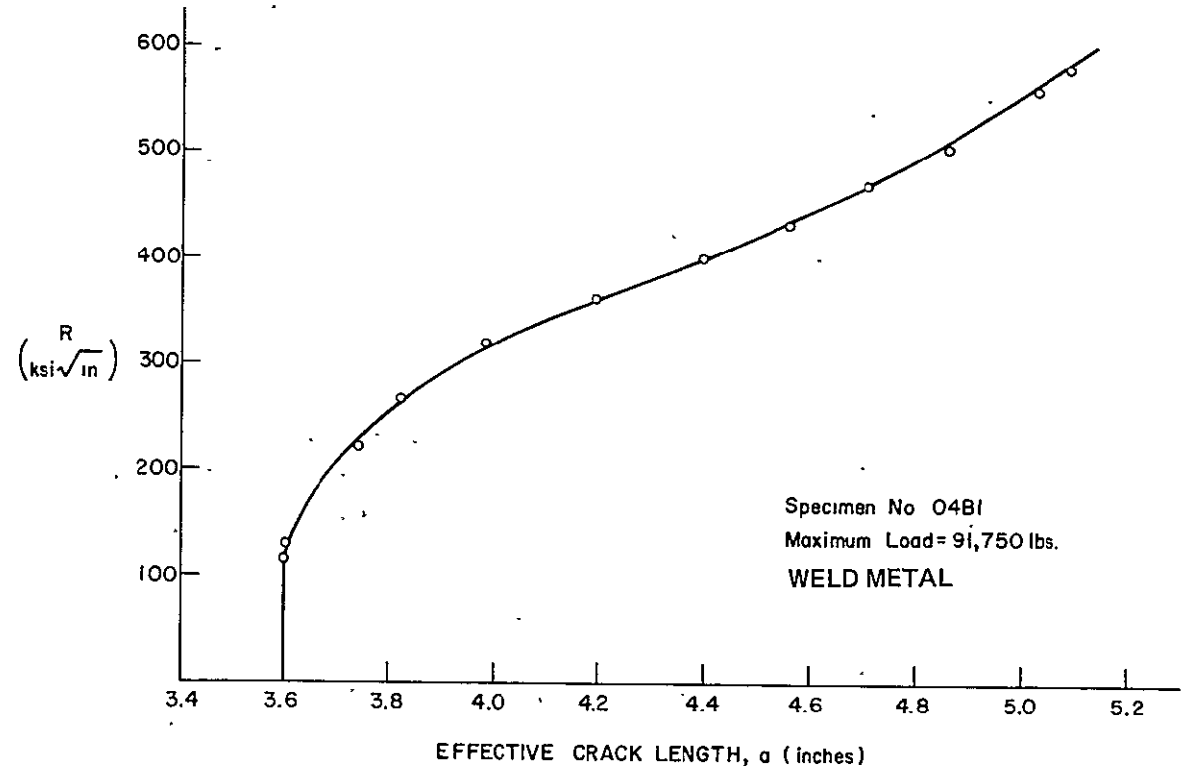

FIGURE 96
WELD METAL AND WELD HAZ FRACTURE TOUGHNESS BEND TEST
RESPONSE CURVES, SPECIMENS B1 AND B2 FROM PANEL W3C04

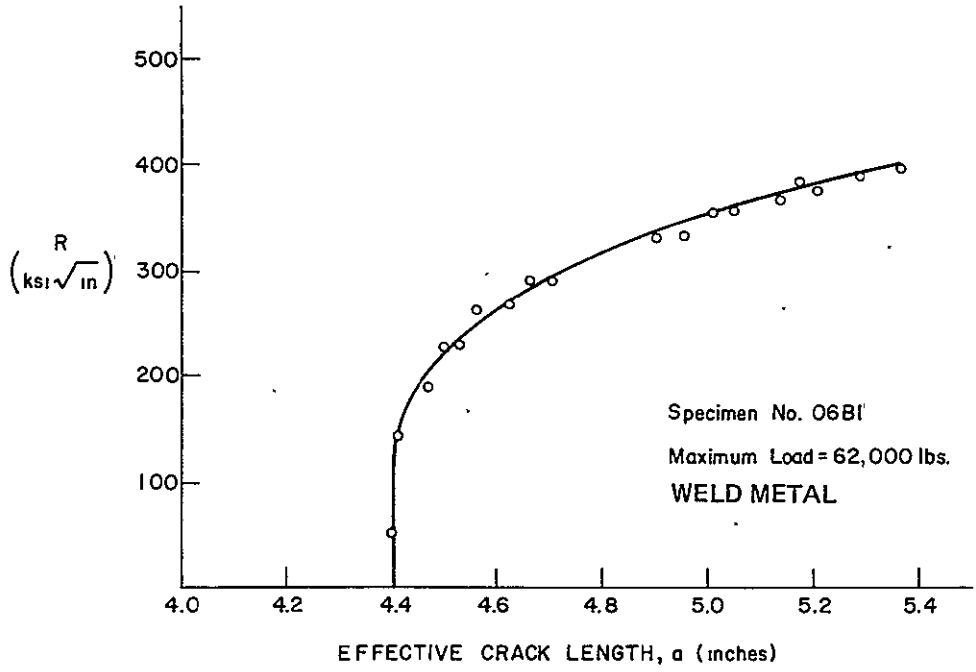

PHOTO CREDIT:
LEHIGH UNIVERSITY

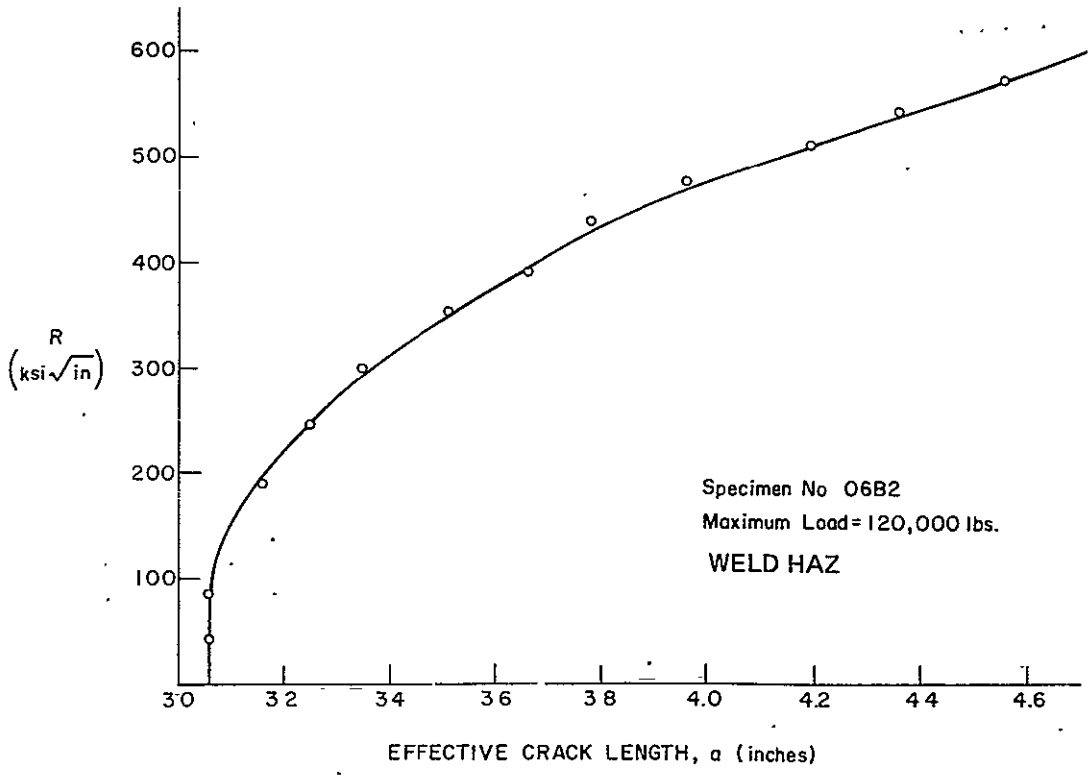

FIGURE 97
WELD METAL AND WELD HAZ FRACTURE TOUGHNESS BEND TEST
RESPONSE CURVES, SPECIMENS B1 AND B2 FROM PANEL W3C06

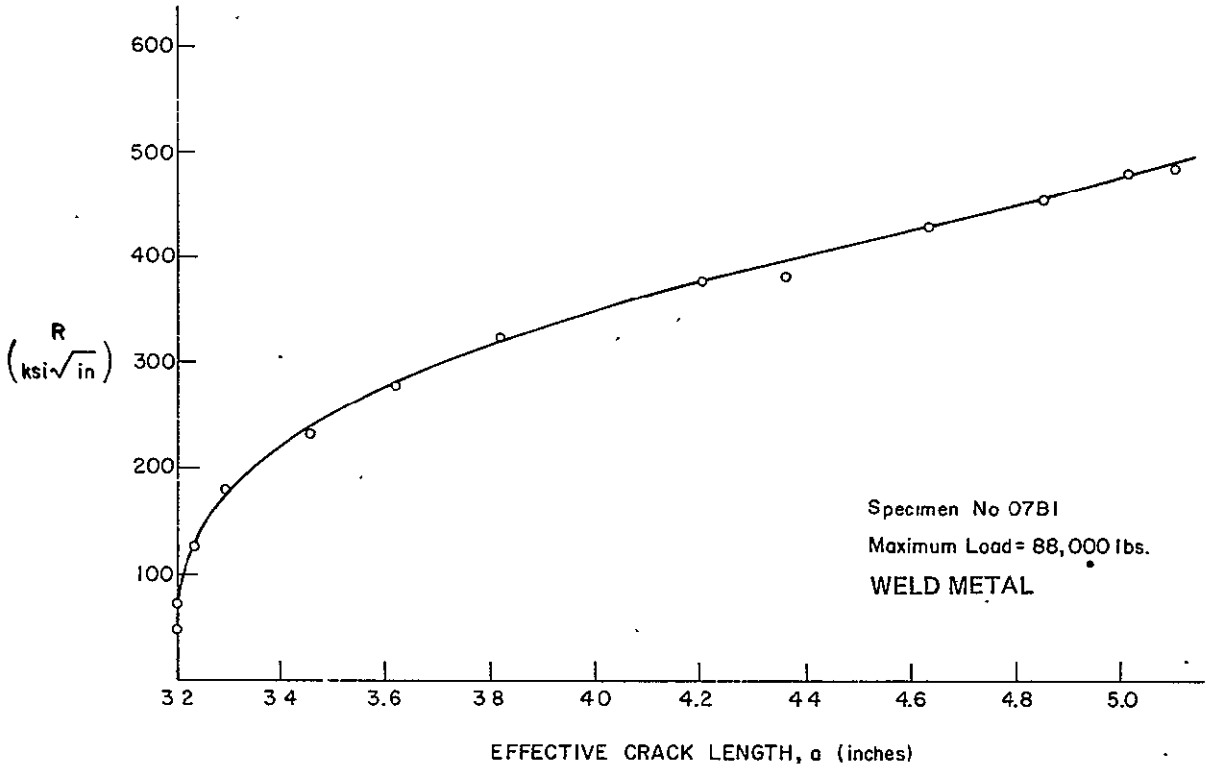

PHOTO CREDIT:
LEHIGH UNIVERSITY

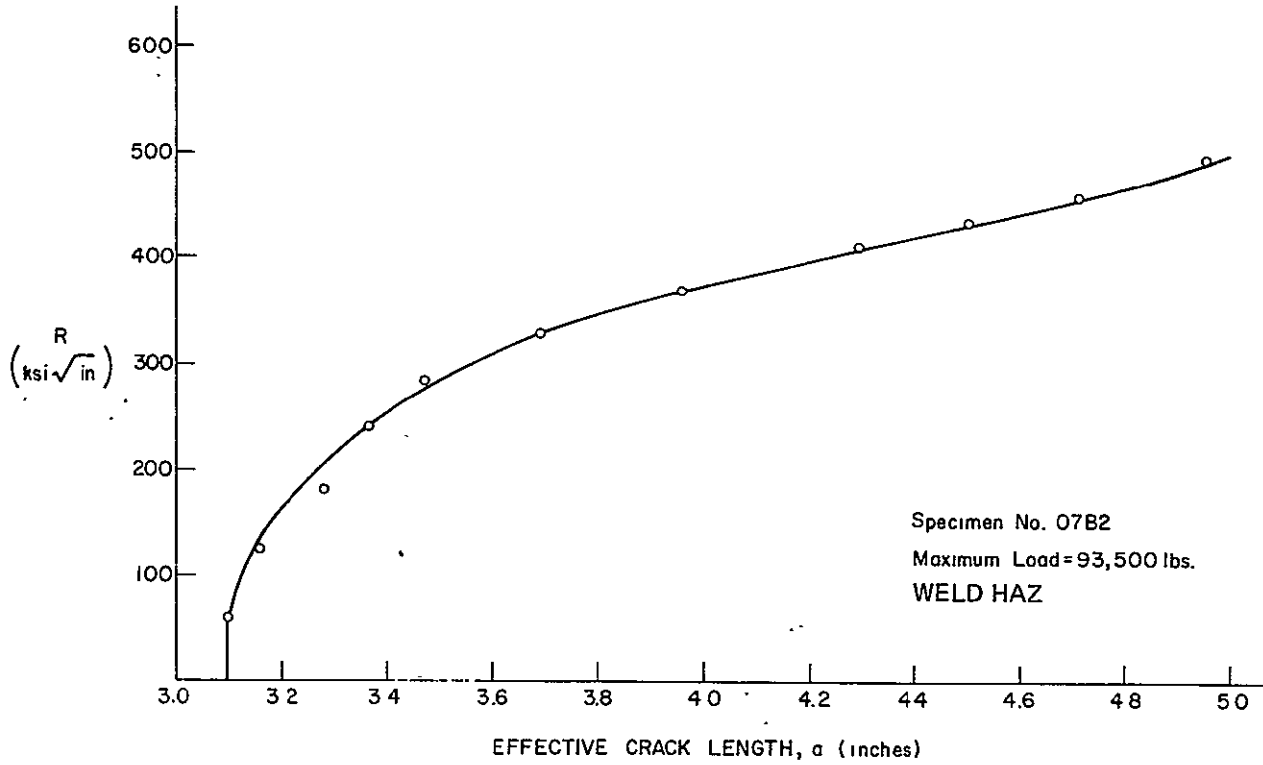

FIGURE 98
WELD METAL AND WELD HAZ FRACTURE TOUGHNESS BEND TEST
RESPONSE CURVES, SPECIMENS B1 AND B2 FROM PANEL W3C07

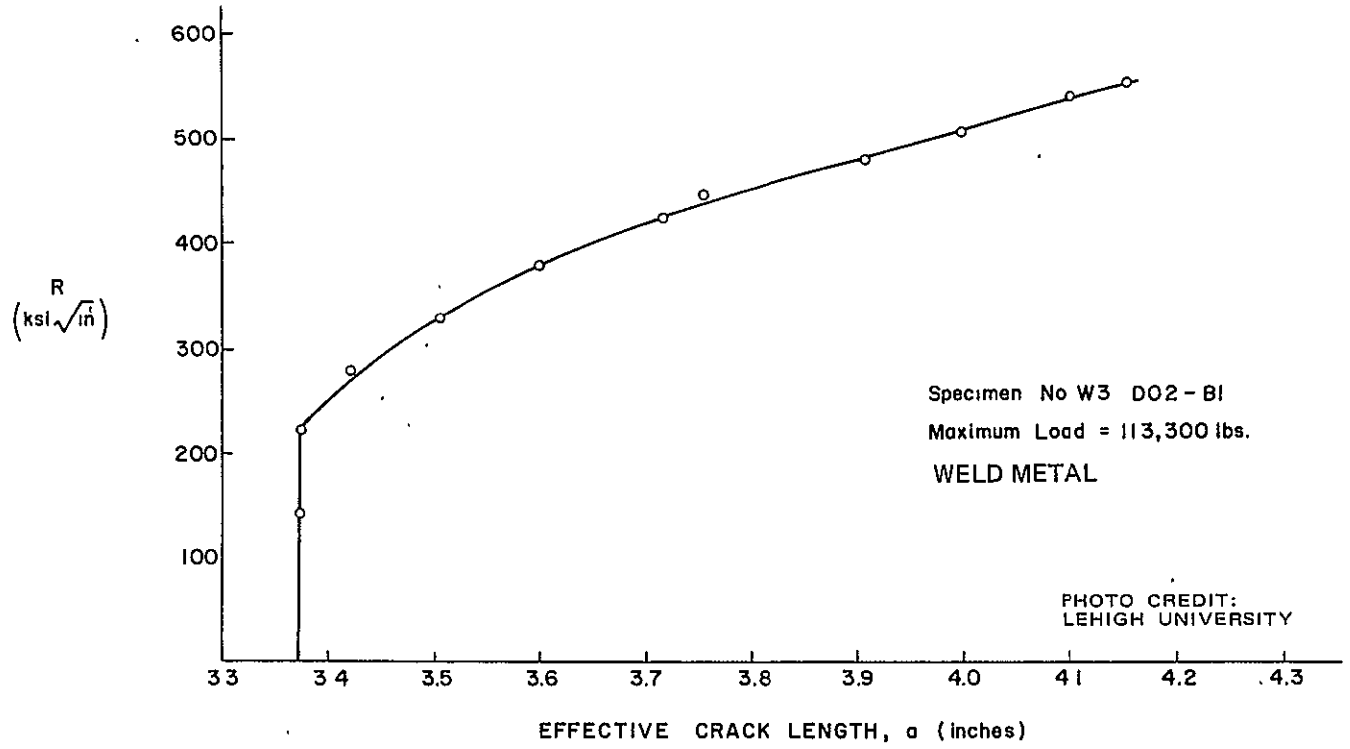

FIGURE 99
WELD METAL FRACTURE TOUGHNESS BEND TEST RESPONSE CURVE, SPECIMEN B1 OF PANEL W3D02

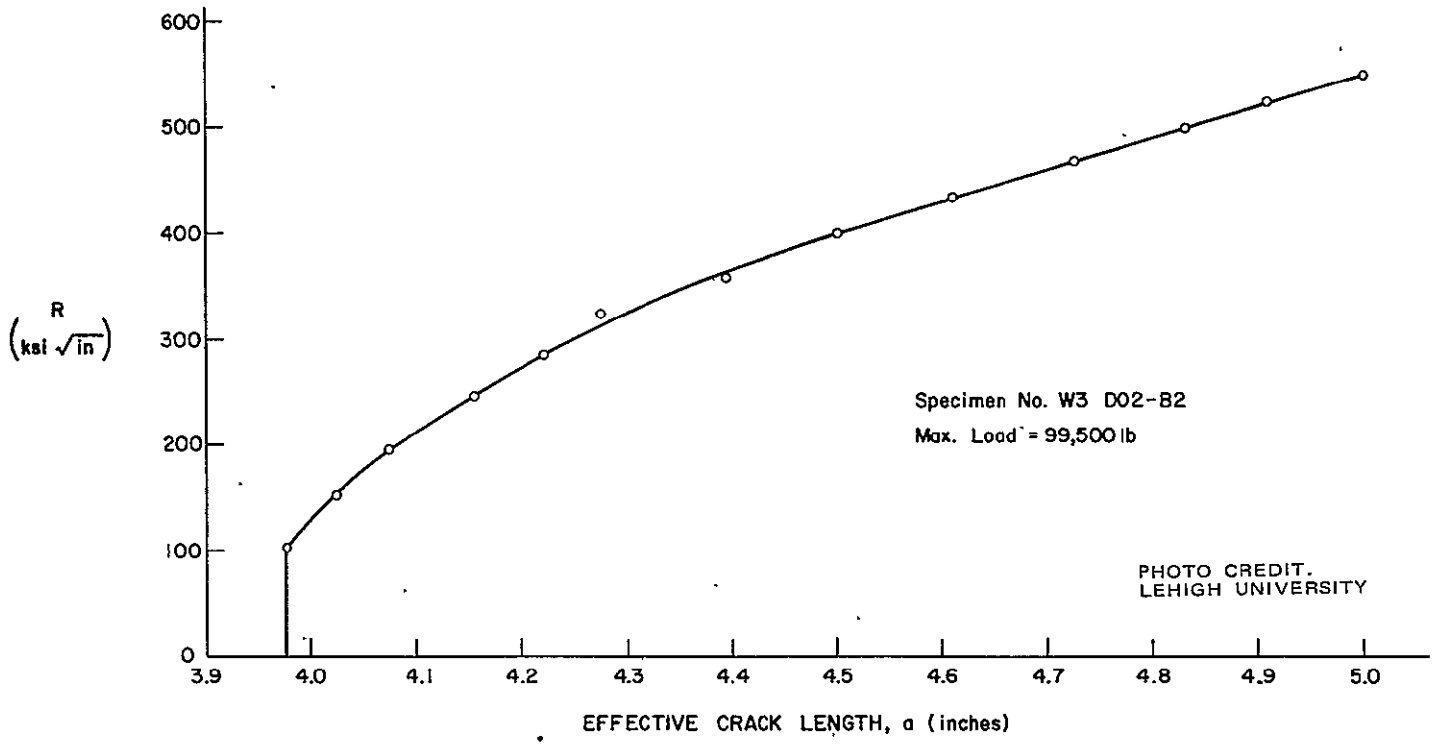

FIGURE 100
WELD HAZ FRACTURE TOUGHNESS BEND TEST RESPONSE
CURVE, SPECIMEN B2 OF PANEL W3D02

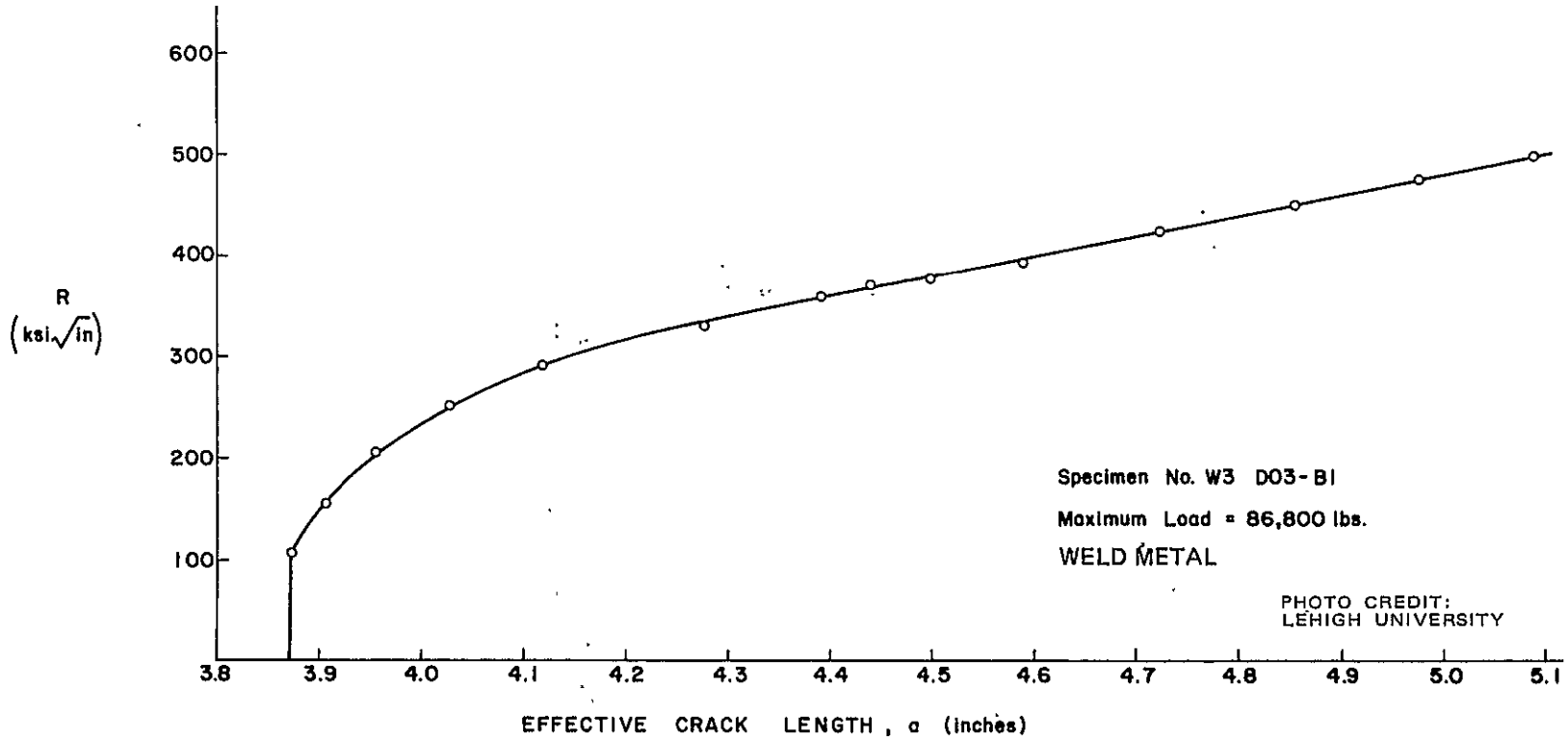

FIGURE 101
WELD METAL FRACTURE TOUGHNESS BEND TEST RESPONSE
CURVE, SPECIMEN B1 OF PANEL W3D03

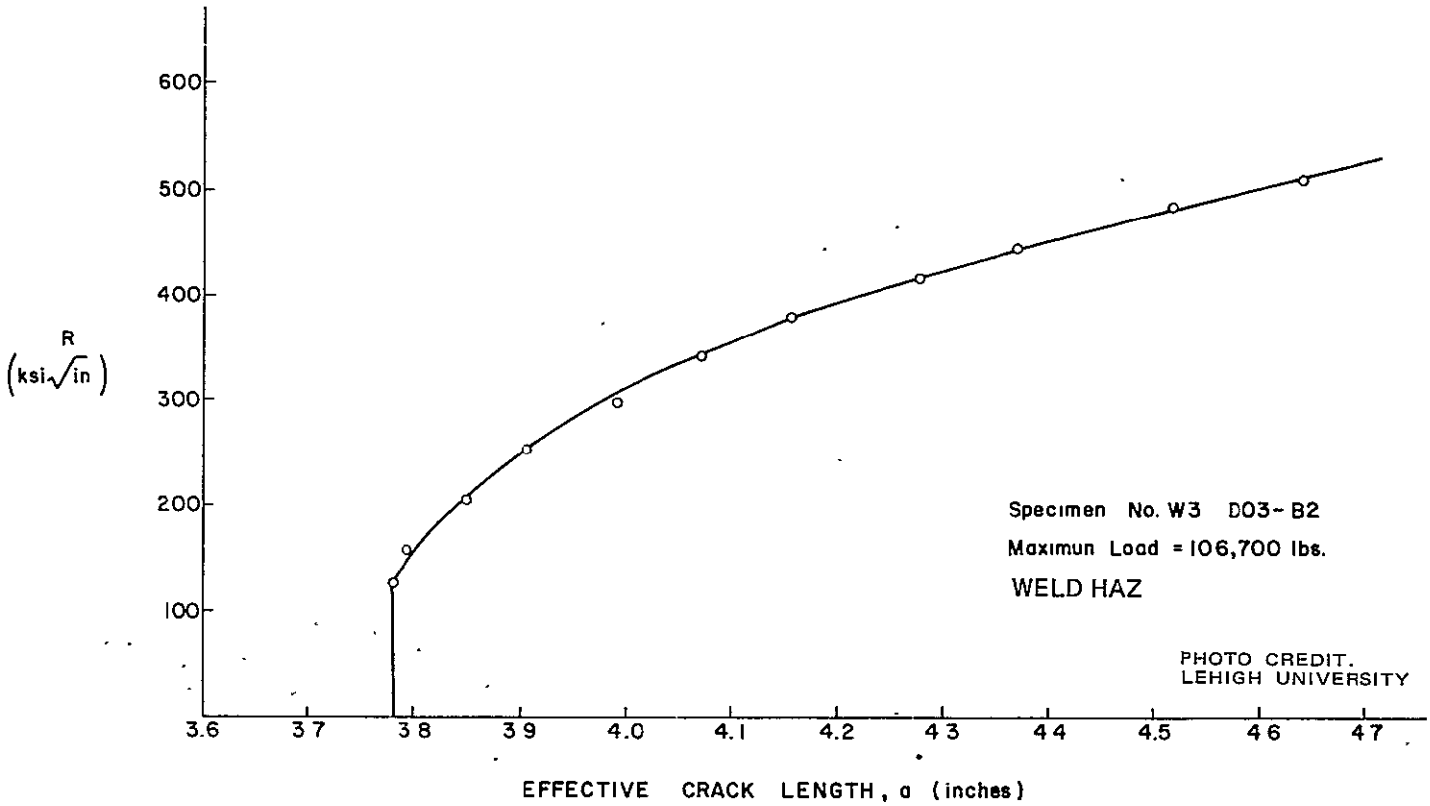

FIGURE 102
WELD HAZ FRACTURE TOUGHNESS BEND TEST RESPONSE
CURVE, SPECIMEN B2 OF PANEL W3D03

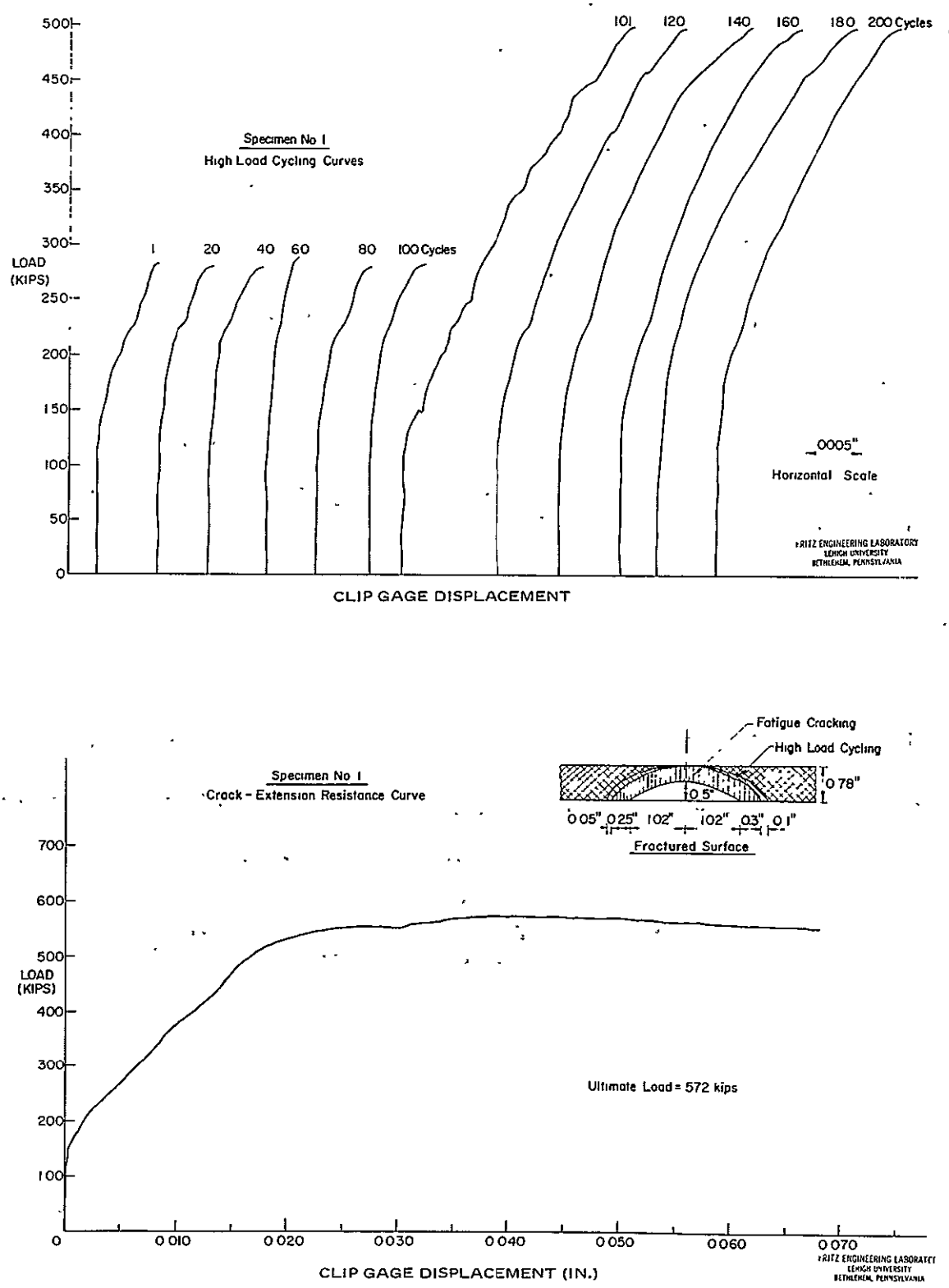

FIGURE 103
LOAD VS CLIP GAGE DISPLACEMENT CURVES RECORDED
PERIODICALLY DURING HIGH LOAD CYCLING AND FINAL TESTING
OF SURFACE FLAW SPECIMEN S1-WELD TEST PANEL W3D04

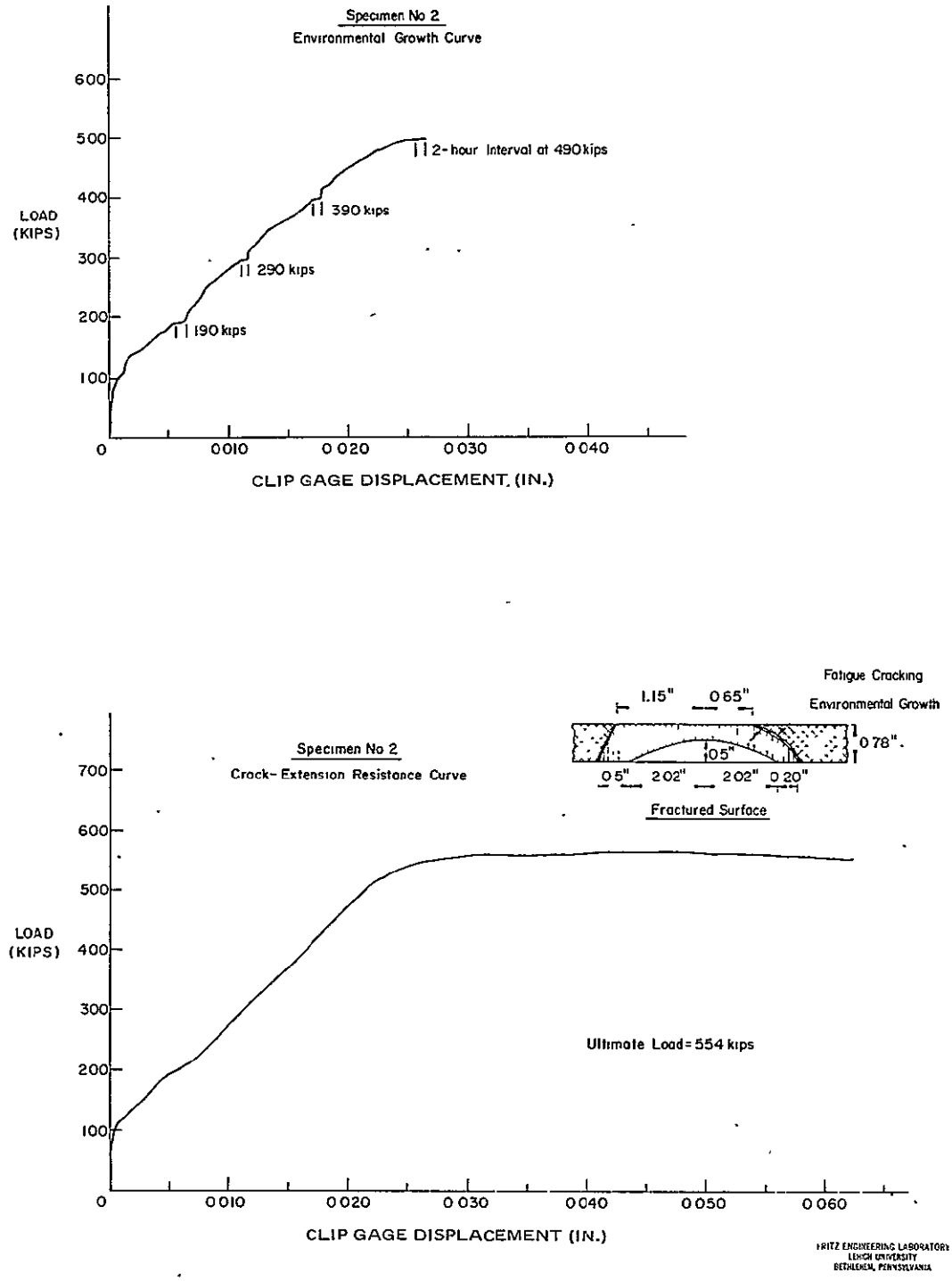

FIGURE 104
LOAD VS CLIP GAGE DISPLACEMENT CURVES RECORDED
PERIODICALLY DURING ENVIRONMENTAL GROWTH RATE STUDIES
AND FINAL TESTING OF SURFACE FLAW SPECIMEN S2
WELD TEST PANEL W3D04

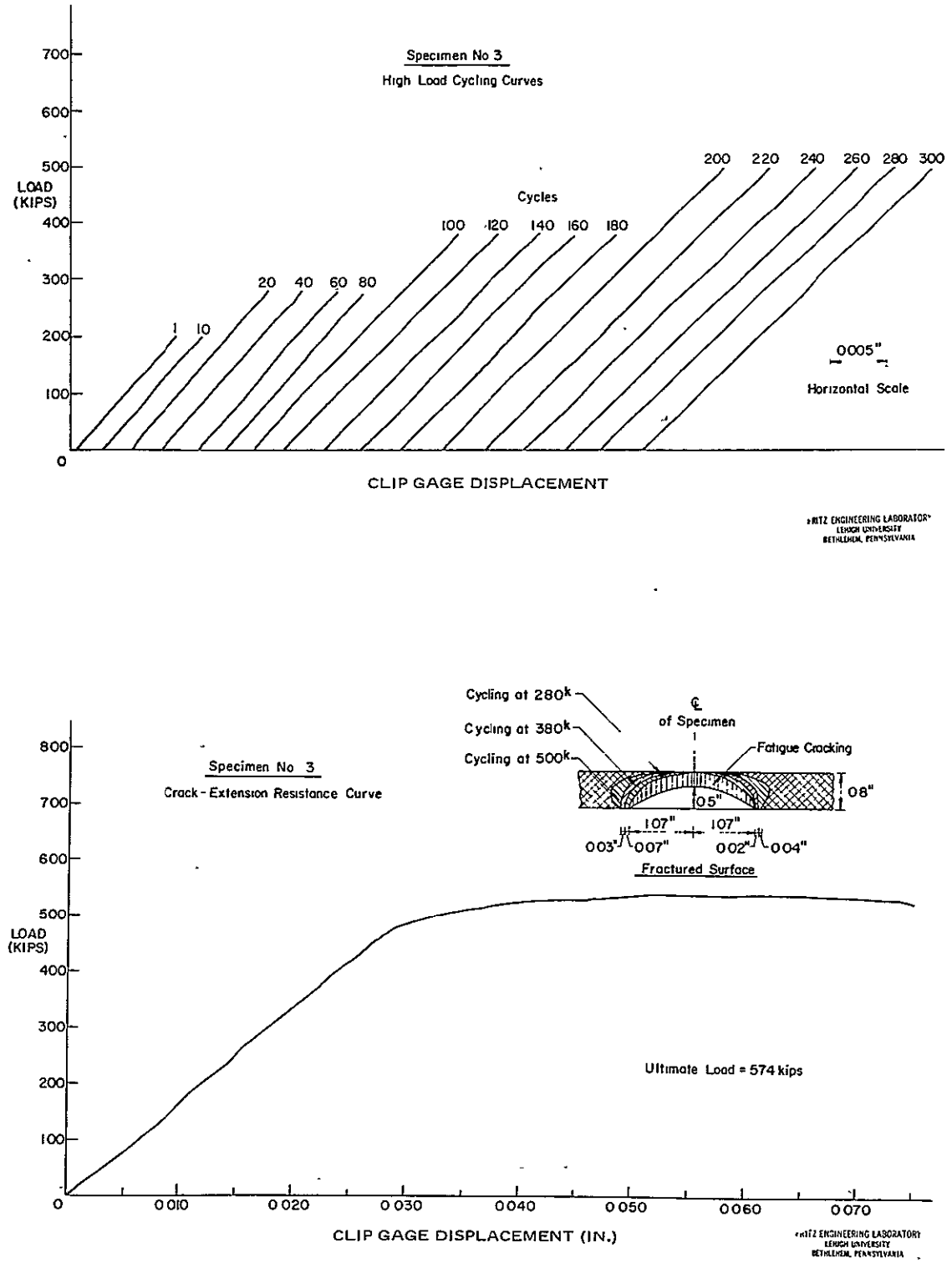

FIGURE 105
LOAD VS CLIP GAGE DISPLACEMENT CURVES RECORDED
PERIODICALLY DURING HIGH LOAD CYCLING AND FINAL TESTING
OF SURFACE FLAW SPECIMEN S3-WELD TEST PANEL W3D04

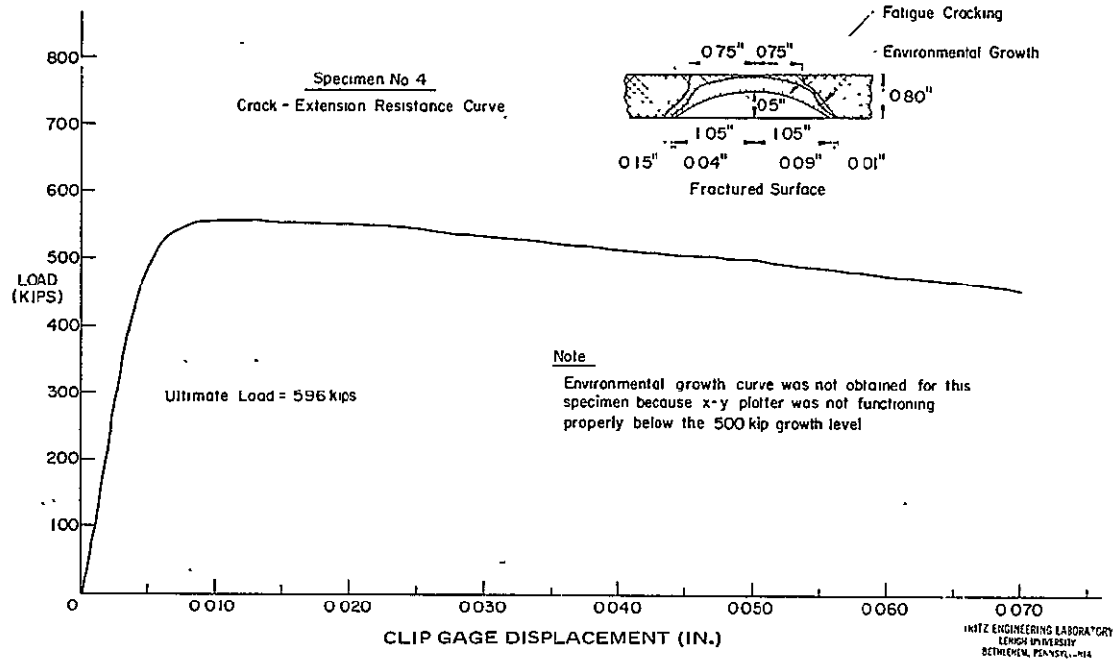

FIGURE 106
LOAD VS CLIP GAGE DISPLACEMENT CURVES RECORDED
PERIODICALLY DURING FINAL TESTING OF SURFACE FLAW SPECIMEN
S4-WELD TEST PANEL W3D04

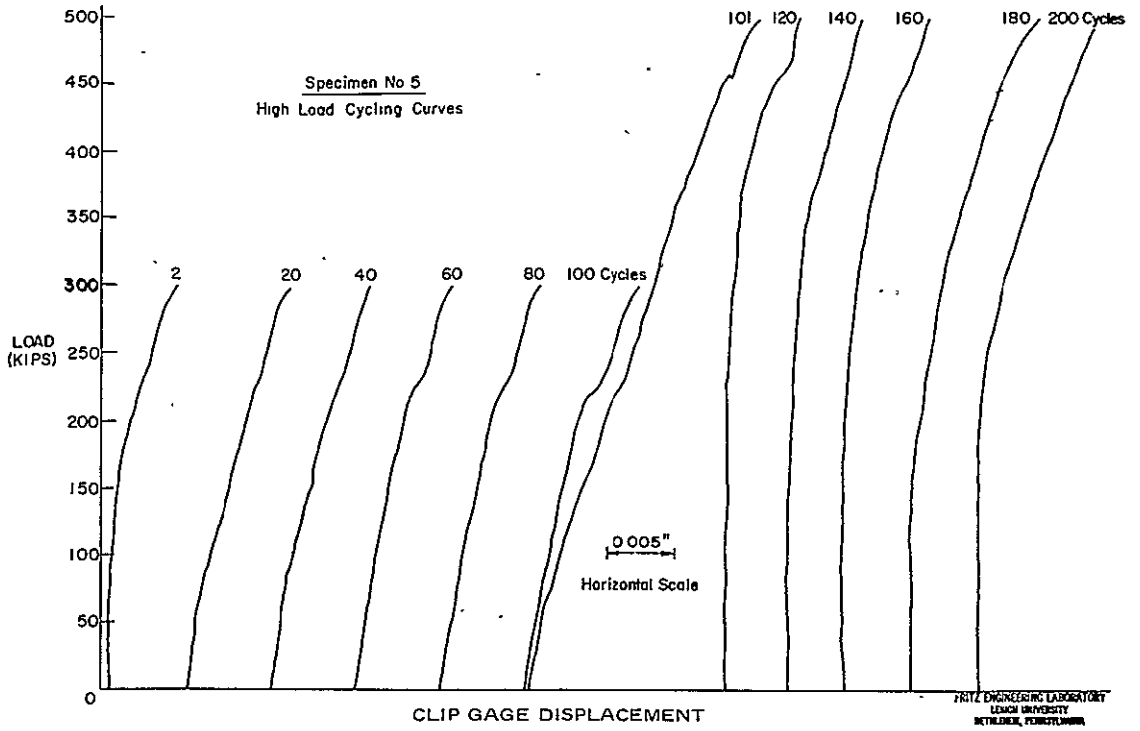

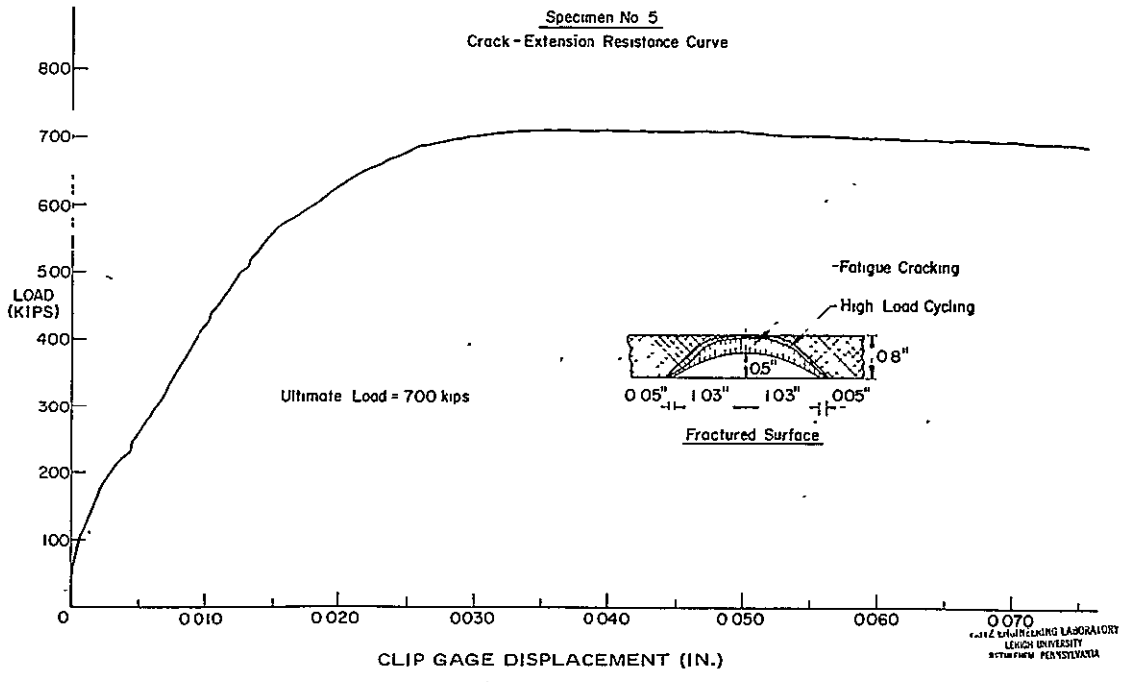

FIGURE 107
LOAD VS CLIP GAGE DISPLACEMENT CURVES RECORDED
PERIODICALLY DURING HIGH LOAD CYCLING AND FINAL TESTING
OF SURFACE FLAW SPECIMEN S5-WELD TEST PANEL W3D04

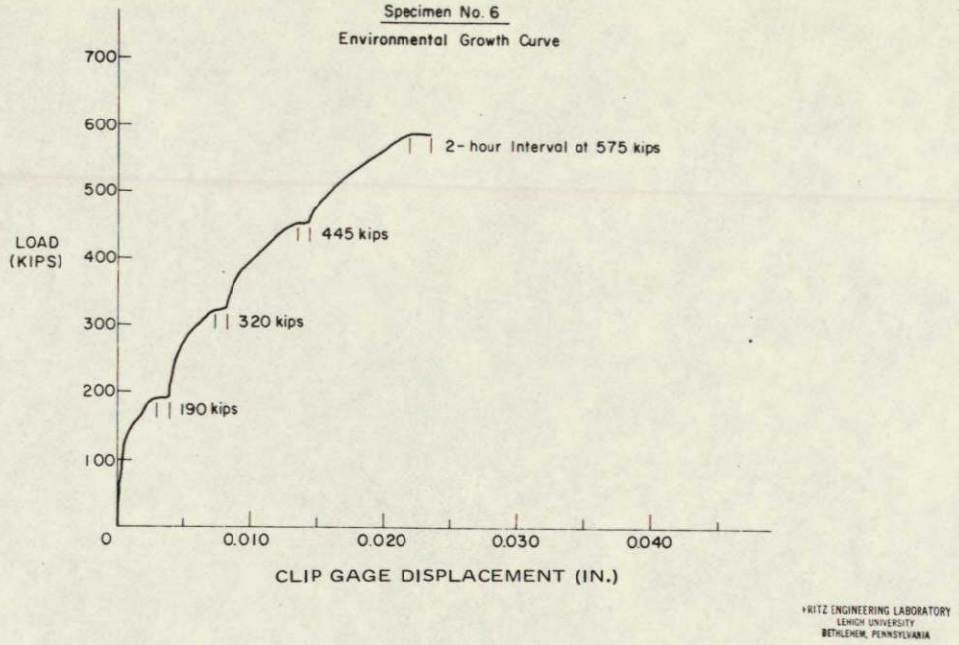

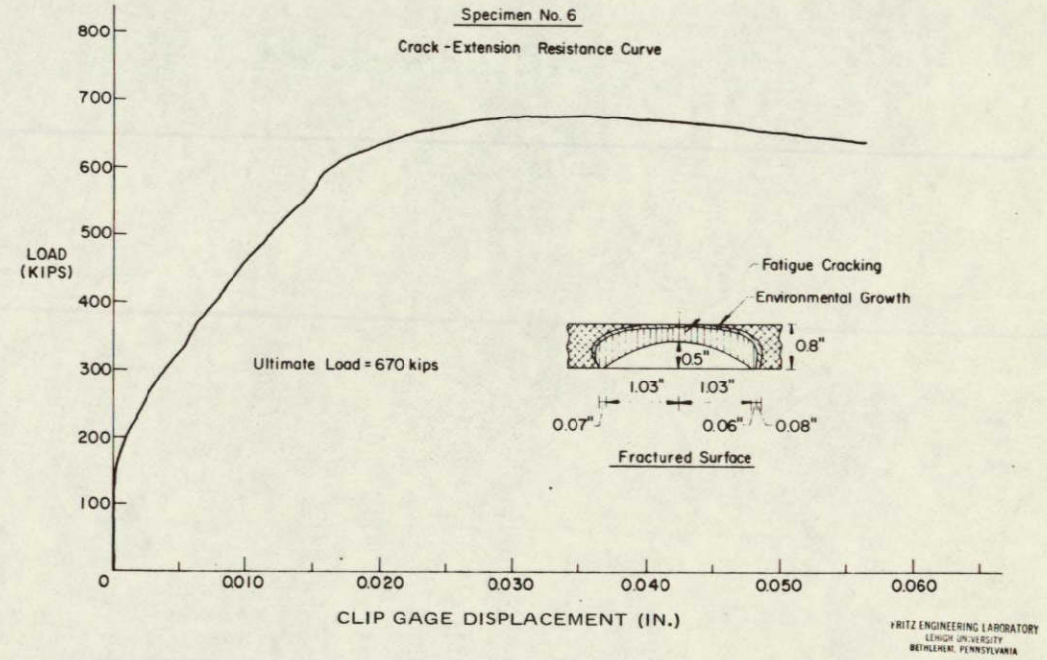

FIGURE 108
LOAD VS CLIP GAGE DISPLACEMENT CURVES RECORDED
PERIODICALLY DURING ENVIRONMENTAL GROWTH RATE STUDIES
AND FINAL TESTING OF SURFACE FLAW SPECIMEN S6
WELD TEST PANEL W3D04

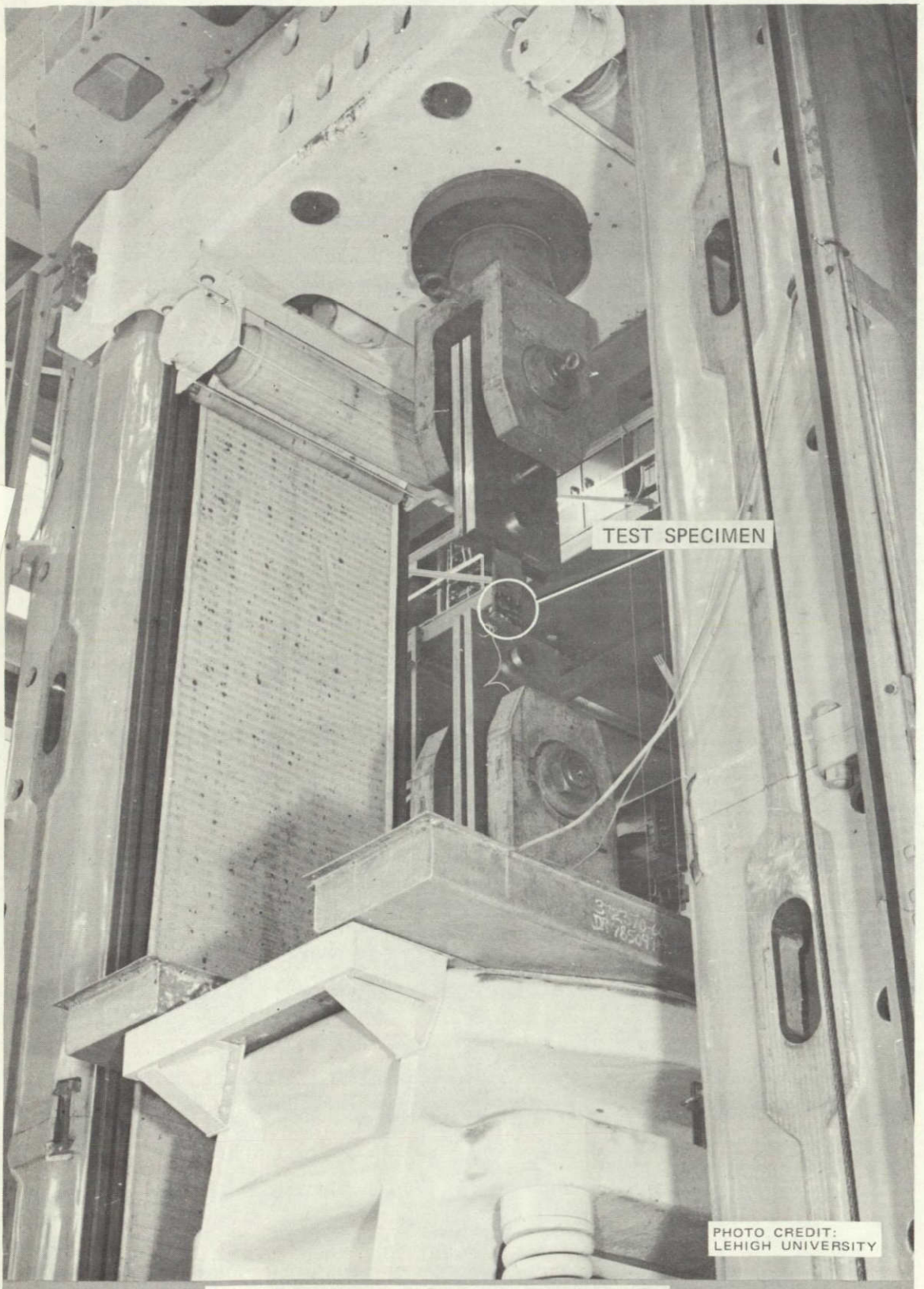

FIGURE 109
SURFACE FLAW SPECIMEN BEING TESTED
IN 5-MILLION LB. TEST MACHINE

FIGURE 110
INSTRUMENTED SURFACE FLAW STRESS-CORROSION
SPECIMEN IN 5-MILLION LB. TEST MACHINE

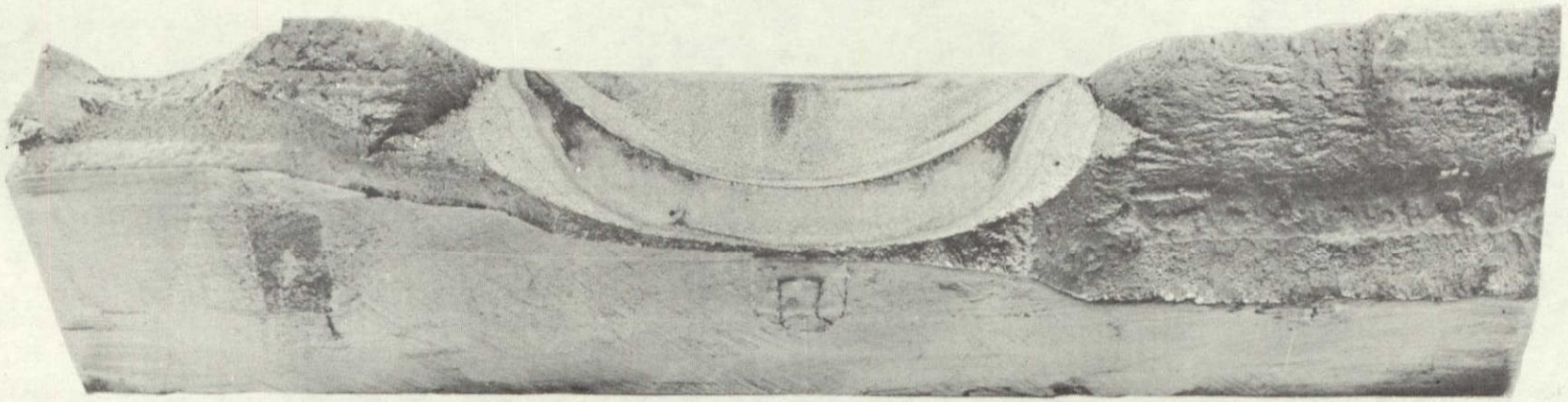

FIGURE 111
FRACTURE SURFACE OF SURFACE-FLAWED TENSILE SPECIMEN W3DO4-S3

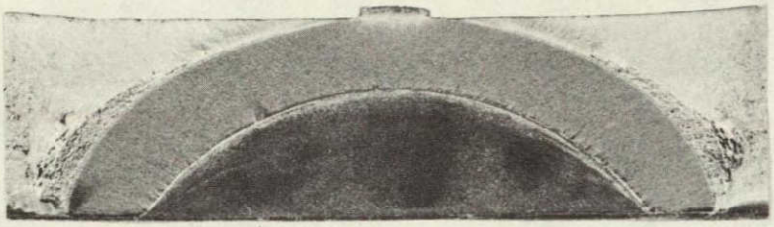

SPECIMEN NO. 1
PLATE W3D03

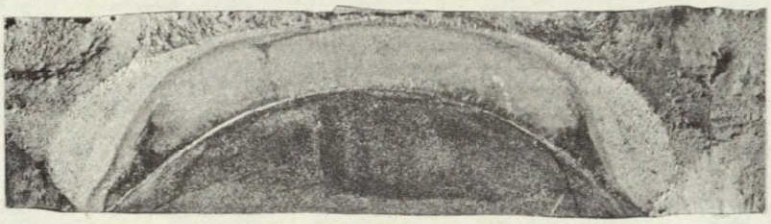

SPECIMEN NO. 3
PLATE W3D03

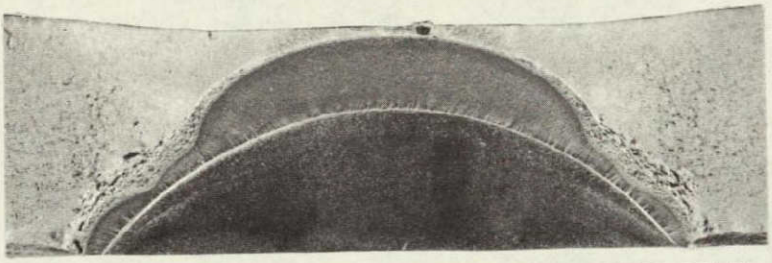

PHOTO CREDIT:
LEHIGH UNIVERSITY

SPECIMEN NO. 5
PLATE W3D03

FIGURE 112
SURFACE FLAWED SPECIMENS, SUBCRITICAL FLAW GROWTH
STUDY, HIGH STRESS CYCLIC LOADING.

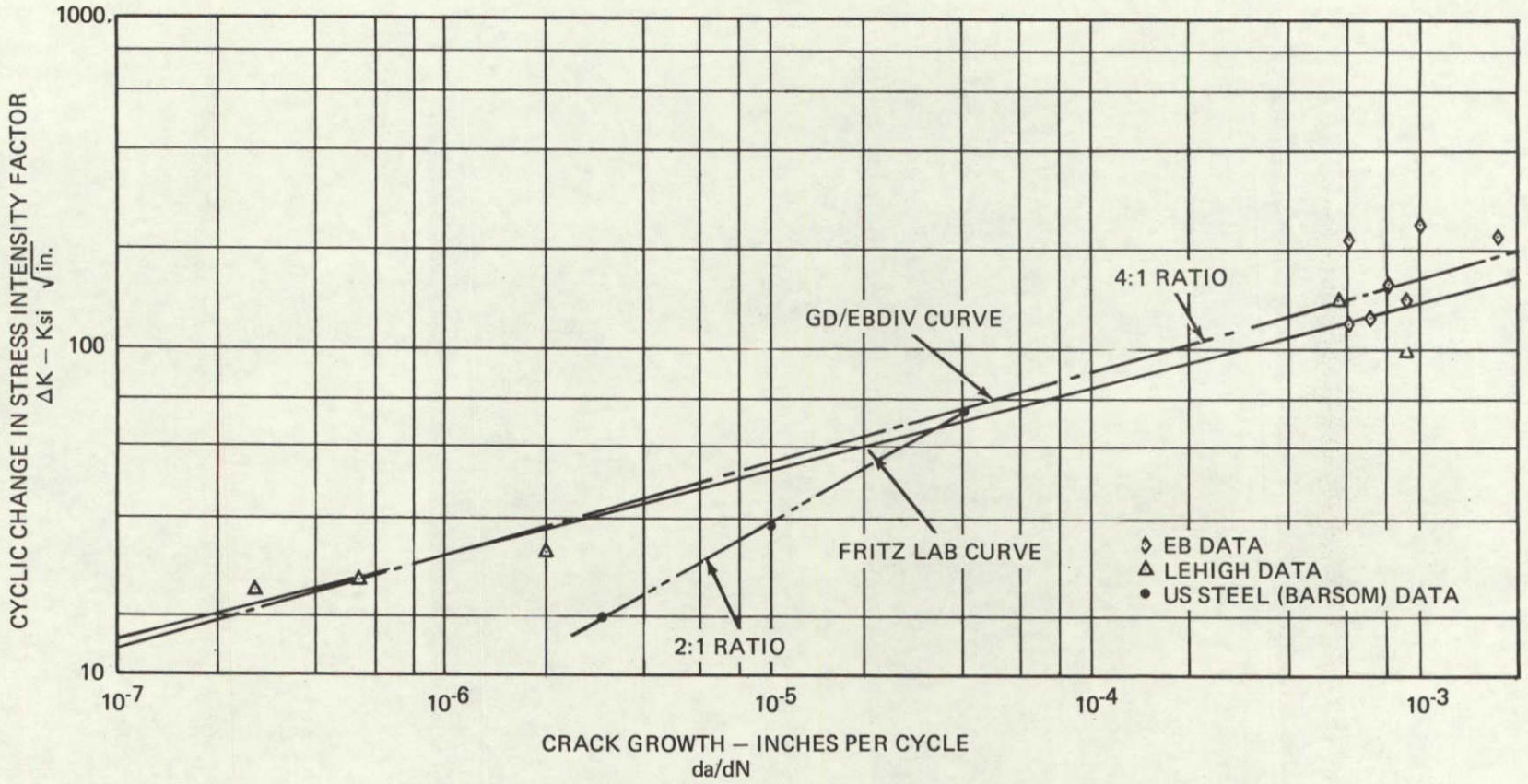

FIGURE 113
LOW CYCLE FATIGUE CRACK GROWTH RATE 12% NICKEL MARAGING STEEL
180 KSI YIELD STRENGTH

SPECIMEN CROSS-SECTION: 6" x 0.80" (APPROX.)
EDM NOTCH: SEMI-ELLIPTICAL, 2" x 0.5" MAX. DEPTH.

SPECIMEN NO. W3D04-S2 (CONSIDERED AS CENTER-CRACK SPECIMEN)

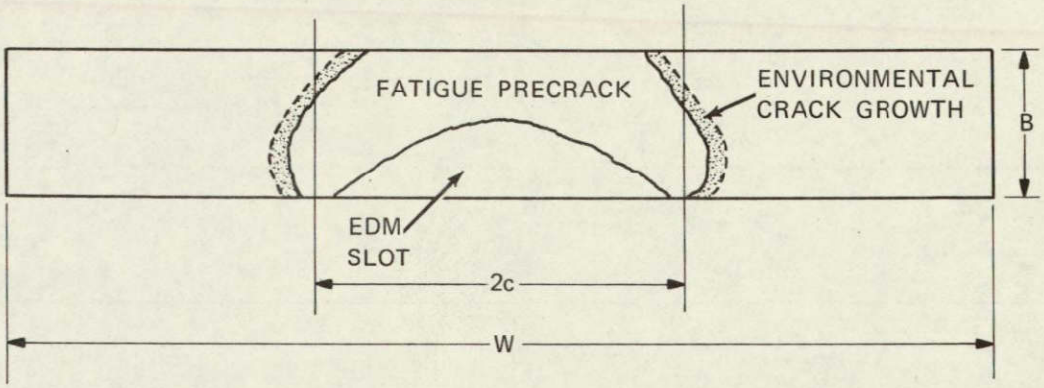

c = 1.13" W = 6"

B = 0.78" 2 c/W = 0.377"

$$K_Q = 1.77\left[1.1\left(\frac{2c}{W}\right) + \left(\frac{2c}{W}\right)^2\right] \qquad \frac{P(c)^{1/2}}{BW} = 0.329P$$

P*, KIPS	K_Q KSI $\sqrt{IN.}$	K_Q^{**} KSI $\sqrt{IN.}$
190	62.5	65.1
290	95.5	99.5
390	128.5	134.0
490	161.6	168.3
554 (ULTIMATE LOAD)	182.5	190.0

*SEE LOAD-DISPLACEMENT CURVE
**FINITE PLATE CORRECTION ADDED: (1)

$$K_Q = CK_Q$$

$$C = \left[1 + 0.3\left(\frac{2c}{W}\right)^2\right]$$

(1) PARIS, PC, AND SIH, G.C. ASTM STP381, P.541

FIGURE 114
COMPUTATION OF STRESS INTENSITY FACTORS
SURFACE FLAWED STRESS-CORROSION SPECIMEN W3DO4-S2

SPECIMEN NO. W3D04-S4 (CONSIDERED AS A CENTER-CRACKED SPECIMEN)

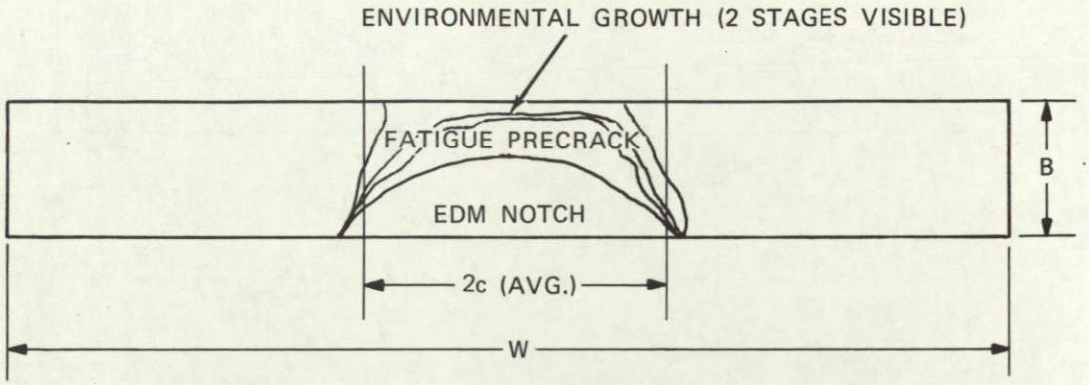

c = 0.993" AVG. W = 6"

B = 0.80" 2 c/W = 0.331"

$$K_Q = 1.77\ [1.1\ (\frac{2c}{W}) + (\frac{2c}{W})^2]\ \frac{P(c)^{1/2}}{BW} = 0.329P$$

P, KIPS	c (AVG.)	K_Q, KSI $\sqrt{\text{IN.}}$	K_Q *
180	0.729	58.5	59.5
280	0.729	91.4	92.9
380	0.864	126.0	129.0
480	0.993	151.3	156.1
596 (ULTIMATE LOAD)	0.993	188.0	194.0

*FINITE PLATE CORRECTION ADDED:[1]

$$K_Q = CK_Q$$

$$CK_c = (1 + 0.3\frac{(2c)^2}{(W)})$$

[1]PARIS. P.C. AND SIH, G.C. ASTM STP 381, P. 541.

FIGURE 115
COMPUTATION OF STRESS INTENSITY FACTORS
SURFACE FLAWED STRESS-CORROSION SPECIMEN W3DO4-S4

SPECIMEN NO. W3D04-S6

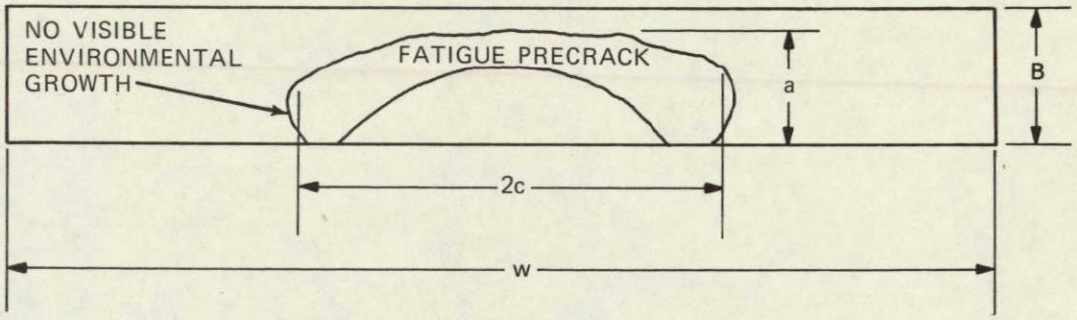

W = 6″ B = 0.8″

c = 1.263″ a/c = .631/1.263 = .499 Φ^2 = 1.46

b = 0.631″ σ_{ys} = 180,000 PSI σ_{ys}^2 = 32.4 x 10^9

NET
SECTION = 3.432 SQ. IN.

$$K_Q = \frac{3.77\sigma^2 b}{\Phi^2 - .212\left(\frac{\sigma}{\sigma_{ys}}\right)^2}$$

P, KIPS	K, KSI $\sqrt{\text{IN.}}$
190	71.0
320	121.6
445	173.0
575	229.0
670 (ULTIMATE LOAD)	271.0

FIGURE 116
COMPUTATION OF STRESS INTENSITY FACTORS
SURFACE FLAWED STRESS-CORROSION SPECIMEN W3D04-S6

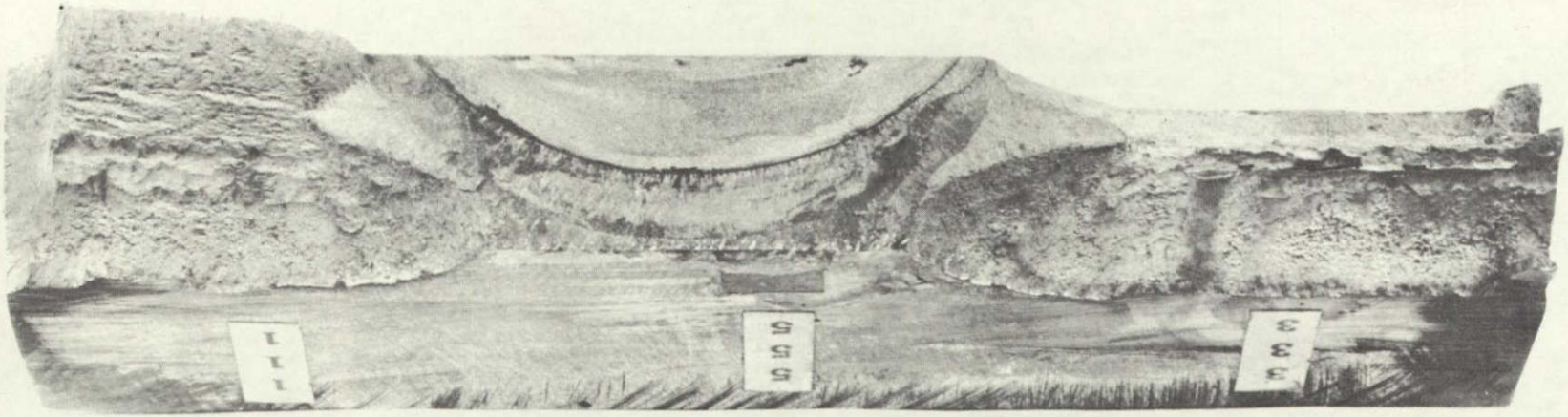

FIGURE 117
FRACTURE SURFACE OF SURFACE-FLAWED STRESS-CORROSION
TEST SPECIMEN W3DO4-S4

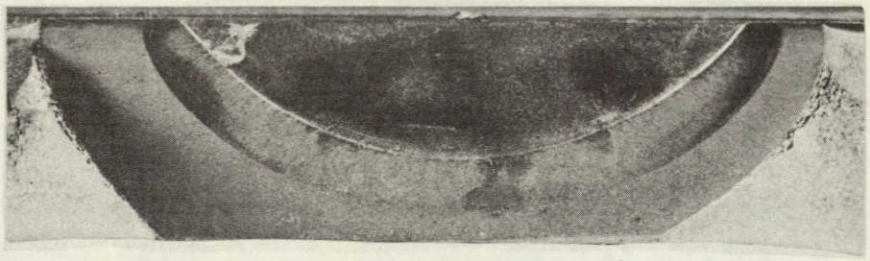

W3D04-S2

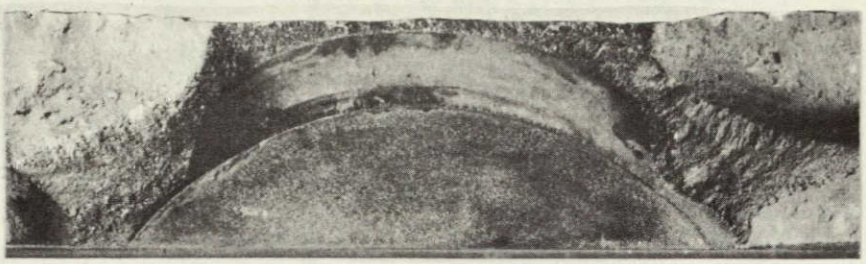

W3D04-S4

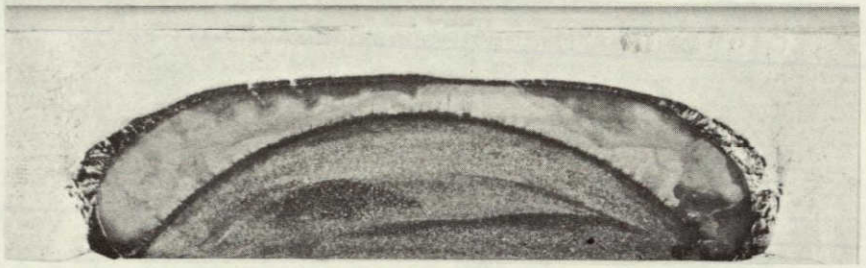

W3D04-S6

PHOTO CREDIT:
LEHIGH UNIVERSITY

FIGURE 118
SURFACE FLAWED STRESS-CORROSION
TEST SPECIMENS

APPENDIX A

Welding and Materials Engineering Department

Process Development Section

SUMMARY OF LITERATURE REVIEW

OF

12% NICKEL MARAGING STEEL

Prepared Under NASA Contract NAS 3-11183

Prepared By: Phillip M. Schmidt

Phillip M. Schmidt

Date: June 25, 1970

GENERAL DYNAMICS
Electric Boat Division

TABLE OF CONTENTS

I. INTRODUCTION

The maraging steels are a relatively new class of materials capable of attaining yield strengths of greater than 300 ksi in combination with exceptionally high fracture toughness. These alloys are termed "maraging" because they are considered to exist as a soft, low-carbon martensite in the annealed condition and derive their high strength from aging at relatively low temperatures. They were initially developed by the International Nickel Company in 1959.

There are essentially four major types of maraging steels: 20 and 25% nickel, each with 1.5-2% total titanium plus aluminum; 18% nickel, with 7-9% cobalt, 5% molybdenum and 0.1-0% titanium plus aluminum; and 12% nickel, with 5% chromium, 3% molybdenum and 0.5-0.8% titanium plus aluminum.

25% Nickel Maraging Steels - The 25% Ni steels are predominantly austenitic in the annealed condition and normally require a preliminary aging treatment (aus-aging) to effect a precipitate in the austenite, thereby decreasing their stability. Transformation to martensite then occurs upon cooling to, or generally considerably below, room temperature. Further strengthening to Rockwell C-50-55 with yield strengths of up to 250 ksi is achieved by a precipitation or aging treatment at 850°F.

The aus-aging treatment generally results in lowered notch and impact properties, probably due to the formation of grain boundary precipitates during the 1300°F aus-aging treatment. The substitution of cold working for aus-aging will overcome this problem and improve the toughness.

This alloy has relatively low toughness compared to lower yield strength maraging steels, and its major advantage is in its exceptional softness and ductility in the annealed condition. A two-step, post-weld treatment (aus-aging or cold working) is required to restore properties to the heat-affected zone of welds in this material.

20% Ni Maraging Steels - The 20% Ni steels are predominatly martensitic as air cooled, but are usually refrigerated to insure complete transformation. The martensitic structure is then precipitation hardened by a 900°F aging treatment. Depending upon time of aging and hardener content, i.e. titanium and aluminum, yield strengths of up to 250 ksi can be obtained. The resultant toughness is only slightly better than for the 25% Ni grades however.

18% Ni Maraging Steels - The 18% Ni alloys [1,2] are the most versatile and widely used of all the maraging steels. They are produced with a wide range of yield strengths, namely 180, 200, 250, 300, and 350 ksi. These strength levels are determined by the aging treatments and hardener content, i.e. titanium, cobalt, molybdenum and limited amounts of aluminum.

This literature review is to provide a summary of the general status of 12% nickel maraging steel technology.

II. GENERAL STATUS OF 12% NI MARAGING STEEL TECHNOLOGY

A considerable amount of research has been conducted on 12% nickel maraging steels since they were initially developed in 1964. In addition, much of the work done on other types of maraging steels, both prior to and since then, has been applicable to the 12% nickel steels. Investigations have encompassed many important areas such as melting, mill processing, strengthening mechanisms, heat treating, fabrication, welding, environmental effects and testing. The results of these efforts have shown that minor variations in either composition or production and processing procedures can significantly affect the physical properties and aging response of these alloys. As more information is gained on the effects of these variables, more consistent aging responses and repeatability of properties are being obtained between different heats of material. Each heat must still be evaluated individually, however, in order to select an aging treatment, which will provide the best possible mechanical properties.

Experience gained in fabricating these steels is leading to increased familiarity with the problems which can develop in machining and welding them and also in the avoidance of solution of these problems. This has also led to the development of improved inspection techniques and precautions.

A. Melting and Production

Maraging steels can be produced successfully by air-melting, vacuum-melting, and vacuum-arc remelting of air and vacuum-melted material. There does not appear to be any consistent difference in tensile properties between the steels produced with these three methods. However, substantial variations in toughness and impact properties have been observed which are attributable to melting practice. In general, air-melt material is not as tough as consumable-electrode vacuum-arc remelted (VAR) material and significantly (20 ft. lbs. or more) less tough than vacuum-induction-melted (VIM) steel.[7, 8, 9, 10, 11]

Vacuum-arc remelting can result in reduced hydrogen contents in maraging steels, but the oxygen and nitrogen levels are not changed much from those found in good vacuum-induction-melted or electric furnace heats. The principal advantage of vacuum-arc remelting is the improved solidification pattern of the remelted ingot.

Vacuum-induction melting allows carbon deoxidation with subsequent slag removal of the carbon. Consequently, carbon contents can be better controlled with this process. This is the principal reason for the greater toughness of VIM steels as compared to VAR air melted material.

Alloy steels in general, and maraging steels in particular, are subject to alloy segregation during solidification. The solidification process, regardless of melting method, results in positive segregation of Ni, Mo and Ti in maraging steels to the extent that austenite may be stabilized in the interdendritic areas. These alloy-rich areas carry through rolling and have been shown to cause minor variations in tensile and impact properties. The water-cooled copper crucible used in the VAR process causes directional solidification, which is predominantly from the bottom because the sides of the solidified ingot shrink away from the crucible wall and radial heat transfer is thus diminished. Because of this directional solidification, the usual segregation pattern associated with ingots poured from air-melted or vacuum-induction-melted heats can be minimized or eliminated.

In addition to producing sound ingots as a result of directional solidification, the VAR process is also more likely to float out low-density, non-metallic inclusions as the molten pool rises in the crucible, and no refractories are picked up from the transfer of molten metal through one or more refractory-lined ladles or vessels, as in vacuum degassing. Also, the dynamic action of the arc is credited with finely dispersing any inclusions which may not float out of the molten metal. The net result is an improvement in mechanical properties over air-melted or vacuum-induction-melted material of similar chemistries.

B. Hot and Cold Working

Maraging steels are readily forged and hot rolled. Soaking of ingots at about 2300°F prior to forging or hot rolling is recommended for homogenization. In hot working these steels a temperature range of 2300°F to 1500°F may be employed. They scale heavily at temperatures near the high end of the range. Starting temperatures (following homogenization) of 1900°F to 2100°F appear to afford a satisfactory compromise between scaling and working characteristics. To assure a fine grain size and optimum mechanical properties, finishing temperatures should be held between 1700°F to 1500°F, accompanied by about 25 percent reduction. Light reductions and high temperatures should be avoided. Fine grain size can be produced only by working and not by thermal treatment.

These materials do not exhibit hot shortness up to 2300°F, nor is cracking a problem when they are finished at or even slightly below 1500°F. As with other low carbon steels, the maraging steels should be free of oil, grease, and shop soil before heating to prevent carburization. The use of cracked ammonia as an oxidation preventive at high temperatures, can result in hydrogen absorption and degradation of plate properties.

The usual solution annealing treatment for maraging steels is 1500°F for 1 hour per inch of thickness followed by an air cool.

A double solution treatment of 1700°F for 1 hour/inch of thickness followed by an air cool or water quench and repeating this treatment at 1400°F has sometimes been found to produce improvements in properties.

When a double solution annealing treatment is used, it is very important that temperatures during the second solution annealing treatment do not go below 1400°F. Temperature should be precisely at, or slightly above this value. Furthermore, no material should be exposed to temperatures above 800°F for any longer time than necessary, since it appears possible to produce aging effects which are not eliminated during the second solution annealing operation.

Annealing should be performed in a furnace atmosphere of about 5% CO_2(1), or argon, and contact with carbon steels or similar carbon sources should be avoided. Furnace fuel oil should not contain more than 0.75 percent sulfur by weight, and fuel gas should not contain more than 100 total grains of sulfur per 100 cubic feet of gas.

Aging can be done without the use of protective atmospheres. An air-cool is normally employed.

Maraging steels work harden quite slowly and can be cold rolled or cold drawn over 75% without intermediate anneals. Fifty percent cold reduction produces increases in hardness of about 5

points Rockwell C before aging. When intermediate annealing is required, a maximum temperature of 1800°F for 60 minutes per inch of section may be used, provided that a final cold reduction of 30% is performed. The standard anneal of 1500°F for 60 minutes per inch of section should be used as a final treatment when best ductility with maraged properties is desired.

It should be noted that even though the work hardening rate of maraging steels is low, the annealed ductility as measured by elongation in 2 inches is comparatively low, ranging from about 10 to 25%. This is of particular importance to forming applications involving an appreciable amount of stretching. In the forming of deep drawn sheels or in cupping operations, drawing of the material rather than stretching should be the basis of tool design. Bending radii should be relatively large.

The strengths of maraging steels, as aged, are increased by prior cold working. Also, cold working tends to decrease slightly the time and temperature at which maximum strength is achieved during aging.

Cold working affects the elastic modulus of maraging steels as shown by dynamic modulus tests.[12] The variation in modulus is not only dependent on the heat treating and cold-working cycles, but also on the orientation of the specimen. Values were observed to range from 25.8×10^6 to 30.6×10^6 psi.

C. Structure and Strengthening Mechanism

The structure of 12% Ni maraging steels when cooled from the solution treating temperature to room temperature is a low-carbon, body-centered cubic martensite with hardness of approximately Rockwell C-32. Martensite start (M_s) and martensite finish (M_f) temperatures are approximately 500 °F and 350°F respectively. As rolled material at room temperature is similarly martensitic, but exhibits excessive variations in properties upon aging.

Strengthening during aging results from the precipitation of various intermetallic compounds which appear to nucleate on dislocations rather than by lattice distortion from carbon. Elements involved in the aging response include nickle, molybdenum, titanium, and aluminum, with the principal precipitates being considered $(Fe, Ni)_3Mo$, sigma FeTi, ordered $(Fe, Ni)_3Al$, and for 18% Ni steels a possible cobalt ordering effect. (13) Because of the very fine size of these precipitates, their indentification is quite difficult. Magnifications of as much as 7500X have failed to reveal them clearly.

Prolonged exposure at temperatures below 1400°F but above 1100°F can result in a large portion of the martensite reverting to stable austenite. The stable austenite will not transform to martensite on subsequent cooling to room temperature, so the yield strength after the usual aging treatment can be much lower than the anticipated value. It is therefore important to avoid extended exposure at temperatures between 1100°F and 1400°F.

D. Aging Response

Variations in "hardener content" and processing history result in differing aging temperatures and times at temperature being required in order to produce optimum mechanical properties. Annealing temperatures also appear to influence the time-temperature relationships of aging.

In one instance it has been reported that higher annealing temperatures have required higher aging temperatures when similar aging times were employed.[7] Lower annealing temperatures are generally desirable, however, in order to obtain fine grain size.[17] Low hardener content alloys have been found to require longer aging times than those having higher hardener contents.[3,18] Likewise, the 12-2-3 and 12-5-3 weld filler wires appear to require different aging treatments.

Extended times at aging temperatures do not produce marked overaging effects.[13,16] Results of one aging study[7] showed one set of specimens to require more than 30 hours at 900°F before overaging was observed, and another one to not show such softening characteristics after 80 hours. Increasing aging time will normally result in increased yield strengths. Toughness decreases with increasing yield strength, however.

E. Effects of Residual Elements on Toughness

The fracture-toughness properties of maraging steels are more sensitive to melting and processing variables than un-notched

tensile properties. Various methods of producing and welding these steels can result in the attainment of 180 ksi or greater yield strengths, but marked differences will be observed in the toughnesses. These differences are very important in that the toughness of a metal determines the maximum allowable flaw size for a given application, and also, if failure should occur, whether it will be of a ductile or brittle nature.

In general, loss of toughness can be related to the formation of thin, dendritic particles and platelets at cellular and dendritic grain boundaries, resulting in a low-energy, intergranular type of fracture in these regions.[14] These particles have tentatively been identified by electron diffraction as Ti_2 , TiC, TiN, and possible $-Al_2O_3$ [13,14] They apparently go into solution at the higher temperatures and precipitate out upon cooling. Other investigators have also reported these compounds reduce toughness,[19] and in addition have reported ZrN, AlN, and TiO.[17,20]

The effects of individual elements are as follow: [10,19,21,22]

Carbon - Carbon should be controlled to 0.02% max. allowable in order to get oxygen and sulfur as low as possible. It has only a slight strengthening effect and drastically reduces the toughness of both base metal and weld metal. A 0.02% maximum is sometimes specified in order to get the lowest possible oxygen and sulfur contents, but this has not always proven worthwhile.

Sulfur -Sulfur contents should be as low as possible, with a 0.005% max. being desirable and 0.008% a definite maximum. Increasing sulfur from 0.002 to 0.015% has resulted in decreases in toughness of as much as 62 ft. lbs. CVN when carbon was at 0.012%.

Silicon - Increasing silicon decreases toughness only when at levels of 0.10% or greater, or when manganese is at fairly high (0.05% or more) levels. Limited grain refinement may result from amounts up to 0.10%.

Manganese - The manganese content of base metal or weld metal does not appear to be detrimental if other element levels are low. Generally, about 0.10% is set as a maximum.

Phosphorus - Phosphorus has an effect similar to sulfur and should be kept as low as possible. 0.005 appears to be a good limitation. Excess amounts can cause hot shortness.

Boron - A very small addition of boron to maraging steels helps control carbide formation however susceptibility to weld metal cracking may be increased and toughness may be impaired. It is therefore not intentionally added and held to a minimum.

Zirconium - Zirconium has been found to form carbides and nitrides in maraging steel which are considered detrimental to toughness. Zicronium therefore is not intentionally added and held to a minimum.

Nitrogen - Undesirable titanium nitrides result from the presence of any nitrogen in maraging steels. Consequently, since these nitrides seriously decrease toughness, the nitrogen level of base material and weld filler wires should be as low as possible. A maximum nitrogen content of 50 ppm seems advisable.

Oxygen - A maximum oxygen content of approximately 30 ppm appears to be desirable, since recent work[23] has shown up to 15 ft. lbs. difference between welds which were identical except for oxygen contents of 7 ppm in the weld of higher toughness and 430 ppm in the lower.

Hydrogen - Hydrogen contents of as low as 6.5 ppm have been reported to have caused cold cracking in 18% Ni weldments.[24] Therefore a maximum hydrogen content of 5 ppm is apparently required.

F. Thermal Embrittlement Effect

Thermal embrittlement has been observed to occur in 12 and 18% Ni maraging steels in both aged and unaged material. It results from slow or interrupted cooling through the 1800°F to 1400°F temperature range after heating above 1800°F.[14,15] This effect is time-temperature dependent and most severe if grain coarsening has first occurred by heating and holding above 1800°F particularly near 2200°F. This embrittlement is believed to result from the formation of various high-temperature grain boundary precipitates on austenite grain boundaries as described in the previous discussion of residual element effects on toughness.

The reduction of residual carbon, sulfur and other residual elements to low levels has helped to overcome this problem.[23]

G. Corrosion Characteristics

General corrosion tests conducted in an industrial atmosphere at Newark, New Jersey indicate the corrosion rate to be less than that of commerical quenched and tempered alloy steels by a factor of approximately ten to one based on weight loss. Similar tests exposed to marine environments at Kure Beach, South Carolina indicate the corrosion rate to be about one-third that of quenched and tempered steels.[3]

The 18 Ni-8Co-3Mo alloys appear to offer good resistance to pitting attack and also to resist, but not be immume to, stress-corrosion cracking. Some of the 12-percent Ni alloys have been found to be quite susceptible to both of these effects however.[26] Mild steel or zinc can be used to cathodically protect base metals from general and stress corrosion, but weld metal can apparently be subject to hydrogen embrittlement when protected with zinc.[3]

Distilled water has been found to be a more aggressive environment for stress-corrosion cracking of 18 percent Ni maraging steels than a 3 percent saline solution, with tap water being the least aggressive.

It has been found that an addition of 1/4 percent sodium dichromate and 4 percent water soluble oil effectively inhibited distilled water so that no failures of 18 percent maraging steel specimens occurred.[7] Use of this inhibitor formulation can be

applied to hydro-testing of 18-Ni pressure vessels, with the possibility of it being equally suitable for use with 12-Ni alloys.

H. Fatigue

Fatigue strengths for rotating beam tests of aged 12-5-3 maraging steel show 90,000 psi at 10^7 cycles and 85,000 psi at 10^8 cycles for unnotched specimens.(3) Cracked specimens show substantially lower values.

III. WELDING AND PROPERTIES OF WELDS

The weldability of 12 percent Ni maraging steels, like other higher nickel grades, is considered excellent. Sound welds can be made in either aged or unaged material, with no need for preheat or post-heat. A post-weld aging treatment is employed to strengthen the weld deposit and to restore the properties of the heat affected zone, which is softened by the heat of welding. Weld metal properties approaching those of the base plate are obtained with the inert-gas shielded-arc processes.

The major problem associated with welding maraging steels is the attainment of maximum fracture-toughness in the deposited metal. Only the inert-gas welding processes give toughness properties approaching those of the base material at yield strengths of 180,000 psi. The gas-tungsten-arc (GTA) process is superior to all others in this regard.

A. Joint Preparation and Welding Cleanliness

The observation of extreme cleanliness is very important in the attainment of optimum weld properties in maraging steels. Even slight contamination of the weld metal with carbon, oxygen, or nitrogen can seriously reduce the toughness of welds in these materials. The absorption of hydrogen must be avoided, since as little as 6.5 ppm has resulted in cold cracking in some instances. Pure argon is generally used as a shielding gas, and all welding should be performed in draft free areas to insure adequate shielding. The use of a gas lens has been found to be beneficial. Oxygen should not be added to the shielding gas, since it detracts from toughness.

Machined weld joint preparations are recommended where highest quality is desired. An acetone or similar type of chemical cleaning technique should be used to remove all traces of dirt and grease prior to welding.

The 12% Ni maraging steels can be cut with the oxy/acetylene process, but cut quality is very poor. Plasma-arc cutting is more satisfactory. If flame or plasma-cut edges are to be used as weld joint preparations, they should be ground to remove all scale and oxidized material. Slight losses of weld toughness may result.

Interpass cleaning with a stainless steel wire brush is usually performed to insure the removal of any possible surface oxides.

Light grinding is recommended to remove any small, tightly adhering chunks of oxide which sometimes form on weld surfaces.

B. Weld Filler Wires[3,21,23]

Three types of weld filler wires are available for inert gas welding 12% Ni maraging steel. These wires are a 17% Ni composition, a low hardener 12% Ni variety, and one of a matching 12% Ni composition.

17% Ni Filler - Until very recently, maximum weld strength-toughness combinations were considered to be obtained from a 17% Ni-2Co-3Mo filler wire using the GTA process. Combinations of 180,000 psi yield strength with 50 ft.-lbs. Charpy V-notch impact energy have been obtained in welds up to 2 inches thick.

When this filler is used with the GMA process or deposited at high GTA deposition rates only 30-35 ft.-lbs. CVN is obtained at 180 ksi yield strengths. High deposition rate techniques are therefore not recommended when maximum toughness is required. The optimum aging temperature for welds made with this filler wire is in the 825-850°F range.

12% Ni Low Hardener Content Filler - GMA or high deposition rate GTA welds having 40-50 ft.-lbs. CVN toughness can be produced in 12% Ni maraging steel using a special low hardener 12% Ni filler wire. This results in weld yield strengths being reduced to 160-175 ksi. The GTA process again offers maximum toughness, but the difference is not as marked as with the 17%

Ni filler. An aging temperature near 900-925°F appears best suited for welds made with this filler wire.

Base Composition Filler - Early efforts with weld wires of base composition did not provide sufficient toughness at the 180,000 psi yield strength characteristic of these wires. The low-hardener 12% Ni wires were consequently developed to improve toughness by reducing the yield strength. Recently, work has been reported which indicates the full potential of matching composition filler wires was not realized in earlier efforts. Wire processing has been found to greatly affect weld toughness, with low gas content matching composition wires exhibiting an average of 15 ft.-lbs. greater toughness than similar wires of high gas content.

GTA welds have been observed to consistently exhibit greater than 50 ft.-lbs. CVN at 180,000 psi yield strengths, while limited work with GMA welding indicates 35-45 ft.-lbs. toughness may be anticipated at similar strengths.

Optimum aging temperatures for welds made with matching filler wire appear to be in the 900-950°F range.

C. Weld Wire Production and Processing

The high purity which is required in filler wires for use with 12% Ni maraging steel indicates it is necessary to produce the material for these wires by vacuum melting or remelting techniques. Vacuum annealing is sometimes helpful in reducing hydrogen contents necessary for maximum weld toughness. Oxygen,

nitrogen and hydrogen contents of as drawn wire should be limited to maximums of approximately 30, 50 and 5 ppm, respectively. In addition, all the residual elements, especially carbon and sulfur, should be as low as possible.

D. Effects of Heat Input and Bead Size

Low heat inputs and small weld beads should be used in welding 12% Ni maraging steel if maximum weld toughness is desired. A maximum heat input of near 40,000 joules/inch has been suggested for GMA welding,[25] was also observed in the work which produced excellent properties in GTA welds made with matching composition weld wire.[23] This work also showed a weld bead size factor of 4 produced maximum toughness, with this factor being defined as inches of 0.062" dia. wire feed per inch of travel. When this bead size factor increased to 12 toughness decreased 12-14 ft.-lbs.

Maximum interpass temperatures of 250°F or less, with no preheat or post-heat and rapid cooling rates are all beneficial in producing welds of maximum toughness.

E. Weld Heat-Affected Zone

In general, the characteristics of the heat-affected zone of 12% Ni maraging steel are similar to those of the 18% Ni alloys. No significant deterioration of toughness occurs in the HAZ of actual weldments, and only a slight softening appears to develop in two regions which experience peak temperatures of 1200°F and over 1800°F.[23,27] This softening is due to the phenomenon of austenite reversion, which is of special interest in regard to welding.

Austenite reversion occurs when maraging steels are exposed to temperatures above 900°F and below the austenitizing temperature, and is most pronounced when temperatures of approximately 1200°F are involved. It can be avoided during aging, but inevitably a narrow region develops in weld heat-affected zones where reversion to austenite occurs.

In earlier studies[28] of maraging steels, decreases in weld strength, ductility, and fracture toughness were generally attributed to austenite reversion. More recent studies[23,27] have demonstrated that the minor variations which occur in the metallurgical structure of weld heat-affected zones have little practical significance on the strength and toughness of weldments. However, the formation of "pools" of austenite in the deposited weld metal is detrimental to strength and should be avoided. Localized temper embrittlement effects are not evident in the weld HAZ.

IV. MACHINING AND GRINDING[29,30,31]

12 and 18 percent Ni maraging steels have similar machining characteristics. Both can be easily machined in the annealed condition, but when aged require more careful selection of cutting tools and machining conditions. The use of premium grades of high speed steel for cutting tools is not justified for annealed material but becomes a necessity for material in the

maraged condition. Aged 12 percent Ni steel has been described as comparable to AISI 4340 quenched and tempered to an equivalent hardness, approximately Rc44.

Soluble oil (1:20) is recommended as a cutting fluid for turning both annealed and aged material and for peripheral end milling of annealed material. Highly chlorinated oil is recommended for face milling and end slot milling with M2 tools for annealed material. It is also suggested for use with maraged steel when face milling with T15 tools, tapping with M1 nitrided tools, or peripheral end milling or end mill slotting with M2 tools. Highly sulfurized oil is recommended for drilling, reaming and tapping annealed material, and for drilling and reaming material which has been aged. C2 carbide tools can be used dry for face milling, side milling and end mill slotting aged material, and for side and face milling annealed material. Turning of aged and unaged material can be accomplished with C3 carbide tools and soluble oil (1:20).

Aluminum oxide, vitrified bonded wheels of medium hardness and medium to open structure are satisfactory for use in grinding the 12 and 18 percent Ni alloys.

Sawing operations are considered impractical for cutting aged 18% Ni material at strength levels above 220,000 psi., but can be accomplished on both 12 and 18% Ni material which is in the rolled and annealed condition or aged lower strength maraging steels without too much difficulty. Wet abrasive cutting with

aluminum oxide, rubber bond wheels of 48 to 60 grit is suggested as an alternative for sawing aged material.

V. PHYSICAL AND MECHANICAL PROPERTIES

The final mechanical properties of 12% Ni maraging steel are, as previously noted, very dependent on production and processing history. The terms design property values or vendor guaranteed minimum properties are for the most part either unreliable or very conservative. In general, allowable values must be established or verified by the user for a given application. The following properties are given for reference only.

TYPICAL 12% NI MARAGING STEEL DATA

Nominal Composition, % by Weight:

Ni	Cr	Mo	Al	Ti	C	Mn	Si	P	S
12	5	3	0.40	0.20	0.02	0.08	0.08	0.008	0.005

Mechanical Properties, 1" Plate - Vacuum Melted:

	0.2% Y.S. Ksi	U.T.S. Ksi	Elong. %	R.A. %	70° CVN Impact Energy Ft.-Lbs.	Typ. Rc
Annealed (1500	115	139	19	76	-	32
Maraged (900 3 Hrs)	180	188	14	65	60	42

Compressive Yield..... 188,000 psi

Fracture Toughness, K_{IC} Aged Plate..... 160,000 psi $\sqrt{in}$

Charpy-V 30 Ft.lb. Transition Temp..... -70°F

Density..... 0.285 lb/cu.in.

Modulus of Elasticity	Dynamic Method	Static Method
Tension.....	26-27 x 10^6 psi	27-28 x 10^6 psi
Compression.....	-	29-30 x 10^6 psi

Shear Modulus..... 10.5 x 10^6 psi

Poissons Ratio..... 0.28

Size Change During Aging..... -0.05%

Coefficient of Expansion

80°F to 800°F..... 6.3 x 10^{-6} in/in/°F

80°F to 1000°F..... 6.6 x 10^{-6} in/in/°F

Fatigue Limit (Polished Rotating Beam, 10^8 Cycles)..... 85,000 psi

TYPICAL 12% NI MARAGING STEEL DATA (Cont'd)

Physical Properties, Vacuum Melted Material:

Magnetic Properties	Annealed	Maraged
Magnetizing Force for Saturation, H, oersteds	2,200	2,150
Flux Density at Saturation, B, Kilogausses	17.5	17.5
Residual Flux Density*, B_R, Kilogausses	5.5	6.3
Coercive Force*, Hc, oersteds	15.5	13.7
Permeability, Mmax	235	300

Electrical Resistivity, microhm-cm

	72°F	180°F	300°F	450°F	613°F	804°F
Annealed at 1500°F	77.3	-	-	-	-	-
Maraged at 900°F, 3 Hrs	74.1	78.5	82.6	85.0	89.4	95.2

	55°	180°	300°	450°	613°	804°
Thermal Conductivity (Btu/(hr)(ft²)(°F/in)	108.3	116.5	128.4	148.8	158.4	160.4

Sensitivity to Radiation Embrittlement..... Very low

Corrosion Resistance

Industrial and Marine Atmospheres..... Good

Sea Water..... Subject to pitting and stress corrosion

"Wet" Fatigue Characteristics..... Good, but crack growth rates still increase

*From Bmax of 10 Kilogausses

VI. BIBLIOGRAPHY

1. Vanadium Alloy Steel Company publication, "18% Nickel Ultra-High Strength Maraging Steels" 1966.

2. R. F. Decker, J. T. Nash, and A. J. Goldman, "18% Nickel Maraging Steel", Transactions of the ASM, Vol. 55, 1962, pg. 58.

3. Inco Bulletin, "Preliminary Data on 12% Ni Maraging Steel" June 1966.

4. G. A. Wacker "Stress-Corrosion Cracking Studies of 10-, 12-, and 18-percent Ni Maraging Steel Alloys in Seawater", U.S. Navy Marine Engineering Laboratory R&D Phase Report 73/66, March, 1966.

5. S. T. Rolfe and S. R. Novak, "Slow-Bend K_{IC} Testing of Medium-Strength High-Toughness Steels", U.S. Steel Corporation Applied Research Laboratory Report No. 39.018-007 (11) August 1, 1967.

6. D. S. Dabkowski, E. G. Hamburg, and L. F. Porter, "Effect of Residual Elements on the Notch Toughness of 12 Ni-5Cr-3Mo Maraging Steels", U. S. Steel Corporation Applied Research Laboratory Report No. 39.018-007 (15) August 1, 1967.

7. L. J. Gagda, "Maraging Steels - Status Report", Martin-Marietta.

8. D. S. Dabkowski, L. F. Porter, and G. E. Loveday, "Evaluation of Production Plates from a Vacuum-Induction-Melted 12 Ni-5Cr-3Mo Steel", U. S. Steel Applied Research Laboratory Report No. 39.018-002 (31) July 1, 1965.

9. D. S. Dabkowski, L. F. Porter, and G. E. Loveday, "An Evaluation of Vacuum-Induction-Melted and Air Melted 12 Ni-5Cr-3Mo Steel", U. S. Steel Applied Research Laboratory Report No. 39.018-002 (36).

10. United States Steel Corporation Publication "Maraging Steels - Air Melt Versus Vacuum Melt", Alloy Products, Alloy Metallurgical, Applied Research Laboratory Report of May, 1966.

11. DMIC Report 200, March 11, 1964.

12. Kula, E. B., and Hickey, C. F., Jr., Evaluation of Maraging Steel at U. S. Army Materials Research Agency", Watertown Arsenal, Watertown, Massachusetts, "Third Maraging Steel Project Review", Report No. RTD- TDR-63-4048, Air Force Materials Laboratory, WPAFB, November 1963.

13. Gross, J. H. "The Development of Steel Weldments" Welding Journal, Vol. 47, No. 6, June, 1968.

14. G. E. Pellissier, "Microstructure in Relation to Fracture Toughness of 18 Ni (250) Maraging Steel Weldments", Paper presented at Symposium on Weld Imperfections, Lockheed Missile and Space Company, Palo Alto, California, September 19 to 21, 1966.

15. G. P. Miller and W. I. Mitchell, "Structure and Hardening Mechanisms of 18% Nickel-Cobalt-Molybdenium Maraging Steels", Journal of the Iron and Steel Institute, Vol. 203, Part 9, (September) 1965, Pg. 899.

16. D. S. Dabkowski, L. F. Porter, and G. E. Loveday, "Evaluation of Production Plates from a Vacuum-Induction-Melted 12 Ni-5Cr-3Mo Steel", U. S. Steel Corporation Applied Research Laboratory Report No. 39.018-002 (31) July 1, 1965.

17. A. J. Birkle, D. S. Dabkowski, J. P. Paulina, and L. F. Porter, "A Metallographic Investigation of the Factors Affecting the Notch Toughness of Maraging Steels", Transactions of the ASM, Vol. 58, 1965, Pg. 285.

18. Private communication with Dr. B. W. Schaaf of International Nickel Company, July 21, 1967.

19. L. P. Connor, L. F. Porter, and S. T. Rolfe, "Second Progress Report: Development of an HY-180/210 Weldment", U. S. Steel Corporation Applied Research Laboratory Report No. 39.018-007 (14) August 1, 1967.

20. R. F. Pitler and G. E. Ansell, "Precipitation in a High-Nickel Maraging Steel", Transactions of the ASM, Vol. 57, 1964, Pg. 220.

21. W. A. Fragetta, "HY-180/210 Weldments, Summary Report on Development of Filler Metals and Joining Procedures", Air Reduction Co., Murray Hill, New Jersey, RE-65-109-CRE-34 (July 15, 1965) Report to Bureau of Ships, Contract NOBS-88540.

22. D. S. Dabkowski, E. G. Hamburg, and L. F. Porter, "Effect of Residual Elements on the Notch Toughness of 12 Ni-5Cr-3Mo Maraging Steels", U. S. Steel Corporation Applied Research Laboratory Report No. 39. 018-007 (15) August 1, 1967.

23. F. H. Lang, "Inert Gas Welding of 12% Nickel Maraging Steel". Paper presented at AWS Fall Meeting in Houston, Texas, October 2, 1967.

24. W. A. Fragetta, K. F. Krysiak, and K. E. Dorschu, "Development of HY-180/210 Maraging Steel Filler Metals and Joining Procedures: Part I", Air Reduction Sales Co., Murray Hill, New Jersey, P&EDD-64-211 (May 12, 1964) Report to Bureau of Ships, Contract Nobs-88540.

25. W. A. Fragetta, "Development of HY-180/210 Maraging Steel Filler Metals and Joining Procedures, Part II", Air Reduction Sales Co., Murray Hill, New Jersey, P&EDD-64-255 (July 15, 1964) Report to Bureau of Ships, Contract Nobs-88540.

26. G. A. Wacker, "Stress-Corrosion Cracking Studies of 10-, 12-, and 18-percent Ni Maraging Steel Alloys in Seawater", U. S. Navy Marine Engineering Laboratory Report 73/66, March 1966.

27. R. J. Knoth and W. A. Petersen, "The Welding of 12% Nickel Maraging Steels" Research Suppliment, Welding Journal, January 1965.

28. L. P. Connor and A. M. Rathbone, "Welding Characteristics of 12 Ni-5Cr-3Mo Maraging Steel - I", U. S. Steel Corporation Applied Research Laboratory Report No. 40.018-002 (12) April 1, 1964.

29. Norman Zlatin and J. F. Kahles "Machining the Maraging Steels", Metal Progress, October 1967.

30. International Nickel Company Bulletin, "Planning, Sawing and Drilling 18% Nickel Maraging Steels" 1967.

31. "Machining Maraging Steels" American Machinist Special Report No. 560, November 23, 1964, McGraw Hill, Inc.

32. Private communication with Carl Binney, Cameron Iron Works, May 10, 1968.

33. Private communication with Tom Landig, International Nickel Company, May 9, 1968.

34. Electric Boat Laboratory Test Reports - M -1487 Specimens 1A-1 through 1A-20.

35. U. S. Steel Test Report - Heat No. L-50897, May 31, 1968.

APPENDIX B

ACOUSTIC EMISSION TESTING OF 12-NICKEL MARAGING STEEL PRESSURE VESSELS

by

H. L. Dunegan

DUNEGAN RESEARCH CORPORATION

June 7, 1970

ACOUSTIC EMISSION TESTING OF 12-NICKEL MARAGING STEEL PRESSURE VESSELS

ABSTRACT

Acoustic emission data was obtained from three point bend fracture toughness specimens of 12 nickel maraging steel, and two pressure vessels of the same material. One of the pressure vessels contained a programmed flaw which was extended by fatigue cycling. It is shown that the flawed vessel had similar characteristics of the fracture specimen, thereby allowing estimates to be made of its nearness to failure during a proof test. Both the flawed and unflawed pressure vessels survived the proof pressure and 5 cycles to working pressure. The acoustic emission response, obtained from the flawed vessel during the proof cycle and 5 cycles to the working pressure indicated that it was very near failure. It did not survive the second proof pressure cycle as the flaw was extended through the vessel wall causing a leak to occur.

INTRODUCTION

This report summarizes the results of acoustic emission tests of 12% Ni maraging steel test specimens and pressure vessels conducted in support of NASA Contract NAS 3-11183. The tests were conducted for General Dynamics Corporation to investigate the feasibility of using acoustic emission monitoring techniques for testing the integrity of welded pressure vessels fabricated from this material.

The tests were performed in two phases. Phase I consisted of monitoring three point fracture toughness bend specimens as they were being tested at Lehigh University. This work was conducted in conjunction with fracture mechanics studies of the material under the direction of Dr. Paul Paris of Del Research Corporation. Phase II tests were conducted on 36-inch diameter pressure vessels during hydrotest at General Dynamics Electric Boat division. Phillip Schmidt was the General Dynamics contract project engineer.

During Phase I, two bend specimens, one with a crack in the heat affected zone and one with a crack in the center of a weld were taken to failure while monitoring the acoustic emission present. These tests gave calibration parameters for the acoustic emission instrumentation to be subsequently used on the pressure vessel tests.

During Phase II one pressure vessel containing a fatigue crack in the weld and one unflawed vessel were taken to failure while monitoring for acoustic emission.

In general, the hydrotest procedure for both vessels was the same. Vessel #1 was proof tested at 7320 psi, cycled 5 times to a simulated work pressure of 6650 psi and then pressurized to failure. Vessel #2 was proof tested at 7210 psi, cycled 5 times to a working pressure of 6550 psi and then, as in the case of Vessel #1, pressurized to failure.

INSTRUMENTATION

One channel of acoustic emission was used on the bend specimens and the unflawed pressure vessel. Two channels were used on the flawed vessel to determine the attenuation present, such that transducer spacing on large structures could be optimized.

Figure B1 shows a block diagram of a single channel of instrumentation. The transducer used contained an active element of PZT-5 that had a fundamental resonance at 150 KHz. The preamplifier had a total gain of 60 db and contained the passband filter shown in the diagram. The filter was set to pass frequencies between 100 and 300 KHz. The power amplifier, digital counter and digital to analog connecter were contained in a single unit and served to integrate the pulses from the preamplifier and give a DC voltage for driving the Y axis of the plotter. The raw rf signal from the preamplifier was fed into the counter such that a large amplitude signal gives more counts than a smaller amplitude signal due to the ring down of the transducer. This gives a weighing factor to the larger pulses and the integrated count is roughly proportional to the energy in the pulse.

The acoustic emission signals were fed into an audio unit containing a local oscillator that is variable between 100-300 KHz, a mixer, and an audio amplifier. This gave an audio record of the acoustic emission occurring during the test.

INSTRUMENTATION (Continued)

An oscilloscope and magnetic tape recorder were used on the flawed pressure vessel. This gave a visual as well as a permanent record of the test.

The acoustic emission instrumentation used was small and durable enough to be transported as luggage aboard an aircraft. This is the transportation mode that was used.

TEST PROCEDURE

During the Phase I tests a single transducer was taped to the bend specimen using a viscous resin to couple the sound from the specimen to the transducer. The Phase II tests involved a separation between the instrumentation and the vessels requiring 100 feet of cable. The preamplifier was placed in the test cell with 20 feet of cable between transducer and preamplifier. One hundred feet of cable was used between the preamplifier and the remainder of the instrumentation which was on the second floor above the test chamber. A single transducer was used on the first test (unflawed vessel). It was placed adjacent to a longitudinal weld at the center of the vessel. Two transducers were used on the flawed vessel, one near the flaw and one at one end of the vessel. The transducer at the end of the vessel was 4 feet from the flaw.

RESULTS

Phase I

Figure B2 shows the acoustic emission response obtained from the three point bend specimen containing a fatigued precrack in the weld metal. Note that no acoustic emission is observed prior to the maximum load used for fatigue cycling. At loads slightly higher than the fatigue load acoustic emission begins to occur. These were primarily large bursts of acoustic emission with each burst in many instances giving several thousand counts. When the total counts exceeded the range used on the counter (100,000 counts full scale) the counter was programmed to automatically reset and start over. This reset is shown by the dashed line.

At 100 kips it became obvious from the acoustic emission that the specimen was nearing failure. At this point a hold cycle of five minutes at constant load was performed. The acoustic emission continued during the hold at constant load and an excess of 30,000 counts was observed during this period. Following the hold cycle period the specimen was taken to failure. The hash marked area represents multiple reset of the counter during this pressure range. The specimen achieved a maximum load of 115 kips prior to failure.

Phase II

Figure B3 gives the results obtained from the two pressure vessel tests. The curve for unit #1 is a composite curve, neglecting 5 cycles to the working pressure of 6650 psi. No acoustic emission was observed on these 5 cycles or on the hold cycle at 7320

Phase II (Continued)

psi which was a good indication no flaw growth was occurring. The portion of the curve on unit #1 up to 7320 psi is the acoustic emission observed on the initial proof test to this pressure. The remainder of the curve is the acoustic emission recorded on the burst cycle. During the burst cycle test no acoustic emission was observed up to the previous proof pressure of 7320 psi. A 5 minute hold cycle was observed at 7320 psi with no emission being observed. This lack of acoustic emission under these conditions was indicative that no flaw growth was occurring and the vessel would probably fail above general yield. The acoustic emission started on the burst cycle at the previous proof pressure and at around 9000 psi went off scale and reset several times out to failure. Most of acoustic emission occurring at pressures greater than approximately 9000 psi was due to general yielding of the vessel and failure occurred at 10,400 psi.

The acoustic emission from the flawed vessel gave an entirely different response. First of all note that no acoustic emission was observed on unit #2 prior to 3400 psi. This was the maximum pressure used to fatigue cycle the vessel in order to generate a fatigue crack at the notch in the weld. This is a good demonstration of the irreversible nature of the acoustic emission. The flaw in the vessel was approximately 2 inches long semi-elliptical in shape and extended over halfway through the 3/4 inch thick materials.

RESULTS (Continued)

Phase II (Continued)

Note that the acoustic emission signals from the transducer located 4 feet from the flaw shows essentially the same fracture as the transducer located 1 inch from the flaw. This information confirmed that the single transducer used on the first vessel provided sufficient coverage of the complete vessel. The hash marked area on unit #2 corresponds to multiple reset of the pen over this pressure range.

Acoustic emission was observed to continue at the proof pressure of 7210 psi over the 5 minute hold cycle at this pressure. This indicated that the vessel was near failure and would have probably failed at this pressure had it been held for a longer period.

After holding for 5 minutes at the proof pressure, the vessel was cycled 5 times to the working pressure of 6550 psi. This data is shown in Figure B4. Note that on each cycle acoustic emission was observed. This indicates that flaw growth was occurring on each cycle to the working load. It was anticipated that failure would have probably occurred in less than 50 cycles to this pressure. The recorder zero was shifted on each cycle which accounts for the vertical displacement at the beginning of each cycle.

RESULTS (Continued)

Phase II (Continued)

After cycling 5 times to the working pressure the vessel was taken to failure. The acoustic emission observed on this failure cycle is shown by Figure B5. We predicted on the basis of the acoustic emission observed on the 5 cycles to the working pressure, that the vessel would fail below the previous proof pressure of 7210 psi. This prediction was confirmed when the vessel began to leak at a pressure of 7150 psi. The test was terminated at this time.

Some additional information using a COD gage was obtained during the test on the flawed vessel. This consisted of measuring the crack opening displacement of the flaw as a function of pressure. The COD readings remained linear until just prior to failure on the last cycle. It would have been difficult if not impossible to have made any prediction based on the crack opening displacement data.

DISCUSSION OF RESULTS

It is apparent from Figure B2 and B3 that a significant difference is observed in the acoustic emission behavior between a flawed and unflawed specimen of the 12 nickel maraging steel. The large jumps in the acoustic emission curves on the fracture specimen and flawed vessel represent large bursts of acoustic emission due to incremental growth of the plastic zone in the vicinity of the flaw.

Phase II (Continued)

Note that acoustic emission was observed at very low pressures on the unflawed vessel, but the summation of counts as a function of pressure has a decreasing slope. We have never observed a failure on a structure under a decreasing slope situation. In all cases an increasing slope to the curve has occurred prior to failure. This low pressure acoustic emission is probably associated with small amounts of localized plasticity due to residual stresses generated during welding. The stress in the vessel is acting as a localized stress reliever, and since no finite flaw is present, the material in this vicinity has a state of redundancy which accounts for the decreasing slope. We also did not observe the large bursts of acoustic emission on the unflawed vessel that were present on both the fracture specimen and fractured vessel.

The flawed vessel was fatigued cycled at a load that was a considerably higher percentage of the failure load than the fracture specimen. This was done so that the flaw in the vessel could be extended in a reasonable amount of time. If one ignores the acoustic emission from the fracture specimen (Figure B2) up to approximately half the failure load, there is a remarkable similarity between the data from the fracture specimen and that from the flawed pressure vessel (Figure B3).

RESULTS (Continued)

Phase II (Continued)

The most significant results of these tests is the large difference in the acoustic emission response between the flawed and unflawed vessel. We were able to predict from the hold cycle emission and the similarity between the behavior of the fracture specimen and flawed vessel that we were very near failure on the first proof cycle - yet the vessel passed the proof test procedure and survived 5 cycles to the working load. Under normal proof test criterion a vessel of this type would have qualified for service.

The 12 nickel maraging steel is an ideal material for monitoring acoustic emission. It is both tough, and high strength. The toughness assures that any flaw present large enough to cause failure below general yield will result in a good sized plastic zone prior to failure. The high strength assures that enough strain energy will be released during the plastic zone formation to assure signals of sufficient magnitude for recording the acoustic emission at a reasonable instrumentation gain.

CONCLUSIONS

The primary conclusions arrived at during this investigation are:

1. Acoustic emission can be successfully used for predicting the presence of flaws of sufficient magnitude to cause failure below general yield in welded 12 nickel maraging pressure vessels.
2. Acoustic emission recorded from fracture specimens of the same welded material of identical thickness to a pressure vessel can be used to predict failures in the vessel.
3. No large differences were noted between the acoustic emission signals from a transducer 4 feet from the flaw and one located within 1 inch from the flaw. We predict that transducer locations could be as much as 10 feet apart and still result in a good test.
4. It was proven that a vessel can withstand a rigorous proof test without failure even though it is very near failure.

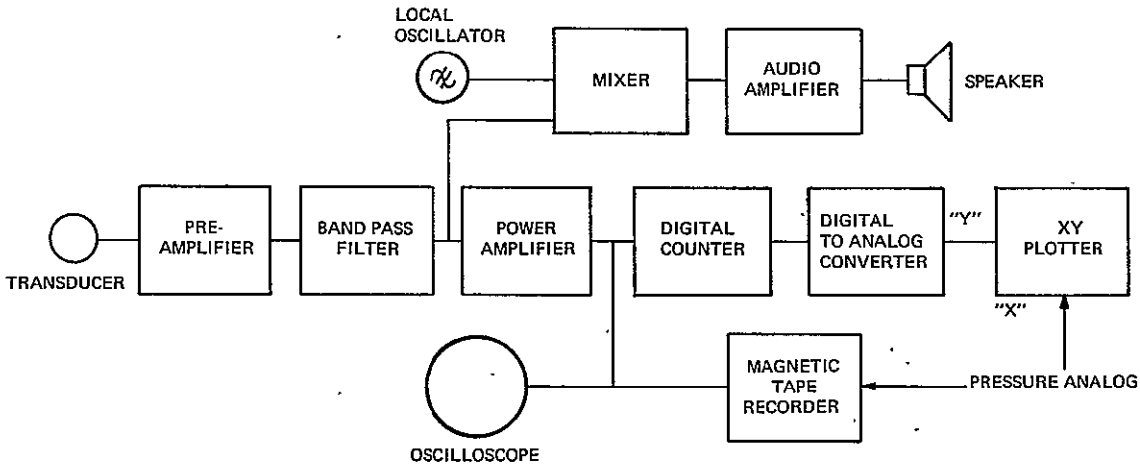

FIGURE .B1

BLOCK DIAGRAM OF INSTRUMENTATION USED IN ACOUSTIC EMISSION TESTS

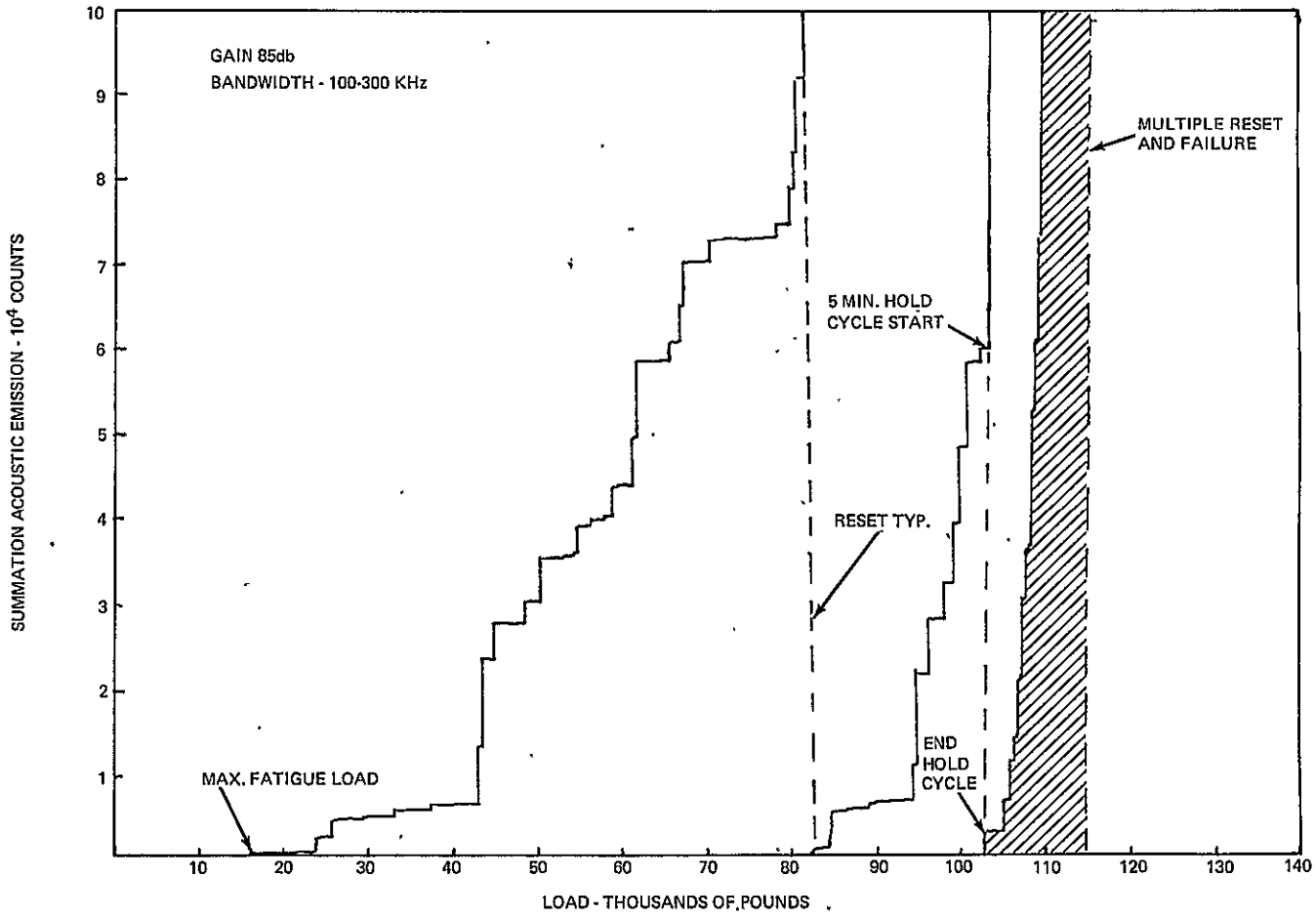

FIGURE B2

SUMMATION ACOUSTIC EMISSION AS A FUNCTION OF LOAD FOR A PRECRACKED 3 POINT BEND SPECIMEN OF 12 NICKEL MARAGING STEEL.

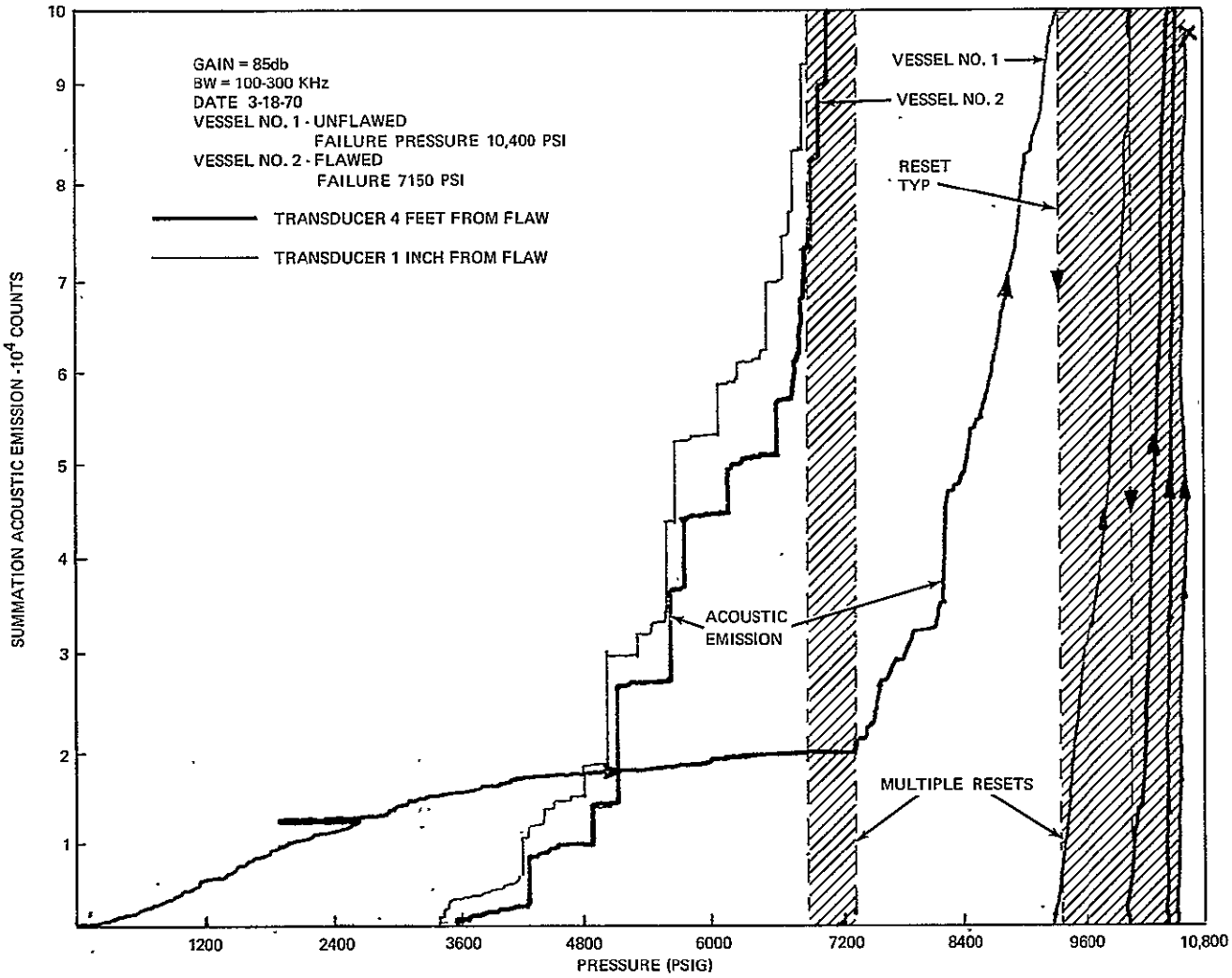

FIGURE B3

SUMMATION ACOUSTIC EMISSION AS A FUNCTION OF PRESSURE FROM -12 NICKEL MARAGING STEEL PRESSURE VESSELS. RECONSTRUCTED PLOT NEGLECTING 5 CYCLE TO 6550 PSI ON UNIT NO 1

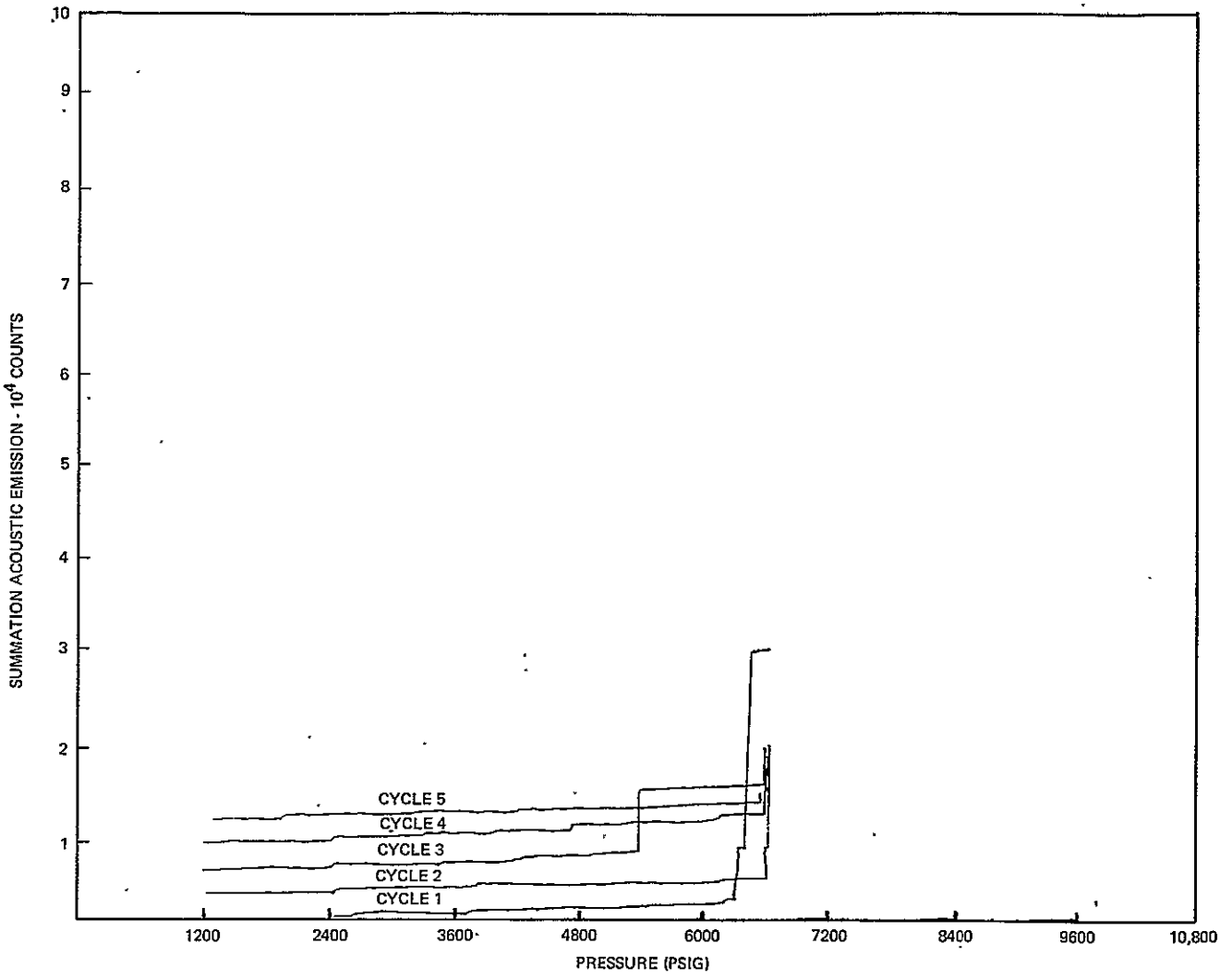

FIGURE B4

SUMMATION ACOUSTIC EMISSION AS A FUNCTION OF PRESSURE ON 5 CYCLES TO 6550 PSI FROM UNIT NO 2

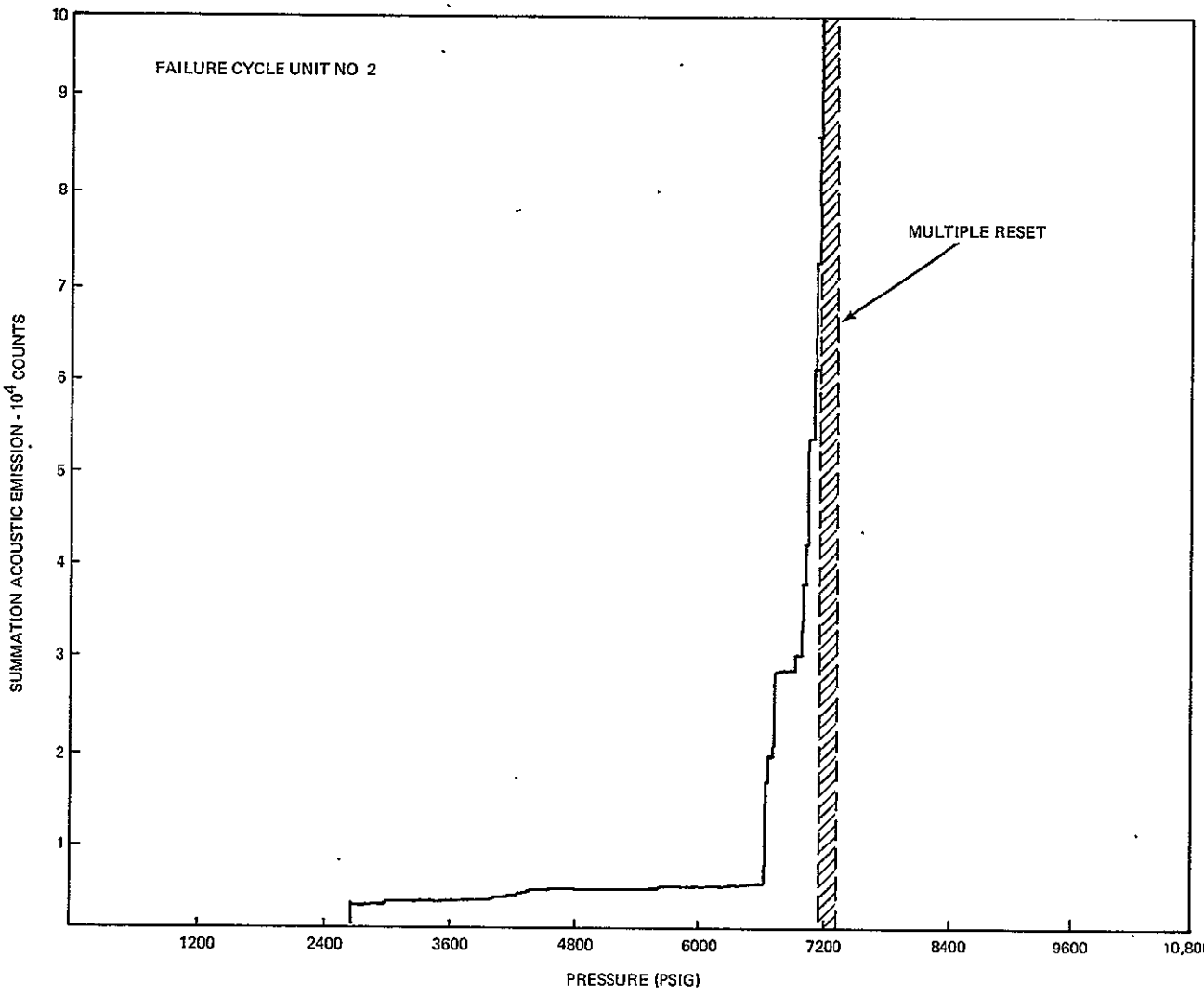

FIGURE B5

SUMMATION ACOUSTIC EMISSION AS A FUNCTION OF PRESSURE ON FAILURE CYCLE
OF UNIT NO 2 FAILURE OCCURRED BY LEAKING AT 7150 PSI